January 2015

Disaggregating Tree And Grass Phenology In Tropical Savannas

Qiang Zhou

DISAGGREGATING TREE AND GRASS PHENOLOGY IN TROPICAL SAVANNAS

By

Qiang Zhou

Bachelor of Science, Hefei University of Technology, 2006

Master of Science, Institute of Remote Sensing Applications Chinese Academy of Sciences, 2009

Master of Science, University of North Dakota, 2012

A Dissertation

Submitted to the Graduate Faculty

of the

University of North Dakota

in partial fulfillment of the requirements

for the degree of

Doctor of Philosophy

Grand Forks, North Dakota

August

2015

This dissertation, submitted by Qiang Zhou in partial fulfillment of the requirements for the Degree of Doctor of Philosophy from the University of North Dakota, has been read by the Faculty Advisory Committee under whom the work has been done and is hereby approved.

Michael Hill (Chairperson)

Soizik Laguette

Jeffrey VanLooy

Bradley Rundquist

Ronald Marsh

This dissertation is being submitted by the appointed advisory committee as having met all of the requirements of the School of Graduate Studies at the University of North Dakota and is hereby approved.

Wayne Swisher
Dean of the School of Graduate Studies

July 28, 2015
Date

PERMISSION

Title	Disaggregating Tree and Grass Phenology in Tropical Savannas
Department	Earth System Science and Policy
Degree	Doctor of Philosophy

In presenting this dissertation in partial fulfillment of the requirements for a graduate degree from the University of North Dakota, I agree that the library of this University shall make it freely available for inspection. I further agree that permission for extensive copying for scholarly purposes may be granted by the professor who supervised my dissertation work or, in his absence, by the Chairperson of the department or the dean of the School of Graduate Studies. It is understood that any copying or publication or other use of this dissertation or part thereof for financial gain shall not be allowed without my written permission. It is also understood that due recognition shall be given to me and to the University of North Dakota in any scholarly use which may be made of any material in my dissertation.

Qiang Zhou

July 14, 2015

Table of Contents

LIST OF FIGURES

LIST OF TABLES

ACKNOWLEDGMENTS

I would like to express my deepest and sincerest thanks go to my committee chair, Professor Michael Hill. His endless patience and the substance of a genius were crucial. Without his guidance, this dissertation could never have been carried out or completed. I would like to thank my committee members, Professor Soizik Laguette, Professor Jeffrey VanLooy, Professor Bradley Rundquist, and Professor Ronald Marsh, who have given encouragement, direction and advice, and finally enabled the study completion.

I wish to thank Professor Crystal Schaaf and Dr. Qingsong Sun. Without their input, the project could not have taken off. In addition, Professor Jane Southworth, Professor Kelley Crews, and Dr. Niti Mishra, who shared their valuable work and contributed to the completion of this study.

I gratefully acknowledge Professor Haochi Zheng, who provided critical support for continuing my doctoral research.

Finally, I would like to thank all faculties and students who have helped me along the way and all contributed to making the study fantastic.

Abstract

Savannas are mixed tree-grass systems and as one of the world's largest biomes represent an important component of the Earth system affecting water and energy balances, carbon sequestration and biodiversity as well as supporting large human populations. Savanna vegetation structure and its distribution, however, may change because of major anthropogenic disturbances from climate change, wildfire, agriculture, and livestock production. The overstory and understory may have different water use strategies, different nutrient requirements and have different responses to fire and climate variation. The accurate measurement of the spatial distribution and structure of the overstory and understory are essential for understanding the savanna ecosystem.

This project developed a workflow for separating the dynamics of the overstory and understory fractional cover in savannas at the continental scale (Australia, South America, and Africa). Previous studies have successfully separated the phenology of Australian savanna vegetation into persistent and seasonal greenness using time series decomposition, and into fractions of photosynthetic vegetation (PV), non-photosynthetic vegetation (NPV) and bare soil (BS) using linear unmixing. This study combined these methods to separate the understory and overstory signal in both the green and senescent phenological stages using remotely sensed imagery from the MODIS (MODerate resolution Imaging Spectroradiometer) sensor. The methods and parameters were adjusted based on the vegetation variation.

The workflow was first tested at the Australian site. Here the PV estimates for overstory and understory showed best performance, however NPV estimates exhibited spatial variation in validation relationships. At the South American site (Cerrado), an additional method based on frequency unmixing was developed to separate green vegetation components with similar phenology. When the decomposition and frequency methods were compared, the frequency method was better for extracting the green tree phenology, but the original decomposition method was better for retrieval of understory grass phenology. Both methods, however, were less accurate than in the Cerrado than in Australia due to intermingling and intergrading of grass and small woody components.

Since African savanna trees are predominantly deciduous, the frequency method was combined with the linear unmixing of fractional cover to attempt to separate the relatively similar phenology of deciduous trees and seasonal grasses. The results for Africa revealed limitations associated with both methods. There was spatial and seasonal variation in the spectral indices used to unmix fractional cover resulting in poor validation for NPV in particular. The frequency analysis revealed significant phase variation indicative of different phenology, but these could not be clearly ascribed to separate grass and tree components.

Overall findings indicate that site-specific variation and vegetation structure and composition, along with MODIS pixel resolution, and the simple vegetation index approach used was not robust across the different savanna biomes. The approach showed generally better performance for estimating PV fraction, and separating green phenology, but there were major inconsistencies, errors and biases in estimation of NPV and BS outside of the Australian savanna environment.

CHAPTER 1 INTRODUCTION

1. Background

Savanna is a discontinuous stratum of trees and shrubs with a grassy/herbaceous understory (Mistry 2000). Tree-grass coexistence has been the subject of much research and has been discussed in a number of reviews (e.g., Bond, 2008; Hanan et al. 2010; House et al. 2003; Scholes & Archer, 1997). The savanna biome may represent a transition zone between forest and grassland, where growth patterns are highly correlated with alternation of wet and dry seasons, and significant disturbance by fire and grazing (Bourliere & Hadley 1983; Staver et al. 2011). Savanna is one of the largest biomes in the world (Figure 1). It is important to the Earth system specifically for water and energy balances, carbon sequestration, and land-atmosphere exchanges through wild fire and production of aerosols (Hill 2013) (Table 1). The savanna tree-grass ecosystem stores carbon in soils and wood, and the patch structure and vegetative cover are critical for water cycling, and support high diversity of plant and animal species (Hanan et al. 2010). In addition, the savanna biome supports one-fifth of the world's population in terms of providing agriculture, grazing, and fuel wood (Mistry 2000).

Major disturbances such as climate change and variability, wildfire, agricultural conversion and overgrazing by domesticated livestock have caused major declines in coverage, and changes in composition of tropical savanna systems (Grace et al. 2006; Higgins et al. 2007; Knapp et al. 2008; Bond 2008; Barlow & Peres 2008; Hanan et al. 2010). The effect of the interaction between climate, fire frequency and intensity and

herbivory is the subject of substantial research interest. Current thinking on tree-grass interactions as represented in process models suggest that (Table 1): 1) grasses suppress juvenile trees through competition for resources, while adult trees suppress grass mainly through water competition (Hanan et al. 2010); 2) fire suppresses tree cover by killing juvenile trees and reducing longevity of adult trees; 3) the magnitude of this suppression is influenced by the grass biomass (as a fuel load) as well as precipitation (as a driver of biomass accumulation and moisture status of the landscape); and 4) herbivores and browsers (including grazing) reduces biomass of both grass and tree layers respectively (Hanan et al. 2010).

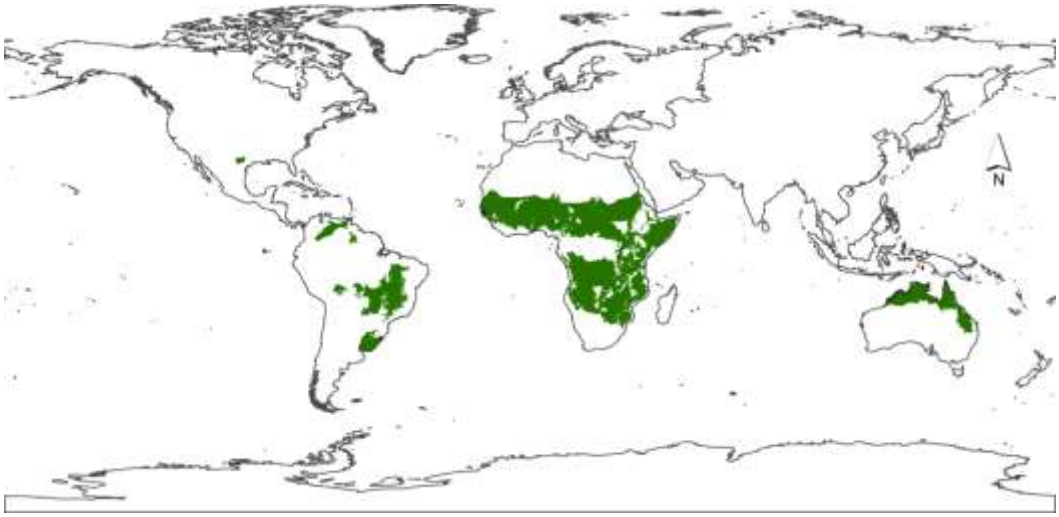

Figure 1. Global tropical savannas (based on WWF Ecoregions, (Olson et al. 2001), and excluding southern and south east Asian tree-grass ecoregions which are heavily converted and altered and not classified as savannas by (Olson et al. 2001))

Table 1. Significance of distinguishing over and under story phenology

	Tree	Grass	Impact	Reference
Ecosystem Functions	○ Support browser (such as giraffe and black rhino) ○ Denser Carbon sequestration than grasses	○ Support herbivore (such as buffalo, burchell's zebra, and cattle) ○ Carbon sequestration	• Provide basis for ecosystem biodiversity • Relieve climate change • Support human society	Ratter et al. 1997; Bustamante et al. 2010
Competition	○ Competition for water and nutrition ○ Grass suppress juvenile trees ○ Adult suppress grass		• The competition amplifies disturbances	De Bie et al. 1998; Sankaran et al. 2005; Goldstein et al. 2008
Fire	○ Kill juvenile trees ○ Reduce longevity of adult trees ○ Dense trees suppress fire	○ Grass provide fire fuel ○ Tend to dominant after fire area	• Leading to deterioration and even desertification • Relieve greenhouse gas • Reduce carbon sequestration source	Higgins et al. 2000; Van Langevelde et al. 2003; Gardner 2006; Verbesselt et al. 2006; Higgins et al. 2007; Verbesselt et al. 2007
	○ Consuming tree foliage and even damaging and uprooting trees	○ Suppress grass distribution ○ Reductions in biomass	• Support local economy • May lead to deterioration and even desertification • Threat to the biodiversity • Reduce carbon sequestration source	Higgins et al. 1999; Van Langevelde et al. 2003; Grace et al. 2006; Ogbazghi et al. 2006; Wiegand et al. 2006
Wood Harvest	Reductions in biomass and species richness			
Agriculture and Urbanization	○ Cause fragmentation ○ Burning or clearing trees and grasses		• Threat to the biodiversity • Reduce carbon sequestration source	Alho & Martins 1995; Cavalcanti 1999; Ogbazghi et al. 2006; Silva et al. 2006; Mitchard et al. 2009

Due to the distinctive functional role of trees and grass, accurate estimation of dynamic fractional cover is important in many fields of research such as biodiversity assessment, deforestation measurement, monitoring of urban expansion (Gessner et al. 2013), assessment and modeling of water balance and hydrodynamics (Guerschman et al. 2009), and fire risks (Verbesselt et al. 2006; Verbesselt et al. 2007). The dynamic of vegetation structure provides a sound base for studying the population of browsers and herbivores that relies on different species. The abundance of dry vegetation is an essential input of fire risk estimation, while tree density, on the other hand, indicates the potential spread of fire. The overall green and dry vegetation allows for better estimation of the carbon sequestration. The fraction of bare soil in time series could be used to identify fire scars, and changes of vegetation structure after fire provides references for fire management. Moreover, the maps of different vegetation provide basis of grazing and woody harvest planning and reducing damage of the savanna ecosystem.

The three major savanna regions are all located at the southern hemisphere at similar latitudes. Due to the broad distribution and its heterogeneous nature, a ground survey is infeasible. Remote sensing provides a practical and timely observation, which makes thoroughly and intensively investigating savanna vegetation dynamics possible. However, because of the diverse vegetation combination and structure, different approaches are needed at various savanna regions.

2. Project Objectives

The objectives of this study were to (Figure 2):

1) Establish a workflow to map the dynamics and phenology of tree and herbaceous vegetation in Australian, South American, and African savannas using remote sensing technology;
2) Compare the accuracy and effectiveness of the methods applied in the three sites; and
3) Compare the vegetation dynamic characteristics across the three savanna sites.

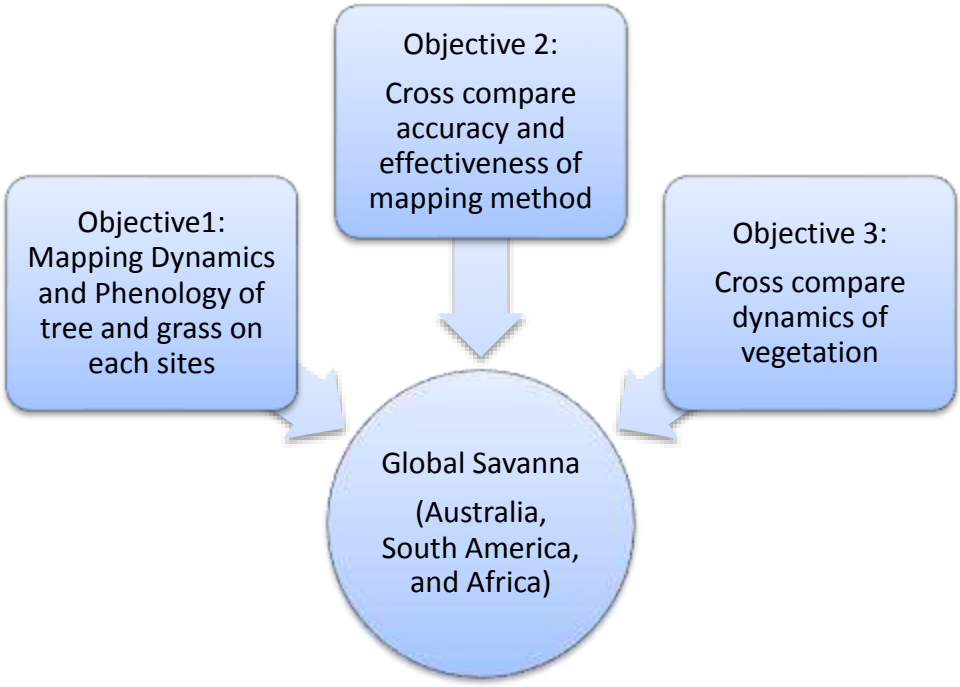

Figure 2. Objectives of the dissertation

The dissertation is structured according to the flow of the research carried out. Figure 3 is an outline of the dissertation with the relationship between chapters. Every chapter starts with an introduction that overviews the task of the chapter and ends with a summary of findings.

Chapter 1 provides information about the vegetation characteristics associated with local climate and human activities. It also reviews previous research and provides background to the ability of mapping vegetation dynamics using remote sensing technology. Then, a concept workflow is established based on previous studies. The unmixing fractional cover from NDVI and SWIR32 distinguishes photosynthetic activities, and time series decomposition separates tree and grass phenology. In **chapter 2**, the workflow and approaches are tested at the Australian savanna where the original approaches are developed further. The results are validated with ground observation and high-resolution images. In **chapter 3,** the workflow is applied at the Cerrado of Brazil where vegetation phenology is similar with the Australian savanna. The approaches are adjusted based on the local vegetation features. The results are validated against high-resolution images and ground survey. The African savanna is studied in **chapter 4** and **chapter 5** due to the distinctive deciduous tree phenology. In **chapter 4**, the unmixing fractional cover is carried out and the results are compared with ground observation and high-resolution images. The performance of vegetation indices in the African savanna is then characterized. In **chapter 5**, a new method is developed to separate the tree and grass phenology. **Chapter 6** describes the variation of accuracy between tropical savannas. Comparisons of the characteristics of the vegetation as well as its dynamics across savanna biomes are also presented.

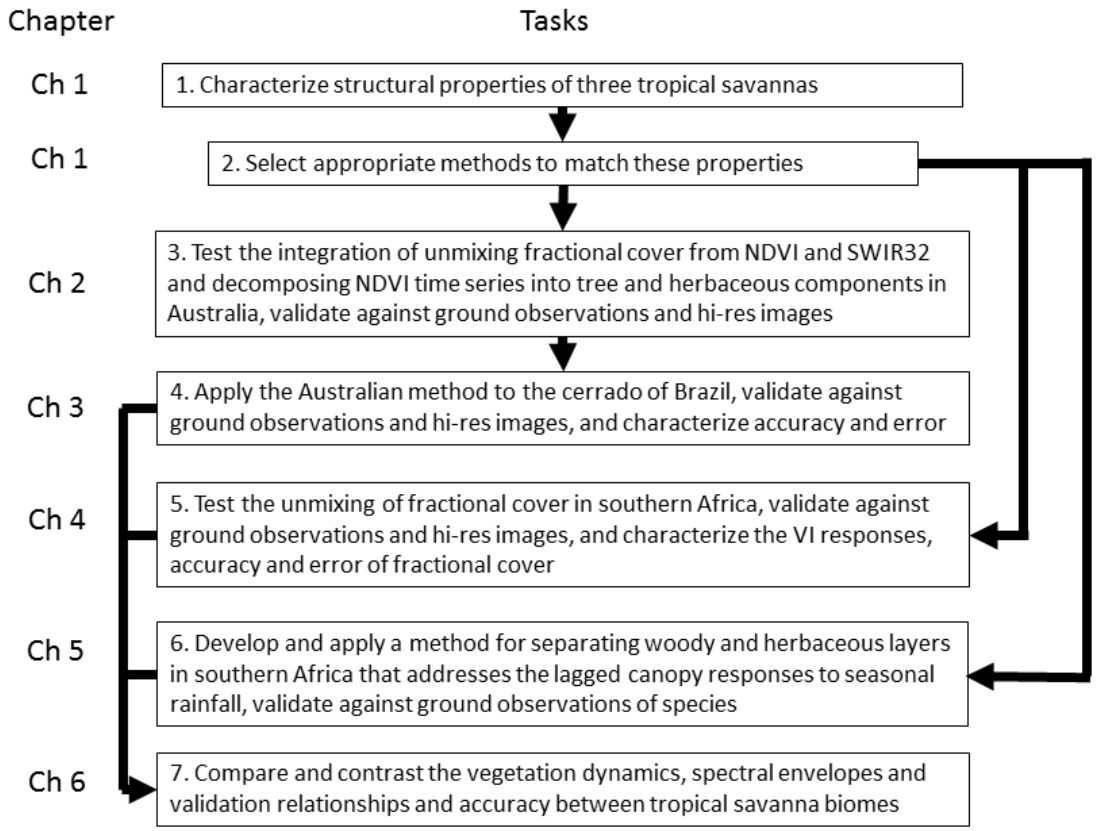

Figure 3. Flow diagram of dissertation chapters and relationship to main contents

3. Tropical Savanna

3.1 Australian Savannas

The Australian savanna zone as defined by the Terrestrial Ecoregions of the World (Olson et al. 2001) includes eight eco-regions: Kimberly tropical savanna; Arnhem Land tropical savanna; Victoria plains tropical savanna; Carpentaria tropical savanna; Cape York Peninsula tropical savanna; Einasleigh upland savanna and Brigalow tropical savanna (Figure 4). The savanna zone covers over 1.6 million km^2. Over 90% of rainfall occurs between November and April (Hutley & Beringer 2010). The land use in the tropical savanna is divided between extensive grazing and conservation or Aboriginal and government land, except in southern Queensland where substantial conversion has occurred (Figure 5). The vegetation cover and types are complex and highly variable

(Figure 6). The study area spans a continuum from closed forest (Cape York Peninsula Tropical Savanna and Arnhem Land Tropical Savanna) to mixed tree-grass systems (Einasleigh upland savanna and Brigalow tropical savanna) and more open woodlands and sparsely treed grasslands (Kimberly tropical savanna, Victoria Plains tropical savanna and Carpentaria tropical savanna). The *Eucalyptus* spp. community is the most widespread woody layer, while C4 grasses dominate the understory (Hutley & Beringer 2010). Other important woody plants include: *Acacia* spp., *Callitris* spp., *Casuarina* spp., and *Melaleuca* spp.. Given the size of the Australian savanna, it stores around one-third of the terrestrial carbon in Australia (Williams et al. 2004; Hutley & Beringer 2010).

3.2 South American Savannas

The central Brazilian tropical savanna, known as Cerrado, covers around 204 million hectares of the country (Figure 7) (Sano et al. 2010). The climate is highly seasonal: summer (October to March) is wet and winter (April to September) is dry (Sano et al. 2010; Miranda et al. 2014). The soils are well-drained and vegetation is tolerant of seasonal aridity (Pennington et al. 2006). The Cerrado landscape varies from a mosaic of grasslands with sparse shrubs and woody cover (Sano et al. 2010; Miranda et al. 2014) to dense woodland. The structural differences in vegetation may be related to soil fertility (Goodland & Pollard 1973) and fire frequency and severity (Ratter et al., 1997). The dominant tree families include *Leguminosae*, *Malpighiaceae*, *Myrtaceae*, *Melastomataceae* and *Rubiaceae* (Ratter et al. 1997). Gallery forests occur along rivers and share many species with rain forests (Pennington et al. 2006). Studies have shown that about 50% of the original Cerrado has been fragmented by deforestation and conversion to agriculture (Klink & Machado 2005; Guimaraes et al. 2006; Sano et al. 2010; Ferreira et al. 2011).

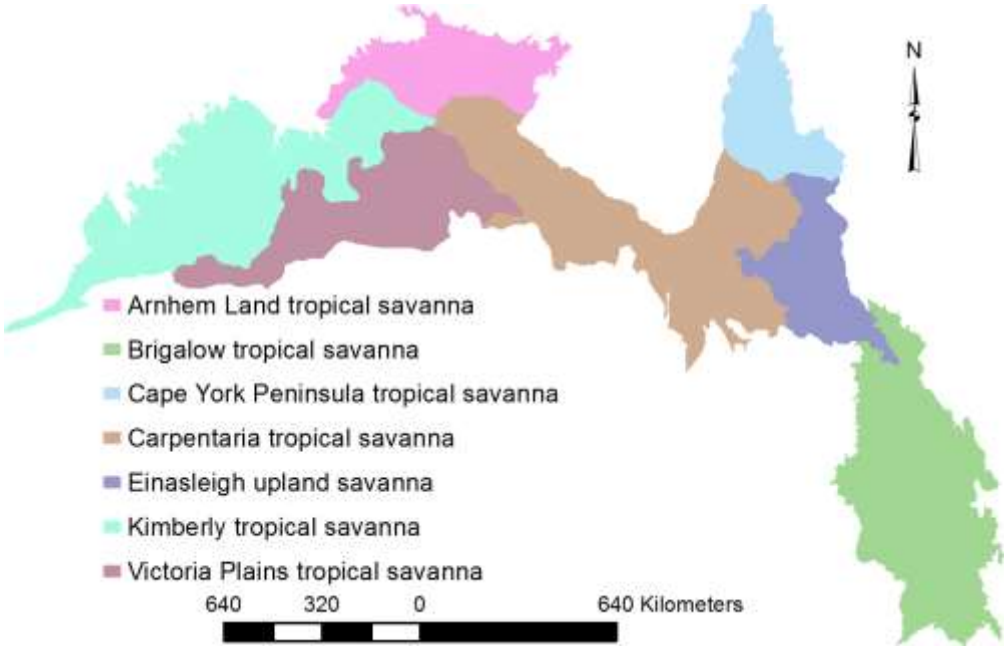

Figure 4. *Australian Tropical Savanna Ecoregions (Olson et al. 2001).*

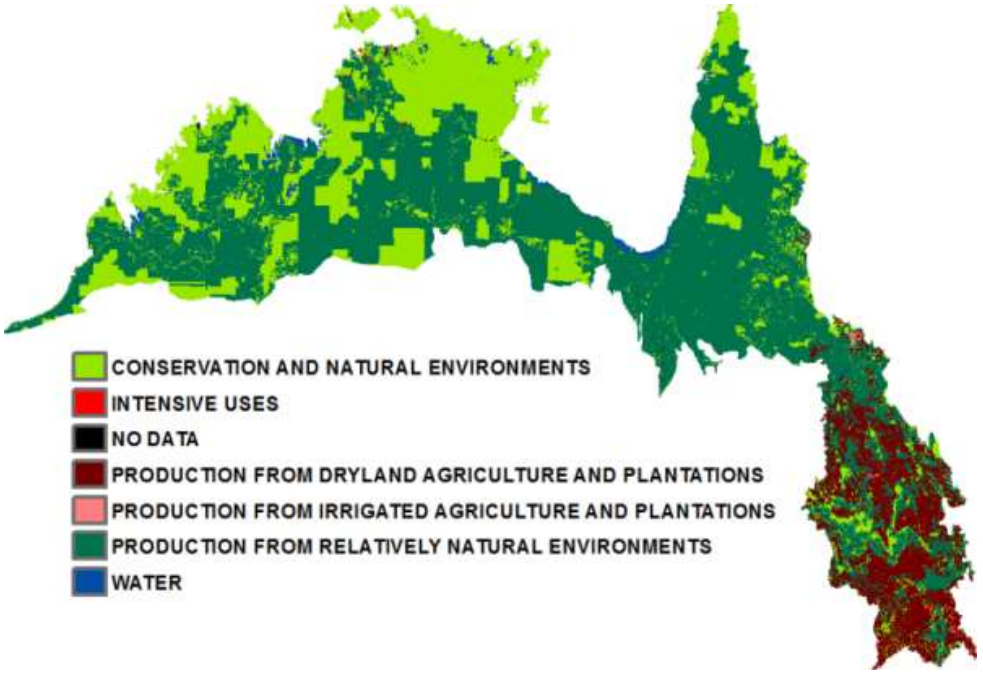

Figure 5. *Land use across the Australian tropical savanna (Bureau of Rural Sciences 2006)*

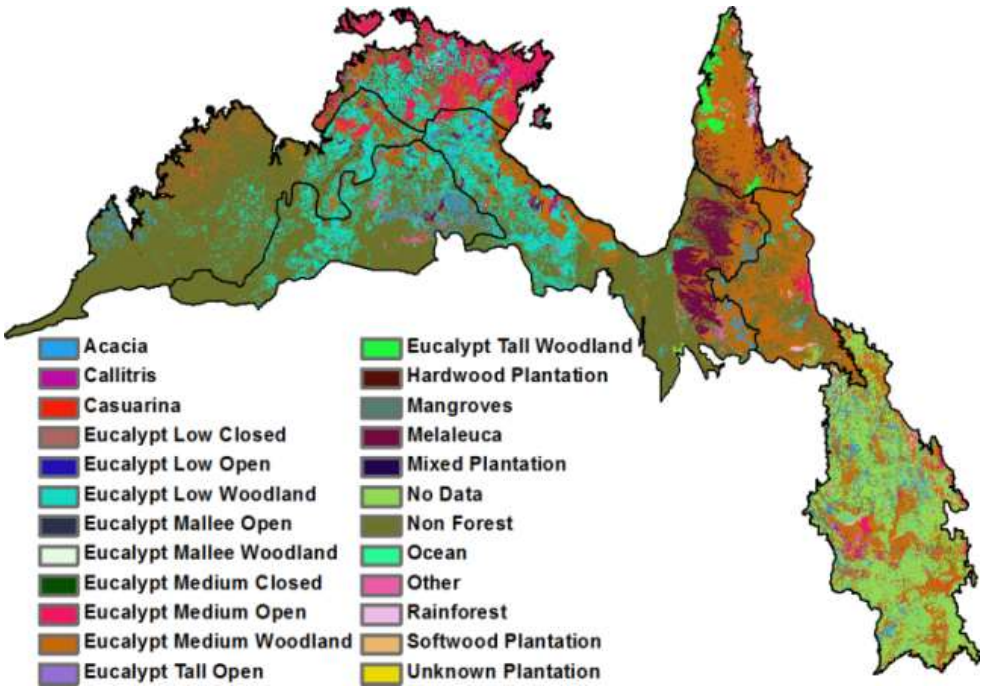

a)

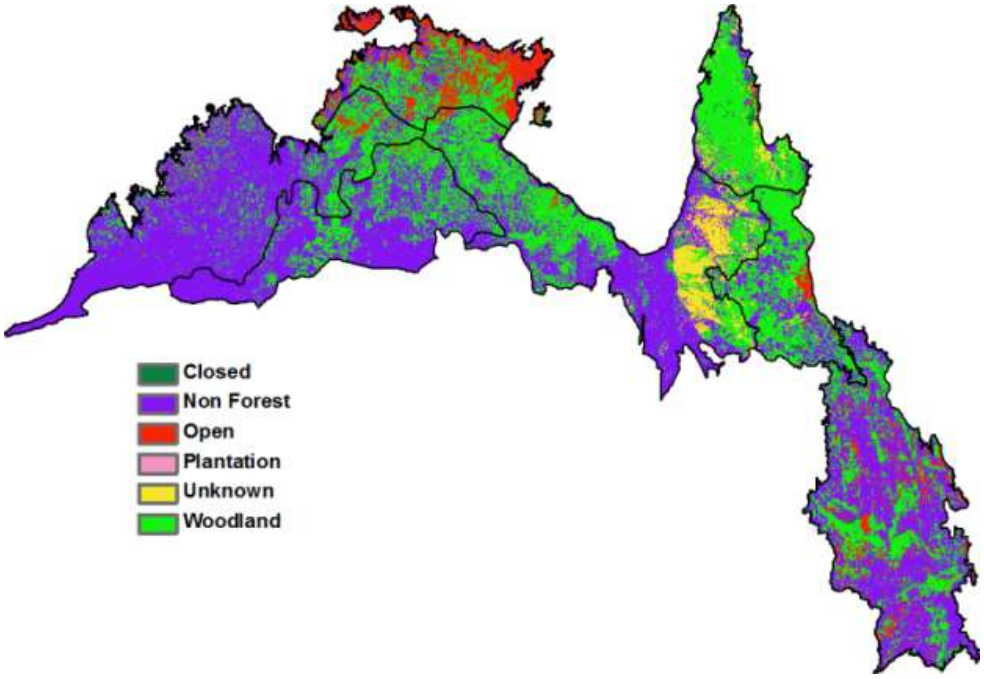

b)

Figure 6. The vegetation of the Australian Tropical savanna vegetation a) vegetation type based on the National Forest Inventory (National Forest Inventory 2003)*; b) the broad plant functional types derived from the NFI.*

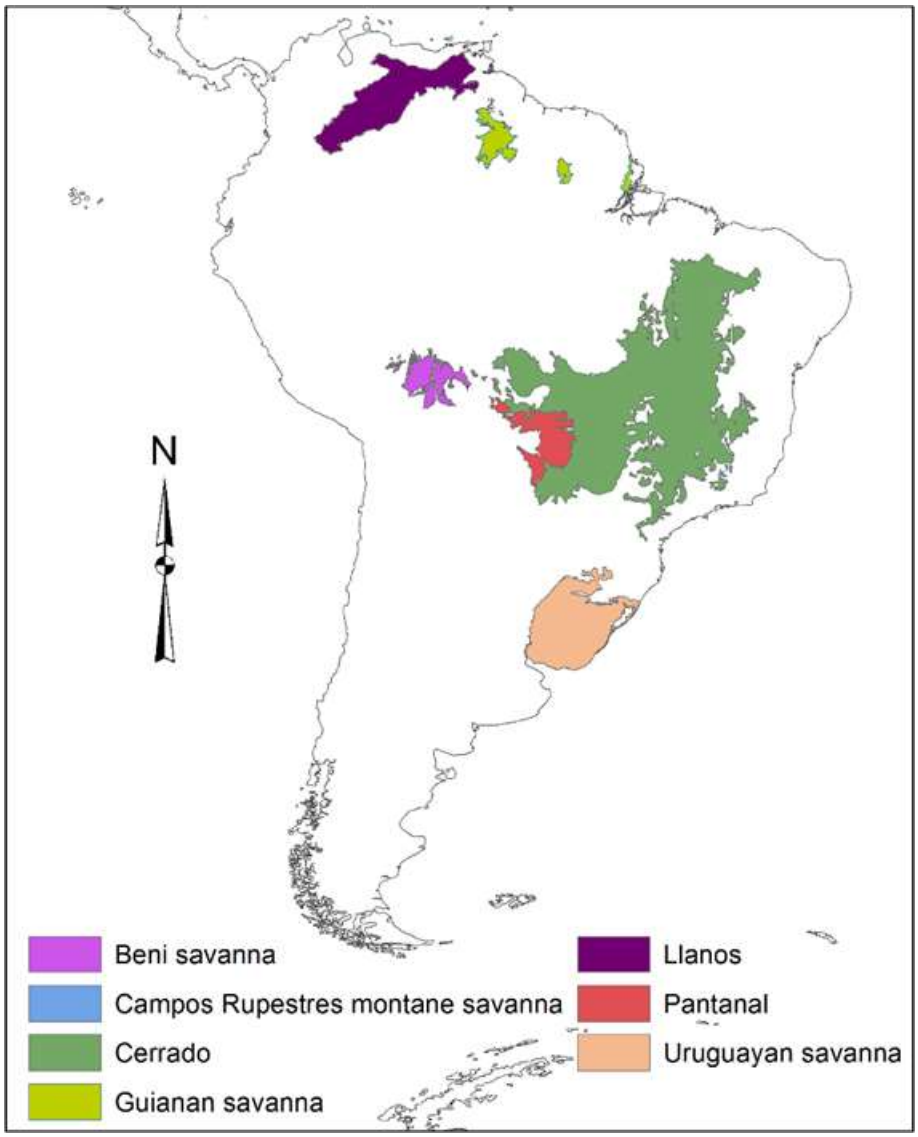

Figure 7. The savanna ecoregions of South America. The Cerrado of Brazil is the largest and the focus of this project.

Another large South American savanna, the Llanos, lies north of the equator and covers about 500,000 km^2 from the eastern coast of Venezuela to the Guaviare River in Colombia (Beard 1953; Blydenstein 1967; Sarmiento 1983; Mistry 2000). Precipitations varies from 800 to 2500 mm and most rainfall occurs between April and November (Monasterio 1970). The woody species are all evergreen: from November to April, leaf flush and fall are concurrent, so the plants are always green, and the leaf flushing stops at the start of the rainy season (Mistry 2000). Smaller savannas also occur in central South

America particularly the Beni savanna and the Guianian savanna which are grassy systems embedded in Amazonia (Hill & Hanan 2010).

3.3 African Savannas

The African savanna can be divided into three regions: West African savanna, East African savanna and the Southern African Savanna (Figure 8) (Hill et al. 2012). The West African savanna covers Mauritania, Mali, Niger, Chad, Sudan, Senegal, Guinea, Burkina Faso, Nigeria, Ivory Coast, Ghana, Togo, Cameroon and Central African Republic. The region experiences a severe rainfall gradient that decreases from south to north. Precipitation ranges from 200 to 1200 mm, and the length of the dry season varies from 6 to 3 months from south to north (Malo & Nicholson 1990; Budde et al. 2004). The vegetation structure ranges from grassland with sparse trees to woodlands and forests along with the increase of precipitation (Mistry 2000). The East African savanna covers Sudan, Ethiopia, Somalia, Kenya, Uganda and Tanzania. The annual precipitation is highly localized and ranges from 500 to 2000 mm (Davenport & Nicholson 1993). Common species include *Acacia* spp., *Commiphora* spp. and *Grewia* spp. (White 1983). The southern African savanna covers Namibia, Botswana, Zimbabwe, Swaziland, Mozambique and South Africa. The savanna covers about 53.7% of southern Africa (Rutherford 1997). The annual precipitation ranges from 200 to 1000mm (Cowling et al. 2004) mostly between October and April (Schulze 1965). From north to the southeast, the vegetation generally changes from woodlands and open deciduous forests to arid shrubland following steep precipitation gradients (Cowling et al. 2004).

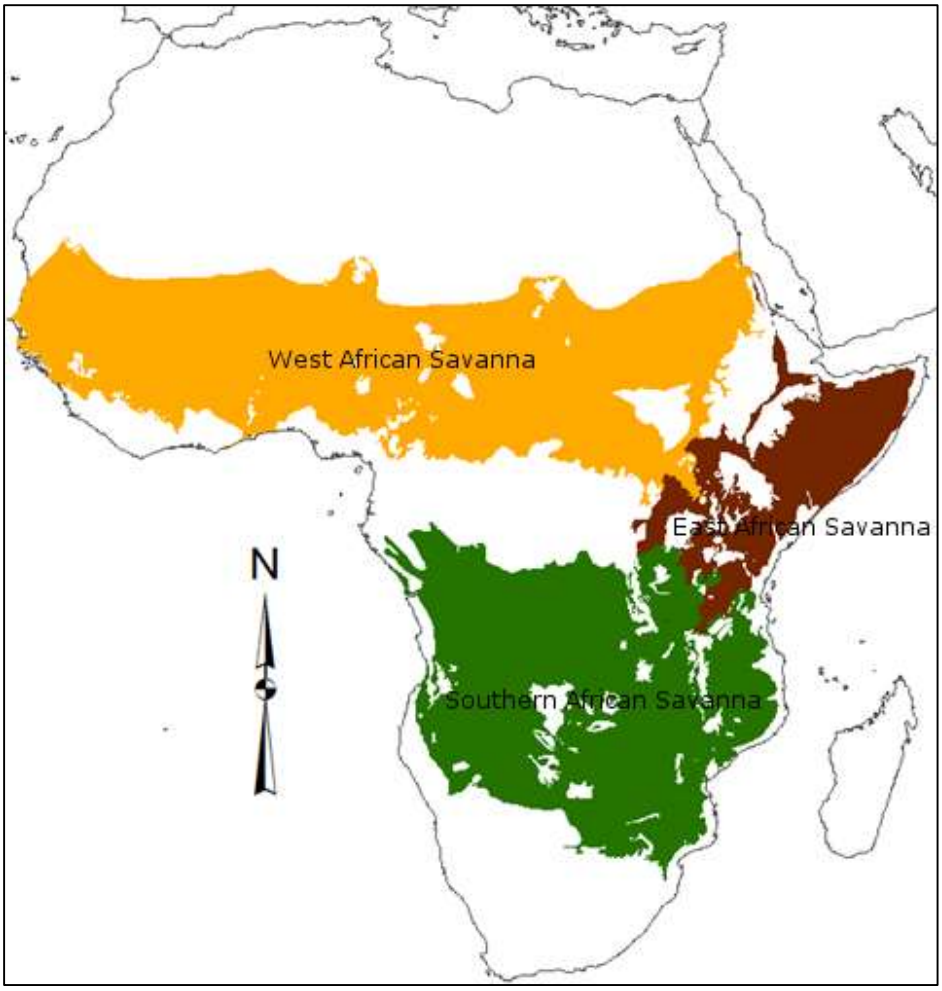

Figure 8. Africa savanna showing the three main regions: east Africa (Brown), West Africa (Yellow) and Southern Africa (Green).

3.4 Asian Savannas

The tropical savanna in East Asia covers Burma, Thailand, Laos, Vietnam and Cambodia (Mistry 2000). Annual precipitation ranges from 1000-1500mm (Stott 1988; Smitinand 1962; Smitinand 1977). The monsoon season starts in May or June and lasts until October or November (Stott 1991). Species in this region include: *A. siamensis, Acacia catechu, Careya arborea, Eupatorium odoratum, Imperata cylindrical, Panicum repens, Pterocarpus macrocarpus, Saccharum spontaneum, Sorghum halepense and Vitiveria zizanoides* (Stott 1991).

4. Remote Sensing of Savannas

Although historically inhabited tropical savannas in Africa, and those recently occupied and exploited in the New World have received considerable attention from researchers, ground observation networks are very limited in both spatial and temporal extent except the Northern Australian Tropical Transect (NATT; Williams & Duff, 1996) and the Kalahari Transect (Scholes & Dowty 2002). Satellite imagery provides a practical and timely resource for modeling and estimating land cover of tropical savanna ecosystems. Early polar orbiting satellites (e.g., Advanced Very High Resolution Radiometer (AVHRR)) were designed mainly for weather analysis, but provided the basis for the development of high frequency global monitoring of vegetation (DeFries 2008). With the development of the normalized difference vegetation index (NDVI, Tucker & Sellers, 1986), and compositing of daily images to create cloud free time series, the dynamics of savanna vegetation in relation to annual climatic cycles was revealed for major parts of western and southern Africa (e.g. Fuller & Prince, 1996; Prince & Tucker, 1986; Prince, 1991; Tucker & Sellers, 1986). Since these early studies, more sensors that are sophisticated have been applied to monitoring and measurement of terrestrial vegetation dynamics. The MODerate resolution Imaging Spectroradiometer (MODIS), launched on the Terra and Aqua platforms in 1999 and 2002 respectively, greatly extended the capability of broad scale analysis by providing higher spatial resolution and more band selection (Hill & Hanan 2010). This allowed savanna studies to spread to Australia (e.g. Guerschman et al., 2009; Guerschman & Scarth, 2015; Guerschman et al., 2012), the Cerrado of Brazil (Ferreira et al. 2003; Hoffmann et al. 2005) and the Llanos of Colombia and Venezuela (e.g. Anaya et al. 2009). The Landsat family of satellites (DeFries 2008), first launched in 1972, and similar sensors (e.g. Satellite Pour

l'Observation de la Terre – SPOT) provided higher spatial resolution for more detailed but less frequent vegetation mapping and monitoring (e.g. Ferreira et al., 2003; Lhermitte et al., 2008; Li et al. 2010; Verbesselt et al. 2006). The availability of data from radar scatterometers further enhanced broad scale assessment of savanna vegetation dynamics (e.g. Frison et al. 1998; Zine et al. 2005).

Over the past 20 years, the number and types of research on remote sensing of vegetation dynamics have greatly expanded. Topics of study include mapping land cover and land use change (Hill & Donald 2003; Budde et al. 2004; Brannstrom et al. 2008; Brink & Eva 2009), fire monitoring (Giglio et al. 1999; Giglio et al. 2000; Verbesselt et al. 2007; Jacquin et al. 2010), fire scar mapping (Roy et al. 2002; Jacquin et al. 2007; Chongo et al. 2007), and surface phenology with climate drivers (Reed 2006; Fuller & Prince 1996; Duchemin et al. 1999; Zhang et al. 2005; Musyimi 2011; Barbosa et al. 2011). In tropical savannas, each of these topics are explicitly concerned with the dynamics and changes occurring in both the woody and herbaceous layers, and hence a variety of methods developed for global vegetation assessment have specific potential for application to tree-grass systems.

4.1 Remote Sensing and Savanna Land Cover Change

A number of temporal analysis methods based on NDVI have been developed for detecting land cover change. For example, Hill & Donald (2003) characterized the time series NDVI using mean, standard deviation, time integrated NDVI, and season duration to estimate spatiotemporal patterns of fragmented landscapes. Rigina & Rasmussen (2003) explored vegetation productivity changes using linear trend lines and principal component analysis (PCA). The analysis suggested that trend line analysis is capable of

distinguishing positive, stable and negative changes in vegetation productivity as well as the magnitude of these changes. PCA could detect general variation and seasonal precipitation changes, while the identified vegetative productivity changes could be both negative and positive at the same time. Budde et al. (2004) defined the local spatial mean +/- standard deviation as the threshold of positive and negative vegetation productivity changes. The study suggested that negative change is related to urban expansion, forest degradation, and heavy grazing, while positive change is related to establishment of forest reserves, presence of undisturbed grasslands, and natural bush land with light grazing/utilization. More recently, tropical savannas (and particularly those in South America) have become a focus for change detection analysis. Brannstrom et al. (2008) analyzed land change in the Cerrado region between 1986 and 2002 using unsupervised classification. The study suggested that nearly 40% of land remained unchanged while 3,646 km^2 (in western Bahia) and 3,011 km^2 (in the eastern Mato Grosso) were converted to agro-pastoral land covers. Brink & Eva (2009) compared land cover types in sub-Saharan Africa between 1975 and 2000 using high spatial resolution images and concluded that nearly 5 million hectare of natural vegetation were lost per year. Romero-Ruiz et al. (2012) classified multi-temporal images between 1987 and 2007 in the Llanos savanna region and found that land cover change was related to local economic development.

4.2 Remote Sensing and Tropical Savanna Fire

Fire is considered an important factor in the dynamics of tropical savannas, especially in the conserved areas where anthropogenic activity is light (Jacquin et al. 2010). For example, Spessa et al. (2005) found that monthly evergreen and monthly rain-

green patterns are strongly associated with fire frequency in the wet-dry tropics of Northern Australia. Some vegetation indices (VIs) were tested or developed for detecting fire scars. For example, a brightness index ($\sqrt{Red^2 + NIR^2}$) was found to be more sensitive for detection of fire scars when compared with NDVI and NBR (Normalized Burned Ratio; +(NIR-MIR) / (NIR+MIR)) (Jacquin et al. 2007). Chongo et al. (2007) found that albedo is most relevant to fire occurrence and sometimes fire scars when comparing with NDVI while the normalized difference water index (NDWI) was unable to detect fire scars. The study tested two methods for fire scar identification: threshold and maximum likelihood classification. The result suggested that the maximum likelihood classification is more effective while the threshold classification needs to be adapted for different areas. Previous studies (Verbesselt et al. 2006; Verbesselt et al. 2007) compared different VIs and found that NDWI could be used as a spatio-temporal source for fire risk monitoring. The author also found that the integral of the Ratio Vegetation Index (NIR/RED) is more sensitive to fuel moisture content than NDVI combined with NDWI and thus could be used to optimize the fire risk prediction (Verbesselt et al. 2006; Verbesselt et al. 2007). Based on previous studies, global fire detection products were then developed from MODIS dataset (Justice et al. 2011): the MODIS Active Fire Product (MOD14) detects actively fire burning areas using the middle infrared bands (Giglio et al. 1999; Giglio et al. 2000; Giglio et al. 2003); the MODIS Burned Area Product (MCD45) characterizes fire affected areas using visible and shortwave infrared bands based on the bidirectional reflectance distribution function (BRDF) (Roy et al. 2002; Roy et al. 2005). Since fire dynamics in savanna depend upon the herbaceous layer

as fuel source, disaggregation of woody and herbaceous layer phenology is of critical importance.

4.3 Remote Sensing and Tropical Savanna Phenology

Savanna phenology is the study of different stages of the vegetation life cycle and its relation with seasonal and inter-annual climate parameters (Maignan et al. 2008). Time series of VIs, in association with climate data, are helpful in revealing dynamics of vegetation corresponding to meteorological forcing. Phenology parameters that have received attention include onset of green-up and senescence, length of growing season, maximum NDVI, amplitude of NDVI, integrated NDVI during growing season, etc. Date of green-up and date of senescence are two key metrics, and a range of different methods has been used to derive these metrics. These methods fit into three general categories: thresholds, derivatives and temporal shifts.

For the first category of methods, the dates of green-up and senescence are defined by the intersection of the smoothed time series with the threshold value in the upward and downward directions. The simplest way to define the threshold is to set it to a constant value; White (1997) used a value of 0.5, while another study used a NDVI value of 0.55 (Duchemin et al. 1999). An alternative approach is to first estimate the general trend of the smoothed time series and then use the trend curve as the threshold. A further way of defining the onset of the growing season is to locate the date when the time series data crosses and persistently exceeds the moving average (Reed 2006; Budde et al. 2004).

The second category of methods applies the assumption that a VI (such as NDVI) time series curve exhibits a concave shape during the non-growing season and a convex shape during the growing season. Thus, the onset of the growing season is defined as the date when the second derivative turns from positive to negative. On the derivative curve,

this date is defined by the inflexion point where the time series curve changes from an upwards to a downwards trajectory (Zhang et al. 2003).

4.4 Remote Sensing and Climate in Tropical Savannas

The dynamics of the savanna are primarily controlled by two factors: plant-available moisture and plant-available nutrients (Mistry 2000). Since tropical savannas are geographically associated with highly seasonal rainfall regimes (Mistry 2000), the question of how meteorological data, like rainfall, affects phenology of savannas has been a major topic of research. Many studies suggest that trajectory of NDVI values (increasing/decreasing) corresponds strongly to increases and decreases in rainfall in tropical savanna regions such as the Northeast of Brazil (Barbosa et al. 2006), Sahel (Herrmann et al. 2005; Capecchi et al. 2008; Huber et al. 2011) and across the savanna ecosystems of Africa (Fuller & Prince 1996; Chamaillé‐Jammes & Fritz 2009). The strong positive correlation is indicative of the way in which water/moisture status constrains vegetation activity in arid or semiarid savanna areas (Roerink et al. 2003). In more mesic savanna environments, on the other hand, the correlation is insignificant (Fuller & Prince 1996; Chamaillé‐Jammes & Fritz 2009).

As a result, attention has been paid to defining the rainfall threshold below which water is the major constraint on savanna vegetation dynamics. Some research suggests that this threshold exists and it relies on both yearly and monthly precipitation (Davenport & Nicholson 1993; Farrar et al. 1994). However, the threshold varies across different savanna ecosystems. For example, in East Africa, the significant correlation between savanna vegetation activity (NDVI) and rainfall occurs when rainfall is below 1000 mm/year and 200mm/month (Davenport & Nicholson 1993). In tropical southern

Africa, this threshold is about 600mm of rain per year (Fuller & Prince 1996). In semiarid Botswana, the threshold is 500mm of rain per year or a monthly rainfall not exceeding 50-100mm (Farrar et al. 1994). However, Santos & Negri (1997) suggested that the absence of simple linear correlation between NDVI and rainfall at wet regime was due to the saturation of the NDVI; an exponential correlation was observed when precipitation is above the threshold (Santos & Negri 1997).

However, more recent research suggests that the best correlation occurs between NDVI and lagged observation of precipitation (Musyimi, 2011), which is due to the temporal delay from the occurrence of rainfall to moisture that available to plant (Barbosa et al. 2011). The shift rate is controlled by both vegetation type and climate patterns (Zhang et al. 2005). For the vegetation type, different species were found to have various leaf flushing lags. Generally, trees show a longer growing season than grasses with early leaf flushing and late senescence (Higgins et al. 2011). Semi-deciduous trees flush earlier than fully deciduous trees and also last 1-2 months longer for senescence (Williams et al. 1997). For the climate factor, research suggests that a high accumulation of rainfall leads to shorter lag of vegetation (Klein & Roehrig 2006).

As the spatial resolution of polar orbiter satellite data used for these analyses varies from a pixel size of 250m (MODIS) to 1.1km (AVHRR), trees and grasses are usually mixed within a pixel and phenology of savanna is a combination of both trees and grasses. Thus, changes of lags observed in the NDVI time series are more strongly associated with major differences in ecosystems (and distinct canopy phenology) or climate regimes (Zhang et al. 2005), which leads to geographical variation in lag observations. For example, in Africa, Martiny et al. (2006) found that the shortest lag of

one month occurs in western Africa and extends to more than 1.5 months in southern Africa; the difference was attributed to the increased rainfall rate before full canopy flushing in west Africa. Nevertheless, other research in the Hwange National Park in Southern Africa suggests that the best rainfall-NDVI correlation was found with a lag of 1 month (Chamaille‐Jammes 2006). In the Sahel region of West Africa, the best correlation lag was 10-20 days (Justice & Dugdale 1991). An interannual effect observed during vegetation green-up was strongly associated with the peak value of the former year NDVI (Philippon et al. 2007).

This dependency of the green-up and senescence and leaf fall on seasonal and interannual variation in timing and intensity of rainfall observed in deciduous tropical savannas of Africa, suggests that separation of woody and herbaceous phenology and dynamics with time series and spectral methods may be difficult due to indistinct and inconsistent behavior of the layers between seasons and years.

5. Separating the Tree and Understory Dynamics

5.1 Retrieving Fractional Cover

As spatial and temporal distribution of abundance of woody and herbaceous vegetation are fundamental to many aspects of the biome such as risk of fire and human subsistence (Scanlon et al. 2002), some attempts have been made to decompose tree grass time series from observed NDVI time series and estimate fractional covers according to the vegetation dynamic corresponding to rainfall patterns. Scanlon et al. (2002) built a linear unmixing three–equation model to estimate the proportion of trees, grass and bare soil within each pixel. The first equation describes the three endmembers making up the overall land cover. The second equation defines the wet season observed NDVI (average

of NDVI from January to March) as the linear combination of the three endmembers weighted by their proportions. The last equation defines the sensitivity of the NDVI to rainfall, described by the ratio between the change in NDVI and the change in rainfall, as a linear combination of the weighted endmembers. The fractional tree cover suggested high positive (R^2=.87) correlation with the mean wet season precipitation. However, NDVI is not very sensitive to dry vegetation or bare soil, since the spectral region most sensitive to cellulose and soil is the high short wave infrared (SWIR ; > 2000nm wavelength).

Huang & Siegert (2006) run unsupervised ISODATA classification based on DEM (Digital Elevation Map) and NDVI images on time slices from the non-growing season, beginning of the season and peak growing season. The overall classification accuracy was 83%. Gessner et al. (2009) derived features including mean, median, min-max, range, standard deviation and sum for rainy, dry seasons and the entire year in Africa. Decision tree regression was used to calculate sub-pixel fractional cover of tree, grass and bare soil, and then validated by high spatial resolution data. The unmixing result suggests less than 0.1 root mean squared errors (RMSE). Guerschman et al. (2009) linearly unmixed savanna into photosynthetic vegetation, non-photosynthetic vegetation and bare soil using NDVI and the Cellulose Absorption Index (CAI) calculated from hyper-spectral images. The approach was then transferred into NDVI and short wave infrared ratio (SWIR32) space, so the MODIS data set is capable of producing dynamic fraction cover. The results were then validated by ten ground observation sites. The coefficient of determination (R^2) varied from 0.55 to 0.98 and the root mean square error (RMSE) varied from 0.05 to 0.54.

One essential element of this study is the effective retrieval of quantitative estimates of fractional cover of PV, NPV and BS across the three study regions. Since the method of Guerschman et al. (2009) is validated and has been used to create MODIS fractional cover products for Australia, this represents the best method to work with for this study, especially since its extension to South America and Africa does not depend upon a substantial ground network of validation sites, as have been applied to more recent refinements of the Australian fractional cover products (Guerschman & Scarth 2015).

5.2 Time Series Methods – Decomposing the Green Signal

After decades of studying dynamics of savanna using remote sensing, a range of methods have been developed and explored. This section reviews essential technologies that had been successfully used to characterize the time series data.

5.2.1 Noise Removal

Before any analysis is undertaken, noise must be removed or minimized, as observations are often contaminated by clouds or aerosols. A number of method are routinely used to correct and smooth the time series: Maximum Value Composition (MVC) (Du Plessis 1999; Musyimi 2011; Budde et al. 2004), Polynomial interpolation (Erasmi et al. 2006; Gaudart et al. 2009), Fourier functions (Wagenseil & Samimi 2006), Best Index Slope Extraction method (BISE) (Viovy et al. 1992; Du Plessis 1999; Lu et al. 2003), and least-squares regression (Bachoo & Archibald 2007; Erasmi et al. 2006). Pettorelli et al. (2005) reviewed time series smoothing methods, and listed some advantages and disadvantages of these methods:

- The MVC model is simple, but unable to remove irregular high values;

- The Polynomial Interpolation and Fourier functions are easy to implement but may lose too much information and the results may also be affected by outliers;
- The BISE is robust for false highs, but the algorithm is designed for high temporal resolution (some research, however, improved the algorithm and made it also suitable for 10-day data (Lovell & Graetz 2001));
- The Least-squares regression works well when outliers are rare, otherwise the result will also be affected.

Once the noise has been removed, two major types of methods were considered for this study: methods that decompose the signal into trends and dynamic components; and methods that decompose the signal into temporal components.

5.2.2 Fast Fourier Transform (FFT)

The harmonic analysis of time series (HANTS) (Menenti et al. 1991) algorithm has been used to remove noise (Jun et al. 2004), correlate with climate data (Lhermitte et al. 2008; Roerink et al. 2003; Bradley et al. 2011), and delineate phenology of vegetation (Leinenkugel et al. 2013). The first two harmonics are mostly used in phenology-related studies. The amplitude of the first harmonic indicates the dominance of evergreen, deciduous or annual habit, while the second harmonic indicates the mixture of two layer system (Moody & Johnson 2001). The phase of harmonic, on the other hand, suggests the timing of leaf-on.

5.2.3 Principal Component Analysis (PCA)

The PCA method converts time series data into linearly uncorrelated series by using orthogonal transformation. The transformed data associates with eigenvalues and higher eigenvalue suggests more information contained. The first component has the

highest eigenvalue and thus contains more of information than the second component etc. Studies suggest that the first component of PCA in savanna time series is associated with main patterns of vegetation types (Gurgel & Ferreira 2003). The second component reveals the seasonal variation of vegetation (Hirosawa et al. 1996), while the fourth component shows 'non-climatic' variation such as slash burning events (Gurgel & Ferreira 2003).

5.2.4 A Seasonal-Trend Decomposition Procedure Based on Loess (STL)

The STL method decomposes time series data into trend, seasonal and irregular components using local regression (LOESS), developed by Cleveland et al. (1990). The method is capable of rejecting noises due to clouds (Lu et al., 2003), separating the long term trend as well as seasonal variation. Jacquin et al. (2010) used STL for characterizing land cover trends and vegetation activity during the growing season. Lu et al. (2003) decomposed savanna tree and grass components from NDVI AVHRR time series based on the STL approach.

Since this method is proven in Australia, it logically becomes the decomposition methods to be applied in concert with the fractional cover retrieval in the Australian tropical savanna. However the predominantly deciduous woody vegetation in Africa means that a frequency decomposition approach will be required, thus the FFT was chosen to be used in comparison and/or combination with the Lu et al. (2003) method for the savannas outside Australia.

6. Study Regions

Three sites were studied (Figure 9): Australian Savanna, Cerrado of Brazil and Southern African savanna. These regions cover major continental savanna biomes with

similar latitude and coverage. However, each site samples different climate, soil type, and species. The variances lead to different vegetation structure and dynamics that produce diverse remote sensing measurements.

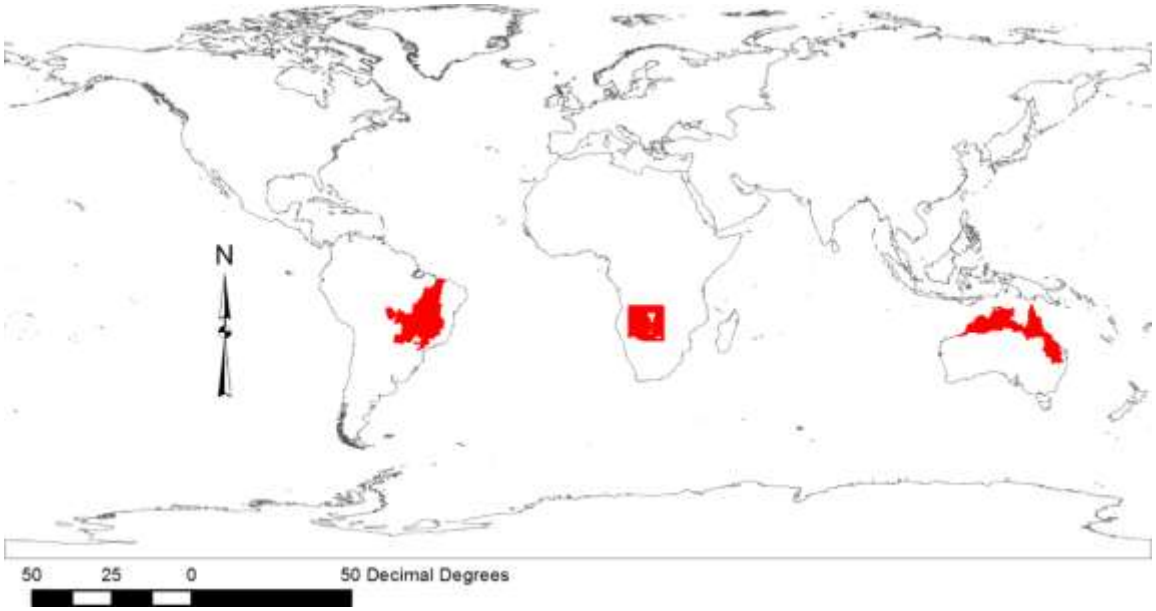

Figure 9. Savanna Study Regions

6.1 Australian Tropical Savanna

The Australian savanna study region is defined by the boundaries of the savanna ecoregions from the Terrestrial Ecoregions of the World (Figure 10) (Olson et al. 2001). The same ecoregions are used by Hill et al. (2012) to explore the dynamics of NDVI and SWIR32 indices across global savanna ecoregions. These ecoregions were selected as they capture the distinctive rainfall gradient (Figure 10) and a continuum of tree-grass composition that ranges from small areas of closed forest, occurring in the Cape York and Arnhem ecoregions, to mixed woodlands in the Einasleigh Upland and Brigalow ecoregions of Queensland, and to open woodland and sparsely treed or treeless grassland in the Kimberly Victoria Plains and Carpentaria ecoregions.

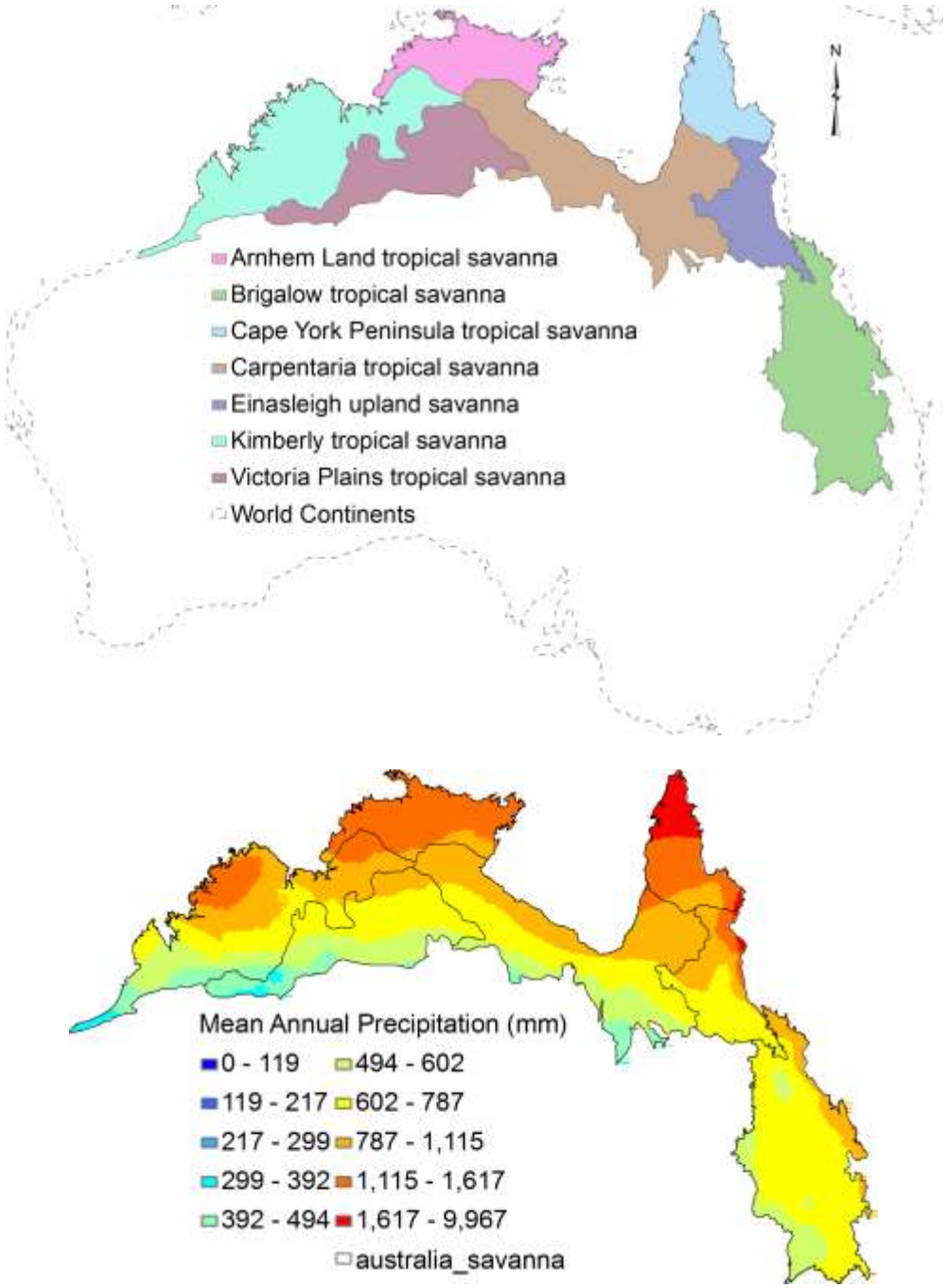

Figure 10. Australian Savanna Ecosystem defined by the Terrestrial Ecoregions of the World (Olson et al. 2001) and Mean annual precipitation (1950-2000) from WorldClim – Global Climate Data (Hijmans et al. 2005)

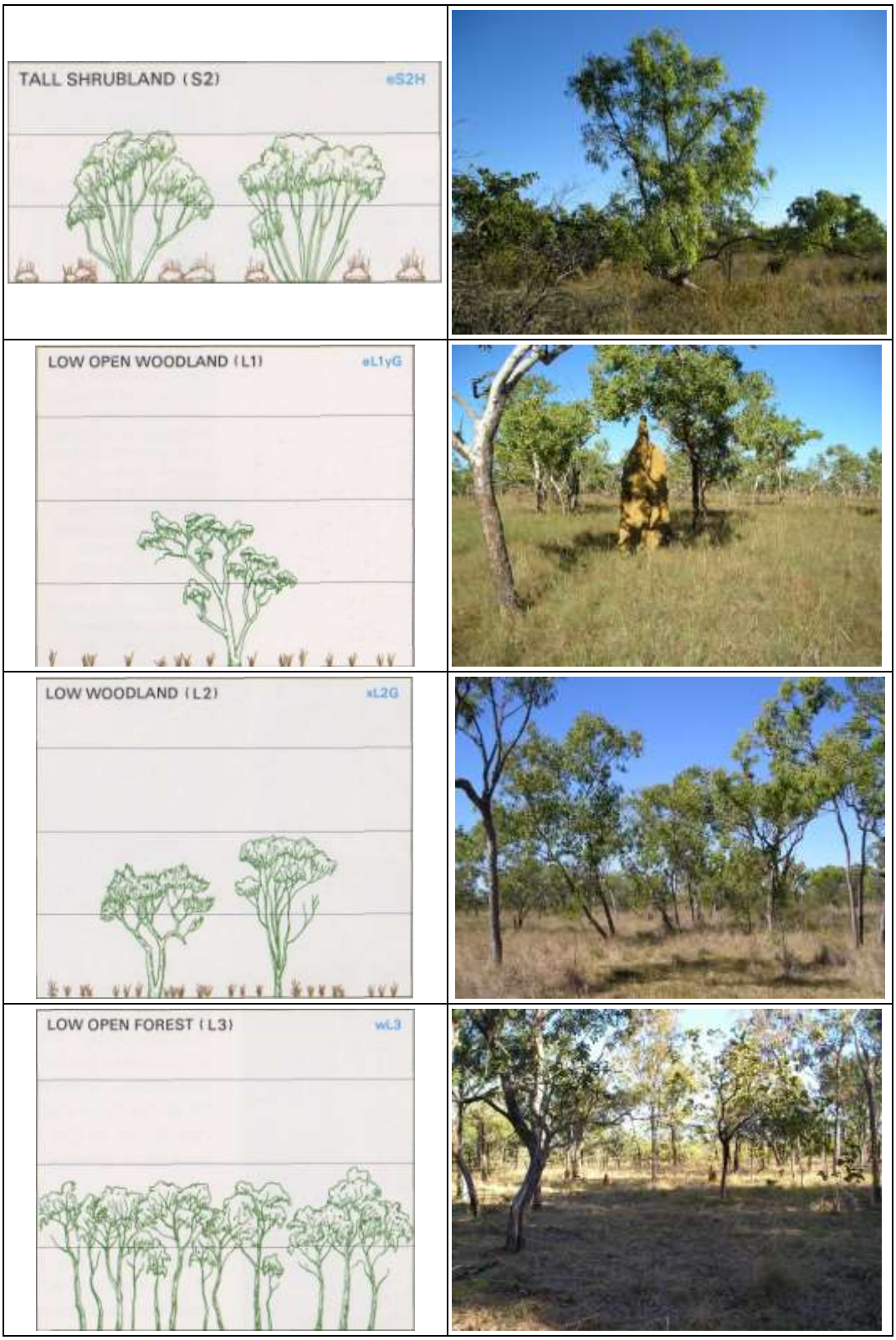

Figure 11. The structure of Australian vegetation and the phenological characteristics (Cartoon source: http://www.ga.gov.au/webtemp/image_cache/GA10362.pdf)

In the Australian tropical savanna, the understory and tree layer are distinctive in height and phenology (Figure 11). The understory is predominantly made up of tropical grasses but includes some palms (*Livistona* spp.) and cycads in the Arnhem and Cape York ecoregions (Olson et al. 2001; Tothill & Gillies 1992) (see table 1. Hill et al., 2012). The tree layer is predominantly *Eucalyptus* spp., interspersed with *Corymbia* spp. *Acacia* spp. are also widespread and *Melaleuca* spp. occur in groves on poorer soils and along water courses (Olson et al. 2001; Tothill & Gillies 1992) (see table 1. Hill et al., 2012). Among the trees and shrubs, there are equal numbers of evergreen, deciduous, semi-deciduous and brevi-deciduous species, however, the dominant species are evergreen, meaning that the tree canopy remains green throughout the year with some modest seasonal fluctuation (Eamus 1999; Williams et al. 1997; Lambin et al. 2003). For this study, we assume that the woody component is 90% evergreen with only small seasonal fluctuation in the green canopy due to natural aging and shedding of old leaves.

6.2 Brazilian Cerrado

The South American savanna study region (Cerrado) is defined by the Conservation and Sustainable Use of Brazilian Biological Diversity Project (PROBIO) (Figure 12). It covers approximately 2 million km^2 in central Brazil (Eiten 1972; Hill et al. 2011), however, it is highly fragmented by agricultural conversion, particularly to African grass pastures for livestock production. The total annual precipitation is between 800 and 2000 mm (Oliveira-Filho & Ratter 2002) (Figure 13), which is much wetter than the Australian savanna. The Cerrado region captures a continuum of tree-grass composition that ranges from grassland to dense woodland (Figure 14). With increasing density of woody species, the ecoregions are also classified into: *Campo limpo* (grassland

without shrubs and trees), *Campo sujo* (grassland with scattering shrubs and small trees), *Campo cerrado* (grassland with scattered shrubs and trees), *Campo sensu strico* (trees and shrubs dominated with more than 30% of crown cover), and *Cerradao* (woodland with crown cover of 50% to 90%) (Oliveira & Marquis 2002; Hill et al. 2011). Those types of physiognomic forms are mixed and intergraded with one another throughout the study region (Mistry 2000). The understory of the Cerrado is predominantly made up of perennial herbs with almost no annual herbs (Coutinho 1990). The woody layer can remain short in height for many years and many have relatively open crowns (Eiten 1994; Eiten 1982). Unlike the Australian savanna, Cerrado does not have a distinctive layer system or phenological difference between trees and grasses. In the Cerrado savanna, grassland is intermingled with palms, dicot, and short woodies. Moreover, due to the high elevation and relatively high annual rainfall, grassland may also retain part of green leaves in the dry season and intermingle with semi-deciduous woody plants.

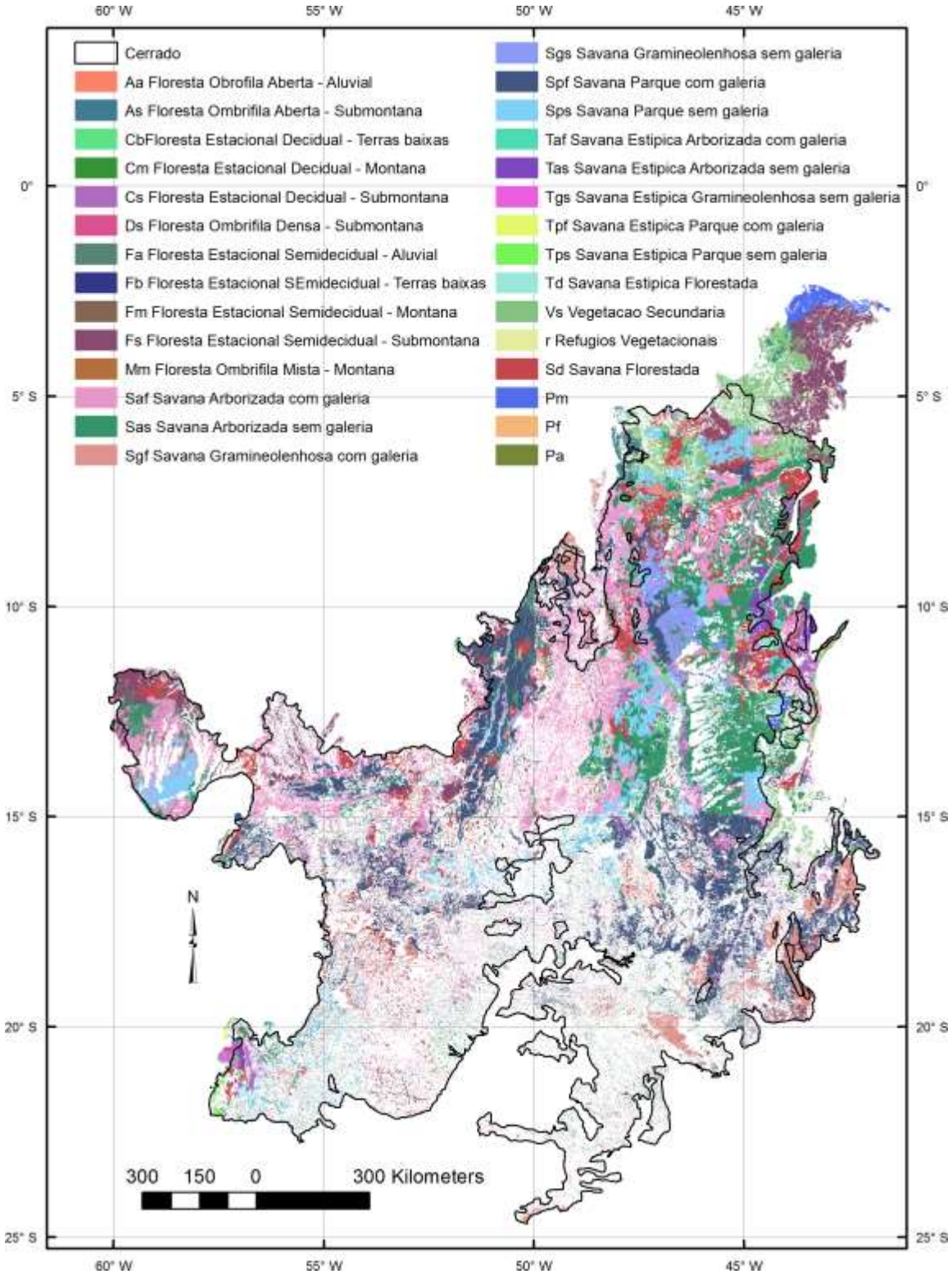

Figure 12. Cerrado Savanna Ecosystem defined by the Conservation and Sustainable Use of Brazilian Biological Diversity Project (PROBIO)

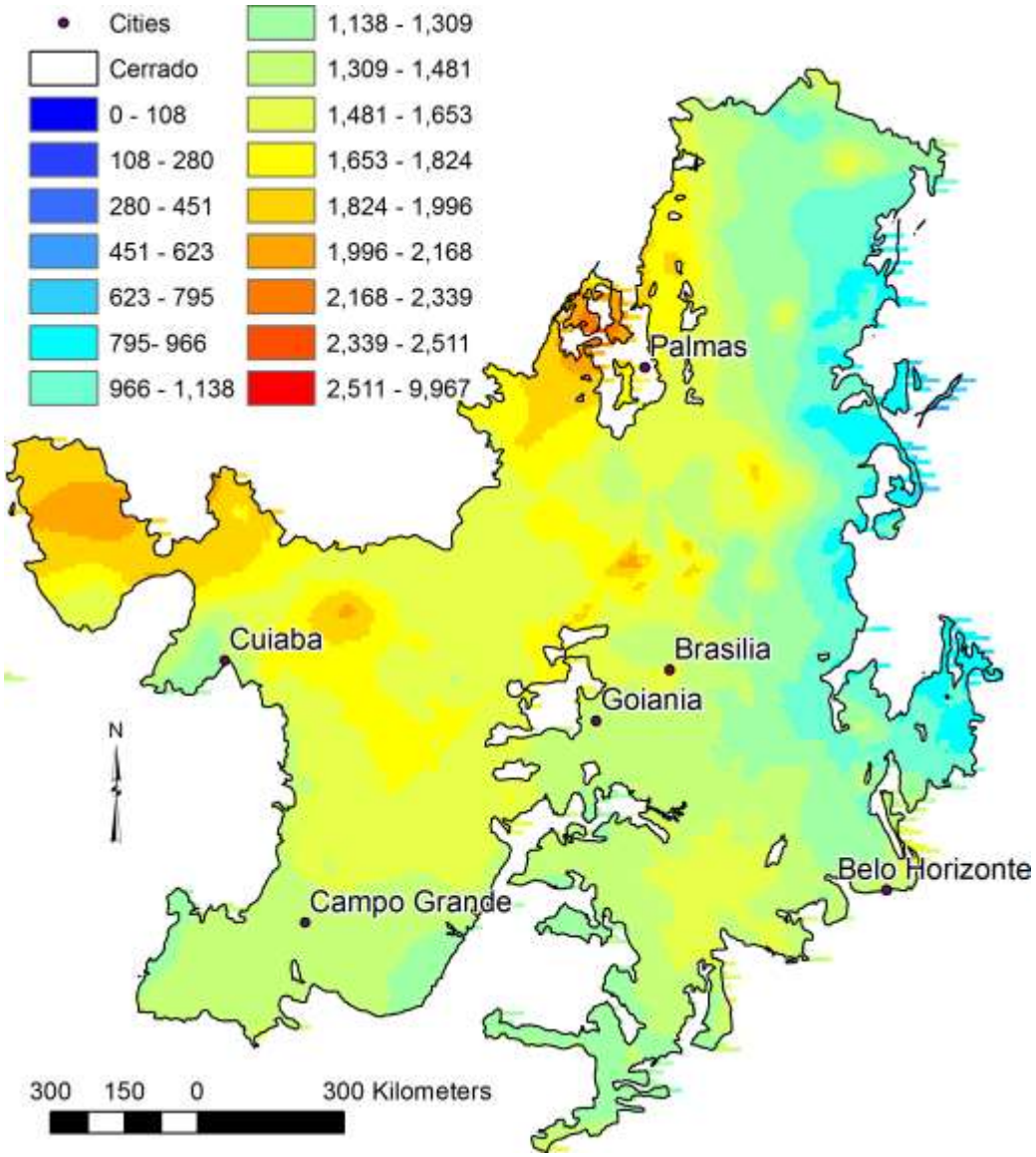

Figure 13 Mean annual precipitation (1950-2000) from WorldClim – Global Climate Data (Hijmans et al. 2005)

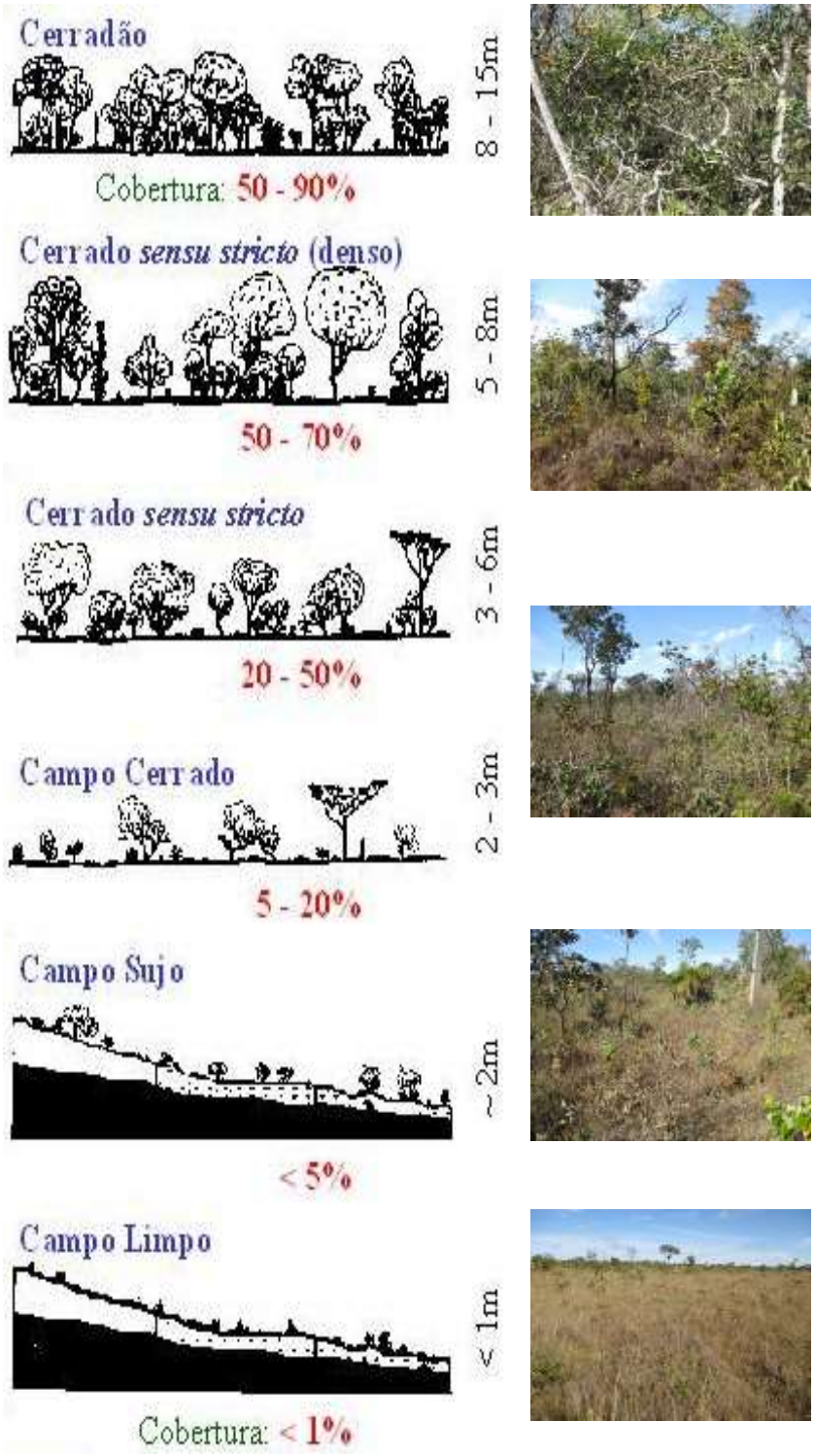

Figure 14. Cerrado Physiognomy (Ferreira et al. 2003)

6.3 Southern Africa

The African tropical savanna is very large. In order to explore the variation in a more manageable way, a study region in southern Africa that spanned the rainfall gradient and diversity of woody vegetation types was chosen. The Southern African savanna square (Figure 15) covers a continuum from dense woody area (Angolan Miombo Woodlands and Central Zambezian Miombo Woodlands) to mixed area (Angolan Mopane Woodlands, Zambezian Baikaiea Woodlands and Zambezian and Mopane Woodlands) and open area (Kalahari Acacia- Baikaiea Woodlands) (Figure 15 and Figure 16). Ecoregions that are excluded in the square include Etosha Pan halophytics, Western Zambezian grasslands, Zambezian Cryptosepalum dry forests, Zambezian flooded grasslands and Zambezian halophytics as defined by the Terrestrial Ecoregions of the World (Olson et al. 2001). Table 2 and Figure 17 show the climate condition of ecoregions. From north to the southeast, the vegetation shifts from woodlands and open deciduous forests to arid shrub land following precipitation gradients (Cowling et al. 2004).

6.4 Influence of Vegetation Structure on Analysis

Distinguishing tree and grass using remote sensing mainly depends on two components: the sensitivity of the vegetation index to spectral differences in trees and grasses and the differences in the shape of the time series curve of the vegetation index that can be decomposed into tree and grass components. The vegetation index describes the spectral characteristics of different vegetation types; however, vegetation structure alters remote sensing measurements. When vegetation is a simple two-layer system, the measurements could be considered as a linear combination of the two layers. By contrast, when trees and grasses are intermingled with each other, the spectrum is an output of

multi-reflection, which reduces the linear relationship. The time series of vegetation index describes the vegetation phenology.

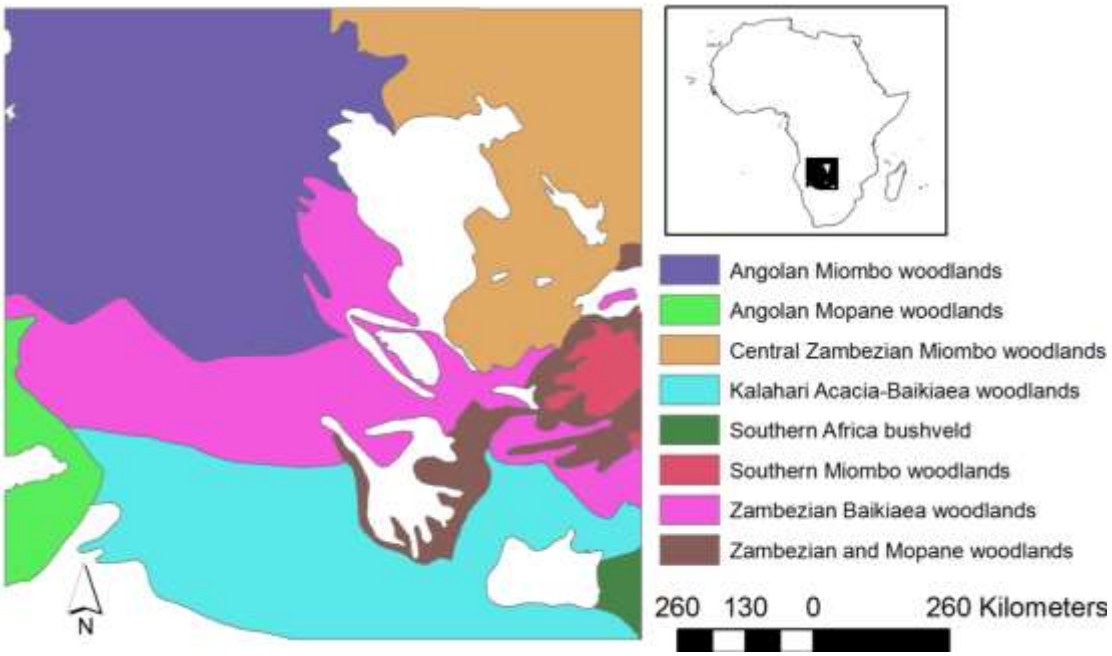

Figure 15 Southern African savanna Ecosystems defined by (David M. Olson et al. 2001)

Table 2. Rainfall pattern of the study area extracted from the World Wildlife Fund

Ecoregion	Rainfall (mm)	Rainfall Period
Angolan Miombo woodlands	less than 800 (south) - 1,400 (north) (Huntley 1974)	Highly concentrated in the summer months
Central Zamezian Miombo Woodlands	600-800	November - March
Angolan Mopane Woodlands	400-600	August and April
Zambezian and Mopane Woodlands	450-710 (Low 1996; WILD & Fernandes 1968; White 1983; Farrell 1968; Smith 1998)	November - April
Zambezian Baikiaea woodlands	400 (Southwest) to more than 600 (East)	November - April
Kalahari Acacia-Baikiaea Woodland	300 (Southwest) to 600 (North)	October -March
Southern African Bushveld	350- 750 (Nix 1983)	4 to 8 months of hot wet season with cool dry season for the rest of the year (M.M. 1986)

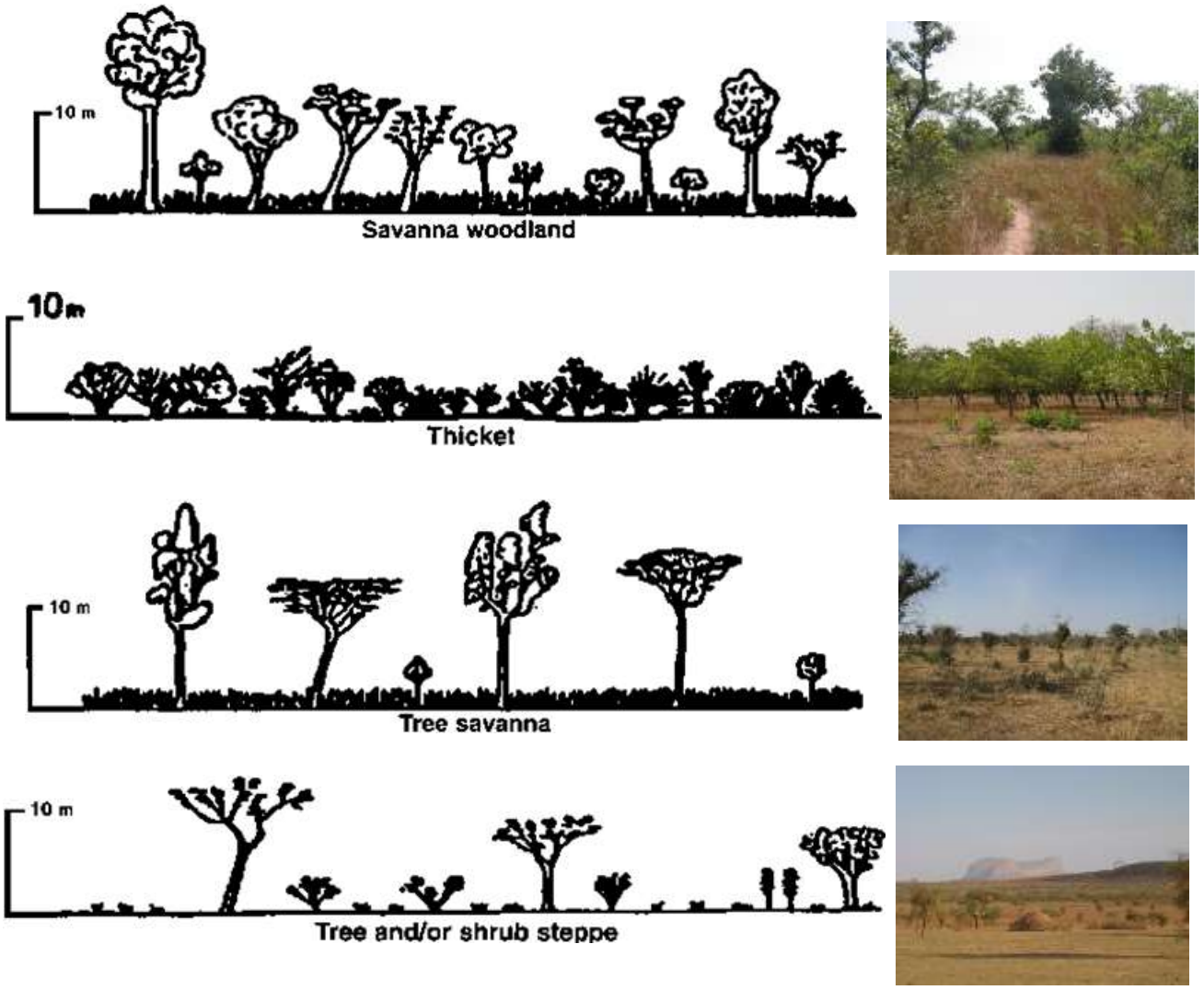

Figure 16. Southern Africa Physiognomy (Cartoon: Bellefontaine, 2000)

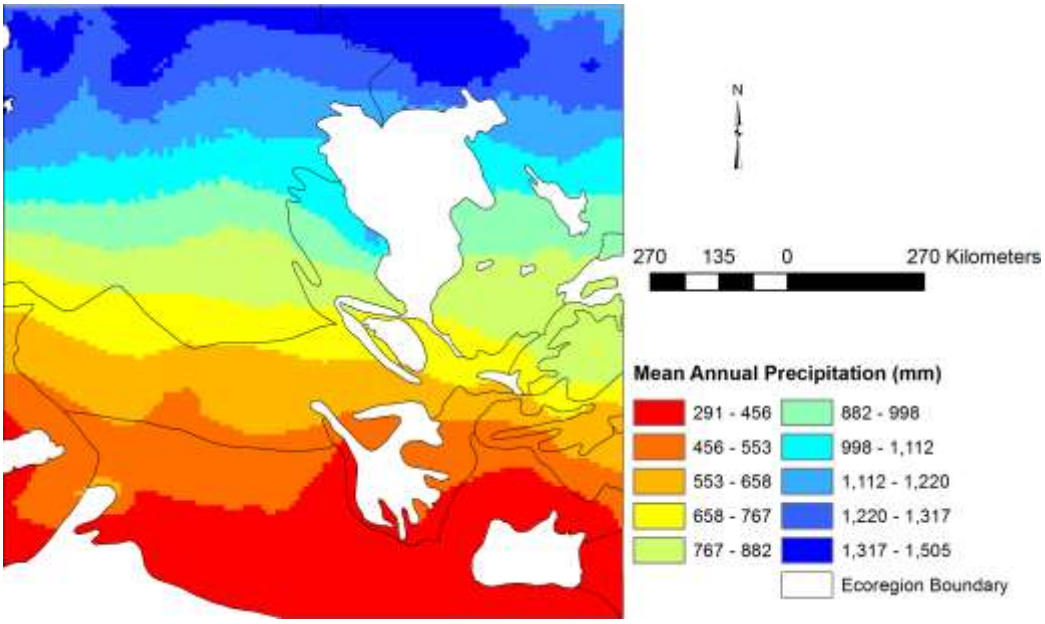

Figure 17. Mean annual precipitation (1950-2000) in the Africa savanna from WorldClim – Global Climate Data (Hijmans et al. 2005)

Table 3 shows the differences of vegetation structure and phenology of the three savanna regions. The Australian savanna shows a clear distinction between woody and herbaceous layers. The woody layer remains green through the whole year with some small seasonal flushing and leaf fall, while the herbaceous layer cures to a dry state almost completely in winter. In the Brazilian Cerrado, the vegetation structure is less distinctive. The land cover types vary from grassland to dense woodland, with a mixture of woody plants, shrubs, palms, dicots, and grass in most area. Moreover, part of grass remains green in winter due to the wet climate, and can be confuse with evergreen woody phenology and introduce higher uncertainty in discriminating less dense woody Cerrado such as *Campo Sujo* and *Campo Limpo*. For the southern African site, the two-layer system is prevalent, but canopy cover varies from broad leaf to fine leaf. The variation in degree of deciduousness mean that detecting differences in the timing of greenup (leaf flush) and senescence (leaf fall) between herbaceous and woody layers is required to separate the woody and herbaceous phenology.

Table 3. Vegetation comparison

Savanna Biome	Savanna structure	Trees	Mid-story (palms, dicots, shrubs)	Herbaceous	Fractional cover method	Green decomposition method
Northern Australia	Mostly two layers – trees and grasses. Occasionally with shrub, palm, dicot mid-story	Evergreen	Evergreen except Terminalia	Perennial grasses except in Arnhem and Carpenteria ecoregions where annuals also occurs	Proven	Proven
Cerrado of Brazil	Patchwork gradient between grassland and woodland with complex woody structure, and complex/diverse mid-story of palms, dicots and small woody plants	Brevi- to semi-deciduous	Evergreen	Perennial grass with cover inversely proportional to woody plant density	Untested	Untested. Potentially requiring adjustment or new method
Southern Africa	Diverse gradient of different species associations varying from broadleaf to fine leafed. Woody cover declines and bare soil increases down steep rainfall gradient	Variably deciduous and highly sensitive to rainfall seasonality and intensity	Highly variable between vegetation associations. Shrubs in more arid areas	Perennial grasses with sparse, patch cover and tussock structure dependent upon soil types and hydrology	Untested	Potentially inappropriate. Method that deals with lack of persistent woody canopies needed

7. Methods

This study depends upon two fundamental assumptions:

1) That a tropical savanna and therefore each MODIS pixel consist of three cover fractions, *f*PV, *f*NPV, and *f*BS. It is essential in the first instance to retrieve a measure of these cover fractions.

2) That the green photosynthetic cover made up of tree canopy, mid-story canopy and grass canopy can be decomposed into

i) Either a persistent component and an seasonal component that represent the evergreen tree canopy and the seasonally green herbaceous material; or

ii) Two or more seasonally green photosynthetic components that are separated in time by different lagged responses to the seasonal rainfall associated with contrasting tree and grass physiology.

Moreover, the study assumes that the PV fraction derived in assumption 1) is made up of green woody (fPV_{woody}) and green herbaceous ($fPV_{herbaceous}$) cover that can be separated by the methods applied in assumption 2).

Clearly, this is a simplification of reality, especially when considering the continuously variable Cerrado and the deciduous African savanna. However, two critical previous studies undertaken in Australia have demonstrated that both the unmixing of fractional cover, and the decomposition of the green NDVI signal are effective in the Australian savanna with evergreen trees (Guerschman et al. 2009; Lu et al. 2003).

It was therefore logical to integrate the two proven methods for the Australian

tropical savanna. However, the applicability of methods and the availability of alternative methods had to be addressed for the South American and southern African savannas. A biome-scale examination of the NDVI-SWIR32 response envelope for all savanna ecoregions in Australia, South America and Africa showed that mean vegetation responses for a number of African and South American ecoregions were not contained inside the end-member response envelope defined for Australia (Hill et al. 2012). Hence, three key analytical steps were required in order to develop, demonstrate and validate methodologies that would be applicable to the three savanna biomes.

a) For each savanna biome the definition of the NDVI-SWIR32 response envelope had to be based on a suite of hyperspectral images that sampled geographical variation and seasonal periods.

b) Deviation of savanna structure and phenology for South America and southern Africa from the assumption of evergreen behavior by woody canopies applicable in Australia made it necessary to test the effectiveness of the time series decomposition method (Lu et al., 2003) and explore methods that incorporated frequency decomposition to deal with semi-deciduous and deciduous woody vegetation and attempt to separate layers based on differences in onset of green-up and senescence/leaf fall.

c) Both fractional cover and woody and herbaceous fraction derived from the analysis are validated against available ground data and available high resolution satellite imagery in order to best define accuracy and error attributable to scale-based issues associated with 500-m MODIS pixels and heterogeneous vegetation targets.,

7.1 Unmixing PV, NPV, and BS fractions

The unmixing model was first established by Nagler et al. (2003) who estimated fractional cover of PV, NPV, and BS by plotting the complementary indices NDVI measuring photosynthetic activities and CAI measuring cellulous of dry vegetation (Figure 18). The land cover plotted forms a triangle in the NDVI-CAI space (Figure 18). The pure PV, NPV, and BS are located at the vertices of the triangle, and mixture of the three endmembers in the triangle can be linearly unmixed. Guerschman et al. (2009) systematically investigated correlation between MODIS bands combination and CAI, and concluded the SWIR32 was the best substitute to CAI in the Australian savanna. The SWIR32, however, measures bare soil and is less sensitive to the difference between BS and NPV, so the new triangle is "flat" and flipped at the NPV and BS end. In the new triangle, green vegetation has highest NDVI and lowest SWIR32; bare soil has highest SWIR32 and lowest NDVI; and dry vegetation has moderate NDVI and SWIR32 (Guerschman et al. 2009; Hill et al. 2012).

If the position of pure land cover types (end members) are known, fractional cover can be solved within the response envelope. In savannas, MODIS pixels are rarely pure especially for NPV and BS. Therefore, endmembers will be extracted at finer resolution images. In this study, Hyperion images, from different vegetation types and seasons, are used to estimate the endmember distribution. The Hyperion imagery was spectrally resampled to MODIS bands using:

$$\boldsymbol{R_w} = \frac{\sum_i \boldsymbol{R_i} \times \boldsymbol{f_i}}{\sum_i \boldsymbol{f_i}} \qquad \textit{Equation 1}$$

Where R_w is the reflectance of simulated MODIS band, R_i is Hyperion reflectance at selected bands and f_i is the spectral response function at the corresponding Hyperion band. The spectral response functions were acquired from OceanColor, NASA. Then NDVI and SWIR32 were calculated using the simulated bands (Guerschman et al. 2009).

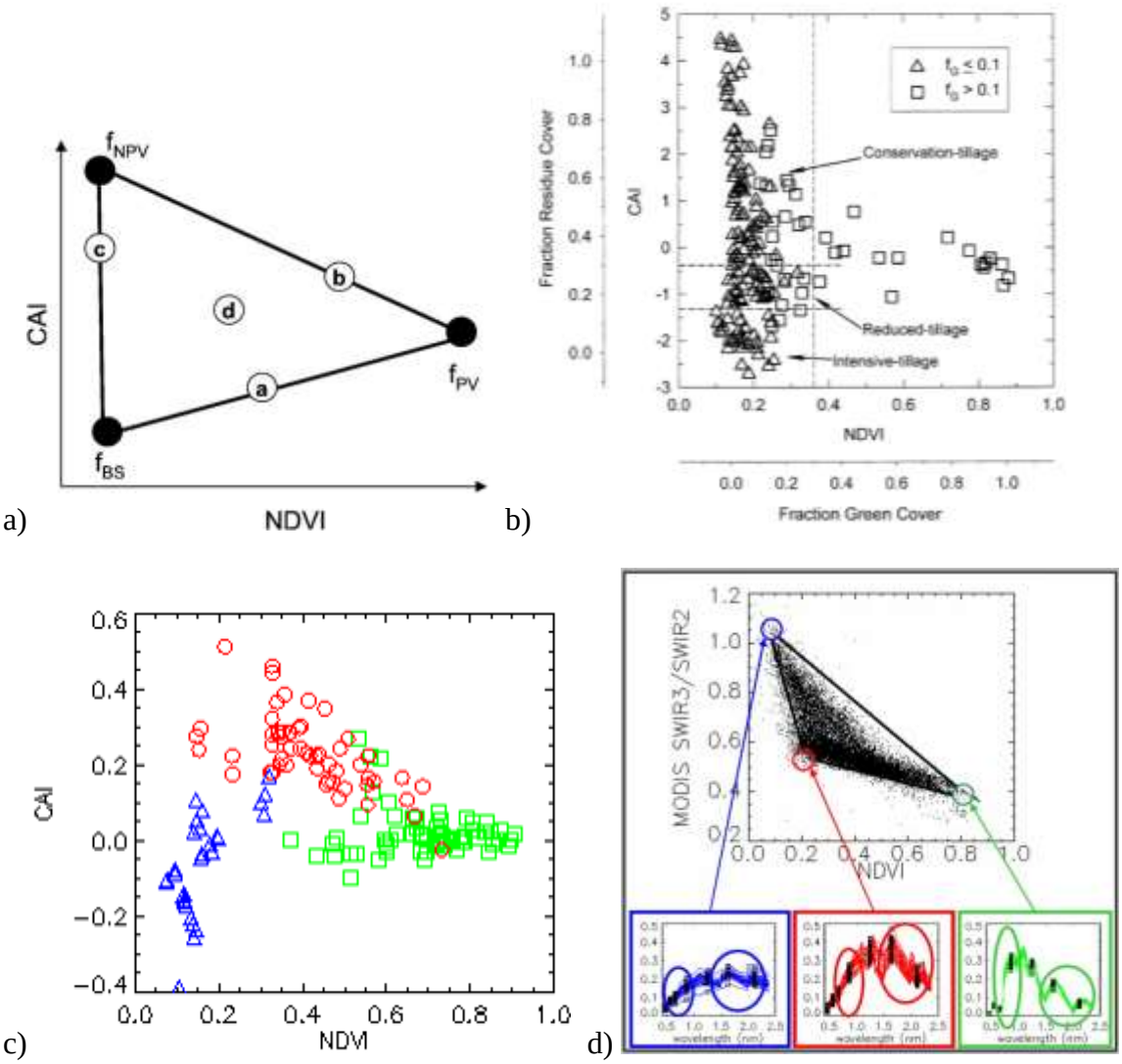

Figure 18. a) Conceptual response envelope for the NDVI-CAI response. b) Example of the NDVI-CAI response for cropland residue cover (from Daughtry et al., 2004). c) Equivalent NDVI-CAI response envelope for Australian tropical savanna and d) MODIS-based NDVI-SWIR32 response envelope that acts as a surrogate approach for unmixing fractional cover (from Guerschman et al., 2009).

The endmembers were extracted by carrying out the following processes in NDVI and SWIR32 space:

1) A two dimensional frequency plot of NDVI and SWIR32 was constructed with pixel number as the z value, and 0.01 units as the bin interval for the resulting response grid (Figure 19 a).

2) A threshold pixel count below which data can be considered as outliers was defined by trial and error iterative reference to images; pixel values with counts below this threshold were set to zero creating a masked two dimensional grid plot of valid pixels (Figure 19 b).

3) The end member pixels were selected as maximum NDVI for pure PV and maximum SWIR32 for pure BS respectively.

4) A Euclidean distance grid from the origin (NDVI = SWIR32 = 0) was calculated for each grid cell of valid pixels (Figure 19 c).

5) The endmember for NPV was estimated as the value within the grid cell that has the minimum distance to the origin:

$$End\ Member_{NPV} = \min_{i=1\ldots G} D = min\sqrt{(NDVI)^2 + (SWIR32)^2} \qquad Equation\ 2$$

where G is the number of valid pixel grid cells in the two dimensional plot; D is the distance to each grid cell in the plot. End-members were validated for correspondence to valid land cover types in selected images by exploring the precise locations in Google Earth.

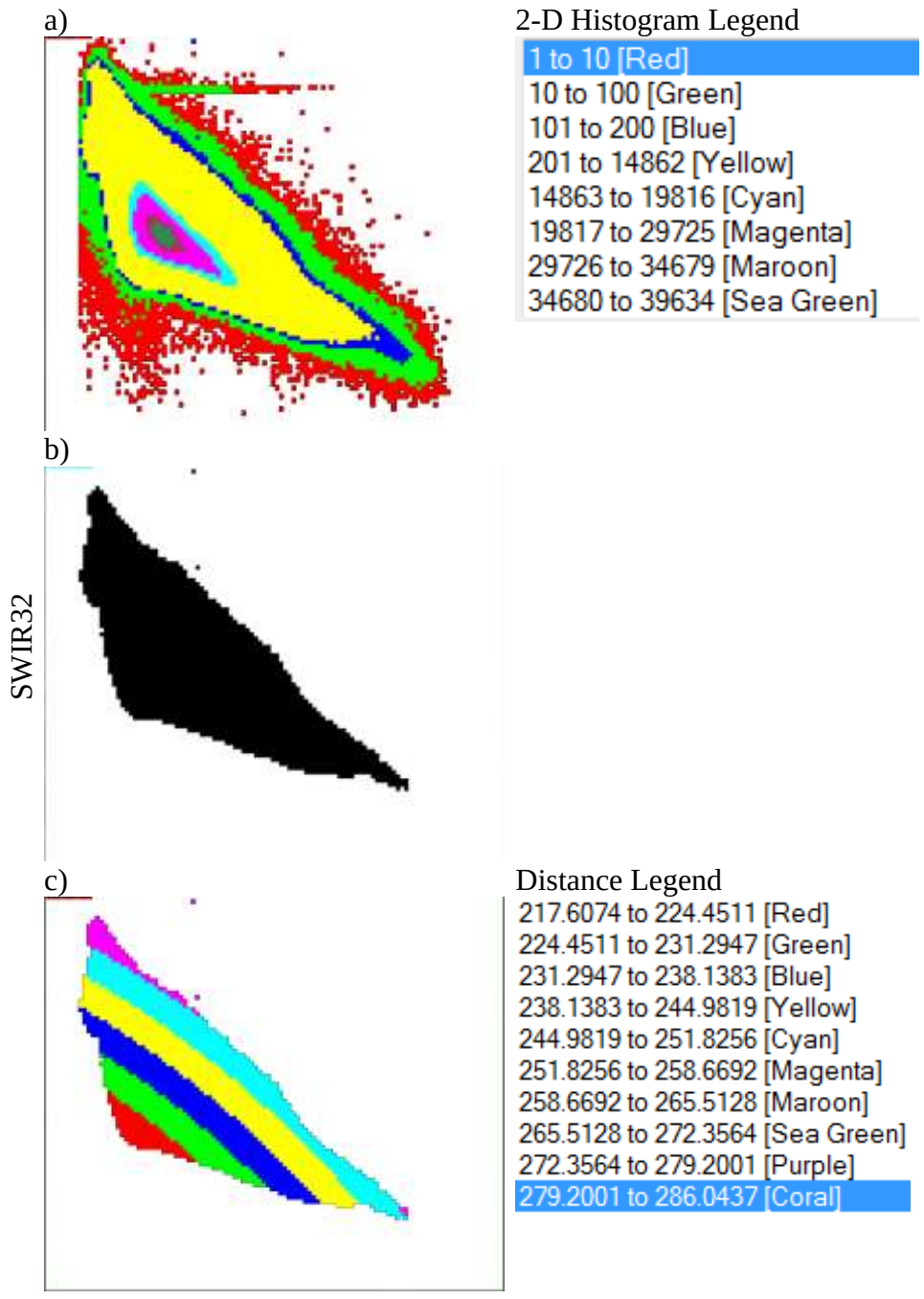

Figure 19. Schematic illustrating the flow for determine the end-member in NDVI-SWIR32 space

Guerschman et al. (2009) used a multiple regression model to convert end member values for CAI (cellulose absorption index) derived from Hyperion to end member values for SWIR32 from MODIS. In this study, we derive end-members for

NDVI and SWIR32 directly from Hyperion imagery. The final end members derived from the combined temporal and geographical coverage are then used directly for MODIS. This meant that end-members derived from this method expanded the response envelope in terms of the upper and lower limits of NDVI and SWIR32 relative to that defined by Guerschman et al. (2009). The fractional covers of PV, NPV, and BS were found by solving the equation:

$$V = f_{PV}V_{PV} + f_{NPV}V_{NPV} + f_{BS}V_{BS} \qquad \textit{Equation } 3$$

$$S = f_{PV}S_{PV} + f_{NPV}S_{NPV} + f_{BS}S_{BS} \qquad \textit{Equation } 4$$

$$f_{PV} + f_{NPV} + f_{BS} = 1 \qquad \textit{Equation } 5$$

where V and S are the NDVI and SWIR32 values in a given pixel, fPV, fNPV, and fBS are the fractions of PV, NPV, and BS and Vpv/Spv, Vnpv/Snpv, and Vbs/Sbs are the NDVI/SWIR32 values of the end-members. For the pixels that fall outside of the response envelope that gives values lower than -0.2 or higher than 1.2 (Guerschman et al. 2009), the negative outliers are set to 0 and positive outliers to 1, while the rest of the fractions are rescaled to sum to 1.0 (Guerschman et al. 2009).

7.2 Time Series Decomposition: Evergreen woody and seasonal herbaceous fractions

The analysis assumes that woody vegetation retains most of its leaf canopy and sheds only a limited percentage of leaves in the dry season, while herbaceous vegetation completely dries out every year. In the current study, this method is used at the Australian site and tested for effectiveness at the South American site where semi-deciduous woody plants are predominant. The decomposition proceeds as follows (Lu et al. 2003):

1) The NDVI is decomposed using Seasonal-Trend decomposition based on the LOESS (STL) method (Cleveland et al. 1990). The decomposition includes three components: seasonal signal, long-term trend, and remainder.

2) The seasonal component is adjusted to rescue vegetation information from the remainder. The procedure is based on the assumption that the remainder contains mainly two parts: irregular noises caused by atmospheric absorption and vegetation information that is due to climate condition (mostly by rainfall). The difference of the two types is that atmospheric absorption only reduces signals, while rainfall usually accelerates growth. Therefore, all positive remainders are added to the seasonal component, and negative remainders are rejected as noise.

3) The maximum and minimum of the adjusted seasonal component are then estimated using a recursive filter. As total herbaceous vegetation dries out in winter, only trees contribute to NDVI. The minimum adjusted seasonal component is considered the slow varied baseline that responds to inter-annual climate changes.

4) Based on the maximum and minimum, the adjusted seasonal component is then rescaled into a range between zero and one. This is the shape factor.

5) Tree signal is the minimum adjusted seasonal component with 10 percent of the shape factor. The remains of the adjusted seasonal component are the seasonal vegetation signal.

7.3 Frequency Decomposition: Seasonal woody and seasonal herbaceous fractions

However, the assumption of a savanna composed only of evergreen woody and seasonal green herbaceous is not always applicable, especially for the African savanna where deciduous woody vegetation predominates in most ecoregions. Therefore, a new method is developed in this study to separate woody and herbaceous vegetation based on

the different senescence phase. The algorithm is the extension of the Fourier Transform. The Fourier transform assumes that time series variation can be separated into a linear combination of sines and cosines; here it is assumed that the time series *f*PV(t) is the linear combination of woody and herbaceous variation only. Another important assumption is that major phenology differences occur between semi-deciduous woody, deciduous woody and herbaceous vegetation, instead of variation due to rainfall pattern. The advantages of linear regression in frequency domain are: (1) avoiding error introduced by the autocorrelation of time series data as mentioned by Musyimi (2011); (2) capturing phenology differences of woody and herbaceous vegetation, and removing high frequency variation due to discrete precipitation events; (3) not only fitting the amplitude of phenology variation but also the phase, which could reduce errors due to the shift of vegetation growing status responding to diverse rainfall patterns.

This algorithm adopts the hypothesis that the evergreen woody vegetation (including semi-deciduous woody) contributes to the long term active photosynthetic wave, while deciduous woody and herbaceous only contains seasonal variation (Lu et al. 2003), so that

$$NDVI_{semi-deciduous}(t) = L(t) + S_{semi-deciduous}(t) \quad \textit{Equation 6}$$

$$NDVI_{deciduous}(t) = S_{deciduous}(t) \quad \textit{Equation 7}$$

$$NDVI_{herbaceous}(t) = S_{herbaceous}(t) \quad \textit{Equation 8}$$

where Evergreen(t), Deciduous(t), Herbaceous(t), are NDVI time series of evergreen woody, deciduous woody, herbaceous, while $S_{semi\text{-}deciduous}(t)$,$S_{deciduous}(t)$, $S_{herbaceous}(t)$ and L(t) represent evergreen woody seasonal variation, deciduous woody seasonal variation, herbaceous seasonal variation and the long term variation.

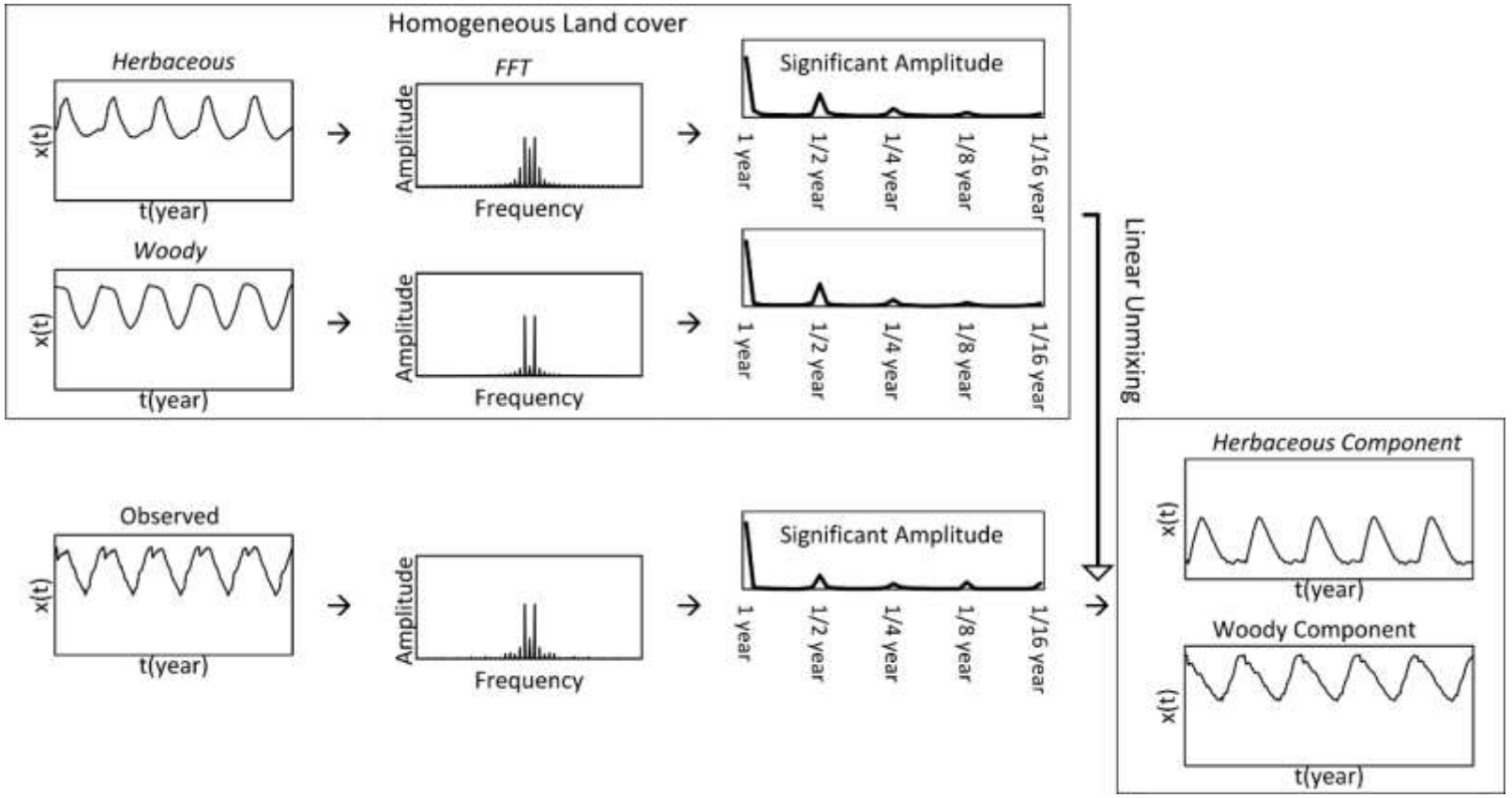

Figure 20. Schematic demonstrating the flow for estimating the partition of woody and herbaceous cover based on the time series f-PV(t).

The seasonal-trend decomposition based on LOESS (STL) is able to generate three components: long-term variation (L(t)), seasonal variation and remainder. The seasonal variation is further adjusted by including positive remainders into the seasonal variation, as the positive remainders may indicate the vegetation response to rainfall (Lu et al. 2003). The adjusted seasonal variation is rescaled into an annual range from 0 to 1 aiming to remove the effect of yearly difference:

$$S^s(t) = \frac{S(t) - S_{min}(t)}{S_{max}(t) - S_{min}(t)} \qquad \textit{Equation 9}$$

where S(t) is the adjusted seasonal variation, Smin(t) and Smax(t) are linear interpolated yearly minimum and maximum. Then the rescaled woody and herbaceous variations are determined by solving equation (4) in the frequency domain.

$$S^s = aS^s_{semi-deciduous} + bS^s_{deciduous} + cS^s_{herbaceous} + \varepsilon \qquad \textit{Equation 10}$$

where S^s , $S^s_{semi-deciduous}$, $S^s_{deciduous}$ and $S^s_{herbaceous}$ are complex vectors that denote the NDVI seasonal variation overall in a given pixel, pure semi-deciduous woody, pure deciduous woody and pure herbaceous in the frequency domain. In order to represent the general phenology feature of vegetation, only low frequencies (from yearly to monthly) are selected in the regression, which aims to capture phenology changes and reject high frequency variation due to individual rainfall events or atmosphere contamination. We assume that the remaining high frequency signals are formed by vegetation types weighted by their proportions. The coefficients a, b and c indicate the proportion of the corresponding vegetation types in the seasonal variation. The product of coefficients and the pure pixel frequency represents the estimated seasonal variation of the corresponding phenology. If the estimated phenology shifts more than one month

away from the overall seasonal variation, the coefficient will be marked as outlier and set to zero. For the remaining vegetation types, high frequency signals were restored according to the amplitude of coefficients.

$$S_{semi-deciduous} = aS^{s}_{semi-deciduous} + \frac{abs(a)}{abs(a)+abs(b)+abs(c)} S^{s}_{r} \quad \textit{Equation11}$$

$$S_{deciduous} = bS^{s}_{deciduous} + \frac{abs(b)}{abs(a)+abs(b)+abs(c)} S^{s}_{r} \quad \textit{Equation 12}$$

$$S_{herbaceous} = bS^{s}_{herbaceous} + \frac{abs(c)}{abs(a)+abs(b)+abs(c)} S^{s}_{r} \quad \textit{Equation 13}$$

where S^{s}_{r} is the remaining high frequency signals of the given pixel, and abs is the amplitude of the complex number. The seasonal variation is then restored to the original scale at the time domain, and the long-term variation is added to the evergreen woody proportion:

$$f_{semi-deciduous}(t) = S_{semi-deciduous}(t) \times \left(S_{max}(t) - S_{min}(t)\right) + S_{min}(t) + L(t) \quad \textit{Equation 14}$$

$$f_{deciduous}(t) = S_{deciduous}(t) \times \left(S_{max}(t) - S_{min}(t)\right) \quad \textit{Equation 15}$$

$$f_{herbaceous}(t) = S_{herbaceous}(t) \times \left(S_{max}(t) - S_{min}(t)\right) \quad \textit{Equation 16}$$

where $f_{\text{semi-deciduous}}(t)$, $f_{\text{deciduous}}(t)$ and $f_{\text{herbaceous}}(t)$ are the fractional cover of vegetation types in time domain. At last the vegetation types are normalized to the sum equal to the overall time series for the consistency.

7.4 Matching Methods and Tropical Savanna Systems

In the following chapters, the *f*PV, *f*NPV, *f*BS will be calculated in each savanna system using the method developed by Guerschman et al. (2009; see section 7.1). The triangle end-members will be adjusted for each savanna system. Fractional cover retrievals will be validated by comparison with field observation and high-resolution

satellite data, and any errors or biases will be reported and examined.

The Lu et al. (2003) method will be applied in Australia to retrieve separate herbaceous and woody phenology from *f*PV (see section 7.2). This method will be explored in South America, while a new frequency decomposition method will also be tested. The frequency decomposition method will be used as the main approach in the southern African savanna to separate deciduous tree canopy and herbaceous phenology based on differences in lag responses to climate (see section 7.3).

Finally, the NDVI-SWIR32 response envelope, validation accuracy of the methods, and estimation of *f*PV, *f*NPV, *f*BS, fPV_{woody} and $fPV_{herbaceous}$ will be compared across the three biomes. The dynamics of the vegetation associated with latitude and rainfall will be compared.

CHAPTER 2 AUSTRALIA

1. Introduction

This chapter seeks to integrate the fractional cover (Guerschman et al. 2009) and greenness decomposition (Lu et al. 2003) approaches to define distinct and separate temporal dynamics for the tree canopy and the herbaceous cover using the Australian tropical savanna with its predominantly evergreen woody vegetation as the initial proving ground. The development of advanced approaches in Australia to decomposing NDVI time series (Roderick et al. 1999; Lu et al. 2003; Guerschman et al. 2009; Scarth et al. 2010; Armston et al. 2011; Muir et al. 2011) that could aid with calibration and validation made the Australian savanna a perfect laboratory for initial exploration of methods.

2. The tropical savanna zone

The Australian savanna study region is defined by the boundaries of the savanna ecoregions from the Terrestrial Ecoregions of the World (Olson et al. 2001): the same ecoregions used by Hill et al. (2012) to explore the dynamics of NDVI and SWIR 32 indices across global savanna ecoregions. These ecoregions were selected as they capture a continuum of tree-grass composition that ranges from small areas of closed forest that occur in the Cape York and Arnhem ecoregions, through mixed woodlands in the Einasleigh Upland and Brigalow ecoregions of Queensland to open woodland and sparsely treed or treeless grassland in the Kimberly, Victoria Plains and Carpentaria ecoregions (Figure 21a). The distribution of forest type and understory is shown in Figure 21 b and c respectively.

In the Australian tropical savanna, the understory is predominantly made up of tropical grasses but includes some palms (*Livistona* spp.) and cycads in the Arnhem and Cape York ecoregions (Olson et al. 2001; Tothill & Gillies, 1992; see table 1. Hill et al. 2012). The tree layer is predominantly *Eucalyptus* spp. interspersed with *Corymbia* spp. *Acacia* spp. are also widespread and *Melaleuca* spp. occur in groves on poorer soils and along water courses (Olson et al. 2001; Tothill & Gillies, 1992; see table 1. Hill et al., 2012). Among the trees and shrubs, there are equal numbers of evergreen, deciduous, semi-deciduous and brevi-deciduous species, however, the dominant species are evergreen, meaning that the tree canopy remains green throughout the year with some modest seasonal fluctuation (Eamus 1999; Williams et al. 1997; Lambin et al. 2003). For this chapter, we assume that the woody component is 90% evergreen with only small seasonal fluctuation in the green canopy due to natural aging and shedding of old leaves.

3. Conceptual Model

The conceptual basis for this chapter is as follows:

1. Savannas consist of up to three vegetation layers with potentially differing canopy phenology: an overstorey woody layer (trees); a mid-story woody layer (shrubs: not always present); and an understory herbaceous layer (grasses, herbs and forbs). In Australia, the woody layers have predominantly evergreen canopies while the herbaceous layers are seasonally green varying from a green understory layer to a completely senescent brown one, following rainfall patterns. Although trunks and branches are also part of the non-photosynthetic component, we assume these are of negligible influence in the Australian savanna where woody plant densities are predominantly low and the main reflectance signal at nadir is provided by the green canopy.

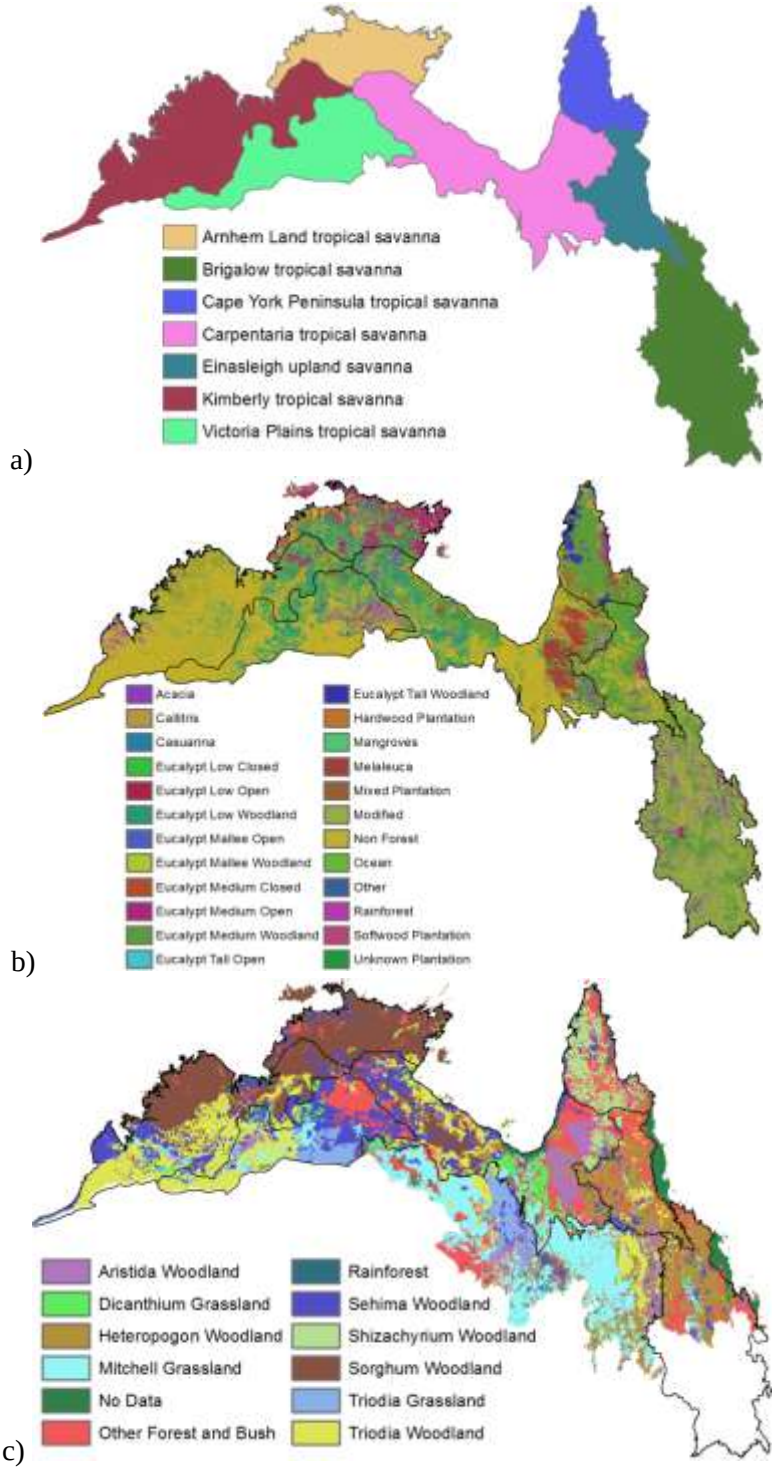

Figure 21. a) Australian Savanna Ecosystems defined by (Olson et al. 2001). b) The National Forest Inventory – Australia (Lymburner et al. 2011). c) Understory Map.

2. For the Australian tropical savanna, it is, therefore, assumed that each MODIS pixel will be a mixture of three cover fractions that sum to unity: photosynthetic

vegetation (PV), non-photosynthetic vegetation (NPV) and bare soil (BS). The PV fraction can be further separated into green tree canopy and green grass/understory cover.

3. NDVI time series track the dynamics of the green canopy (photosynthetically active) part of the woody overstorey and the midstorey layer, and the herbaceous understory layer. Time series decomposition methods such as those of Lu et al. (2003) have frequently been applied to the NDVI to attempt to separate the phenology of the woody layers from the herbaceous layer. Since the green cover signal detected by the sensor is made up of a predominantly evergreen tree canopy and highly seasonal understory green canopy, it is assumed that a time series of NDVI can be decomposed into a persistent and seasonal green signal using the method of Lu et al. (2003).

4. The response space between the NDVI and the SWIR32 can be unmixed to derive fractional cover of PV, NPV and BS (Guerschman et al. 2009). The SWIR32 vegetation index exhibits its highest values with high bare soil cover fractions these values decrease as the fraction of NPV increase and reaches their lowest values when PV cover is maximal (Guerschman et al. 2009; Hill et al. 2012). In savannas, MODIS pixels are never pure in terms of NPV and BS, and rarely pure in terms of PV (combined tree and herbaceous canopy). Therefore, end members will be derived from the response space between NDVI and SWIR32 at Hyperion pixel scale and these will be applied to MODIS unmixing.

5. The PV fraction derived from unmixing (*f*PV) can be considered to be equivalent to the combined woody and herbaceous PV obtained from the decomposition

of NDVI time series (fPV_{woody} and $fPV_{herbaceous}$). The NPV fraction from unmixing can be regarded as representing the senescent component of the herbaceous layer (fNPV).

6. Therefore, the woody fraction can be calculated from the ratio of fPV_{woody} and fPV (described in section 5.6). The herbaceous fraction can also be calculated from the ratio of $fPV_{herbaceous}$ and fPV, and by adding in the fNPV to integrate the herbaceous senescence cycle (described in section 5.6).

4. Data

4.1 Satellite data

4.1.1 MODIS NBAR Data

A 10 year time series (2002-2011) of the MODIS 8-day 500-m nadir BRDF-adjusted reflectance product (MCD43B4) (Schaaf et al. 2002) provided the high quality data for the time series decomposition and unmixing analysis. The MODIS data were masked to the Australian savanna zone as defined by the ecoregions (Figure 1a). A time series of NDVI and SWIR32 VIs was calculated from the reflectance (R) data using R_{645} and R_{858} for NDVI, and R_{1640} and R_{2130} for the SWIR32. The vegetation index time series data were then smoothed to reduce noise, and gaps were filled using linear interpolation (Lu et al. 2003). The noise was identified based on three criteria: 1) either calibration band suggests lower than "best quality" as described by the MCD43A2 product (Schaaf et al. 2002); 2) vegetation index value is higher than threshold 1.2 as both indexes suggest a range from 0 to around 1.0; 3) change of vegetation index is higher than 0.5 times of standard deviation within a search window of six 8-day intervals (Lu et al. 2003). The noise was then replaced by spline interpolation. The final data set consisted of 460 8-daily, 500-meter resolution composites for the period of January 2002 to December 2011.

$$SWIR32 = \frac{R_{2130}}{R_{1640}} \qquad \textit{Equation 17}$$

$$NDVI = \frac{R_{858} - R_{645}}{R_{858} + R_{645}} \qquad \textit{Equation 18}$$

4.1.2 Hyperion Data

Available EO-1 Hyperion L1R cloud-free images were acquired from the USGS Earth Explorer in order to provide the fullest possible coverage of savanna vegetation types across the study region (Figure 22a). Images were grouped by ecoregion, by seasonal period and by broad east-west geography, since the western ecoregions tend to be dryer and more sparsely treed than the eastern ecoregions (Figure 22b). Images were distributed throughout the complete growing season, but some ecoregions had fewer images and less ideal coverage of seasonality than others did.

The images were radiometrically calibrated and atmospherically corrected using ACORN 6.1®. The imagery was processed to remove bad bands, de-striping, remove noise from the short wave infrared region, and remove the major water interference regions following a comprehensive suite of procedures (Jupp et al. 2002; Apan & Held 2002; Datt et al. 2003; Datt & Jupp 2004). The final images contain 152 bands for subsequent analysis - this retained the following wavelength ranges: 447 – 1114 nm; 1154 nm – 1336 nm; 1487 – 1790 nm; and 1981 – 2365 nm. Minimum noise fraction (MNF) was applied to the visible (447 – 854nm) and SWIR bands (864 – 2365nm) separately for each image. Only bands with significant eigenvalues were used for the later inverse transformation. The imagery was then geometrically corrected using ENVI image-to-image registration from the Hyperion L1GST product. The RMSE (Root Mean Square Errors) ranged in value from 0.3 to 0.6 pixels.

4.1.3 Orbview-3 Data

The Digital Globe Corporation has made a global archive of high-resolution multi-spectral imagery collected between 2003 and 2007 publically available. Six geo-corrected 4m L1Gst Orbview-3 images were acquired from the USGS Earth Explorer and used to validate the tree and herbaceous fractional data produced by the analysis. The images had acquisition dates ranging from June 9, 2006 to September 23, 2006 (Figure 22a). According to the National Forest Inventory map (Lymburner et al. 2011), the June 09, 2006 images (ID = 172; 232; 292) are mostly not forest except some small patches of "Eucalypt Medium Woodland" or "Eucalypt Medium Open". The image 302 is most covered by "Eucalypt Low Woodland" and part of the east area is "Eucalypt Medium Woodland". The image 572 covers some scattered patches of "Eucalypt Medium Woodland" at the northern part and some "Acacia" at the central part and the rest are not forest. The northern part of image 372 is covered by "Eucalypt Low Woodland" while others are all "Non Forest".

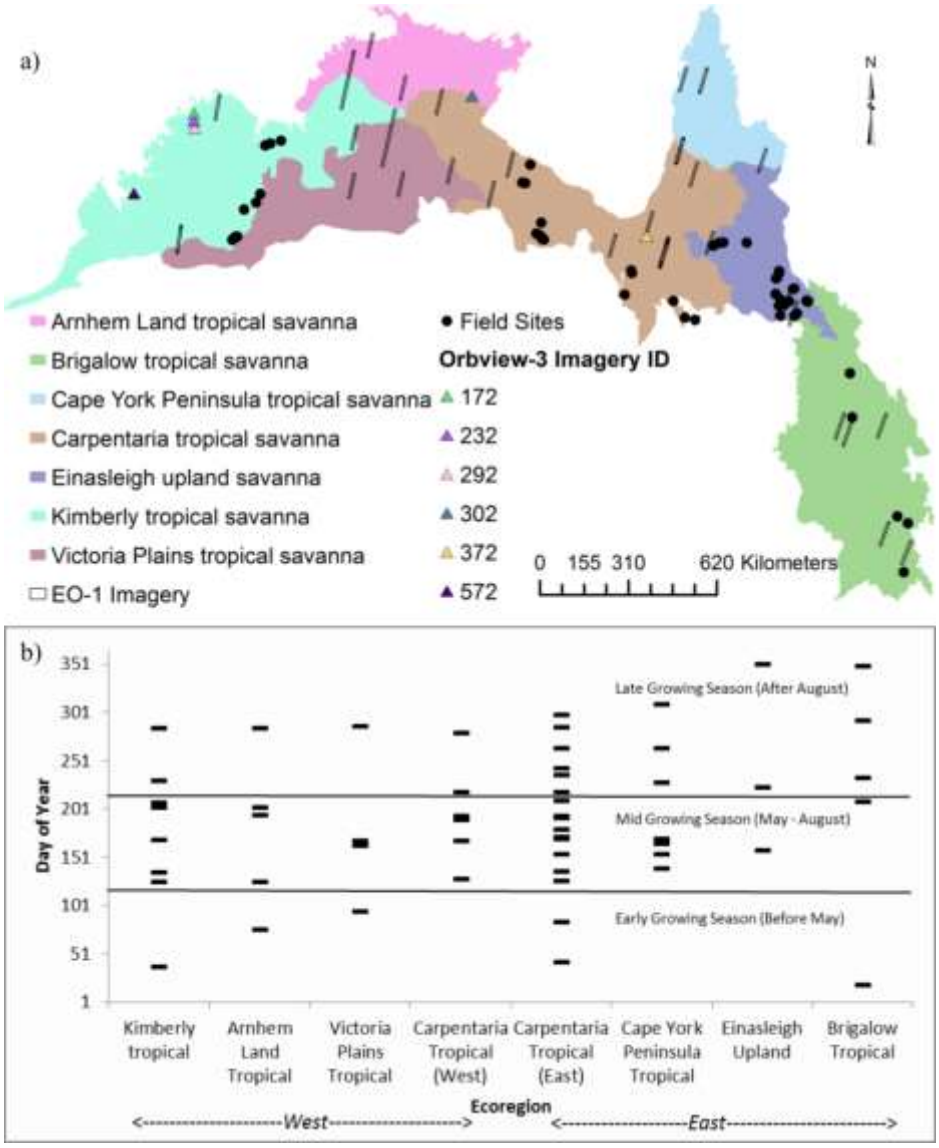

Figure 22. a) Study region showing the savanna ecoregions, distribution of EO-1 Hyperion imagery used in end-member analysis, location of Orbview-3 imagery using in validation of disaggregated tree and herbaceous cover fractions and distribution of field sites from the Australian Ground Cover Reference database used in validation of disaggregated tree and herbaceous cover fractions. b) Temporal distribution of EO-1 images across ecoregions as well as East-West part of Australia.

4.1.4 Landsat persistent green product

The persistent green vegetation fraction and wooded mask over the whole Australian savanna were derived from dry season Landsat 5 TM and Landsat 7 ETM+ images from 2000 to 2010 and made available by the Joint Remote Sensing Research Program (Johansen, et al., 2012). The product provides an estimate of the projected

persistent green fraction, which is considered as nominally woody vegetation with an overall classification accuracy of 0.826, and an $R^2 = 0.859$ for a linear regression against field measured foliage projected cover (http://www.auscover.org.au/xwiki/bin/view/Product+pages/Persistent+Green-Vegetation+Fraction).

4.2 Field Data

Ground measurements were extracted from the Australian Ground Cover Reference Sites database (ABARES, 2013) and masked for the study region (R. Trevithick, pers. comm.) (Figure 22). The measurements were collected beginning in 1998 and were concentrated from fall to spring. The observations are based on a "star" arrangement of three 100-meter transects (recording data on understory, midstorey and overstorey) (Muir et al. 2011). The measurements included percentage ground cover for crust, disturbed, rock, green leaf, cryptogam, dead/dry and litter; percentage mid-level cover for green, dead and branch; percentage overstorey cover for total crown, overstorey green, overstorey dry/dead and overstorey branch; and calculated proportion of persistent green (R. Trevithick, pers. comm.). Image subsets of 500 x 500 pixels from topographically and atmospherically corrected Landsat surface reflectance were also obtained for each field site. Landsat subsets contaminated by clouds were removed. A final total of 93 ground points and Landsat subsets were used for validation.

5. Analysis

The processing scheme for the analysis is shown in Figure 23. The analysis involved: i) exploration of geographical variation in the response space between NDVI and SWIR32 with Hyperion imagery to derive 30 m scale end member values for PV, NPV and BS; ii) linear unmixing of MODIS NDVI and SWIR32 images at each time interval for the 2002-2011 time series into PV, NPV and BS fractions; iii) decomposition of the MODIS

NDVI time series into persistent and seasonal components; iv) calculation of seasonal green ($NDVI_{seasonal}$) and persistent green ($NDVI_{persistent}$) components and comparison with the Landsat persistent green fractional cover product aggregated to MODIS resolution; v) partition of *f*PV based on proportions of $NDVI_{persistent}$ and $NDVI_{seasonal}$ to derive fPV_{woody} and $fPV_{herbaceous}$; vi) mapping green tree (fPV_{woody}), green herbaceous ($fPV_{herbaceous}$) and dry herbaceous ($fNPV_{herbaceous}$) cover for the Australian tropical savanna; vii) validation of tree and total herbaceous cover against field observations; and viii) validation of tree and total herbaceous cover against tasseled cap transforms of Orbview-3 data classified into green tree canopy, green herbaceous cover, dry herbaceous cover and bare soil.

5.1 Exploration of geographic variation in NDVI and SWIR32 end members in EO-1 Hyperion imagery

Scatterplots of NDVI versus SWIR32 were constructed for the east and west parts of Australian savanna, as well as each ecoregion. It was necessary to use an automated system for endmember extraction with such a large image suite. The endmembers for each ecoregion and sub-region were extracted. The end-member variation was assessed and compared for final overall end member definition. The goal of this comparison was to capture and evaluate the variation of the response envelope patterns across different soil and vegetation covers. The final end-members were selected based on the most extent of the response envelope to enclose others.

5.2 Linear unmixing of MODIS NDVI and SWIR32 images using refined end members

The linear unmixing method was applied to each pair of NDVI and SWIR32 images in the time series by following the method described in Chapter 1. In order to assess the linear unmixing results:

1. First, the fractional cover of PV, NPV, and BS from this analysis was compared to that created from the original analysis by Guerschman et al. (2009) by accessing data layers from the AusCover Remote Sensing data facility in Australia. Simple regression was undertaken between corresponding image dates to determine any offsets associated with the different end-members used.

2. Then, the fractional cover from this analysis was overlaid with fire scar data (http://www.firenorth.org.au/nafi2/about/firescarmaps.htm) for the same date in 2005 as used by Guerschman et al. (2009).

5.3 Deriving separate tree cover and total herbaceous cover

The relative fraction of tree ($rfPV_{woody}$) and herbaceous ($rfPV_{herbaceous}$) vegetation contributing to *f*PV is based on relative magnitudes of the decomposed and the total NDVI signals at time (t), and can be equated to the fraction of that signal attributable to the persistent ($NDVI_{persistent}$) and seasonal ($NDVI_{herbaceous}$) components, where the sum of the two ($NDVI_{total}$) is scaled from 0 – 1.0:

$$rfPV_{woody}(t) = \frac{NDVI_{persistent}}{NDVI_{total}} \qquad \textit{Equation 19}$$

$$rfPV_{herbaceous})(t) = \frac{NDVI_{seasonal}}{NDVI_{total}} \qquad \textit{Equation 20}$$

Then the fractional cover of the tree and herbaceous parts of PV at any time slice can be separated by multiplying *f*PV by the ratio of the persistent or seasonal proportion of the NDVI signal to the total of the two components:

$$fPV_{woody}(t) = fPV(t) \times \frac{NDVI_{persistent}(t)}{NDVI_{Seasonal}(t) + NDVI_{persistent}(t)} \qquad \textit{Equation 21}$$

$$fPV_{herbaceous}(t) = fPV(t) \times \frac{NDVI_{H}(t)}{NDVI_{seasonal}(t) + NDVI_{persistent}(t)} \qquad \textit{Equation 22}$$

$$fTotal_{herbaceous}(t) = fPV_{Herbaceous}(t) + fNPV(t) \qquad \textit{Equation 23}$$

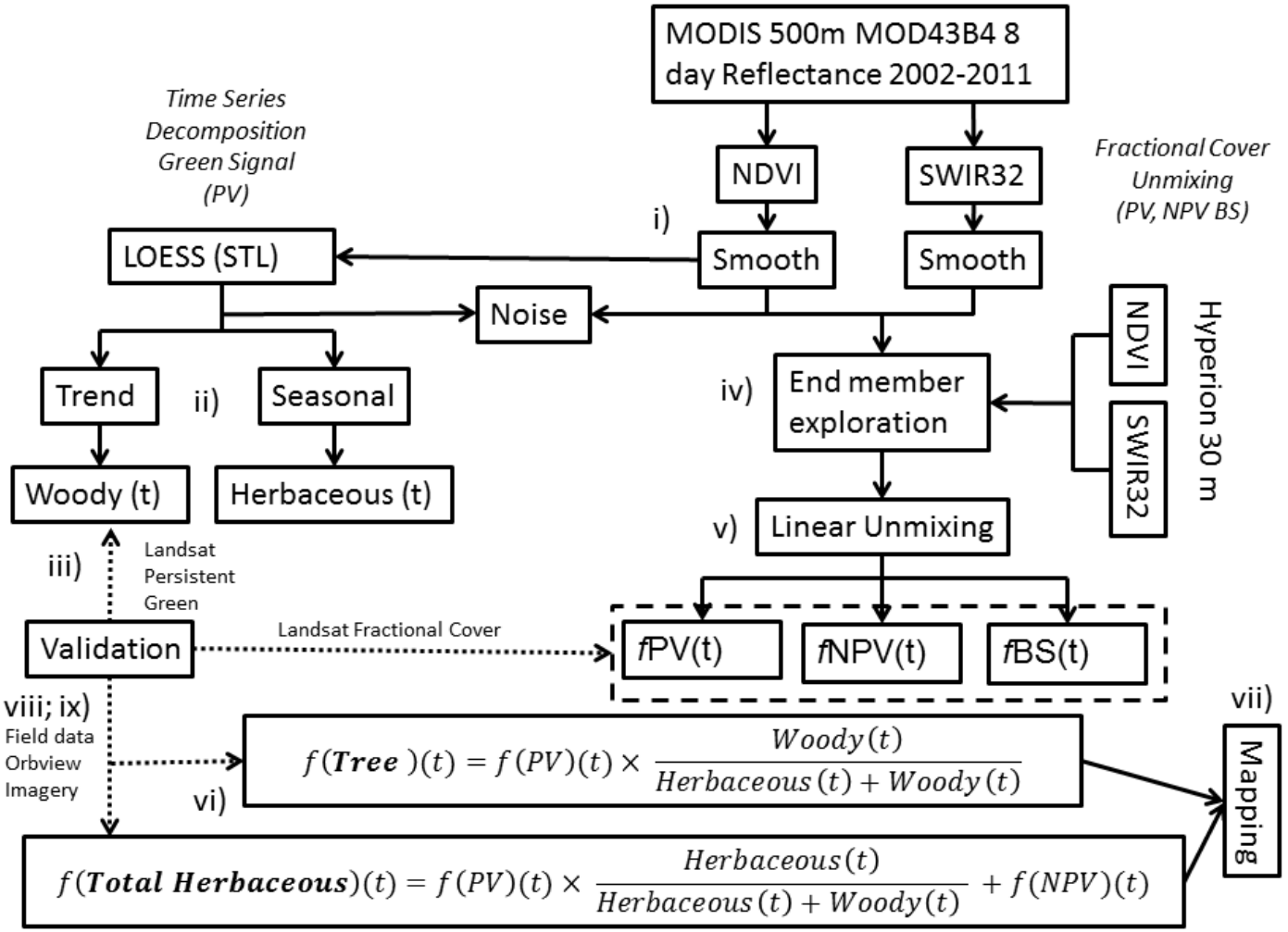

Figure 23. Brief illustrating the approach for assessing the fractional of woody, herbaceous, NPV and BS cover based on time series of vegetation index

5.4 Decomposition of NDVI into persistent and seasonal components

The tree and grass NDVI is estimated based on Lu et al. (2003) time series decomposition method (see Chapter 1, section 7.2).

5.5 Mapping fractions of green tree cover, green herbaceous cover, and dry herbaceous cover

The integrated algorithm incorporating the r*f*PVwoody and r*f*$PV_{herbaceous}$ from the NDVI time series decomposition and the *f*PV and *f*NPV fractions from the unmixing (Figure 2) was applied to the 10-year time series (2002-2011). This created a sequence of 460 three-band images containing fractional cover of green trees (*f*PV_{woody}), green herbaceous (*f*$PV_{herbaceous}$) and dry herbaceous (*f*NPV~ *f*$NPV_{herbaceous}$) material. The three fractions are displayed in an RGB composite where *f*PV_{woody} is displayed as green, *f*$PV_{herbaceous}$ is displayed as red, and *f*$NPV_{herbaceous}$ is displayed as blue. Black areas indicate regions where bare soil predominates and vegetation fractions are all below the minimum value confidence threshold for the method. The time series of tree and herbaceous components was examined for its capacity to characterize differences in tree and herbaceous phenology by extracting temporal profiles for selected savanna land cover types using classes from the National Forest Inventory (Lymburner et al. 2011) and an understory map derived from the tropical savanna vegetation map (Fox 2001).

5.6 Validation of Woody fraction using Landsat Persistent Green

The estimates of r*f*PV_{woody} derived from the decomposition of the NDVI times series were validated by comparing it with the 30 m resolution Landsat persistent green product (Johansen, et al., 2012). The 10-year average of the r*f*PV_{woody} estimate at the time of maximum NDVI in each year was used for comparison. The average r*f*PV_{woody} was classified into 32 classes with unique values evenly distributed from 0 to 1. Then the

mean and standard deviation of the 30 m pixel values of the Landsat persistent green fractional cover within each unique 500 m scale fPV_{woody} value was calculated. The values were then compared by linear regression and Reduced Major Axis (RMA) regression (Sokal, & Rohlf 1995; Legendre & Legendre 2012).

5.7 Validation of tree and total herbaceous cover against field observations

Since the savannas are very heterogeneous at 500 m pixel scale, the representativeness of the field sites in relation to the 500 m MODIS pixels was assessed for the NDVI and SWIR32 indices using Landsat subsets. NDVI and SWIR32 (Equation 9) were calculated for the 500 x 500 pixel Landsat images (corresponding to a 3 x 3 MODIS pixel array) at each site (Figure 1a). Several measures of spatial representativeness were developed by Román et al. (2009). One measure, the ST_{score} is a combination of a number of statistics derived from a variogram function:

$$ST_{score} = \left(\frac{|R_{CV}|+|R_{ST}|+|R_{SV}|}{3} + R_{SE}\right)^{-1} \qquad \textit{Equation 24}$$

R_{CV} = Relative coefficient of variation
R_{ST} = Scale requirement index
R_{SE} = Strength of spatial dependence
R_{SV} = Relative landscape variability (Roman et al., 2009)

Another measure, the RAW_{score} is a first order measure from the semivariogram analysis based on the R_{CV}.

$$RAW_{score} = |2R_{CV}|^{-1} \qquad \textit{Equation 25}$$

Both the ST_{score} and the RAW_{score} are proportional to site representativeness meaning that high values indicate the most representative sites. However, the two measures do illustrate different elements of the site variation. Román et al. (2009) reported a range of ST_{score} values from 0.6 to 36.4 across a set of Ameriflux sites with values less than 3.0

being considered relatively unrepresentative. The ST_{score} was calculated for NDVI and SWIR32 for each site. The square root mean of ST_{score} and of RAW_{score} for NDVI and SWIR32 were then used to assess the representativeness of field observations. MODIS fPV_{woody} and $fPV_{herbaceous}$ were compared with field observations using linear regression and RMA.

5.8 Validation of tree and herbaceous cover against classified Orbview-3 imagery

High-resolution multispectral imagery provided a means to accurately quantify the proportion of tree canopy and bare soil within a MODIS pixel. The Tasseled Cap transform (Kauth & Thomas 1976), originally developed for Landsat data (Kauth & Thomas 1976; Crist & Kauth 1986), rotates multi-band data into Greenness, Brightness and Wetness layers and provides the means to define the tree, herbaceous and soil cover in these high resolution images. For these dry season Orbview-3 images, we assumed that the greenness band corresponded to green tree canopy and the brightness band was indicative of bare or near bare soil areas. The remainder of the image area was then assumed herbaceous cover. The Tasseled Cap transform was applied to the Orbview-3 images. The transform for IKONOS data was developed by Horne (2003) based on the different spectral characteristics. Our study use the coefficients developed for IKONOS, as the band settings were similar for the two sensors.

$$T_{Brightness} = 0.326R_{blue} + 0.509R_{green} + 0.56R_{red} + 0.567R_{nir} \quad \textit{Equation 26}$$

$$T_{Greenness} = -0.311R_{blue} - 0.356R_{green} - 0.325R_{red} + 0.819R_{nir} \quad \textit{Equation 27}$$

$$T_{Wetness} = -0.612R_{blue} - 0.312R_{green} + 0.722R_{red} - 0.081R_{nir} \quad \textit{Equation 28}$$

The Tasseled Cap indexes were then classified into 30 discrete classes using an ISODATA method (ENVI®) and the classes were aggregated into bare soil, green tree

canopy, green herbaceous and other vegetation by comparing the classes with Google Earth data. This classification has to assume that each Orbview-3 pixel is pure (which at 4 m pixel scale is unlikely in the majority of cases) in order to form a suitable summary of the fractional cover of 500 m MODIS pixels. Given that a MODIS pixel will contain 15625 Orbview-3 pixels, it is necessary to make the assumption that within pixel mixtures will introduce a small but acceptable error relative to the benefit of fine scale sampling of the major fractional components in a MODIS pixel.

Linear interpolation was used to estimate the MODIS woody and herbaceous fractional cover at the exact dates corresponding to Orbview-3 images. In order to correctly align MODIS pixels with Orbview-3 classifications, MODIS NDVI was regressed against Orbview-3 NDVI for corresponding image dates, and the images were aligned to maximize the linear regression fit in terms of RMSE and R^2. For validation, the MODIS pixel coverage within the Orbview-3 image was converted to a vector lattice, with polygon values corresponding to every 1 % variation in cover fraction. Then MODIS tree and herbaceous cover fraction was regressed against the tree and herbaceous cover fraction from Orbview-3 images using linear regression and RMA.

6. Results

6.1 Geographic and seasonal variation in NDVI and SWIR32 endmember in EO-1 Hyperion imagery

The EO-1 reflectance spectra formed the triangular shape in the NDVI/SWIR32 scatterplot for all ecosystems. NDVI ranged from 0 to 0.8 and SWIR32 range from 0.4 to 1.1. A visual examination based on the Google Earth software was conducted to assess the land cover types near the potential endmembers. The result suggested that the locations that derived from endmembers were mostly homogeneous.

Figure 24 shows the range of the potential end-members derived directly from the geographic and temporal array of Hyperion NDVI and SWIR32 data, at 30 m pixel resolution. The potential end-members derived here extend the vertices of the end member response envelope to lower values of NDVI than those derived from the regression relationship between the Hyperion-based NDVI-CAI response space and the MODIS NDVI-SWIR32 response in Guerschman et al. (2009). Among ecoregions, the potential end-members of NPV and BS are more clustered compared to those for PV; it reflects the wide range of tree canopy density across the wetter and dryer parts of the Australian savanna. Hence, even at a 30 m pixel scale, it is difficult to find pure pixels of green tree canopy except in the Cape York area. As the figure shows, the Brigalow tropical savanna has the least PV and the highest BS while Cape York Peninsula tropical savanna has the highest PV. Other ecosystems show relatively similar end-member distribution including the Kimberly tropical savanna, Victoria plains tropical savanna, Carpentaria tropical savanna and Einasleigh upland savanna. Though endmembers vary by ecoregions, the overall plot still shows a unique response envelope shape with other endmembers falling inside.

Thus, the end member set was selected across the ecoregions to include all potential selections and was defined as follows:

PV: NDVI = 0.838, SWIR32 = 0.338

NPV: NDVI = 0.119, SWIR32 = 0.523

BS: NDVI = 0.035, SWIR32 = 1.081

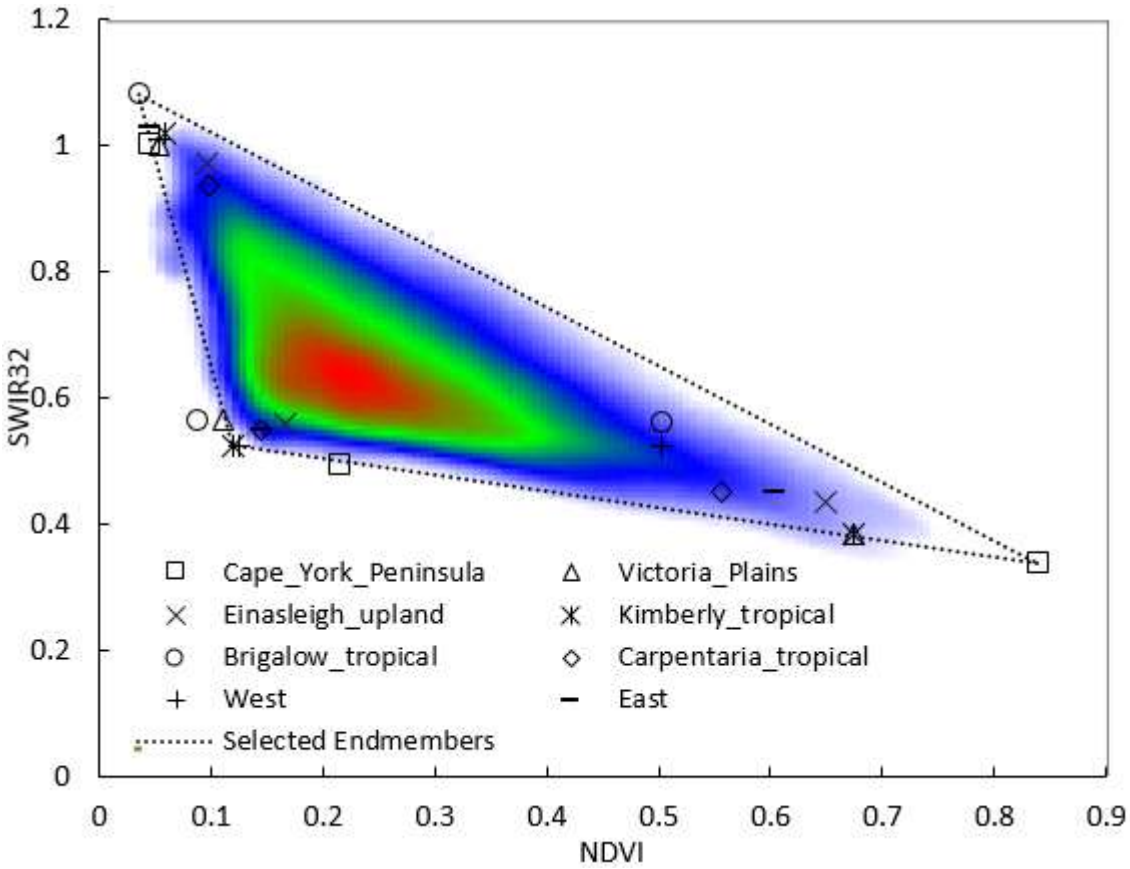

Figure 24. Distribution of the potential endmembers across ecoregions compared with the selection from Guerschman et al. (2009)

6.2 Assessment of Fractional Cover derived from unmixing the refined endmembers

The time series of NDVI and SWIR32 was unmixed using the end-members defined above. The resulting data showed a strong agreement with the original Australian fractional cover product based on the 2005 spatial distribution of *f*PV, *f*NPV and *f*BS. Comparison of the fractional cover data derived here, with the fire scars that occurred in 2005 near Darwin (http://138.80.129.56/nafi3/) described by Guerschman et al. (2009), showed a good correspondence of high *f*BS for burned areas, and high *f*NPV for areas that were not burned.

Figure 25 shows a scatter-plot comparison of *f*PV, *f*NPV and *f*BS estimated from this study and the product data derived by Guerschman et al. (2009) (TERN/AusCover, 2013).

Comparisons are made for the beginning, middle, and end of the dry season (1-May-2005; 4-July-2005; 6-September-2005), corresponding to the three Hyperion images used in the Guerschman et al. (2009) study. The scatter plots show overall linear correlation. However, this study shows an approximately 20 percent higher *f*PV at low leaves of green cover than the Guerschman et al. (2009) study. The disagreement diminishes as green cover increases. On the other hand, this study shows an approximately 20 percent lower *f*NPV at high NPV coverage than the Guerschman et al. (2009) study. The differences diminish as senescent cover decreases. The estimation of *f*BS shows strong agreement and is close to a 1:1 ratio. These differences were expected based upon the application of end-members for BS and NPV shown in Figure 24. They extend the scale of the response space, principally on the PV-NPV axis, and would be expected to increase sensitivity to PV at low cover fractions. The results indicate that the fractional cover derived here matches the original product, except for differences created by the refining of the end-members based on Hyperion imagery documented here.

6.3 Decomposition of NDVI into persistent and seasonal components

Figure 26 shows examples of NDVI and its decomposition results for different vegetation types based on the National Forest Inventory (Lymburner et al. 2011). The "Eucalypt Tall Woodland" and "Eucalypt Medium Open" have high persistent NDVI signals and low seasonal NDVI signals, while "Melaleuca" exhibits less persistent NDVI signal and more seasonal NDVI signal. The "Non Forest" class shows a very low persistent NDVI signal and a predominant seasonal NDVI signal. Both "Eucalypt Tall Woodland" and "Eucalypt Open" show a significant drop that is considered to be because of atmospheric contamination (Lu et al. 2003). Nevertheless, the woody and herbaceous NDVI indicated that the decomposition method is able to reject the excursion.

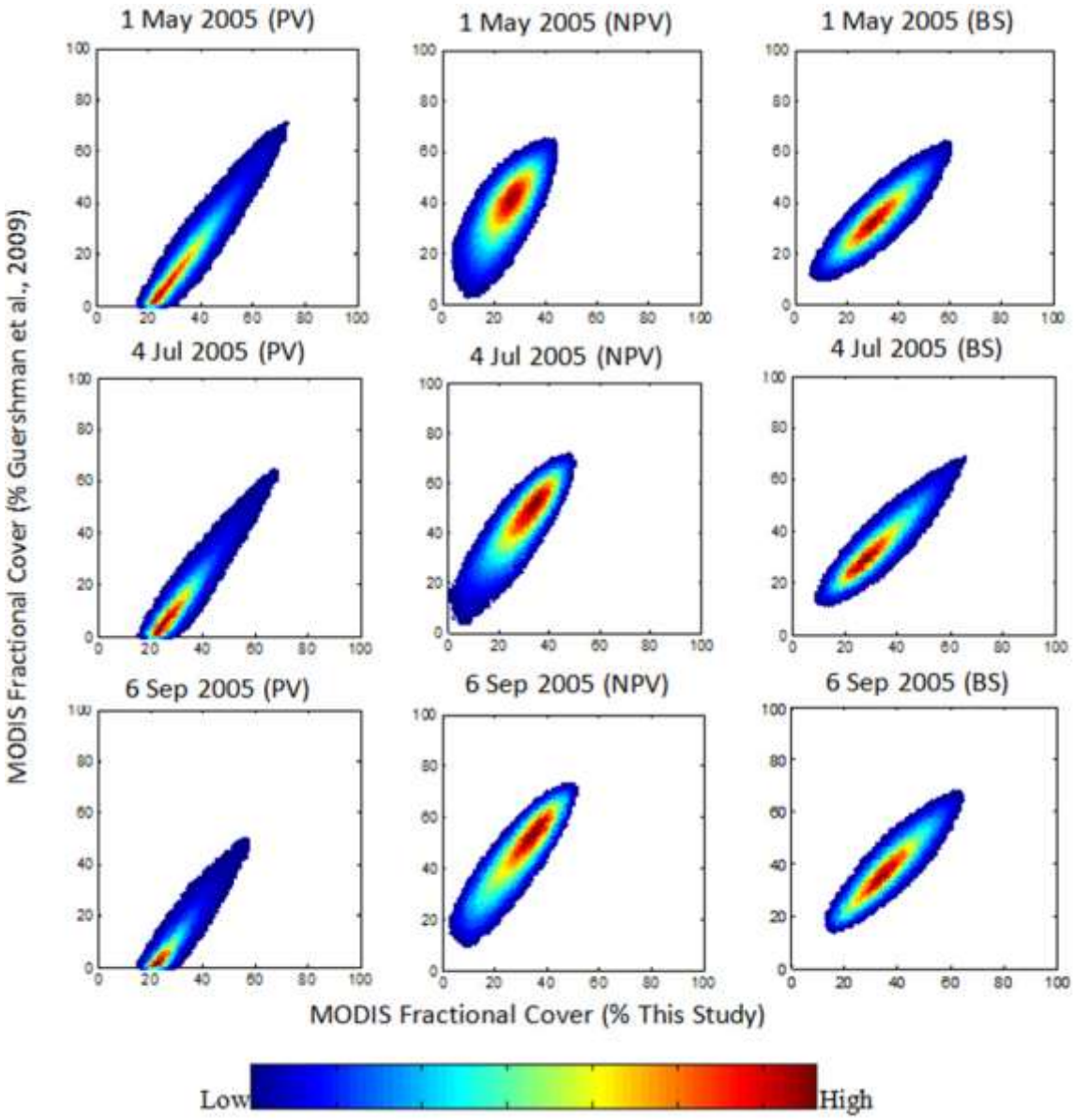

Figure 25. Scatter plot of PV, NPV and BS fractional cover from this study versus data from Guerschman et al., 2009. The frequency of combinations is shown in heat map color scale

6.4 Validation of persistent green cover fraction

The scatter plot of the Landsat persistent green fractional cover versus the MODIS persistent green is shown in Figure 27. The validation result showed an overall linear correlation with a R^2 of 0.99 and a slope of 0.89. The slope indicates a slightly overestimation at low woody fraction cover area and underestimation at very high woody fraction cover area. One of the reasons is that 10% of the seasonal variation contributed

by woody vegetation is not applicable for sparse and dense woody area. Besides, both sparse and dense woody land cover types are minor compared to the overall savanna region (fewer MODIS pixels), which introduces uncertainty related with statistically significance. The standard deviation varies from 0.08 to 0.23, but with the increase of the number of MODIS pixels, the STD is close to 0.1. The stabilized STD suggested overall accuracy of the combined approaches in this chapter.

6.5 Mapping fPVwoody ,fPVherbaceous, and fNPVherbaceous

The average monthly values for fPV_{woody}, $fPV_{herbaceaous}$, and $fNPV_{herbaceous}$ in the Australian savanna zone are mapped as RGB composite images in Figure 28. A subset of the savanna in the Northern Territory region is shown in close-up for May and September. As observed, the Cape York Peninsula tropical savanna and Arnhem Land tropical savanna are mostly covered by evergreen trees. Herbaceous vegetation starts growing in November from the west coast of the Arnhem Land tropical savanna to the inland. The peak of greenness arrives around March. Then, herbaceous vegetation starts drying out from the inland to the east coast of Queensland. In corresponding to NPV, the dead biomass and litter start to increase from April through to September. The region where black predominates, especially between November and January, indicates areas with high *f*BS and low fractional cover of all three vegetation components.

6.6 Description of Overstory and Understory Cover Dynamics

The time series of fPV_{woody}, $fPV_{herbaceous}$, and $fNPV_{herbaceous}$ were extracted from typical vegetation combinations with a focus on understory types (Figure 29). *Heteropogon* (black spear grass) woodlands (Figure 29a) are located in the eastern part of the savanna; *Triodia* (spinifex) woodlands occur in the southern arid margins (Figure 29b); *Dichanthium* (Queensland blugrass) grassy woodland is predominantly located at

the base of the Gulf of Carpentaria (Figure 29c); *Sehima* woodlands (Figure 29 d) occur in a band of better soils and intergrade with the annual grassland; and the annual *Sorghum* woodlands dominate the poorer soils nearer to the coast in the Northern territory (Figure 29: e; f).

The data show a slight upwards trend in the fPV_{woody}. *Dichanthium* grassy woodlands show a higher seasonal peak in $fPV_{herbaceous}$ and a stronger seasonal oscillations but shorter growing season compared to other more heavily treed woodlands. Besides considering the slightly overestimation of fPV_{woody} at the sparse woody fractional cover area (Chapter 2, section 6.4), the actual woody coverage in *Dichanthium* grasslands is expected to be lower. The relative proportions of fPV_{woody}, $fPV_{herbaceous}$, and $fNPV_{herbaceous}$ between the vegetation types match expectations; *Sorghum-Eucalyptus* open woodlands have higher tree densities and lower herbaceous cover than Sorghum woodlands, while *Triodia* woodlands would generally have low $fPV_{herbacoues}$ fractions since spinifex is a xeric bunch grass suited to harsher environments. Besides, $fNPV_{herbaceous}$ shows opposite oscillation trend when compared with $fPV_{herbaceous}$, which shows the growing cycling of the herbaceous vegetation. The overall higher $fNPV_{herbaceous}$ than $fPV_{herbaceous}$, on the other hand, indicates the prevalence of litters in each season.

6.7 Validation of tree and total herbaceous cover against field observations

The ground observations of green herbaceous cover showed a very broad scatter of values for a given level of $fPV_{herbaceous}$. The ST_{score} was mostly less than 1 indicating that the sites were not a good representative of the pixel scale variation (Figure 30). The ST_{score} ranges from 0.94 to 3.15; sites with values less than 3.0 were considered relatively unrepresentative by Román et al. (2009). The RAW measure also exhibited mostly very

small values; a few high values indicating sites that are more representative were clustered around low levels of woody cover, and very low levels of herbaceous cover. There was a 0.1 unit offset between ground observations and fPV_{woody} retrieved at 500 m scale, and a wide scatter of ground values at $fPV_{woody} < 0.3$. The ground data were also relatively unrepresentative of fPV_{woody}. Given the low tree canopy cover in these savannas, and the consequent poor representativeness of ground data at the MODIS scale, the 0.1unit offset between ground observations and fPV_{woody} retrieved at 500 m scale, and the scatter of ground values at $fPV_{woody} < 0.3$ is not surprising. As a result, the ground validation data did not provide a convincing validation case for the estimates of $fPV_{herbaceous}$ and fPV_{woody+} retrieved here.

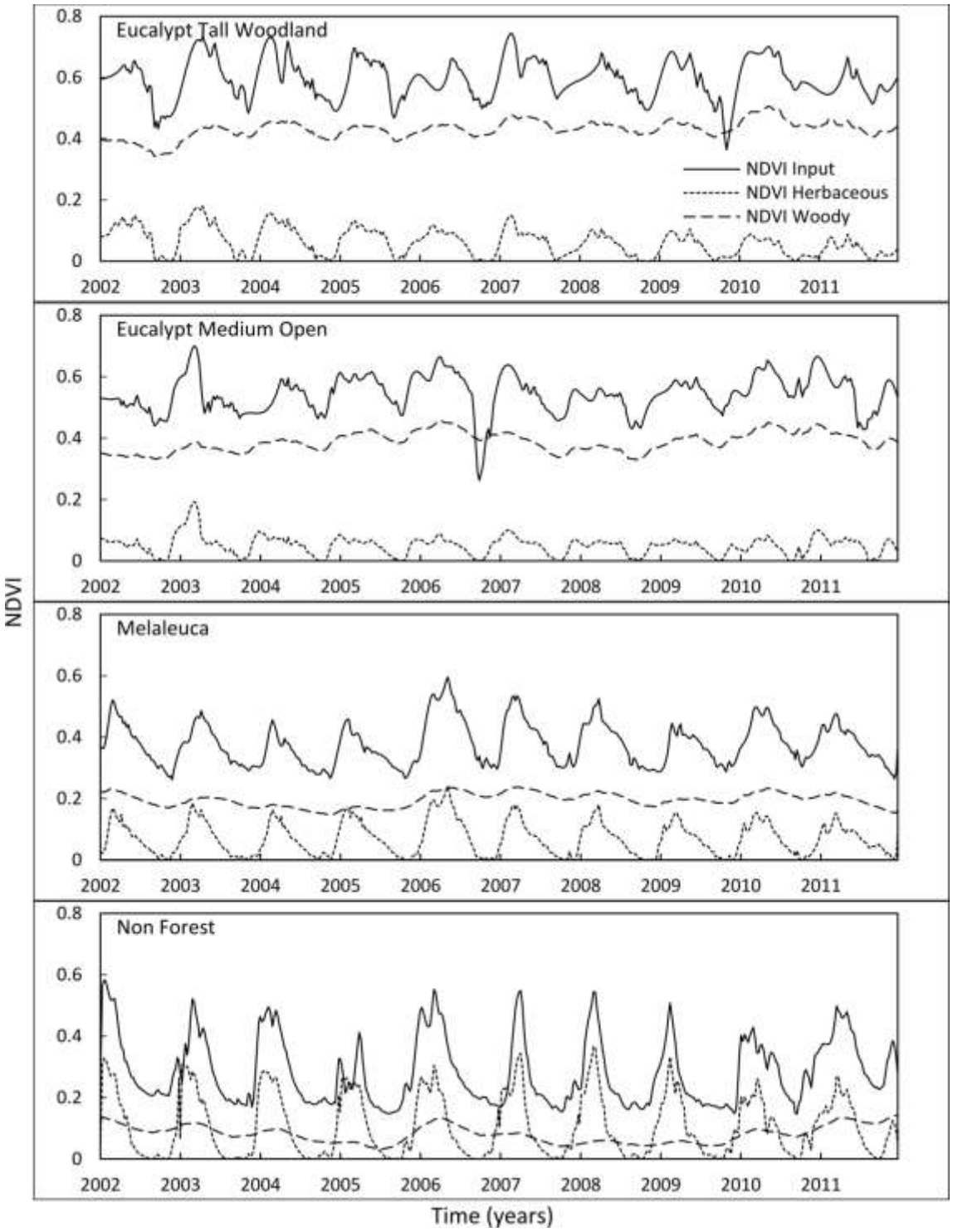

Figure 26. Decomposition NDVI into Woody NDVI and Herbaceous NDVI for different vegetation covers. "Eucalypt Tall Woodland" in Cape York Peninsula tropical savanna (14.03S, 142.31E); "Eucalypt Medium Open" in Arnhem Land tropical savanna (13.82S, 132.52E); "Melaleuca" in Carpentaria tropical savanna (18.07S, 141.76E); "Non Forest" in Victoria Plains tropical savanna (17.92S, 129.06E)

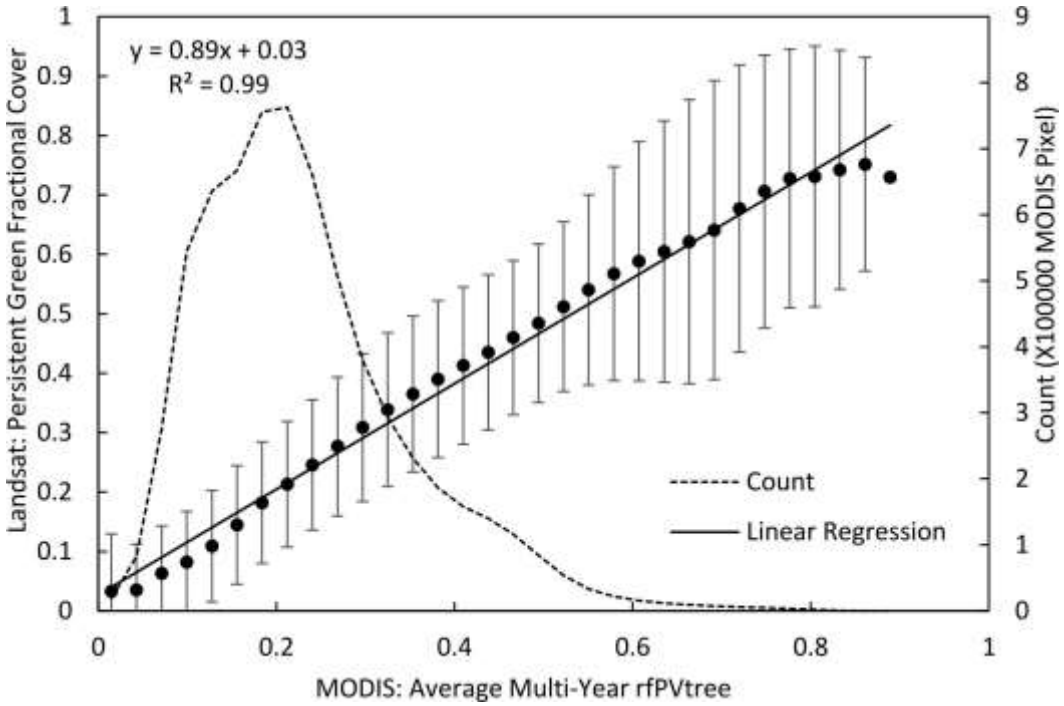

Figure 27. Linear relationship between the MODIS woody fraction cover from this study versus the Landsat persistent green fraction product

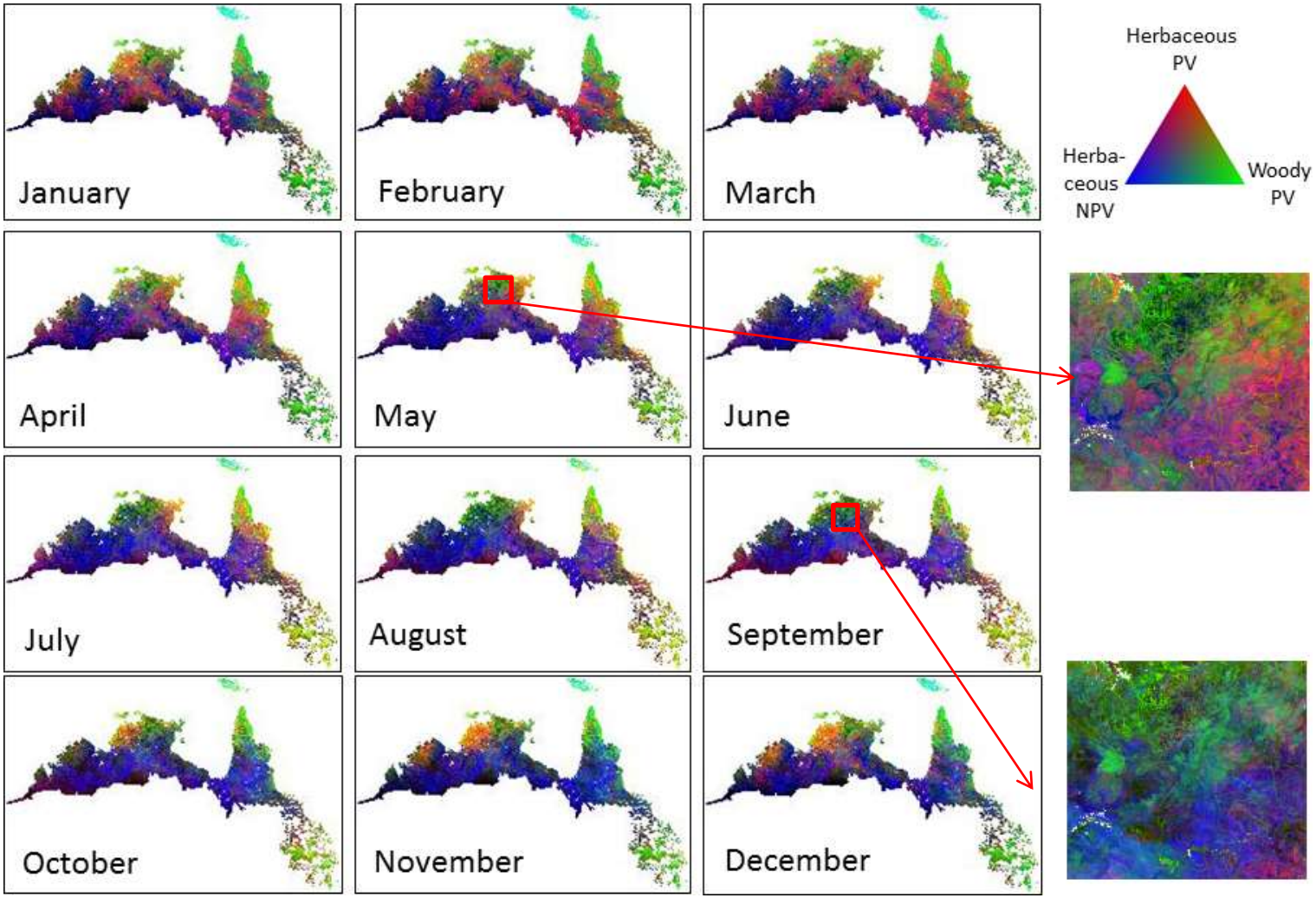

Figure 28. Monthly average of fractional cover for green tree canopy, green grass and NPV grass in the Australian savanna zone. The proportions of land covers are shown in RGB as specified in the color legend. The dark area suggests high proportion of bare soil

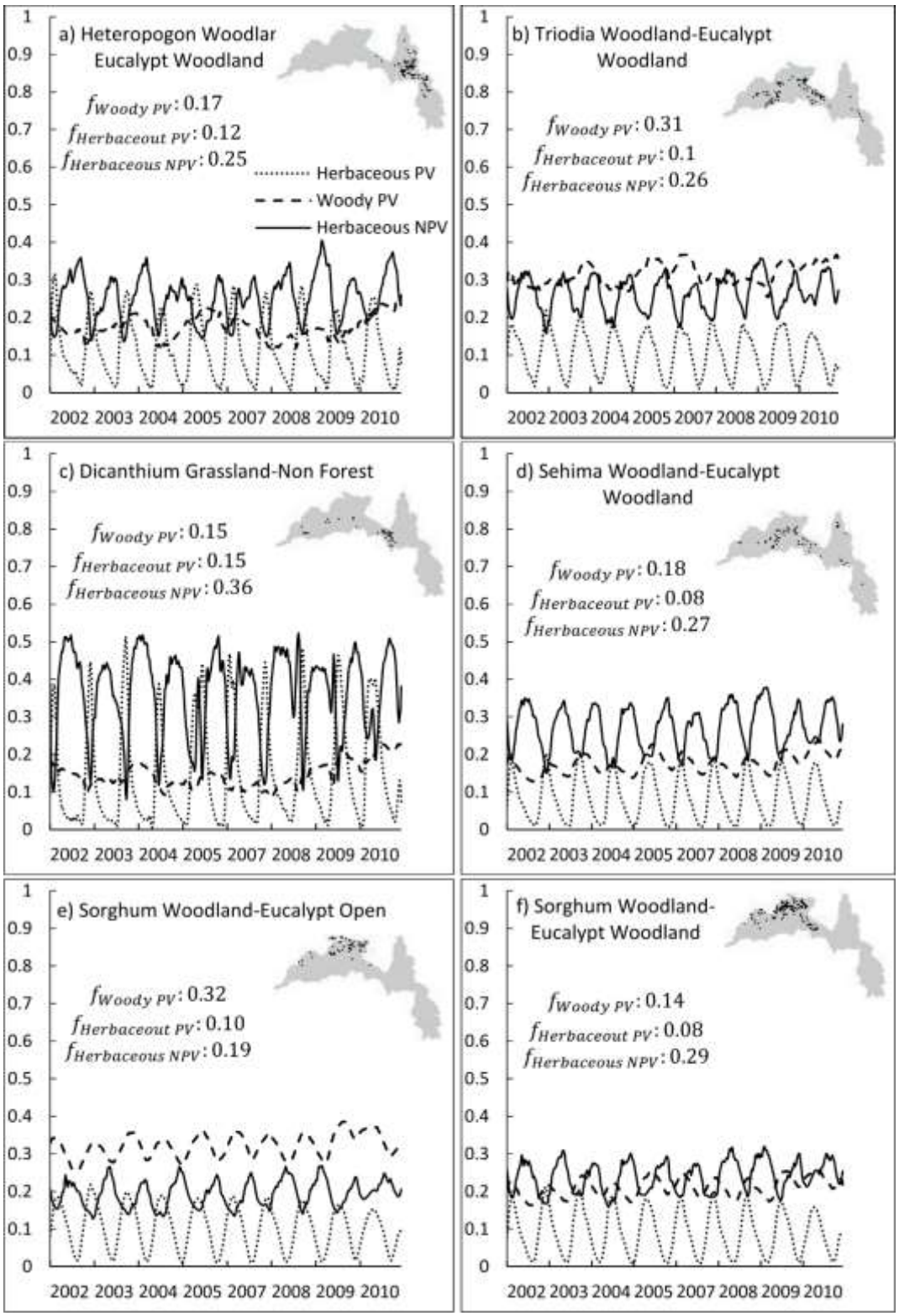

Figure 29. a) Heteropogon grassland with sparse trees. b). Triodia grassland with sparse woodland. c)Dicanthium grassland. d)Sehima grassland sparse Eucalypt woodland. Sorghum grassland with e) open and f) sparse Eucalypt woodland

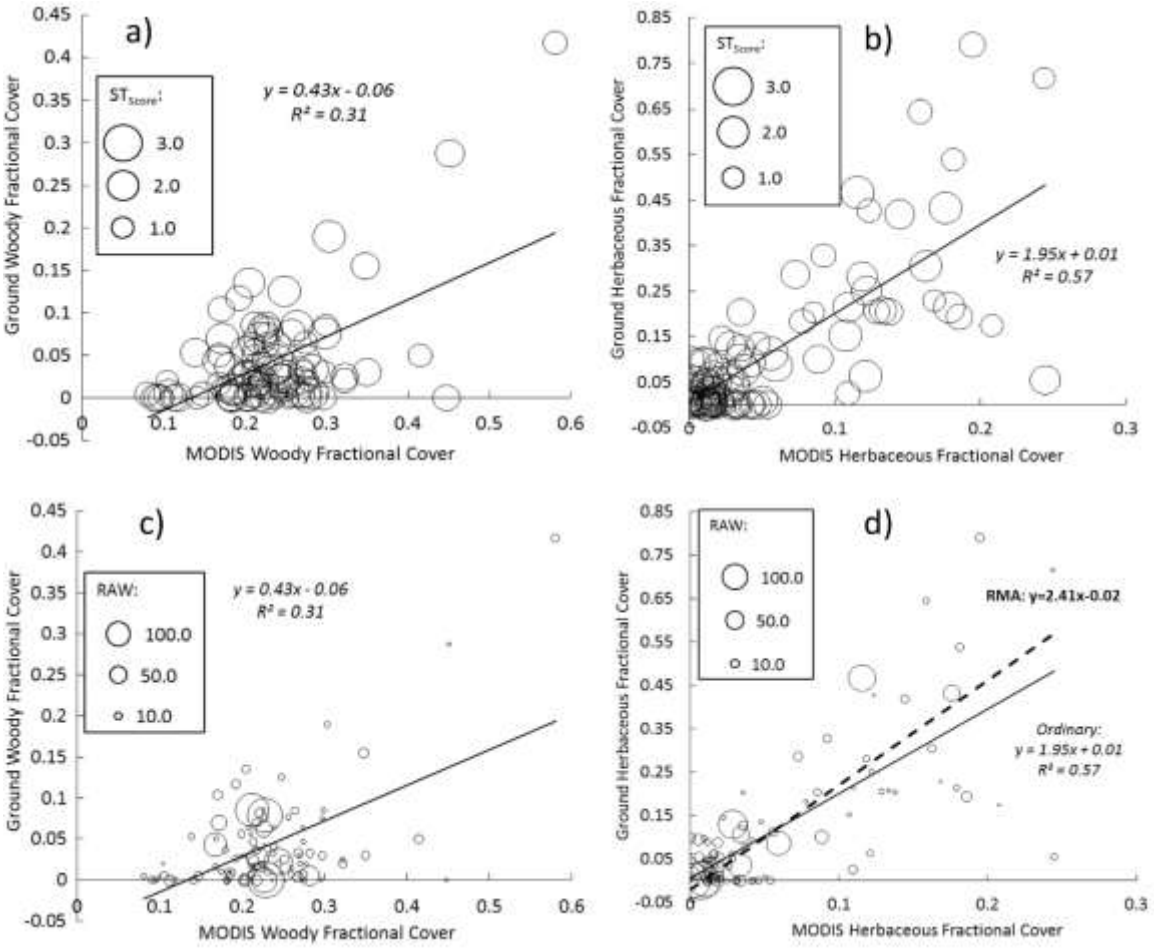

Figure 30. Ground validation based on field observations from the Australian Ground Cover Reference Database. a) Relationship between derived tree cover fraction and field data. b) Relationships between derived total herbaceous cover fraction and field data. The circles indicate the representativeness of 100 x 100 m NDVI and SWIR32 data at field sites at the MODIS pixel scale

6.8 Validation of woody and herbaceous cover against classified Orbview-3 imagery

The relationship between variation in spectral values and spatial distribution of classes derived from Orbview-3 images, and the variation in cover fractions captured at MODIS scale can be visually examined in Figure 29. The dense woody patches in the classified Orbview-3 images show strong matches with the fPV_{woody}. On the other hand, there are some herbaceous patches in images 572 and 372, which are also distinctive in the herbaceous fractional cover map. The Orbvivew-3 fPV_{woody}, $fPV_{herbaceous}$, and $fNPV$ at the 500m scale were estimated based on the classified images and compared to the

MODIS corresponding fractional covers (Figure 31). Scatter plots suggested substantial linear correlation especially for fPV_{woody} and $fPV_{herbaceous}$ with RMSE less than 0.1 (Figure 32). The *f*NPV was plotted into two groups as two sets of images showed different linear relationships. Images in group one are closer to the inland and predominated by seasonal grasses, which mostly dry out and are partly degraded in winter. The fPV_{woody} and *f*NPV showed high intercept which means there is an overestimation from the MODIS data due to the limited sensitivity to minor fractional cover change at 500-meter scale. Nevertheless, the less than 1 coefficient meant better agreement with the increase of fractional covers, which indicated better performance of the MODIS data when woody fractional cover is significant. Meanwhile the 95% confidence interval for MODIS estimations, within separate Orbview-3 value ranges, was also calculated. The lower interval suggested more stable estimation from the MODIS. The intervals were generally less than 0.05 given that the sample size was mostly less than 10 at each value range. The *f*NPV showed more variation against the Orbview-3 classification, especially for the low NPV covers. One of the reasons could be that the MODIS method would be expected to be more effective at the higher fractional covers due to the scale limitation. Another reason could be that MODIS is less sensitive to distinguishing NPV from soil as suggested in the "flat triangle" envelope. Finally, the disagreement could also be because MODIS differentiates PV, NPV, and BS based on the spectral differences, while validation tends to identify patches as pure land cover types. This means, when vegetation spectrum gradually changes from fully developed to totally dried out or degraded, MODIS considers it a combination of PV, NPV, and BS, whereas validation data simplified it into one of the endmembers.

6.9 Variation in herbaceous fraction across the Tropical Savanna

Figure 33 shows the statistics of the average annual maximum (10 years) green herbaceous vegetation ($fPV_{herbaceous}$), dry herbaceous ($fNPV$), and total herbaceous ($fPV_{herbaceous} + fNPV$) cover fraction. The maximum fraction may be retrieved from different times of year. The Brigalow tropical savanna was excluded from these maps due to the high level of land cover fragmentation. Some patches shows low average value of all three components in the coast area of Cape York Peninsula tropical savanna and the southern part of the whole study region (Figure 33 a, c, e). The constant low herbaceous average fraction suggests the dominance of trees or bare soil. The maps of temporal standard deviation exhibit less patches structure. However, the southern dry margins, and grasslands on cracking clays in the Gulf country are still distinct.

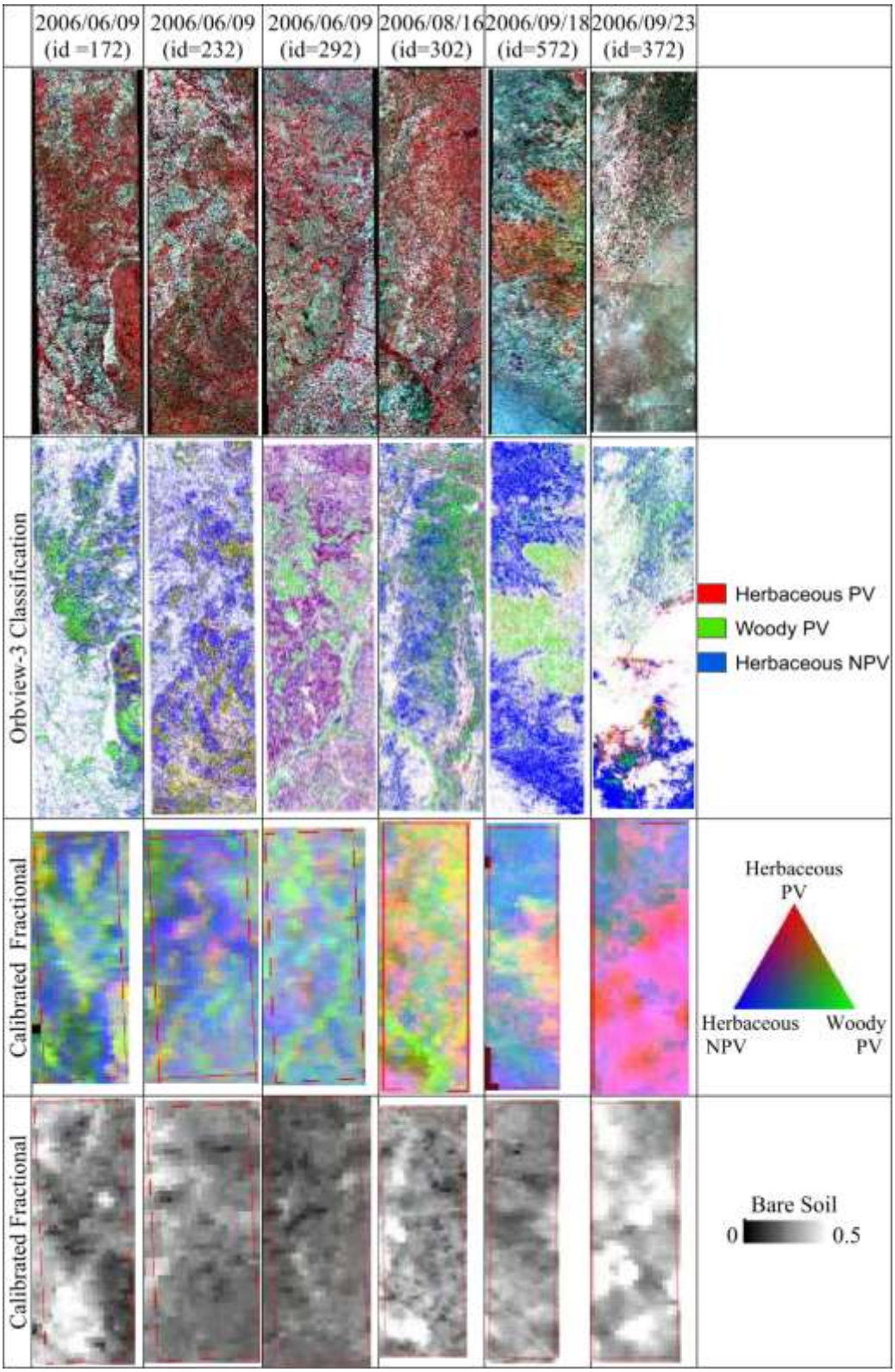

Figure 31. The composition in RGB color space of Orbview-3 images as well as MODIS tree and herbaceous cover fractions at corresponding dates

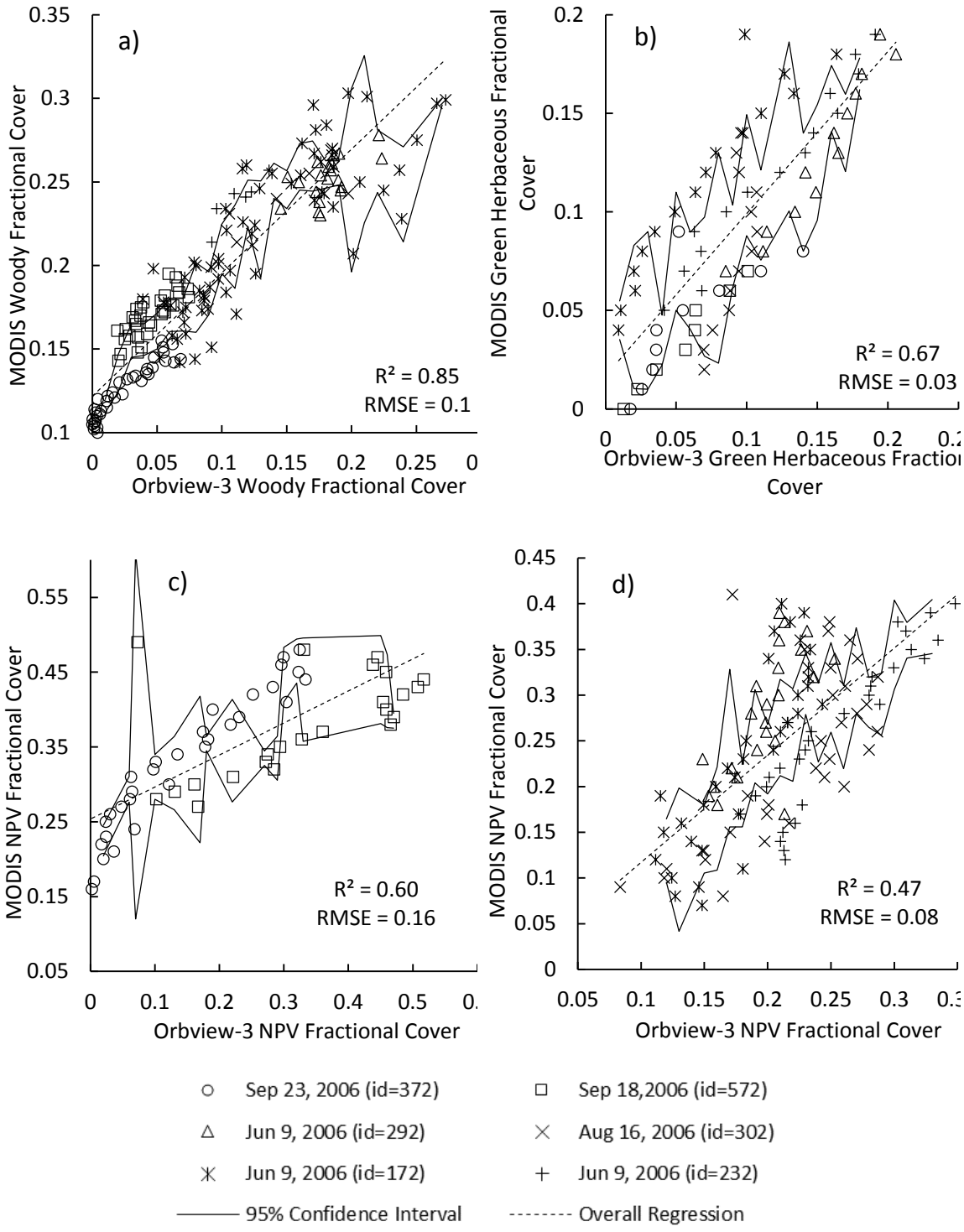

Figure 32. Linear relationship between the MODIS herbaceous and woody fraction cover versus the fraction cover based on the Orbview-3 classification

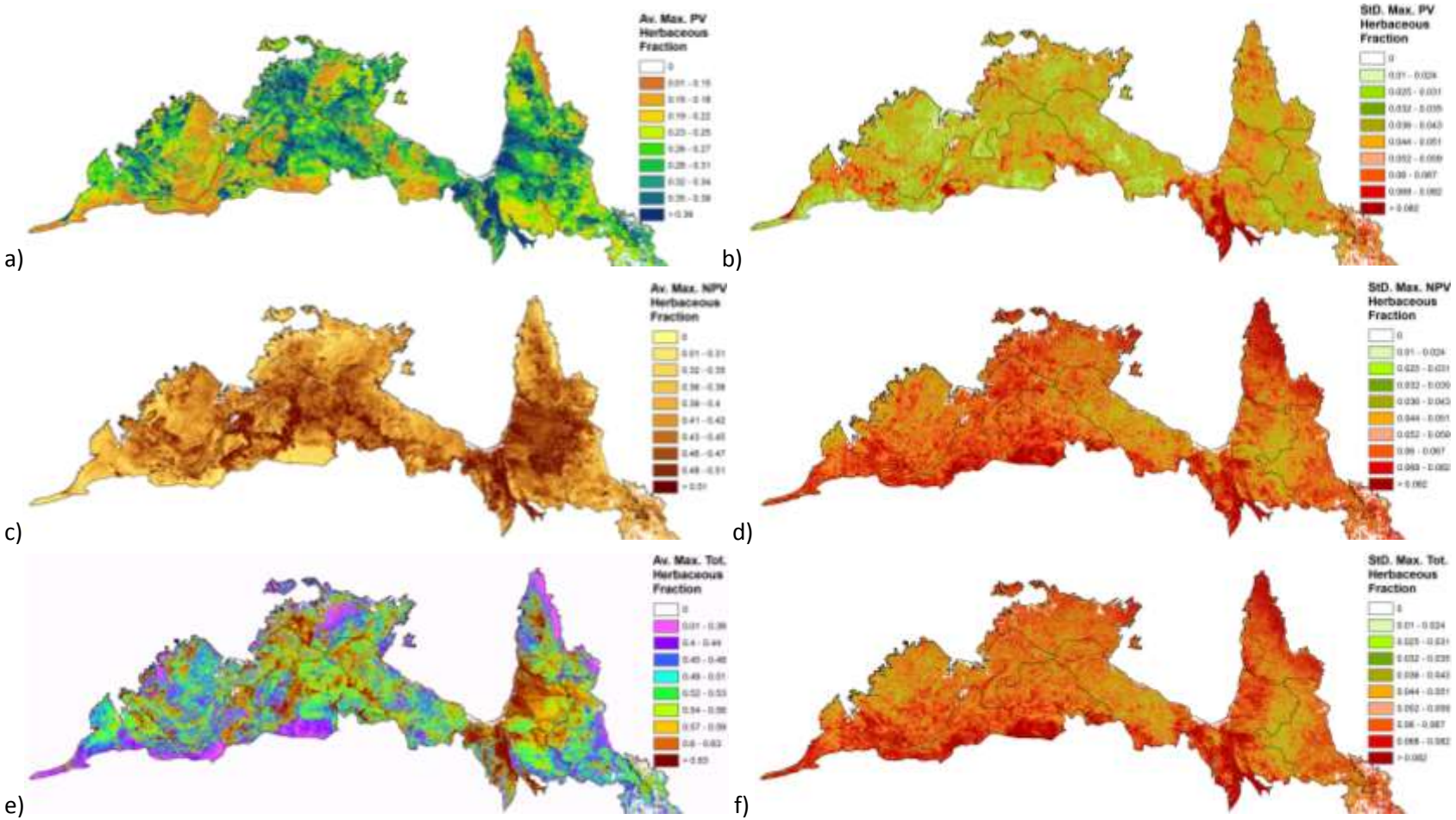

Figure 33. a) Average annual maximum $fPV_{herbaceous}$*; b) Standard deviation (over 10 years) of maximum* $fPV_{herbaceous}$*; c) Average annual maximum* $fNPV_{herbaceous}$*; d) Standard deviation (over 10 years) of maximum* $fNPV_{herbaceous}$*; e) Average annual maximum total herbaceous cover fraction (*$fPV_{herbaceous}$ + $fNPV_{herbaceous}$*; f) Standard deviation (over 10 years) of maximum total herbaceous cover fraction.*

7. Discussion

This analysis has shown that the fractional cover of green and dry herbaceous cover can be resolved from that of woody green canopies and bare soils by combining time series decomposition and linear unmixing approaches with the NDVI and SWIR32 VIs. While the NDVI and SWIR32 space derived fractions of green vegetation, dry vegetation, and bare soil, the time series of NDVI extracted fraction cover of green tree cover and green herbaceous cover from green vegetation fractional cover. Guerschman et al. (2009) developed the NDVI-SWIR32 linear unmixing method and later the method was applied to the whole of Australia (Guerschman et al. 2012). However, Guerschman et al. (2009) selected the endmembers based on three Hyperion images from the same location, but Hill et al. (2012) found that the endmember envelope could vary with ecoregion. In this chapter, the endmember set was systematically compared across ecosystems and refined for the specified savanna land cover types. The endmembers extended at the low end of NDVI compared with Guerschman et al. (2009). This is because the better coverage of spatial and temporal variation in this chapter is able to capture the drier landscapes.

Most of the previous studies (e.g. Gessner et al., 2009; Lu et al., 2003; Scanlon et al., 2002) aimed to discriminate tree, grass, and bare soil, while some studies explored the potential of mapping fractional cover of green vegetation, dry vegetation, and bare soil in savanna areas (Guerschman et al. 2009; Guerschman et al. 2012; Guerschman & Scarth 2015). Here, one further step is estimating fractional cover of overstorey and understory as well as their senescent phase. The maps of average maximum herbaceous cover identify areas dominated by herbaceous cover, and the temporal standard deviation shows

the variation in over a 10-year time period. The maps could be used as an indicator of vegetation condition in relation to water balance, nutrient flow, and biomass in sparsely wooded area (Ludwig et al. 2000; Ludwig et al. 2002; Bastin et al. 2002; Bastin & Ludwig 2006).

The woody fractional cover was validated by comparing the fPV_{woody} and Landsat persistent green product, which shows strong agreement ($r^2 \approx 0.99$). The fPV_{woody} was then compared to Orbview-3 image classifications. Given that the Orbview-3 images captured mainly non-forest areas during the dry season, this comparison provided a closer examination of the performance of the fPV_{woody} at the low end of the woody coverage scale. The result suggested overall strong linear correlation. There was an offset in the intercept value for the fPV_{woody} validation curve of about 0.1 units; this meant that MODIS data estimated 10% tree cover where Orbview-3 classification showed no trees were present. This could be explained by the assumption that 10% of the seasonal variation in NDVI is contributed by woody vegetation (Lu et al. 2003).

The $fPV_{herbaceous}$ was also validated against Orbview-3 image classifications, providing a relationship and R^2 value. The validation of *f*NPV produced different regression lines for northern and southern image locations, with regression coefficients substantially less than 1.0. A reason for this could be that the MODIS method would be expected to be more effective at higher fractional covers where *f*NPV would represent more of the surface signal retrieved in a MODIS pixel.

The validation against the ground observations suggests overall less agreement. The low performance could be attributed to: 1) a potential alignment problem between

MODIS and ground measurements as shown between MODIS and Orbview-3 data set; 2) a lack of representativeness of all field observations at 500-meter scale due to the heterogeneous nature of savanna. 3) field measurements focusing on the dry season when most green vegetation coverage was low; and 4) ground measurements assuming that the distribution of the understory is not affected by the "clumpiness" of the overstorey (Guerschman et al. 2012). This assumption could cause problems especially during the dry season because previous studies have suggested that the overstorey could affect soil moisture and hence delay the water restriction in the understory (Maranón et al. 2009). Finally a difference between the validation data and the MODIS estimations can be due to the fact that NDVI and SWIR32 are not only related to the coverage but also to the spectral feature of vegetation, while validation data tends to classify the vegetation into either pure green or complete dry out entities. For example, while MODIS results would consider withering grass in open area as overall low green coverage ($fPV_{herbaceous}$), the field observation or the Orbview-3 grass class would suggest this to be pure green grassland.

As this chapter is a combination of two approaches, assumptions from the approaches are also inherited. Nevertheless, there are some possible problems with those assumptions. Firstly, the mixing of PV, NPV, and BS in the NDVI and SWIR32 space is linear. This assumption is supported by Guerschman et al. (2009), as they suggested a linear mixture relationship in the NDVI and CAI space, and a high linear correlation of SWIR32 with NDVI and CAI. Secondly, the assumption that 10% of seasonal oscillation is contributed by woody cover is overall applicable, but would cause errors when the

woody cover is low or absent. Thus, the contribution of seasonal oscillation needs to be adjusted according to the land cover in future studies.

8. Conclusion

In this chapter, sub-pixel fractional cover of herbaceous, woody, dry vegetation, and bare surface from 2002 to 2011 were delineated for savanna in Australia. The fraction values were derived with linear regression (Guerschman et al. 2009; Guerschman et al. 2012) and STL time series decomposition (Lu et al. 2003) based on 8-day MODIS data. The analysis has shown that the method allows for the description of the features of savanna landscapes. The woody and herbaceous fractional cover could be estimated when compared to Landsat persistent green products and high-resolution (Orbview-3) classification images.

The workflow tested in this chapter is generally suitable for mapping tree/grass dynamics when both tree and grass fractions are significant at 500-meter scale. The original approach was to first unmix the PV, NPV, and BS fractions where, PV and NPV are prevalence. Then *f*PV is decomposed into persistent green and seasonal green. The second approach relied on the assumption that overstory is persistent green and contributes 10% of seasonal variation of *f*PV. This assumption, however, highly depends on local species and climate condition, which need to be tested outside of the Australian savanna. The Cerrado in South America presents a similar vegetation phenology where overstory is prevalently evergreen, and understory contributes to most of the seasonal variation of *f*PV. Thus, the workflow will be tested in South America in the next chapter.

CHAPTER 3 CERRADO FRACTIONAL COVER AND GREEN FRACTION

1. Introduction

Since the proposed integrated method using unmixing and time series decomposition was successfully applied to Australia in Chapter 2, this chapter aims to apply the same approach to define distinct and separate temporal dynamics for the woody canopy and the herbaceous understory in the Cerrado Savanna. This chapter is divided into two sections. First, the data collected from EO-1 Hyperion imagery are used to explore the NDVI-SWIR32 response space. The endmember envelope defined in the NDVI-SWIR32 space is then used in the linear unmixing of *f*PV, *f*NPV, and *f*BS based on MODIS based time series. Second, the time series *f*PV are used to explore the green woody and green herbaceous fractions. Both time series decomposition (Lu et al. 2003) and frequency decomposition will be tested in this chapter.

2. Data

2.1 Satellite data

2.1.1 MODIS NBAR Data

MODIS 8-day 500-meter BRDF adjusted reflectance product (MCD43B4) (Schaaf et al. 2002) was acquired for the Cerrado savanna from January 2002 to December 2011. Time series of NDVI and SWIR32 indices were calculated, then filtered to reduce noise, and the contaminated data were replaced with spline interpolation (Lu et al. 2003). The Cerrado is heavily fragmented by local agriculture activities, then the savanna regions were extracted based on the PROBIO natural land cover classes (year

2004-2006, 1:250,000, based on Landsat 5 - TM) (Sano et al. 2007) and all converted land was removed.

2.1.2 EO-1 Hyperion Data

In total 15 Hyperion images were acquired (Table 4) from the USGS Earth Explorer in order to provide the more exhaustive possible coverage of vegetation types and different phases of phenology (Figure 34). The image pre-processing included: removing the bad bands, de-striping, removing the noise from the short wave infrared region, removing the major water interference regions following a comprehensive suite of procedures, atmospherically correcting the image using ACORN 6.1®, smoothing visible (447 – 854nm) and SWIR bands (864 – 2365nm) separately using the minimum noise fraction (MNF) and weighted running average (Jupp et al. 2002; Apan & Held 2002; Datt et al. 2003; Datt & Jupp 2004). The final images contain 152 bands retaining the following wavelength ranges: 447 – 1114 nm; 1154 nm – 1336 nm; 1487 – 1790 nm; and 1981 – 2365 nm. The images were then geometrically corrected based on the Hyperion L1GST product with the RMSE (Root Mean Square Errors) ranging from 0.3 to 0.6 pixels.

2.1.3 Quickbird-2 Data

Launched in 2001 Quickbird-2 has one panchromatic sensor (resolution: 0.61-0.72m) and four multispectral sensors (resolution: 2.44-2.88m; blue band: 450-520nm; green band: 520-600nm; red band 630-690nm; and near-IR: 760-890nm). Seven Quickbird-2 images were available (Figure 35, provided by Mike Palace) capturing the vegetation phenology from February to September and covering approximately 120 MODIS pixels. Those seven images sample different vegetation types across the whole study region. The multispectral bands with 2.4-meter spatial resolution were fused with

the 0.6-meter panchromatic band. The results were four pan-sharpened bands of 0.6-meter spatial resolution images.

Table 4. Hyperion Images analyzed for end-member determination

ACQ_DATE	Latitude	Longitude
2001/07/18	-10.062	-50.043
2001/07/20	-15.916	-48.077
2001/08/19	-10.130	-50.050
2001/08/21	-15.878	-48.064
2003/02/09	-9.525	-45.057
2003/05/23	-15.523	-48.009
2003/06/24	-12.134	-48.326
2004/03/23	-13.051	-58.315
2004/03/31	-5.708	-44.068
2006/05/27	-18.115	-52.993
2006/06/16	-18.197	-53.012
2006/08/22	-18.208	-53.015
2007/04/22	-18.148	-52.999
2008/07/27	-18.203	-53.012
2008/09/19	-18.216	-53.018

2.1.4 RapidEye Data

The RapidEye imagery has a 5-meter pixel resolution and 25km by 25km swath. RapidEye has five bands: Blue (440nm - 510nm); Green (520nm – 590nm); Red (630nm - 685nm); Red Edge (690nm - 730nm); and Near IR (760nm - 850nm). Three available RapidEye images were acquired on August 30, 2012 (Figure 35). All three images were located in the Brasilia national park region (provided by Mercedes Bustamante).

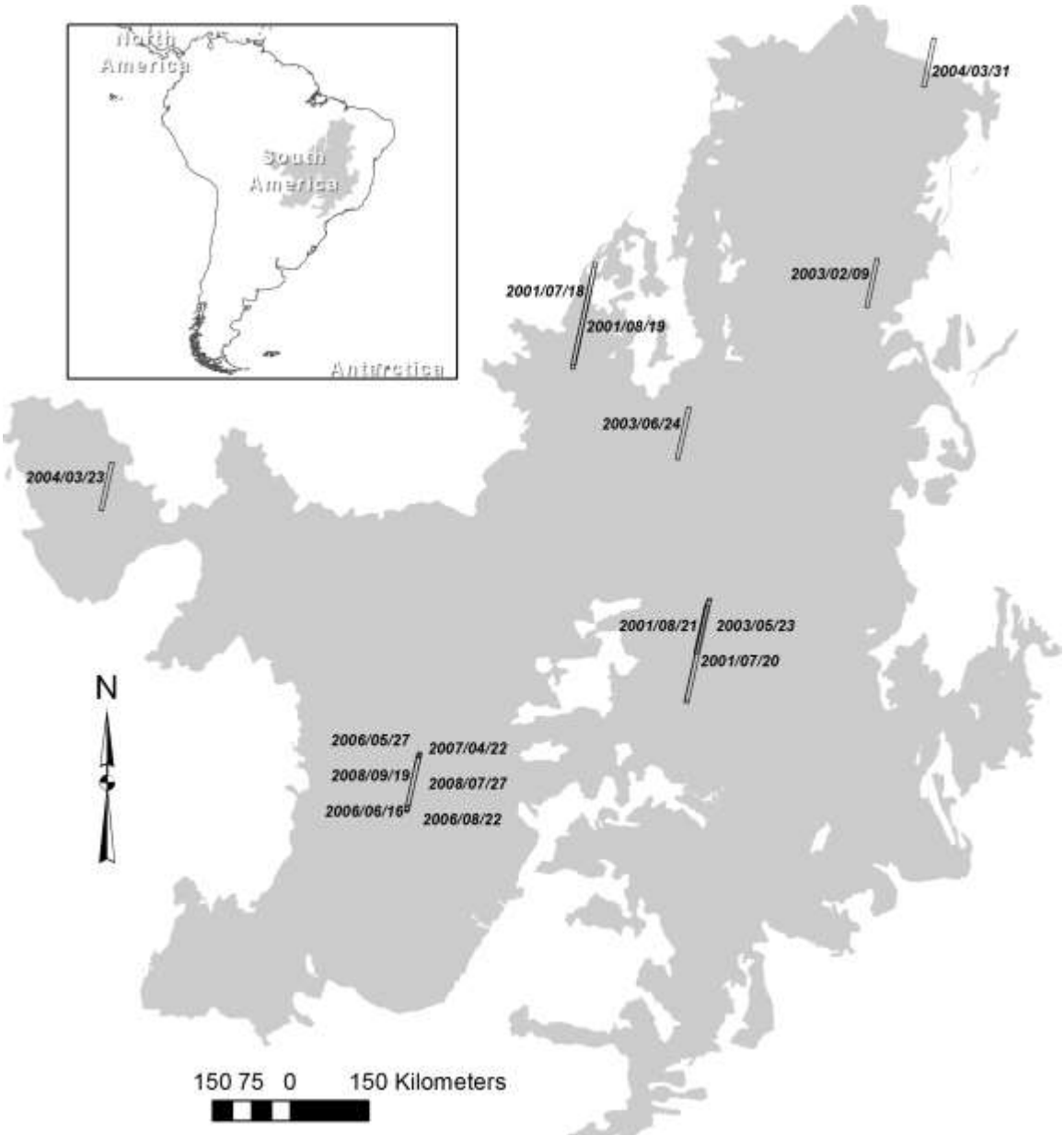

Figure 34. The location of the EO-1 images collected for determine unmixing endmembers

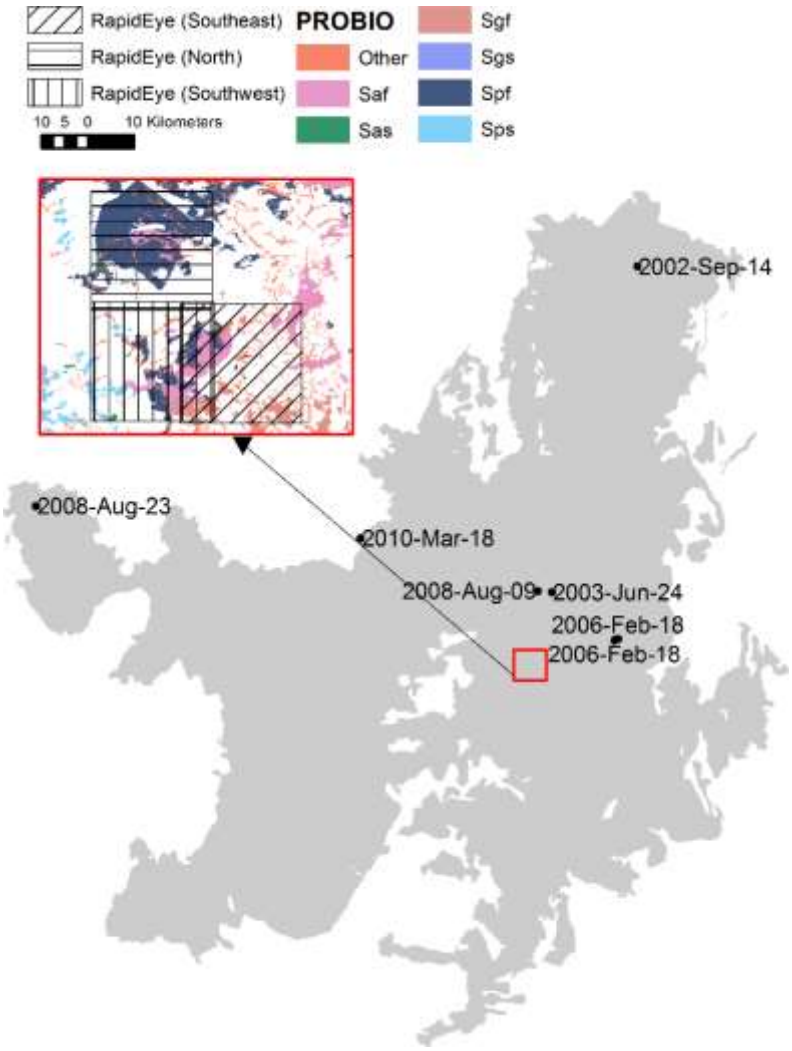

Figure 35. Location of RapidEye and Quickbird imagery used in validation

2.2 Ground Data

2.2.1 Cerrado Fuels survey

Ground measurements were extracted from the United States Department of Agriculture (Ottmar et al. 2001) stereo photo survey to quantify Cerrado fuels. The measurements were collected during the dry season (July and August). According to the vegetation structure, the observation sites were grouped into five series: *campo limpo* (CL), *campo sujo* (CS), Cerrado *ralo* (CR), Cerrado *sensu stricto* (CSS), and Cerrado *denso* (CD). Each site was surveyed with a field of view angle of 32 degree within a 45.7-meter radius. The measurements included elevation, year since last fire, grass height,

grass inflorescences height, understory height, tree height, canopy cover, woody biomass, tree biomass, grass biomass, dicots biomass, litter biomass, percentage cover of trees with or without foliage, and stem density.

2.2.2 Terrestrial Precipitation: 1900-2010 Gridded Monthly Time Series

Monthly precipitation data (mm) from 2002 to 2010 were acquired from NASA's Innovation in Climate Education (NICE) Program (Matsuura & Willmott 2012). The precipitation data from station were compiled from several updated sources and interpolated to a 0.5 by 0.5 degree latitude/longitude grid. The precipitation data associated with the Cerrado fuel survey were used to validate the vegetation fractional cover. The average precipitation during the dry season (July and August) over nine years was calculated to match the fuel survey.

3. Analysis

The analysis involved the following steps: i) specifying the end-members response envelope from Hyperion imagery; ii) calculating the *f*PV, *f*NPV and *f*BS by linear unmixing of MODIS NDVI and SWIR32 images; iii) exploring and decomposing the different phenology of woody and herbaceous vegetation; iv) validating *f*PV, *f*NPV, and *f*BS against RapidEye imagery; v) validating fractional cover against Quickbird imagery; vi) validating the fractional cover against ground observations and precipitation; and vii) mapping fPV_{woody}, $fPV_{herbaceous}$, and *f*NPV.

3.1 Exploration of geographic variation in NDVI and SWIR32 endmembers in EO-1 Hyperion imagery

Scatterplots of NDVI versus SWIR32 were constructed using two data sets: Hyperion simulated MODIS indexes (30 meter); MODIS average indexes at the yearly maximum (and minimum) NDVI period (500 meter). The Hyperion data set aims at

capturing pure pixels of NPV and BS during the dry season, and the MODIS data set aims at capturing pure pixels of PV when vegetation reaches a peak of leaf flushing. The endmembers were selected using the same procedure described in chapter 2.

3.2 Linear unmixing of MODIS NDVI and SWIR32 images using refined endmembers

A linear unmixing approach was applied for each pair of NDVI and SWIR32 images in the time series, following the method described in Chapter 1.

3.3 Exploration and Decomposition of phenology characteristics of woody and herbaceous vegetation

In this chapter, two methods are explored for decomposing the NDVI into woody and herbaceous fractions. Lu et al. (2003) method may not be well suited to the Cerrado site because the different vegetation phenology characteristics were defined from the Australian savanna site. One of the important differences is the assumption that 10 percent of seasonal variation comes from the woody layer. Vegetation data (Ottmar et al. 2001) show that the herbaceous understory of the Cerrado is intermingled with small dicots, palms and woody plants in patchwork of more or less woody associations, meaning that a distinct layer structure of woody and herbaceous plants is not consistently present. This section therefore explores two methods for decomposing the *f*PV into woody and herbaceous components: the frequency decomposition method outlined in Chapter 1 (section 4.3), and the method of Lu et al. (2003) outline in Chapter 1 (Section 4.2) and applied in Chapter 2.

The frequency decomposition method is able to dynamically detect the proportion of seasonal variation from the woody and herbaceous phenology, though it is incapable of separating the baseline of trees from that of grass vegetation. The method of Lu et al. (2003) sets both seasonal variation and baselines to a constant value. These constant

values represent the average condition of the overall study area, but because they do not distinguish between vegetation species and structures, are unable to indicate the diversity at those sites.

3.3.1 Frequency Decomposition

The amplitude and phase of the first three harmonics were used to explore the time series characteristics of the Cerrado vegetation. Then significant frequencies from yearly to monthly variation at the USDA sites were compared in order to test the effectiveness of distinguishing the woody and herbaceous vegetation using selected frequencies.

In order to extract the typical phenology pattern of woody and herbaceous vegetation in Cerrado, both time series of NDVI and *f*PV were used. The woody and herbaceous phenology patterns were extracted by implementing the following processes: (1) extracting key frequencies that define seasonal variations (yearly to monthly); (2) classifying the key frequency images using the ISODATA unsupervised classification approach; (3) calculating the pure pixel index (PPI) (Boardman 1994) and the average index value for individual classes; (4) identifying the "pure" pixels that represents the typical phenology patterns based on the PPI and the high resolution images from Google Earth; 5) calculating the average *f*PV time series for woody and herbaceous pixels.

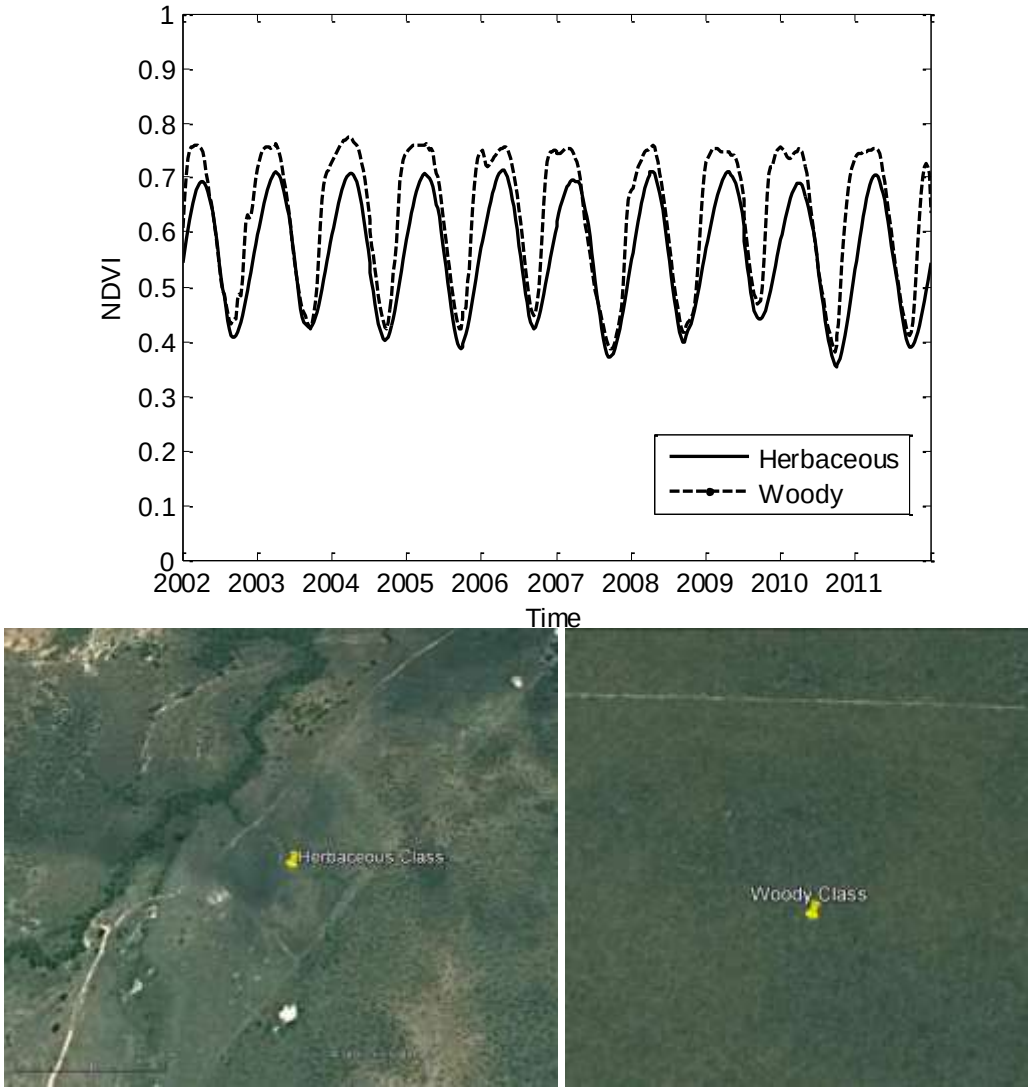

Figure 36. The distinctive growing patterns selected for frequency decomposition and the example of landscapes from Google Earth

By comparing the time series of classes via PPI and Google Earth over the whole study region, two growing patterns were selected (Figure 36) for the frequency unmixing. The first pattern indicates that vegetation starts flush leaves later and slower than the second pattern. The second pattern retains most of its leaves longer than the first type of vegetation. Figure 36 shows examples of the two types of vegetation on Google Earth. The first growing pattern (geographic location: -7.714, -47.899) is used to represent the

herbaceous vegetation and the second growing pattern (geographic location: -11.458, -44.630) to represent the woody vegetation.

The frequency decomposition was then applied on the *f*PV time series by following the method described in chapter 1. The fPV_{woody} was calculated as the slow varying baseline with the woody seasonal oscillation while the herbaceous seasonal oscillation was as calculated as $fPV_{herbaceous}$.

3.3.2 Time Series Decomposition

The method of Lu et al. (2003) was tested in the Cerrado by adjusting parameters based on particular metrics from the time series of NDVI. One of the essential parameters to be regulated is the proportion of seasonal variation attributable to the woody components. Moreover, in order to represent the grass component during dry season, the baselines NDVI values for grass had to be defined.

The proportion of the woody seasonal variation (λ) is calculated based on the grass seasonal variation from the "CL" group and dense woody seasonal variation from the "CD" group. Thus, Vw and Vg can be solved

$$V_s = f_{cc}V_w + (1 - f_{cc})V_g \qquad \textit{Equation 29}$$

$$\lambda = \frac{V_w}{V_w + V_g} \qquad \textit{Equation 30}$$

Vs, Vw, and Vg are seasonal variations of NDVI, pure woody vegetation, and grassland respectively, while fcc is the canopy cover. The canopy cover is known from the fuel survey for each site, and Vs can be extracted based on the location of sites. Then Vw and Vg can be estimated and the average λ can be calculated ($\lambda = 0.26$).

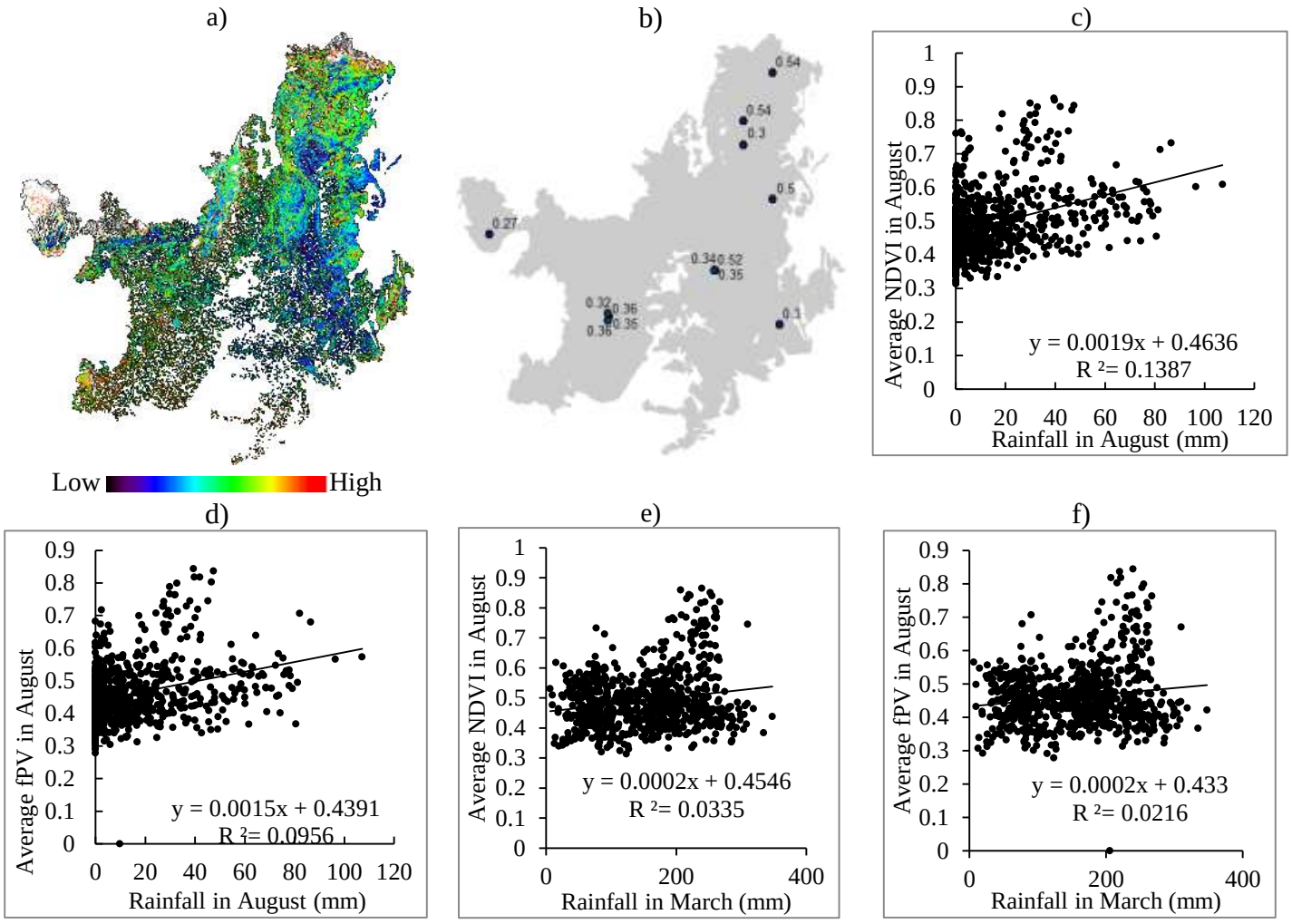

Figure 37. Procedure of determine woody/herbaceous baseline. A) NDVI at dry season; b)NDVI of grassland at dry season; c) scatter plot of rainfall versus NDVI at dry season; d) scatter plot of rainfall versus fPV at dry season; e) scatter plot of wet season rainfall versus NDVI at dry season; f) scatter plot of wet season rainfall versus fPV at dry season

In order to determine the baseline of green grass, the NDVI during dry season is mapped (Figure 37 a), b)). The dry seasonal NDVI is displayed at "CL" sites and other grasslands selected from Google Earth. The result shows that the baseline varies from 0.27 to 0.54. Figure 37 c) and d) shows that the proportion of green vegetation during the dry season depends on water availability. Figure 37 e) and f) show a bottom at around 0.35, which indicates the range of grassland baseline.

3.4 Validation of PV-NPV- BS Fractional Cover against RapidEye Imagery

The RapidEye images were classified into 30 classes using the unsupervised classification method and integrated into PV, NPV, BS and water. The *f*PV, *f*NPV, and *f*BS were then estimated based on the grid defined by MODIS images. This procedure assumes that PV, NPV, and BS components are commonly predominant at the 5-meter scale. The assumption, however, is precarious due to the highly mixture of woody and herbaceous vegetation in most of the Cerrado region.

3.5 Validation of Fractional Cover against Quickbird Imagery

The Tasseled Cap transformation was applied on the fused Quickbird images to convert the spectrum into Greenness, Brightness and Wetness. The transformation was first developed using the Landsat TM dataset (Kauth & Thomas 1976; Crist & Kauth 1986) and later applied to Quickbird by (Yarbrough et al. 2005).

$$T_{Brightness} = 0.319R_{blue} + 0.542R_{green} + 0.49R_{red} + 0.604R_{nir} \quad \textit{Equation 31}$$

$$T_{Greenness} = -0.121R_{blue} - 0.331R_{green} - 0.517R_{red} + 0.78R_{nir} \quad \textit{Equation 32}$$

$$T_{Wetness} = 0.652R_{blue} + 0.375R_{green} - 0.639R_{red} - 0.163R_{nir} \quad \textit{Equation 33}$$

The Tasseled Cap indices were classified into 30 classes using the unsupervised classification method and integrated into green tree, green herbaceous vegetation, NPV,

BS, and water. The fPV_{woody}, $fPV_{herbaceous}$, fPV (green tree and green herbaceous vegetation), $fNPV$, and fBS were then estimated based on the grid defined by the 500-meter pixel of MODIS images. Each grid represents one MODIS pixel.

3.6 Validation of Fractional Cover against Cerrado Fuel survey and Climate data

Average of fractional cover from July and August were calculated to be compared with the fuel survey. Stepwise multiple regression and least square analysis were used to test the relationships between the fractional cover and field observed vegetation information. Statistics of monthly rainfall data were also used to interpolate the validation.

Table 5. Parameters used for validation

Fuel Survey Variable	Comment	Climate Variable	Comment
YrSB	Years since last fire	Precipitation_mean	mean
GHt1	Grass Mean Height	Precipitation_sd	standard deviation
GHt2	Grass inflorescences Mean Height	Precipitation_median	median
UHt	Understory Height	Precipitation_trimmed	trimmed mean (with trim defaulting to .1)
Cover	Canopy Cover	Precipitation_mad	Median absolute deviation (from the median)
BiomT	Woody material Biomass	Precipitation_min	minimum
BiomTree	Tree Biomass	Precipitation_max	maximum
BiomG	Grasses Biomass	Precipitation_range	range
BiomD	Dicots Biomass	Precipitation_skew	skew
BiomL	Litter Biomass	Precipitation_kurtosis	kurtosis
BiomTot	Total Biomass	Precipitation_se	standard error
WHt	Tree Mean Height		
X.Fol	Tree Percentage of total		
StemDens	Tree Density		

Time series of fractional cover of NPV, green woody, and green herbaceous vegetation were also plotted for the Fuel survey sites in order to test the phenology characteristics of different vegetation structures.

3.7 Mapping fractions of green woody and herbaceous cover and dry vegetation cover

The outputs of the overall model include 8-day time series of fPV_{woody}, $fPV_{herbaceous}$, *f*NPV and *f*BS from 2002-2011. The RGB color ramp was used to illustrate the average monthly distribution of fPV_{woody} (green), $fPV_{herbaceous}$ (red), and *f*NPV (blue). The dark areas suggest prevalent bare surface while vegetation is sparse.

4. Result

4.1 Exploration of geographic variation in NDVI and SWIR32 endmembers in EO-1 Hyperion imagery

Both EO-1 Hyperion and MODIS reflectance spectra formed the triangular shape in the NDVI/SWIR32 space (Figure 38). The endmembers extracted from the individual data sets were also displayed. The Hyperion endmembers cover triangles formed by MODIS data, thus our study selects the Hyperion endmember set for the unmixing.

PV: NDVI = 0.98, SWIR32 = 0.24

NPV: NDVI = 0.08, SWIR32 = 0.57

BS: NDVI = 0.07, SWIR32 = 1.00

4.2 Results of Frequency Decomposition

The first five harmonics over the fuel survey sites were plotted in Figure 39. The harmonics were grouped and colored from lightest woody density ("CL") to heaviest woody coverage ("CD"). The plots show that:

1. The most significant (high amplitude) harmonics appears at only the first two frequencies;

2. Woody vegetation tends to have lower amplitude at the first two harmonics than herbaceous vegetation

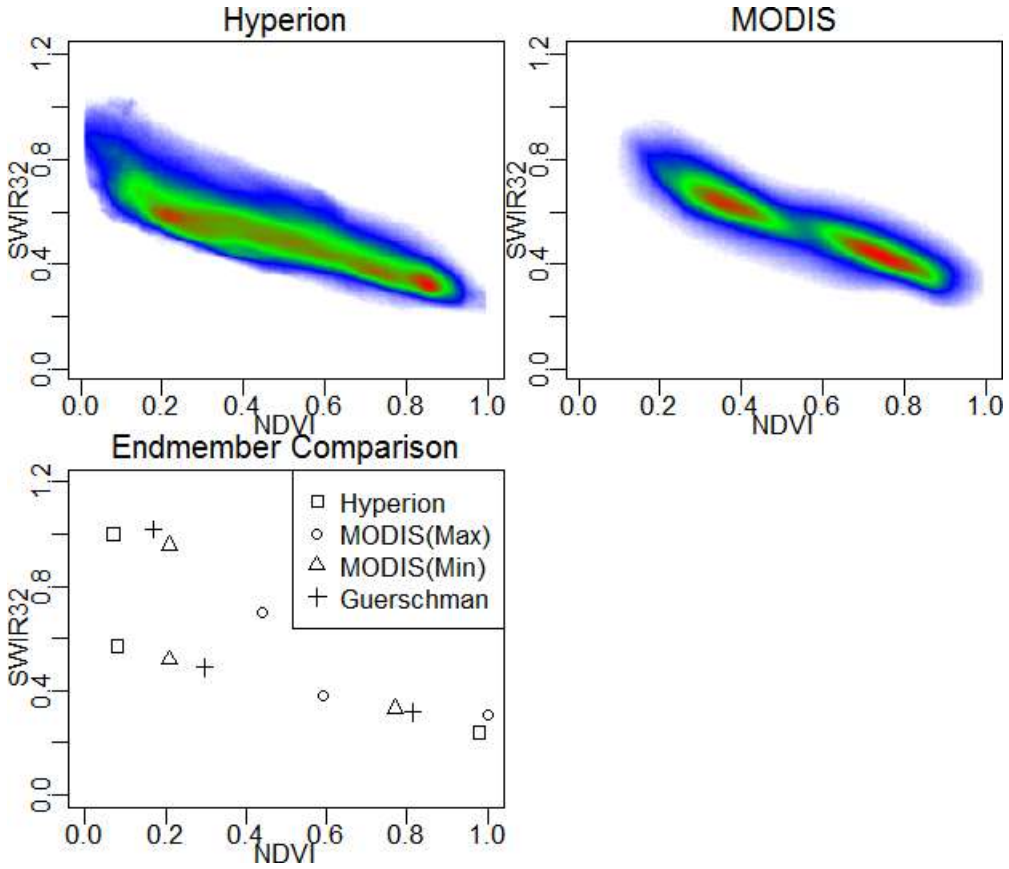

Figure 38. Distribution of the potential endmembers extracted from Hyperion imagery and MODIS compared with the selection from Guerschman et al. (2009).

The phase shows a similar pattern at the first frequency except for two heavy woody vegetation sites.

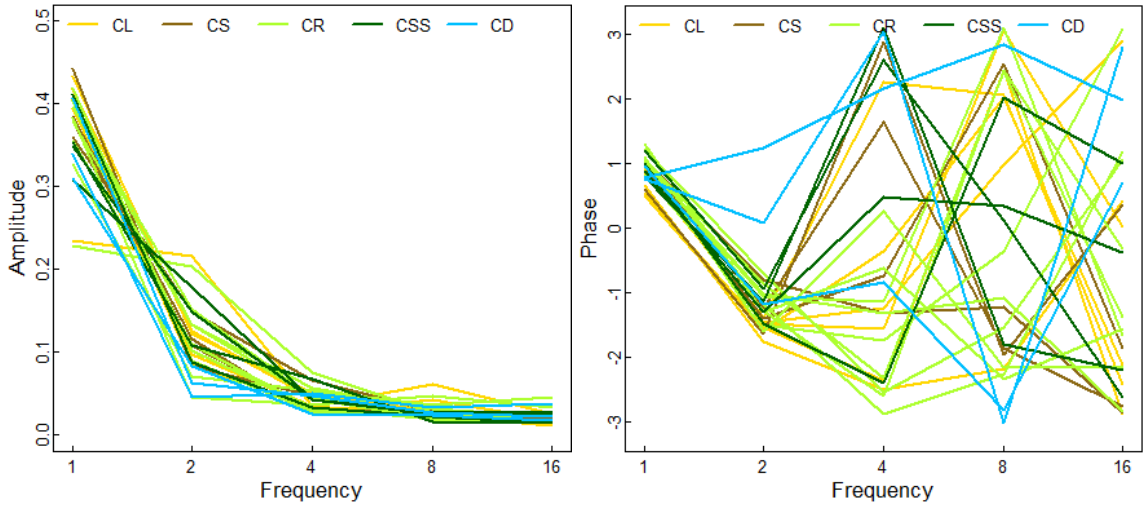

Figure 39. NDVI FFT amplitude and phase (first five components) in Fuel survey sites. The sites are colored in groups of vegetation structures.

The amplitude and phase of the first three harmonics were mapped in Figure 40 and Figure 41. The amplitude map indicates the strength of variations at different frequencies. The red color means significant single annual pulse that may suggest the dominance of single phenology, while the yellow color suggests an overall annual pulse and two types of distinctive phenology. The blue color shows the wetland areas of the study region. The phase map, on the other hand, shows overall less variation.

Figure 42 shows the dynamics of green vegetation fraction and its gradual senescence for the fuel survey sites. In general, the woody vegetation fractional cover should increase from "CL" (*Campo limpo*) to "CD" (*Cerradao*). However, the method retrieves a high proportion of green woody vegetation at the "CL" (*Campo limpo*) grassland sites, suggesting that the algorithm is unable to consistently distinguish between woody and herbaceous NDVI signals. This suggests that there is no basis for consistently separating woody and herbaceous dynamics using a frequency decomposition approach as there is no consistent phase of amplitude difference on which to base discrimination.

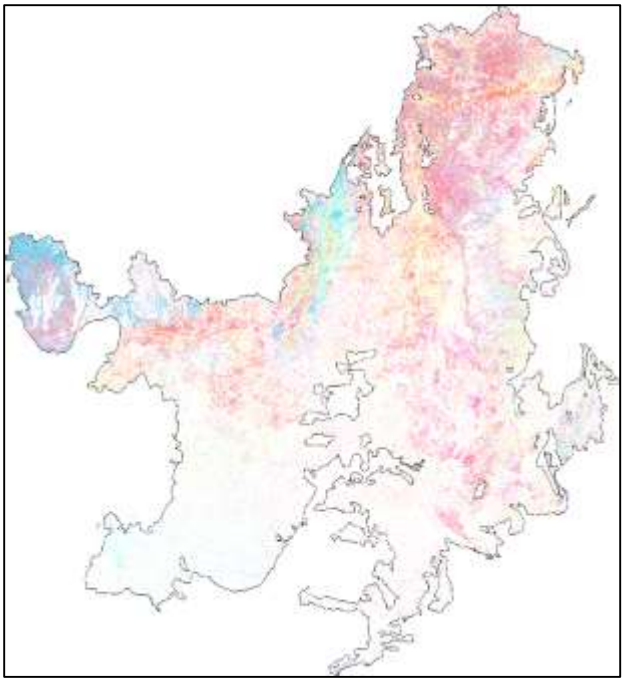

Figure 40. NDVI FFT amplitude (first three components) for the Cerrado savanna zone. The value is show in Red (first harmonic), Green (second harmonic), and Blue (third harmonic).

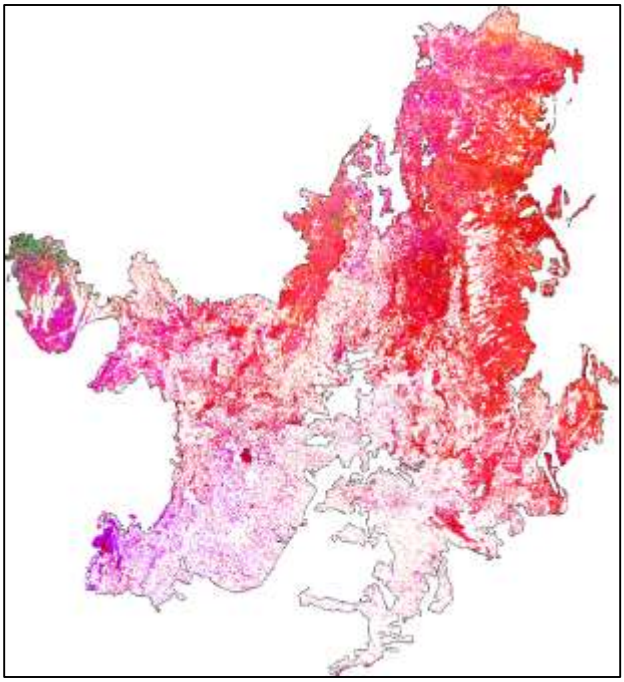

Figure 41. NDVI FFT phase (first three components) for the Cerrado savanna zone. The value is show in Red (first harmonic), Green (second harmonic), and Blue (third harmonic).

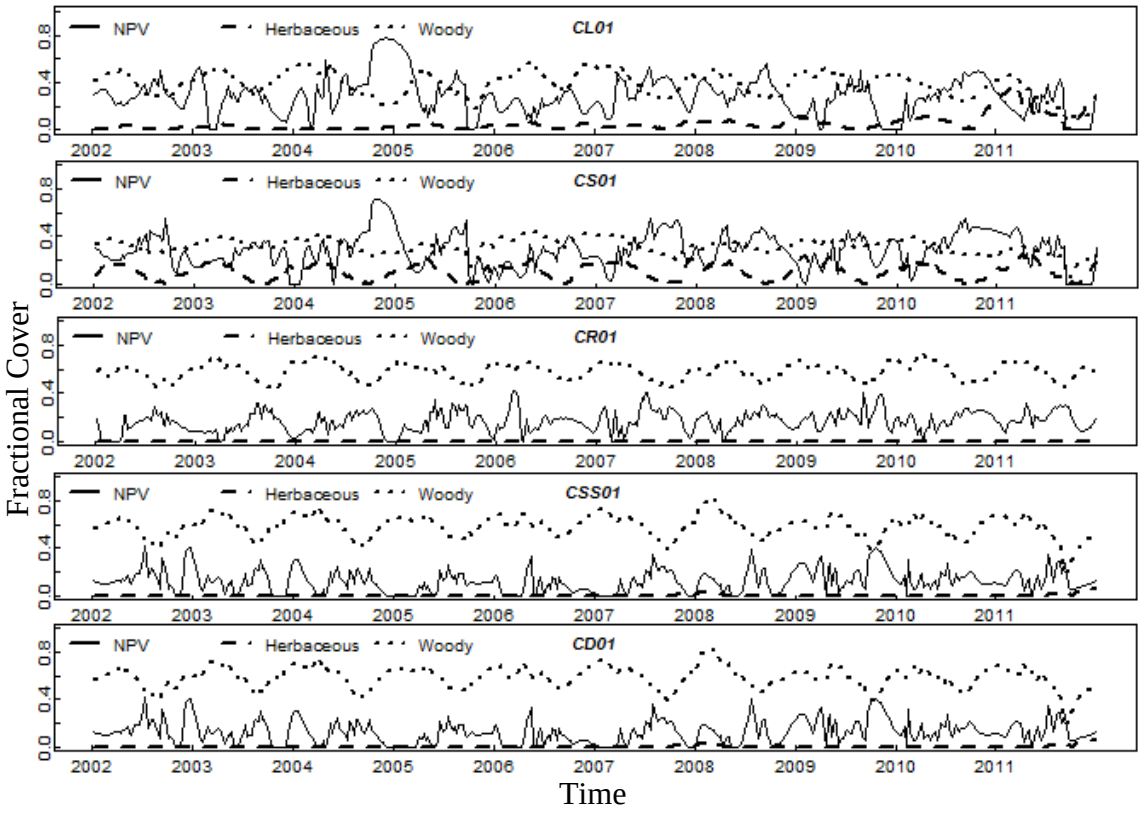

Figure 42. Examples of time series of fNPV, fPV_{Woody}, and $fPV_{Herbaceous}$ for different vegetation structures based on fuel survey.

4.3 Results of Time Series Decomposition

The *f*PV was decomposed into fPV_{woody} and $fPV_{herbaceous}$ using the grass baseline values equal to 0.3 (Figure 43, left) and 0.35 (Figure 43, right). The different baselines produce similar results. The *Campo limpo* and *Campo sujo* sites have high herbaceous fractional cover and a near-zero woody component. The average woody fractional cover generally increases from the "CL" group to the "CSS" group (from 0.03 to 0.09 when the grass baseline is 0.35). However, woody fractional cover is underestimated in dense woody areas. This indicates that Lu's et al. (2003) method with the grassland baseline is limited when separating the highly mixed Cerrado vegetation.

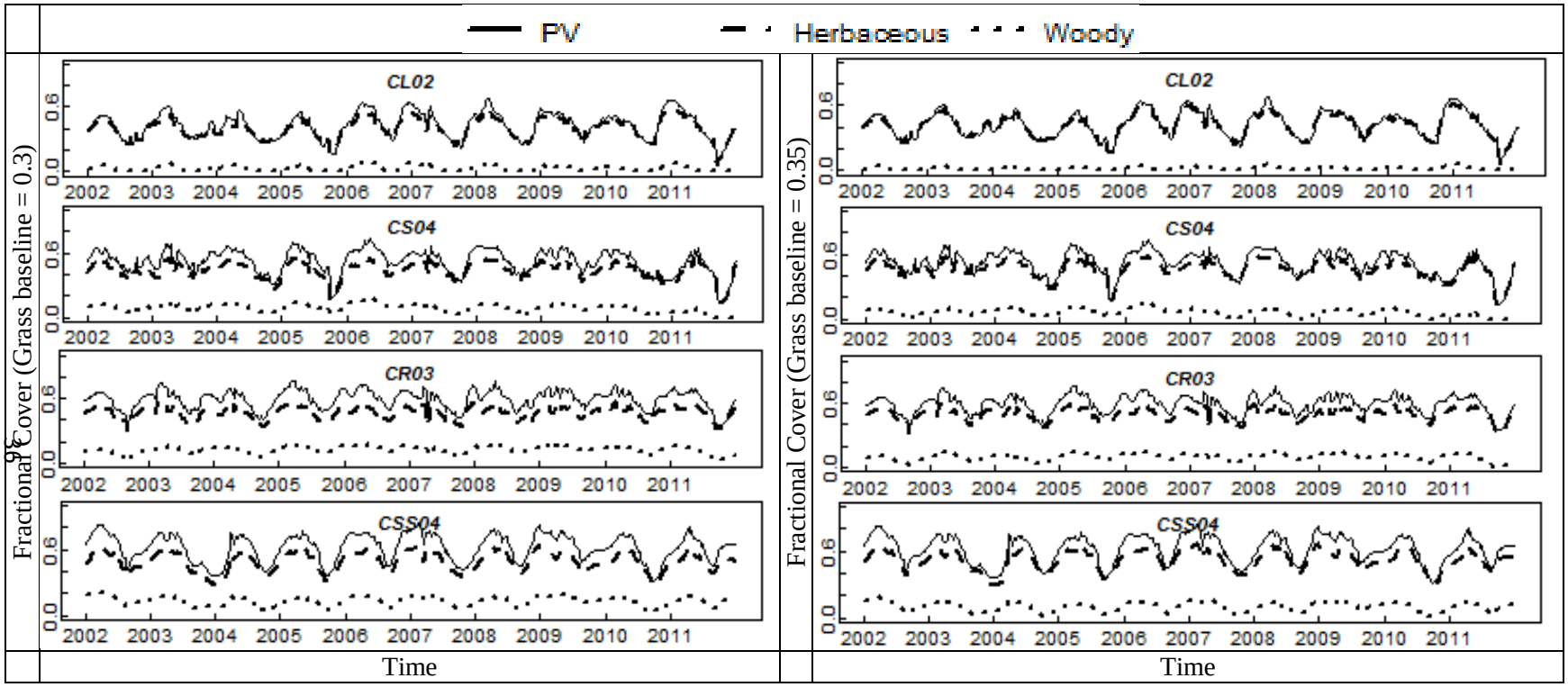

Figure 43. Decomposition input fPV into fractional cover of woody and herbaceous components for fuel survey sites. Grass baseline equal to 0.3 (left) and 0.35 (right)

4.4 Validation of fPV, fNPV, and fBS against RapidEye Imagery

The respective scatter plots of the RapidEye derived *f*PV, *f*NPV, and *f*BS versus the MODIS estimation are shown in Figure 44. The linear regression shows higher r-squared for *f*PV, and *f*BS. All three comparisons show less variation from MODIS fractional cover. The linear regression indicates that MODIS fractional cover tend to overestimate the low fractional cover, but underestimate the high fractional cover compared to the RapidEye classification. The MODIS fractional cover ranges between 0 and 0.6, while the RapidEye suggests ranges from 0 to 1.0. The possible reason is that RapidEye classified tree/grass mixture into pure PV, NPV, and BS at 5-meter scale, which essentially categorized vegetation structures instead of pure components. This classification gave overestimation of one component and underestimation of the rest, which exaggerated the fractional cover variations.

4.5 Validation of Fractional Covers against Quickbird Imagery

Figure 45 shows the validation of *f*BS, *f*NPV, *f*PV, and frequency derived fPV_{woody} and $fPV_{herbaceous}$ against Quickbird imagery. The linear regression shows that the two data sets produced similar results on fractional cover of photosynthetic vegetation and green woody vegetation. Non-photosynthetic vegetation and green grass, however, have little coverage in the Quickbird images. The *f*BS validation, on the other hand, is clumped by image date and suggests different linear correlation. The disagreement confirms the different linear relationship of *f*NPV in the Australian savanna validation, and suggests a lower sensitivity for SWIR32 to distinguish *f*NPV and *f*BS components. Nevertheless, the MODIS estimation still captures the variation of fractional cover at the RMSE range from 0.13 to 0.19.

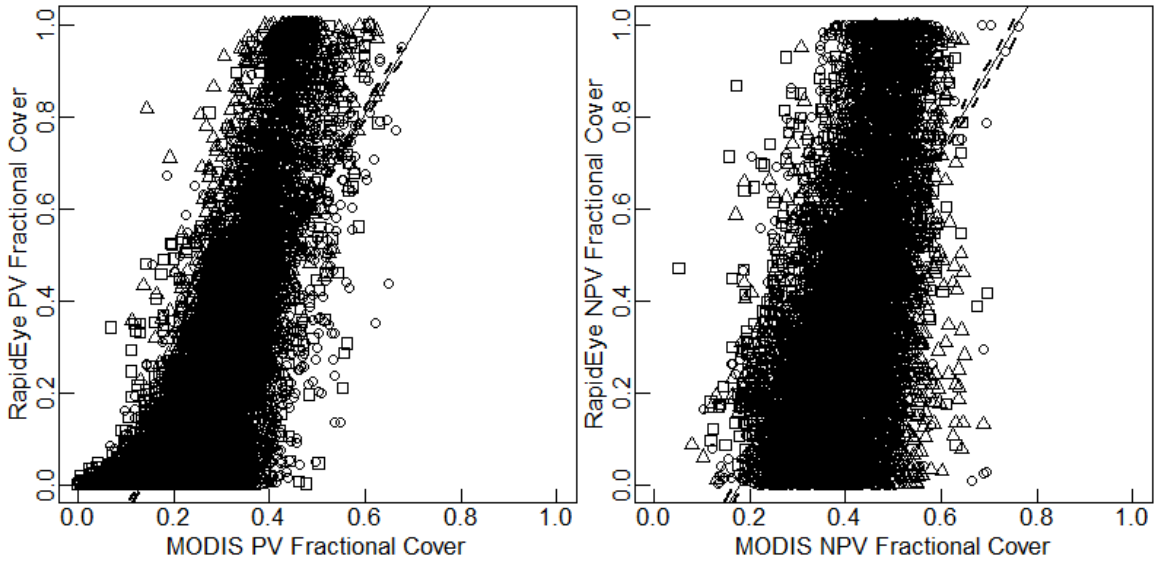

y=1.73x-0.23

R^2: 0.5 RMSE: 0.21

y=1.73x-0.31

R^2: 0.26 RMSE: 0.27

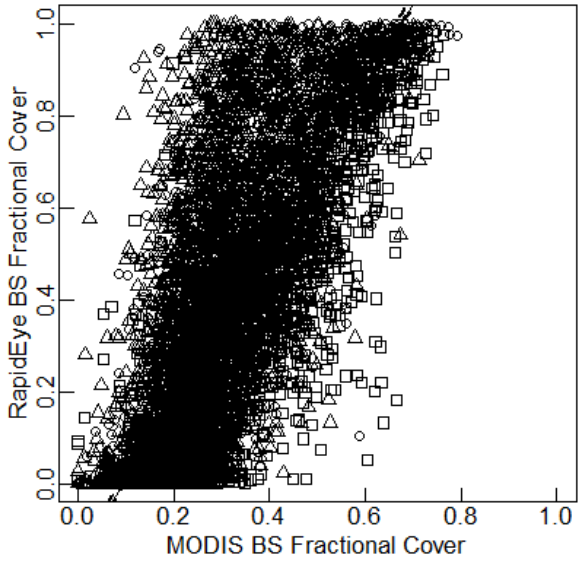

y=1.73x-0.16

R^2: 0.6 RMSE: 0.24

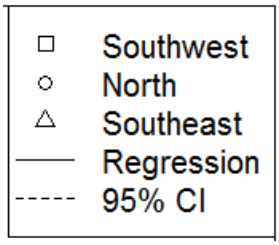

Figure 44. Linear relationship between the MODIS PV, NPV, and BS fraction cover versus the fraction cover based on the RapidEye classification

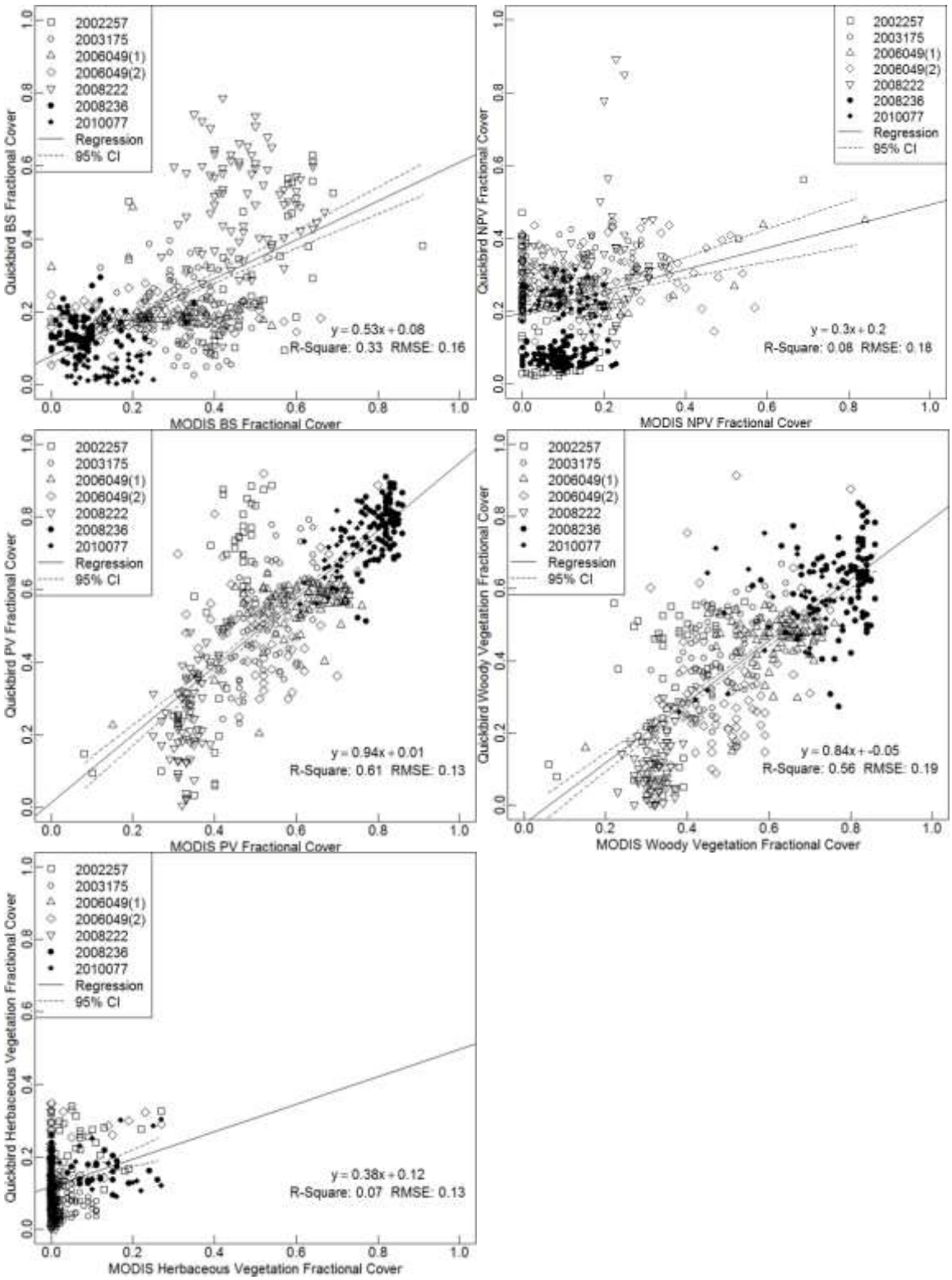

Figure 45. Linear relationship between the MODIS fPV, fNPV, fBS, fPV_{Woody}, and $fPV_{Herbaceous}$, versus the fraction cover based on the Quickbird classification

4.6 Validation of Fractional Cover against Cerrado Fuel survey

Stepwise multiple linear regressions are used to see if remote sensing retrievals of cover fractions can be related to a detailed breakdown of the vegetation cover components described in the USGS Fuel Survey (Ottmar et al. 2001). In addition, precipitation data were included to account for geographical variation of seasonal precipitation patterns across the USGS sites that may have influenced the timing and magnitude of the green canopy development at each site. The result of stepwise multiple regressions suggest the parameters that are most correlated with fractional covers (Table 6), which reveals the biological driver of the fractional cover variation. The first three rows show the fractional cover of PV, NPV, and BS in relation to the field observed vegetation structure and climate variation. As results show, adding precipitation data improves the regression in all three models. The standard deviation of monthly rainfall affects all three components, while the average of overall precipitation mostly affects the coverage of dry vegetation and bare soil during the dry season. For the vegetation survey parameters, woody material biomass is significant in the PV and BS components, while biomass of grass is more correlated with the NPV component. Years since last fire and understory height also affect all three components.

The last two rows show the vegetation structure and rainfall variation in relation to the fraction cover of green woody and herbaceous vegetation from the two decomposition methods. The time series decomposition shows significant advantage for the herbaceous fraction estimation, but a similar performance for the woody fraction. The green woody fractional cover shows correlation with woody related parameters as well as “grass mean height” and “grasses biomass”. The correlation with the understory and grass height indicates the sheltering between woody and herbaceous vegetation due to the

absence of layer structure in the Cerrado. The green herbaceous fraction derived from the time series decomposition shows correlation with various precipitation parameters in comparison to the fraction derived from the frequency decomposition. This is because the frequency decomposition assumes that grass dry out during dry season hence, it is less correlated to rainfall.

Figure 46 shows scatter plots between calculated fraction and predicted value from stepwise regressions. The precipitation shows minor improvement in the multiple linear regressions in *f*PV, *f*NPV, and *f*BS. The time series decomposition gives less variation on both herbaceous and woody fractions. In comparison with the frequency decomposition, the time series decomposition shows overall high herbaceous fraction and low woody fraction which is consistent with the time series in Figure 43.

*4.7 Mapping f*PV, *f*NPV *and f*BS

Since neither method for separation of fPV_{woody} and $fPV_{herbaceous}$ gave satisfactory results, a final map product could not be developed. However, validation indicated that the unmixed *f*PV, *f*NPV and *f*BS results were good, so monthly averages of these as RGB composites can be presented (Figure 47). The proportions are shown in RGB as indicated in the color legend. The fractional cover map shows more vertical gradient patterns in comparison to the Australian savanna. As observed, the southwest Cerrado savanna is covered by dense evergreen or semi-deciduous vegetation. The southeast, however, shows a high seasonal proportion of dry vegetation and bare soil. A strip in the northwest shows converse seasonal variation where Greenup starts in May and senescence begins in August. The Brasilia national park is shown for April and August. The subset in April

shows a generally high proportion of green vegetation. The subset in August shows a track of forest along rivers while most of other area is covered by dry vegetation.

Table 6. Results of stepwise multiple regression and r-square of fPV, fNPV, fBS, fPV_{woody}, and $fPV_{herbaceous}$ against fuel survey and precipitation

Unmixed cover fractions	**Regression without Precipitation**	**R^2**	**Regression with Precipitation**	**R^2**
PV	YrSB, UHt, BiomT, BiomL	0.6	YrSB, BiomT, BiomL, StemDens, Precipitation_sd	0.68
NPV	YrSB, UHt, BiomG, BiomL	0.76	YrSB, UHt, Cover, BiomL, Precipitation_mean, Precipitation_sd, Precipitation_trimmed	0.83
BS	YrSB, UHt, BiomT, StemDens, X.Fol	0.70	YrSB, GHt1, UHt, BiomT, BiomD, StemDens, Precipitation_mean, Precipitation_sd, Precipitation_trimmed	0.80
Decomposed green cover fractions	**Time series Decomposition (with precipitation, grass baseline = 0.35)**	**R^2**	**Frequency Decomposition (with precipitation)**	**R^2**
Green Woody	YrSB, GHt1, UHt, BiomT, BiomTree, BiomG, BiomD, BiomL, X.Fol, Precipitation_mean, Precipitation_sd, Precipitation_trimmed Precipitation_mad	0.91	YrSB, GHt1, Cover, BiomT, BiomTree, BiomL, WHt, X.Fol, StemDens, Precipitation_mean, Precipitation_sd, Precipitation_median, Precipitation_trimmed, Precipitation_mad	0.92
Green Herbaceous	YrSB, Cover, BiomT, BiomD, BiomL, X.Fol, Precipitation_mean, Precipitation_sd, Precipitation_trimmed. Precipitation_mad, BiomTot	0.85	YrSB, GHt2, Cover, Precipitation_trimmed, BiomTot	0.50

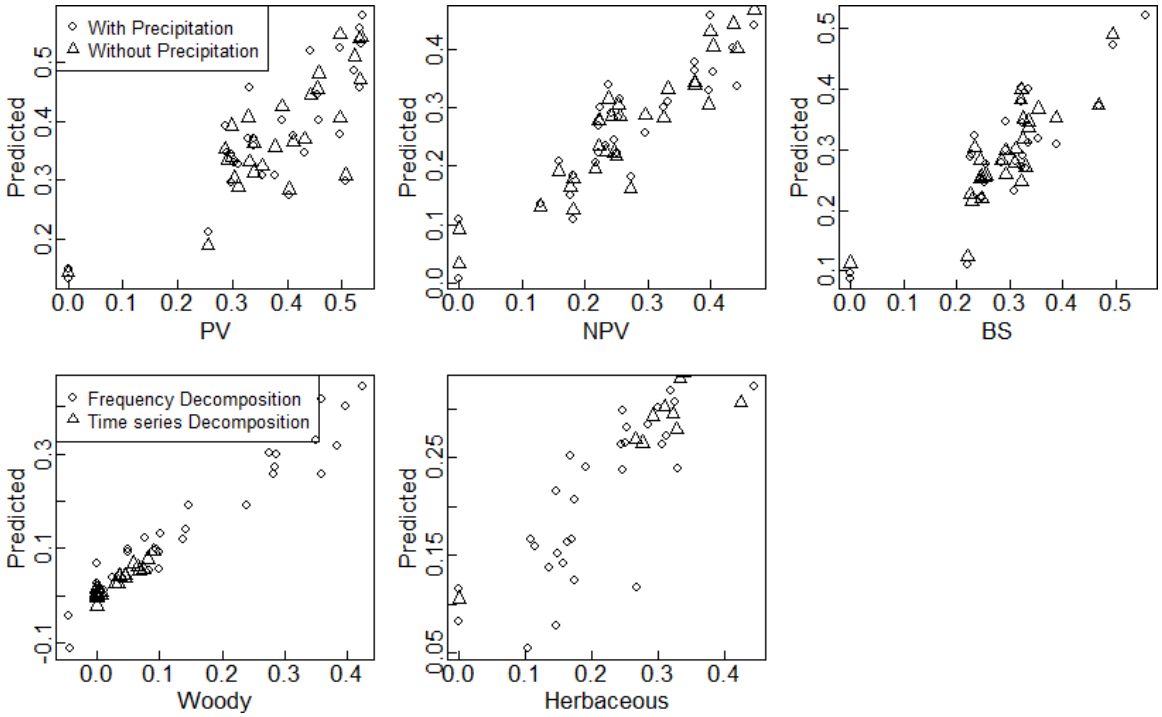

Figure 46. Calculated fraction versus predicted value based on the multiple linear regression in Table 6. The first row compares the regression results w/o precipitation data. The second row compares the regression results of woody and herbaceous fractions from different decomposition methods.

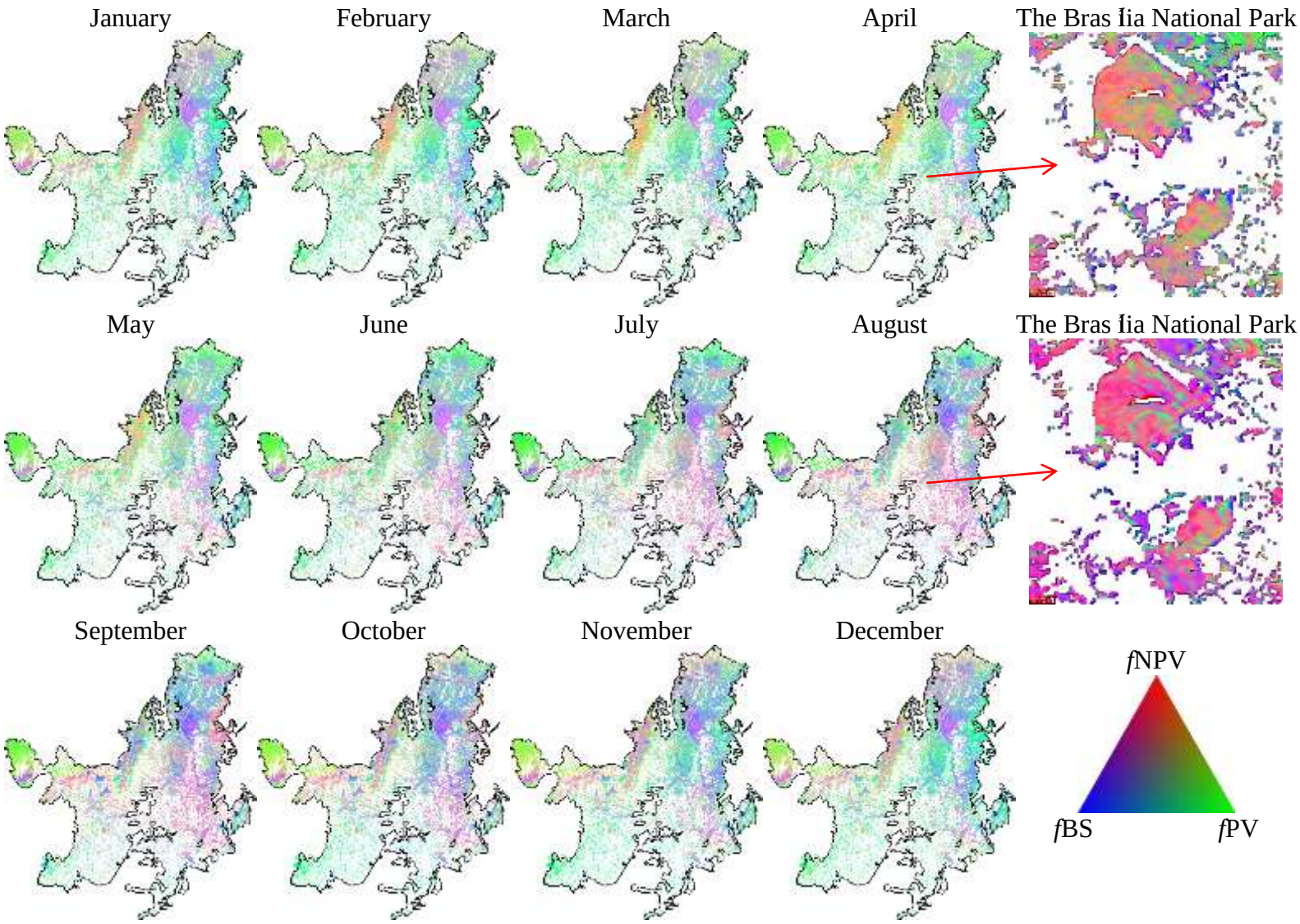

Figure 47. Monthly average of fractional cover for PV, NPV, and BS in the Cerrado savanna zone. The proportions of land covers are shown in RGB as specified in the color legend

5. Discussion

The result shows that *f*PV, *f*NPV, and *f*BS in the Cerrado savanna can be separated within the NDVI and SWIR32 space (Guerschman et al. 2009; Guerschman et al. 2012). Guerschman et al. (2009) found that green vegetation, dry vegetation, and bare soil formed a triangle shape in the NDVI and SWIR32 space and developed the linear unmixing model to estimate the *f*PV, *f*NPV, and *f*BS. On the other hand, Hill et al. (2012) concluded that the response envelope vary across ecoregions and needs to be refined when applied to local landscapes. Thus, this chapter adjusted the endmember envelope based on the local vegetation structure.

Furthermore, this chapter distinguished the green woody (fPV_{woody}) and the green herbaceous ($fPV_{herbaceous}$) vegetation using both the time series and the frequency decomposition. The time series decomposition, first developed by Lu et al. (2003), separated evergreen trees from seasonal grass using NDVI time series. However, the method was based on the Australian tropical savanna vegetation and ignored the effect from bare soil and dry vegetation (Lu et al. 2003). This chapter adjusted the parameters of seasonal variation and baseline for the Cerrado vegetation.

Furthermore, this chapter tested the frequency decomposition to estimate the woody and herbaceous seasonal variation. The approach was developed based on the previous studies that there is distinctive seasonal variation between grass dominated Cerrado and tree dominated Cerrado (Ferreira et al. 2003; De Bie et al. 1998; Higgins et al. 2011). The fPV_{woody} and $fPV_{herbaceous}$ were calculated based on the *f*PV in order to reduce the effect from bare soil and dry vegetation. One of the important assumptions for the frequency decomposition is that pure MODIS pixel of grassland and forest existents

in the study area. The coverage of *Cerradao* (dense woody area) and *Campo limpo* (clean field) provides a sound base for the pixel selection. The *Cerradao* covers 17.1 million ha, while the *Campo limpo* covers 9.4 million ha in Cerrado (Fearnside 2000; Vourlitis & Rocha 2011).

The fractional cover results were validated against the high-resolution imagery. The fractional cover of PV, NPV, and BS were first examined based on three RapidEye images acquired on August 30, 2012. The comparison showed good linear correlation but less variation from the MODIS fractional cover, hence, an overestimation at the low fractional cover and an overestimation at the high fractional cover area. One of the potential reasons for this result is that the vegetation cover at the RapidEye 5-meter resolution is also a mixture of trees, green grass, and dry grass. So when one component is dominant in a RapidEye pixel, others are ignored, causing an underestimation of low fractional cover and an overestimation of the dominant component. The fractional cover results were also validated against Quickbird imagery. The comparison showed better linear correlation with *f*PV, and fPV_{woody}. Both *f*NPV and $fPV_{herbaceous}$ are low over the validation area (mostly less than 0.2), which MODIS data may not be sensitive enough to detect. The better performance of *f*PV could be explained by the shape of the response envelope in the NDVI-SWIR32 space. SWIR32 is a substitute for CAI, however, is less sensitive to dry vegetation (Guerschman et al. 2009). The less sensitivity of SWIR32 leads to more uncertainty from the impacts of different soil backgrounds.

Stepwise multiple regressions were used to validate fractional covers against field observation and precipitation. The regression suggested a strong agreement with PV, NPV, and BS. The time series decomposition showed overall a better performance when

distinguishing woody and herbaceous vegetation. $fPV_{herbaceous}$ derived from the frequency decomposition showed poor agreement with observation, and the regression parameters suggested that covering between woody and herbaceous vegetation may significantly affect the accuracy of estimation.

6. Conclusion

In this chapter, a combined decomposition method, utilizing both spectra and time series analysis, has been built for evaluating fPV_{woody}, $fPV_{herbaceous}$, fNPV, and fBS over the Cerrado region. The spectral analysis was initially developed for the Australia savanna (Guerschman et al., 2009), and this chapter has refined the approach for the Cerrado ecosystem.

This chapter explored both time series and frequency decomposition methods to separate green woody and green herbaceous components. The complex and variable vegetation structure of vegetation and its phenology limited the effectiveness of both Lu et al. (2003) decomposition method and the frequency decomposition method. The time series decomposition showed better agreement at the *Campo limpo* sites; however, it underestimated the woody component of woodland. The frequency decomposition, on the other hand, overestimated woody component at the *Campo limpo* sites as this method is unable to determine a grass baseline. The time series decomposition showed a better estimation at grassland, but the fixed baseline and the seasonal variation may not suit the overall study area. The frequency decomposition performed better in woodland area, but is unsuccessful at some site when herbaceous vegetation remains green during the dry season.

Taking into account the cumulative conclusions from the two decomposition methods applied to the Australian savanna and the Cerrado, the frequency decomposition method will be used for the African savanna where seasonal variation of vegetation widely varies between species but grass completely dries out in winter.

CHAPTER 4 FRACTIONAL COVER RETRIEVAL IN SOUTHERN AFRICA

1. Introduction

Chapter 2 and Chapter 3 discussed the potential of mapping the dynamic fractional cover of overstory and understory in the Australian tropical savanna and the South American savanna. This chapter describes the work undertaken to explore the feasibility of mapping the fractional cover of PV (*f*PV), NPV (*f*NPV), and BS (*f*BS) in the southern African savanna. The African savanna is a highly productive and heterogeneous system (Vanak et al. 2012), where water availability is one of the most significant limitations (Hill et al. 2011). The carbon dynamics of African savanna are of vital global importance in terms of fire emission, land use emission, and degradation (Williams et al. 2007; Nicholson 2000). Accurate estimation of vegetation dynamics of African savanna would be helpful to better understanding global environmental changes. The method used in Chapter 2 for retrieval of the fractional cover of PV, NPV and BS can be applied here. The southern African savanna, however, has very different vegetation types and land cover characteristics. In this chapter, a set of Hyperion images that sample different geographical areas and seasonal variation is again used to establish an African refined version of end-member set for unmixing fractional cover. Since the African savanna is very large, the analysis is carried out over a study area in Southern Africa that samples a wide range of vegetation and climate variation.

The selected area of the southern African savanna samples a gradient of precipitation and a continuum of tree-grass composition ranging from woody savanna semi-deciduous Miombo woodland to deciduous Acacia Baikiaea and Terminalia fine leafed savanna. This area corresponds to a region well studied by the Southern African Fire Atmosphere Research Initiative (SAFARI) 2000 NASA campaign (Scholes & Dowty 2002; Scholes et al. 2004; Privette & Roy 2005; Privette et al. 2004), where some specific sites have been much researched (e.g. Gibbes et al. 2010; Mishra et al. 2014; Mishra & Crews, 2014). Those previous studies with field observations and high resolution fractional cover studies enable better bases for our validation.

2. Study area

The Southern African savanna square covers a continuum of vegetation from dense woody area (Angolan Miombo Woodlands and Central Zambezian Miombo Woodlands) to mixed area (Angolan Mopane Woodlands, Zambezian Baikaiea Woodlands and Zambezian and Mopane Woodlands) and open area (Kalahari Acacia-Baikaiea Woodlands). Ecoregions that are not present in the study area are Etosha Pan halophytics, Western Zambezian grasslands, Zambezian Cryptosepalum dry forests, Zambezian flooded grasslands and Zambezian halophytics as defined by the Terrestrial Ecoregions of the World (Olson et al. 2001). From north to the southeast following precipitation gradients, the vegetation shifts from woodlands and open deciduous forests to arid shrub land (Cowling et al. 2004).

Figure 48 shows land cover types produced from MODIS data (MDC12Q1). The product describes land cover between 2001 and 2010 with 500-meter resolution (Broxton et al., 2014). The map shows a continuum of tree-grass combination from woody savanna

(Northern part) through tree-grass mixture (middle) to grassland (Southeastern part). Figure 49 shows land use characteristics with livestock density from the Soil and Terrain database for Southern Africa (FAO/ISRIC, 2003). The map shows more detail of vegetation structure in the middle part of the study area than Figure 48, which suggests dominance of shrubs in Zambezian and Mopane woodland as well as the western part of the Zambezian Baikiaea woodlands. *Table 7* is the list of primary vegetation combination in the different ecosystems (Burgess et al. 2004; Hill et al. 2011). Typical overstories include: 1) Miombo that often forms a dense coverage, and varies from evergreen to deciduous dominant (Fuller 1999; Chidumayo 2002; Richer 2008; Vancutsem et al. 2009); 2) Mopane is a winter deciduous and mostly forms open woodland (Fuller 1999; Veenendaal et al. 2008); 3) Kalahari, mostly a deciduous, with the dominant pattern varying due to the climate condition.

Table 7. Vegetation characteristics of African savanna ecoregions (Burgess et al. 2004; Hill et al. 2011)

Ecoregions	Tree	Phenology	Grasses
Angolan Miombo Central Zambezian Miombo Southern Miombo	*Brachystegia; Isoberlinia; Julbernardia* spp.	D	*Loudetia; Hyparrhenia; Tristachya* spp.
Zambezian & Mopane Angolan Mopane	*Colophospermum mopane; Combretum; Acacia; Kirkia* spp.; etc.	D	*Aristida; Digitaria; Erarostis; Echniochloa* spp.
Southern Africa Bushveld	*C. mopane; Acacias; Terminalia spp.* *Burkea* spp.	D	*Hyparrhenia* spp.
Zambezian Baikiaea	*Baikaiea plurijuga*	D	Sparse grasses
Kalahari Acacia-Baikiaea	*Lonchocarpus; Terminalia; Burkea; Combretum; Grewia; Acacia; Commiphora* spp.	D	*Aristida; Eragrostis; Heteropogon; Digitaria* spp.

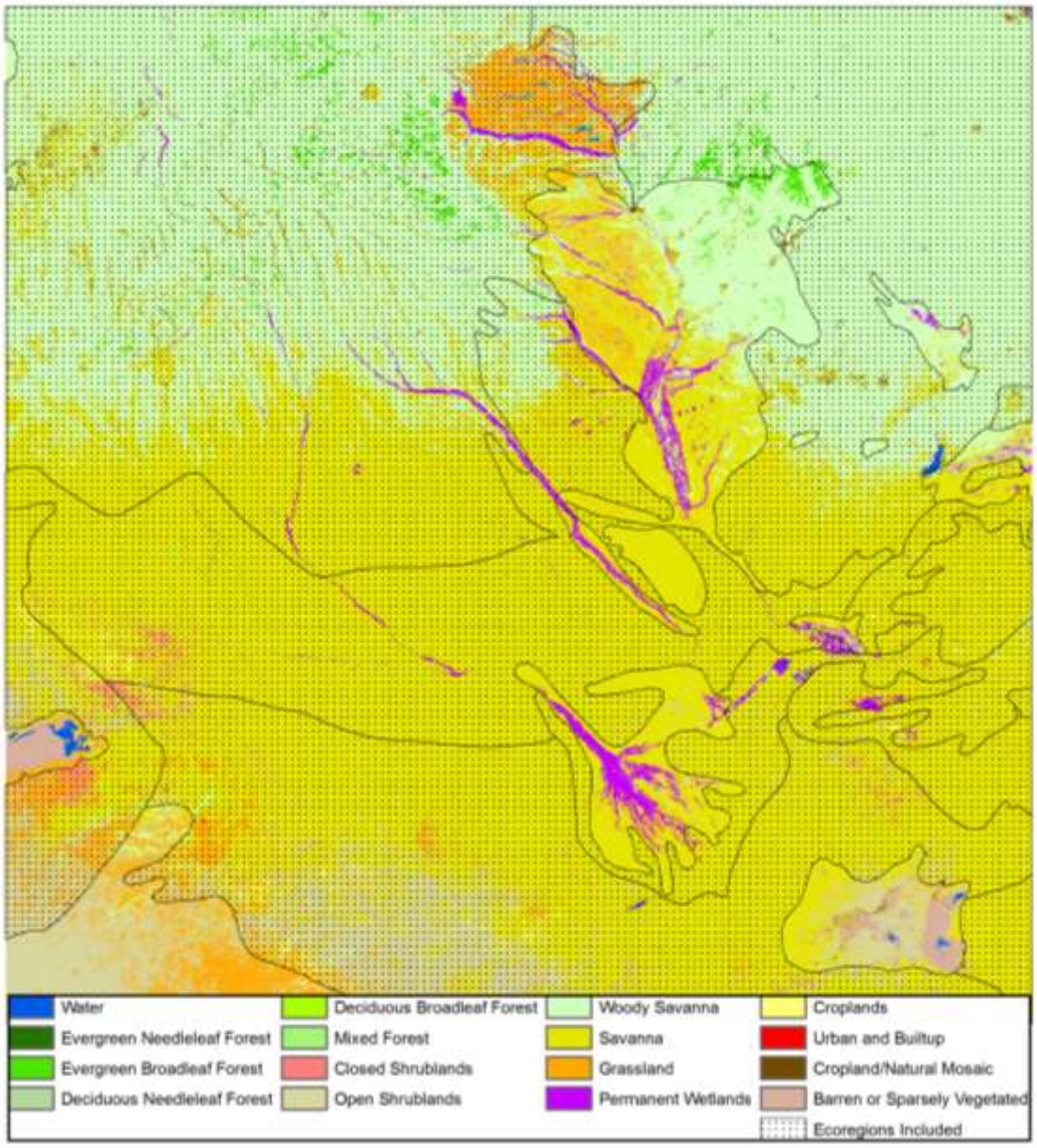

Figure 48. Vegetation, land cover and land use characteristics of the study region. a) MODIS IGBP Land Cover dominant class for 2001-2011 (MDC12Q1) (Broxton et al., 2014)

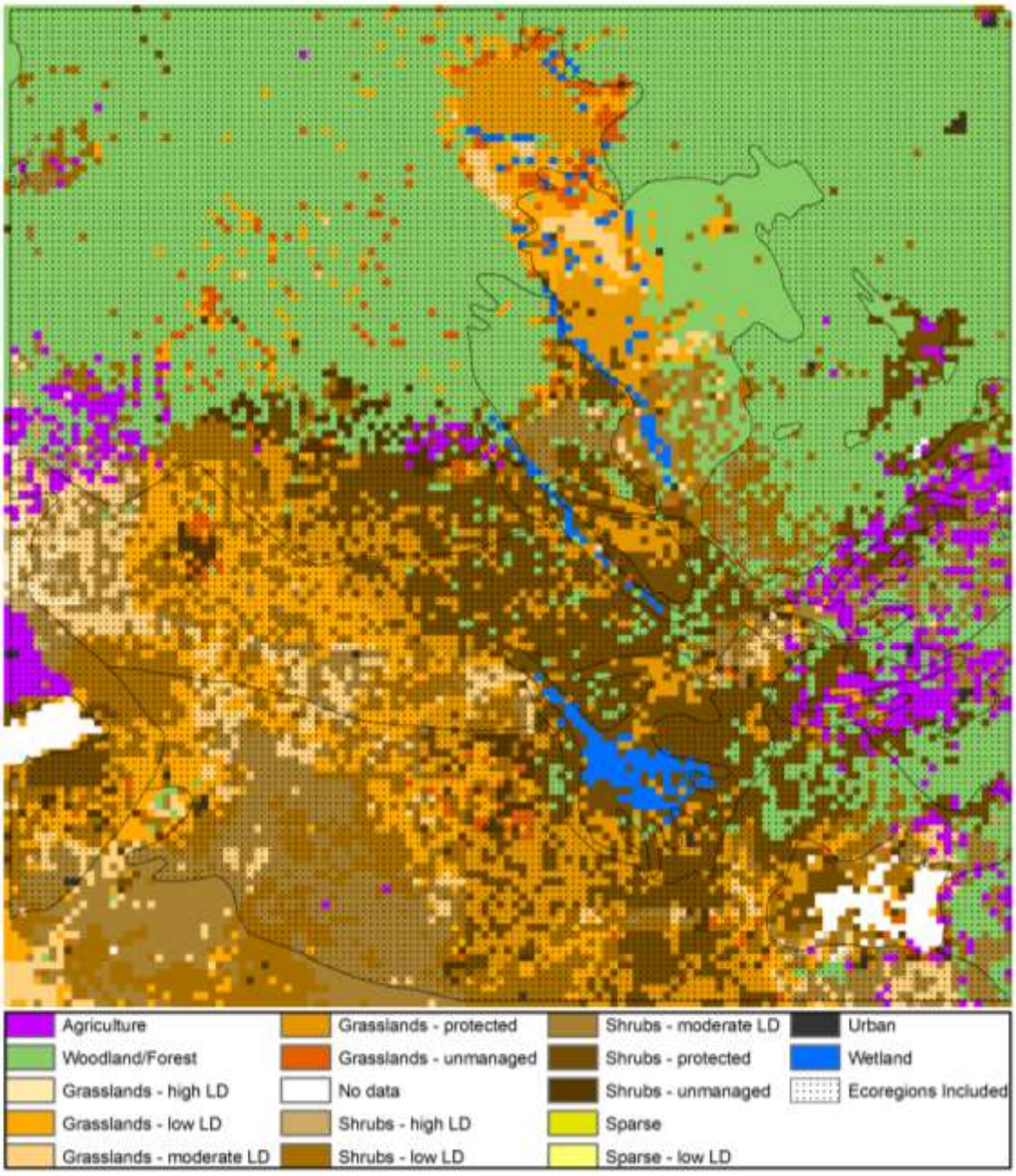

Figure 49 FAO Land Use characteristics including indications of livestock density (LD) (FAO/ISRIC 2003)

3. Data

3.1 MODIS

MODIS 8 day MCD43B4 BRDF adjusted reflectance product (Schaaf et al. 2002) was acquired for Southern Africa from January 2002 to December 2011. The spatial resolution is 500 meter. NDVI and SWIR32 were derived and noise was reduced by using a linear interpolation (see section 4.1.1 in chapter 2).

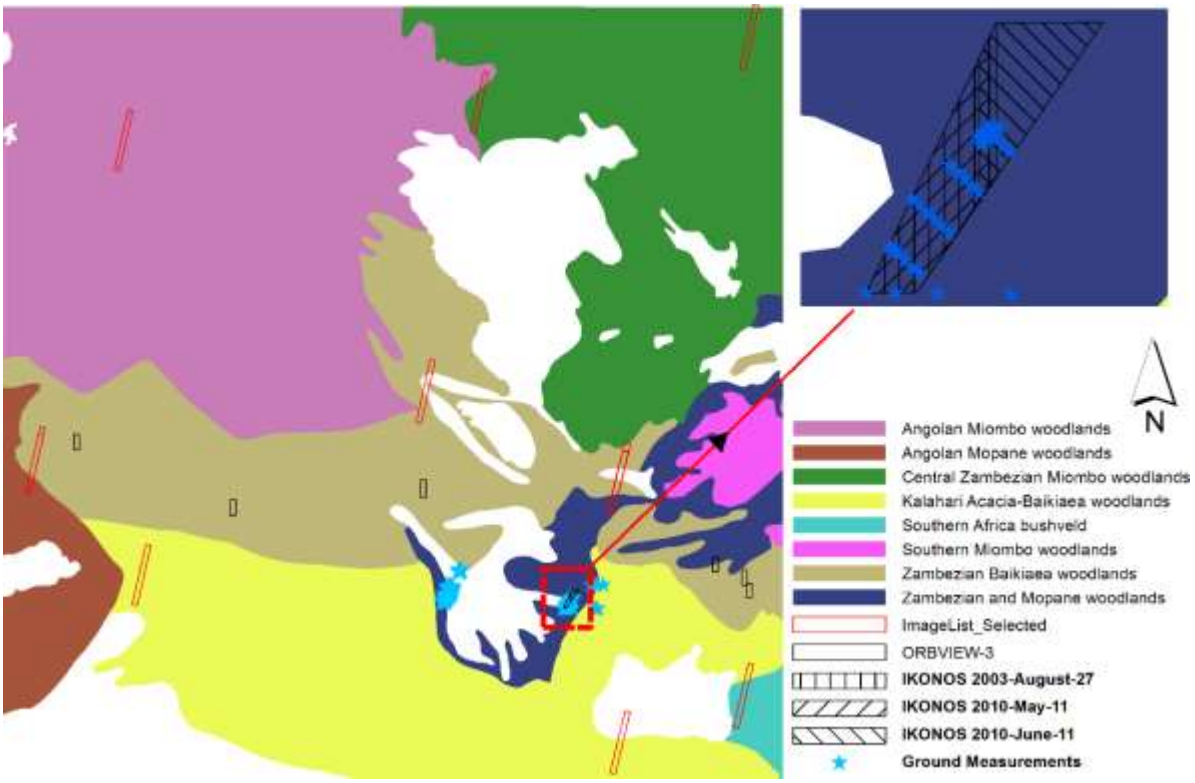

Figure 50. Southern African savanna Ecosystems defined by Olson, Dinerstein, Wikramanayake, Burgess, Powell, Underwood, D'amico, Itoua, Strand, Morrison, et al. (2001) showing the location of EO-1 Hyperion images, IKONOS, Orbview-3and GeoEye images and field data sites

3.2 Hyperion

Twelve Hyperion images were acquired from the USGS Earth Explorer (Figure 50, *Table 8*). The selection aims at covering various vegetation combinations as well as different stages of phenology. The imagery was processed to remove bad bands, major water interfering regions, noises in the short wave infrared regions and strips (Jupp et al.

2002; Apan & Held 2002; Datt et al. 2003; Datt & Jupp 2004). Further image processing includes: 1) radiometrical and atmospherical correction using ACORN 6.1R; 2) spectra smoothing of visible (447 – 854nm) and SWIR bands (864 – 2365nm) separately using Minimum noise fraction (MNF); 3) geometrical correction based on the Hyperion L1GST product with a RMSE (Root Mean Square Errors) ranging from 0.3 to 0.6 pixels. The MODIS bands (Band 1, 2, 6, 7) were then simulated and VIs (NDVI and SWIR32) were calculated.

Table 8. Hyperion Images analyzed for end-member determination

ACQ_DATE	Latitude	Longitude	Eco-regions
2003/05/26	-18.872	17.938	Kalahari Acacia-Baikiaea woodlands
2003/06/18	-12.750	17.688	Angolan Miombo woodlands
2004/05/07	-11.297	26.504	Central Zambezian Miombo woodlands
2004/08/23	-17.313	16.428	Zambezian Baikiaea woodlands
2004/09/07	-20.575	26.420	Southern Africa bushveld
2005/03/03	-17.210	16.452	Zambezian Baikiaea woodlands
2005/10/25	-16.288	21.943	Zambezian Baikiaea woodlands
2006/08/12	-12.218	22.702	Central Zambezian Miombo woodlands
2008/02/24	-17.569	24.654	Zambezian Baikiaea woodlands
2010/09/29	-21.231	24.682	Kalahari Acacia-Baikiaea woodlands
2011/06/17	-17.442	24.684	Zambezian Baikiaea woodlands
2011/09/21	-17.567	24.653	Zambezian Baikiaea woodlands

3.3 IKONOS

Three IKONOS images were available, (Figure 50) August 27, 2003, and May 11 and June 11, 2010 on representing different stages of dry season and covered by (248, 475 and 428 respectively) MODIS pixels. Each 4-meter resolution multispectral bands of an image was fused with the 1-meter panchromatic band to create four pan-sharpened bands at 1-meter spatial resolution images.

3.4 GeoEye-1

The GeoEye-1 image was acquired on 16 May 2010. The image is composed of 4 multispectral bands (Blue: 450nm-510nm; Green: 510nm-580nm; Red: 655nm-690nm; NIR: 780nm-920nm) at 2 meter resolution. The *f*PV, *f*NPV, *f*BS, and the average of each land cover type at MODIS scale were estimated by Mishra et al. (2014).

3.5 Ground Measurements

The ground measurement set was extracted (Thomas Brandt, personal communication) over Mababe (Botswana, Africa. Latitude: -19.1; Longitude: 22.2) in 2012 from May to August (Figure 50). Percentages of understory were estimated at 5-meter and 20-meter away from each individual site along the sampling path. All transects (1 X 1 meter) run either parallel or at a 45-degree angle to the latitude. The canopy readings were taken at the same location on each site using a densitometer. The readings were taken at each location looking at four directions (N, W, S, E or NW, SW, SE, NE). The measurements included percentage of ground cover for tree, grass, litter, and soil; and percentage of overstorey cover for canopy openness.

4. Analysis

The analysis was conducted as follow: i) exploring the geographical and seasonal variation of the response space between NDVI and SWIR32; ii) selecting of end-members for linear unmixing of MODIS NDVI and SWIR32 images to the fractional cover of PV, NPV and BS; iii) validating of PV, NPV and BS against field data, and classified IKONOS and GeoEye-1 images; iv) Exploring the relationships between cover fractions unmixed using the NDVI-CAI response envelope, and the NDVI-SWIR32 response envelope using Hyperion imagery; v) exploring of the seasonal and land cover-derived variation of the relationships between the key VIs for a time series of images

over the dry savanna and wetlands in the Caprivi region; vi) linear unmixing of PV, NPV and BS fractions using the MODIS times series; viii) exploring of the temporal profiles of PV, NPV and BS for selected vegetation types as defined by the SAFAR 2000 vegetation maps, and checking for purity using Google Earth;.

4.1 Exploration of geographic variation in NDVI and SWIR32 endmembers

The workflow in this section remains the same as the section 5.1 in chapter 2. Scatterplots of NDVI versus SWIR32 were constructed using Hyperion simulated indexes. The data sets were selected to capture pure pixels of NPV when the vegetation was completely dry, PV when the vegetation was reaching full leaf canopy and BS during the driest part of the season. The endmembers for each image were extracted. The end-member variation was assessed and compared for final overall end member definition. The goal of this comparison was to capture and evaluate the variation of the response envelope patterns across different soil and vegetation covers. The final end-members were selected based on the most extent of the response envelope to enclose others.

4.2 Linear unmixing of MODIS NDVI and SWIR32 images using refined end members

As already mentioned, the linear unmixing approach was developed for the Australia savanna by Guerschman et al. (2009). In our study, the assumption that the mixing of land covers in the NDVI and SWIR32 space is linear was explored and supported using IKONOS extracted *f*PV, *f*NPV, and *f*BS as well as the corresponding NDVI and SWIR32. The linear unmixing approach was then applied based on the endmembers assessed in the previous section.

4.3 Validation of PV-NPV-BS Fractional Cover against Field Observations

For each site of field observation, the average of each category was calculated and the final percentage of ground cover was derived by multiplying the average canopy openness, while the canopy closeness was one minus the average canopy openness. As all measurements were taken during the dry season, ground percentage of grass was compared with MODIS *f*NPV. The standard deviation of each category was also calculated to assess the heterogeneous of field observations.

4.4 Validation of MODIS Fractional Cover Estimation against GeoEye-1 and IKONOS imagery

The GeoEye-1 fractional cover calculated by Mishra et al. (2014) was used directly for comparison.

The fused IKONOS images were converted to Greenness, Brightness and Wetness using the Tasseled Cap transformation. As a remind, this method was first developed using Landsat TM dataset (Kauth & Thomas 1976; Crist & Kauth 1986) and later applied to IKONOS by Horne (2003).

$$T_{Brightness} = 0.326R_{blue} + 0.509R_{green} + 0.56R_{red} + 0.567R_{nir} \quad \textit{Equation 34}$$

$$T_{Greenness} = -0.311R_{blue} - 0.356R_{green} - 0.325R_{red} + 0.819R_{nir} \quad \textit{Equation 35}$$

$$T_{Wetness} = -0.612R_{blue} - 0.312R_{green} + 0.722R_{red} - 0.081R_{nir} \quad \textit{Equation 36}$$

The Tasseled Cap indices were classified into 30 classes using an unsupervised classification method and integrated into PV, NPV, BS and other. The proportions of PV, NPV and BS were then estimated based on the grid defined by MODIS images.

4.5 Comparison of NDVI-CAI and NDVI-SWIR32 Unmixing with Hyperion

Hyperion images were first unmixed into *f*PV, *f*NPV, and *f*BS in the NDVI-CAI space and the NDVI-SWIR32 space. The two sets of results were then compared in order to test the reliability of the NDVI-SWIR32 response space. As the main concern is the substitution of CAI by SWIR32, only *f*NPV and *f*BS were assessed in the two response spaces. The comparison was grouped by ecoregions, so that the variation of NDVI-SWIR32 performance may be identifying for different vegetation combination.

4.6 Exploration of Seasonal and Land Cover Variation in Spectral Relationships

The NDVI-SWIR32 space was also assessed by testing the variation of the relation between CAI and SWIR32; SWIR2 and SWIR3; and NDVI and SWIR32. This assessment allows to better understanding the response of SWIR32 over vegetation for different season and land cover types, hence the performance of linear unmixing in the NDVI-SWIR32 space.

5. Result

5.1 Geographic variation in NDVI and SWIR32 endmembers

Figure 51 shows the response envelope for Hyperion imagery of the NDVI-CAI and NDVI-SWIR32 relation. Although the imagery was acquired at different time and cover different ecoregions, all images form one distinctive response envelope in the NDVI-CAI space. The response envelope extents are similar at the PV and NPV vertex in both 30 meter and 500-meter scale, but the BS vertex shrinks at the coarser scale. When using SWIR32 to replace CAI, most images still form the response envelope, except for two images at the 30-meter scale. Visual examination shows that the response envelope outliers are salty pan in the images. The outliers suggest that the SWIR32 is less robust and introduced more uncertainty related with different soil types in the African savanna.

The other images show that response envelopes are also similar between the 30-meter and the 500-meter scale, except slight shrink at the BS vertex at the 500-meter scale. The shrinks at the BS vertex in both response envelopes indicate the lack of pure bare soil pixels at the 500-meter scale.

The endmember sets were then selected from the 30 meter scale using the procedure described in chapter 2 (Figure 52, Table 9). Figure 52 shows the distribution of selected endmember set with dense plot of Hyperion derived indexes. The dense plot shows blank when pixel number is low, however, the endmember set captures the higher NDVI at PV vertex. When comparing with the Australian endmember set, the Cerrado also shows higher NDVI at the PV vertex, which indicates the denser woody coverage at some area of Cerrado.

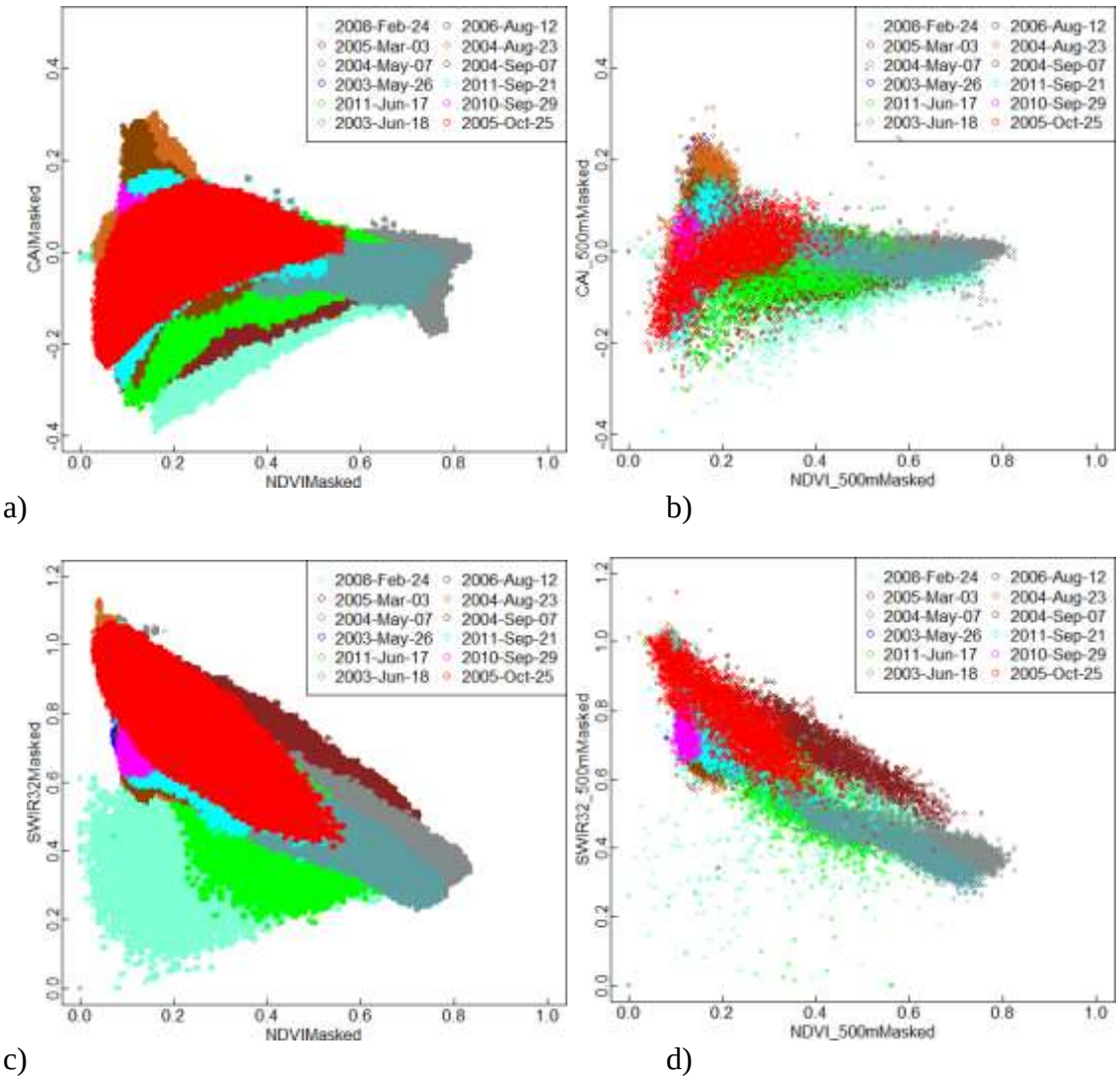

Figure 51. Comparison of the two dimensional response envelop from Hyperion data for a) NDVI vs CAI; and b) NDVI vs SWIR32 at 30 m pixel resolution; and c) NDVI vs CAI; and d) NDVI vs SWIR32 rescaled to 500 m MODIS pixel resolution. Colors correspond to the image acquisition data. The locations can be seen in Figure 1. Data have been filtered to remove outliers according to the method described.

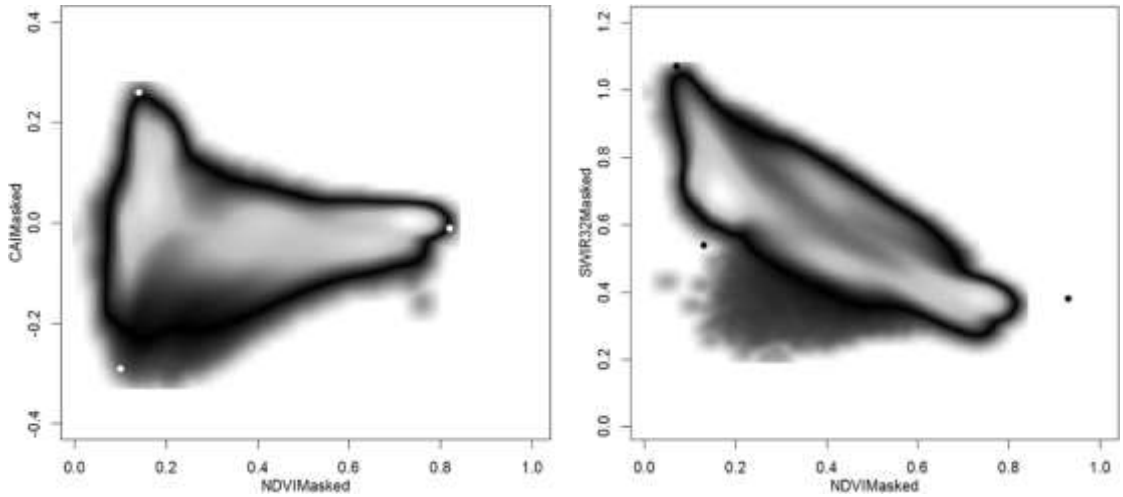

a) b)

Figure 52. The final response envelopes and selected end members from Hyperion at 30 m resolution for: a) NDVI vs CAI; and b) NDVI vs SWIR32.

Table 9 Endmembers used in the fractional cover calibration

	PV	**NPV**	**BS**
NDVI	0.82	0.13	0.07
SWIR32	0.35	0.56	1.05
	PV	**NPV**	**BS**
NDVI	0.82	0.14	0.1
CAI	-0.01	0.26	-0.29

5.2 PV-NPV-BS Fractional Cover

The unmixing approach was applied to 8-day MCD43B4 BRDF MODIS imagery from 2002 to 2011. The average monthly fractional covers are shown in Figure 53. It shows a general temporal pattern, however, different vegetation combinations in the study region. Angolan Miombo woodlands and Central Zambezian Miombo woodlands are mostly dominated by evergreen or semi-deciduous woody with distinctive grassland patch in between (Figure 53). In the Zambezian Baikiaea woodlands, dominant woody vegetation dries out between April and October and there is significant bare surface even during the wet season. In the Kalahari Acacia-Baikiaea woodlands, on the other hand, there is a relative high proportion of NPV through the whole year and the vegetation dries out between March and November.

The temporal pattern of *f*PV, *f*NPV, and *f*BS was extracted for some sampled land cover types shown in Figure 54. The sampling sites were selected based on the vegetation maps (SAFARI 2000). These maps provide a more detailed separation of vegetation types in the eastern half of the study area. The temporal profiles for the sample sites are displayed in Figure 54 in ascending order of latitude, which corresponds to decrease of precipitation. With the reduction of water availability, the vegetation type shifts from forest (Figure 54 a-d) to shrub (Figure 54 e-i) and to grassland (Figure 54 l). The *f*PV, *f*NPV, and *f*BS are highly correlated in all vegetation types. Highest *f*PV occurs during the wet season, while highest *f*BS happens during the dry season with the highest *f*NPV occurs in between. The main ecological differences among vegetation types are:

1. A higher baseline *f*PV in dense woody area and a higher baseline *f*BS in shrub and grassland

2. A wider *f*PV peak and a lesser variation of amplitude in dense woody compare to shrub and grassland

5.3 Validation of PV-NPV-BS Fractional Cover against Field Observation

The respective scatter plots of the ground validation samples versus the *f*PV, *f*NPV, and *f*BS are shown in Figure 55. The standard deviation of ground-based fractional cover ranges from 0.05 to 0.42; the spread and magnitude of standard deviation values suggests that within-pixel variation is much greater than between pixel variation making application of these data to validation problematic. The ground observation of NPV and BS show very broad scatter values for a given level of *f*NPV and *f*BS, and the high standard deviation indicates that the sites are heterogeneous at the pixel scale. Besides, without considering the "clumpiness" of the overstorey, estimation of the ground NPV

and BS introduce error under different vegetation structures. The best linear correlation occurs between the ground overstorey and the *f*PV. Given the low tree cover and the high heterogeneousness of these savannas at the MODIS scale, the 0.1 unit offset is not surprising.

5.4 Validation of PV-NPV-BS Fractional Cover against IKONOS imagery and GeoEye imagery

The respective scatter plots of IKONOS and GeoEye derived *f*PV, *f*NPV and *f*BS versus MODIS estimation are shown in Figure 56. Linear regression and the 95% confidence interval of the regression were also displayed. The validation suggested that MODIS overestimated *f*PV (Figure 56 a) when green vegetation is sparse but showed better agreement when more green cover was present. Comparatively the *f*NPV showed good agreement with the IKONOS cover fractions in August (Figure 56 b), but exhibited an underestimation of NPV cover when dry vegetation cover is lower in May and June (Figure 56 e). The *f*BS fraction shows two different linear correlations (Figure 56 c, f). The two linear relationships have similar slopes but a different intercept.

5.5 Comparison of NDVI-CAI and NDVI-SWIR32 Unmixing with Hyperion

The results of the validation analysis indicated some significant bias and error was present in the MODIS-derived *f*NPV and *f*BS estimates. Since these estimates depend heavily on the validity of the SWIR32 index as a surrogate for the CAI (see Chapter 1, section 5.1), some additional investigation of this relationship for the African study region was required.

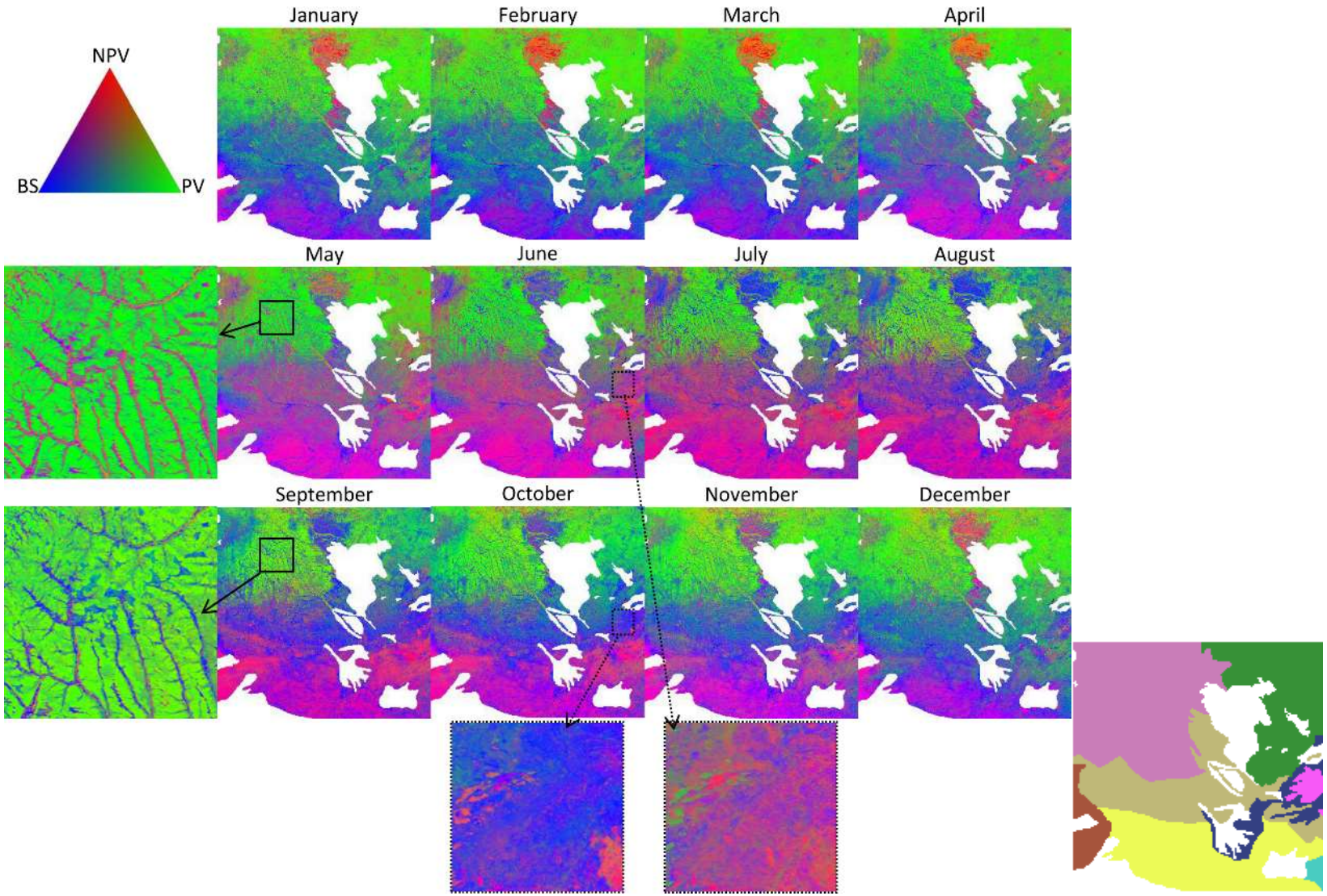

Figure 53. Average monthly fractional cover for the study region. Insets show fractional cover at two dates in the Angolan Miombo woodlands and two dates in the Zambian Miombo and Mopane woodlands; the overview map in right shows ecoregions of the study area (Figure 50)

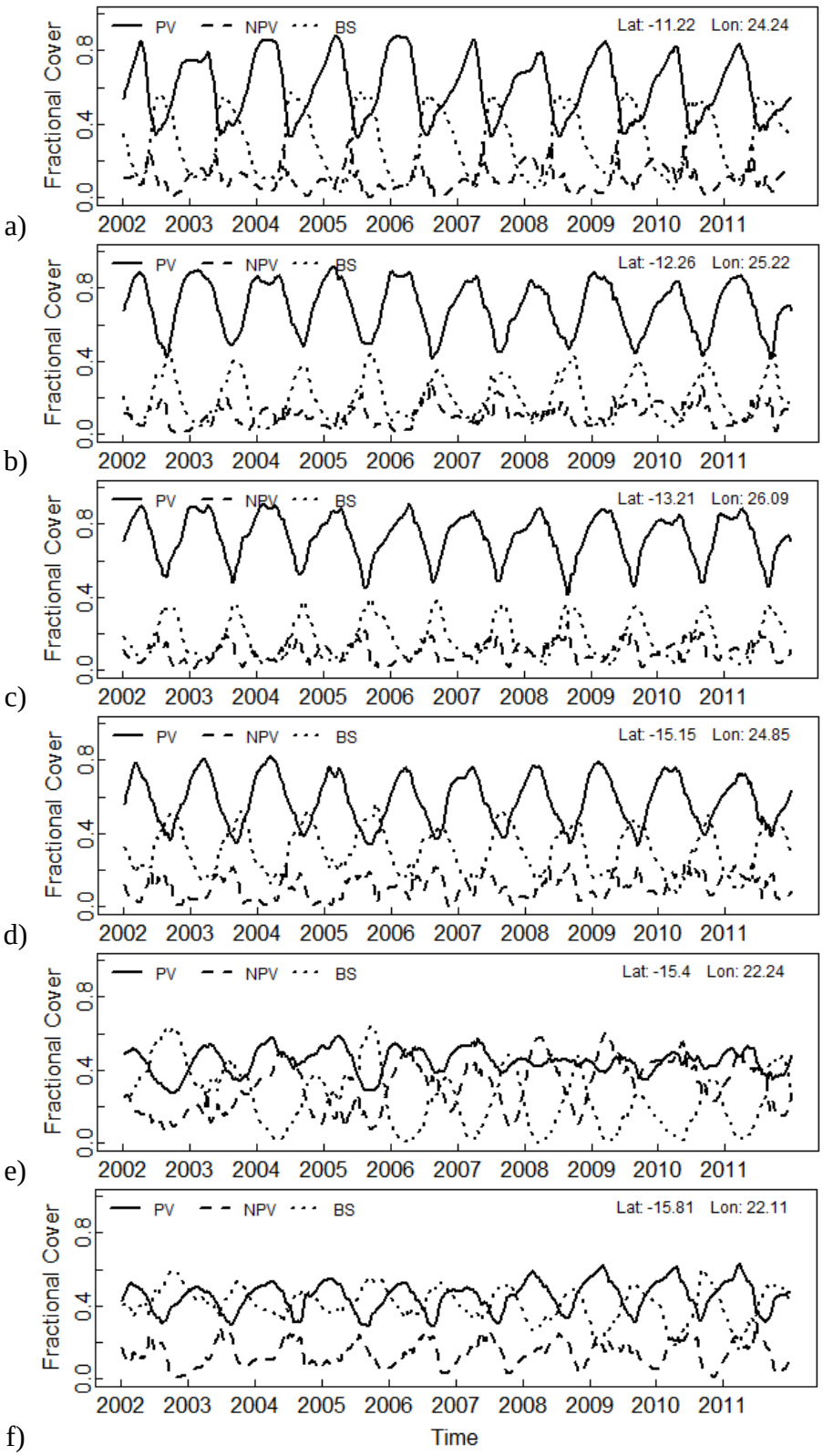

Figure 54. (Part 1) a) Erythrophleum woodland; b, c) Brachystegia/Julbernardia woodland; d) Brachystegia woodland on Kalhari sand; e) Diplorynchus savanna; f) Loudetia grassland.

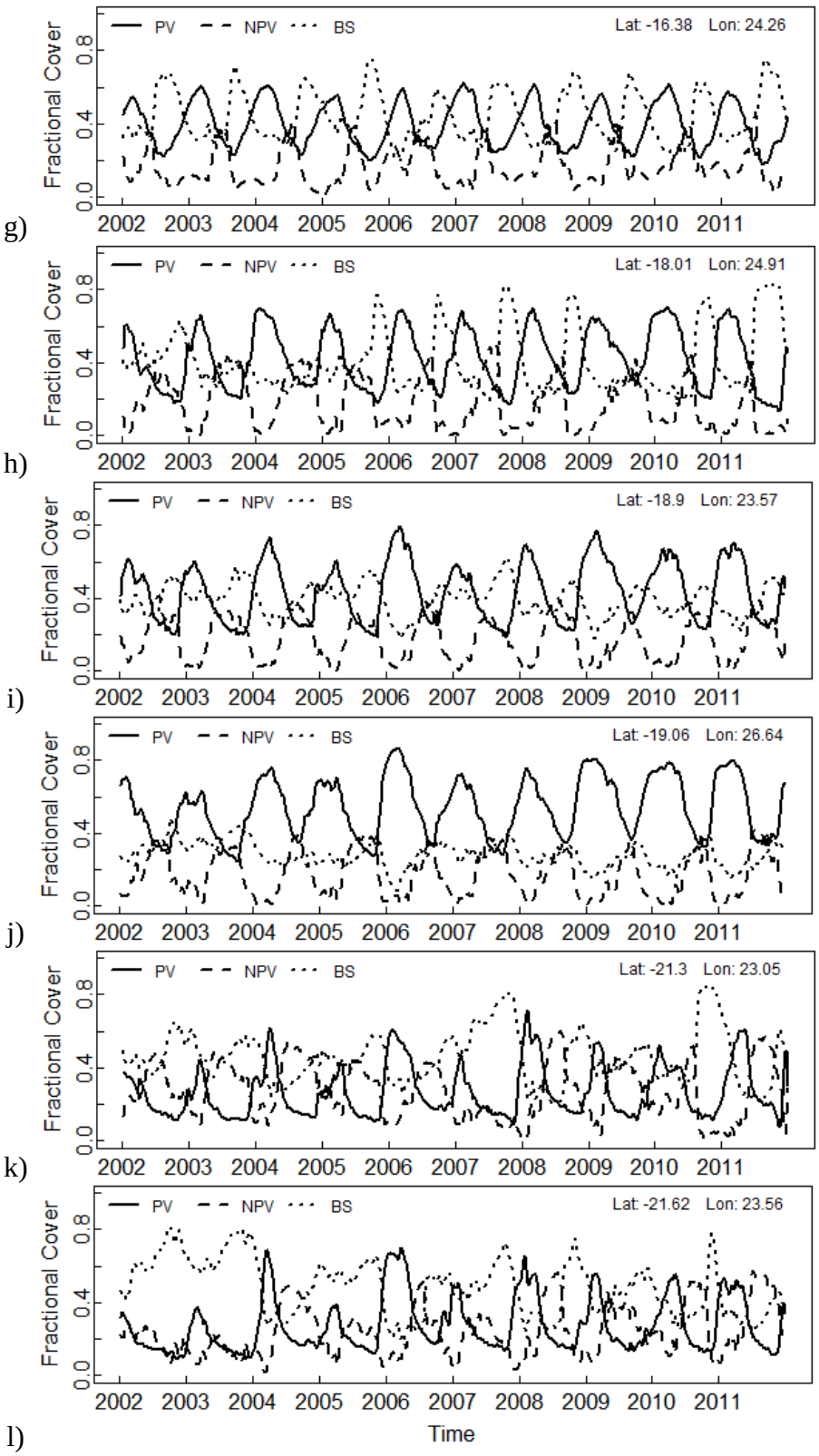

Figure 54 (Part 2) g) Brachystegia woodland on Kalahari sand; h) Baikiaea savanna; i), Colophospermum mopane savanna; j) Acacia-Lonchocarpus shrubland; k, l) Terminalia sericea arid savanna

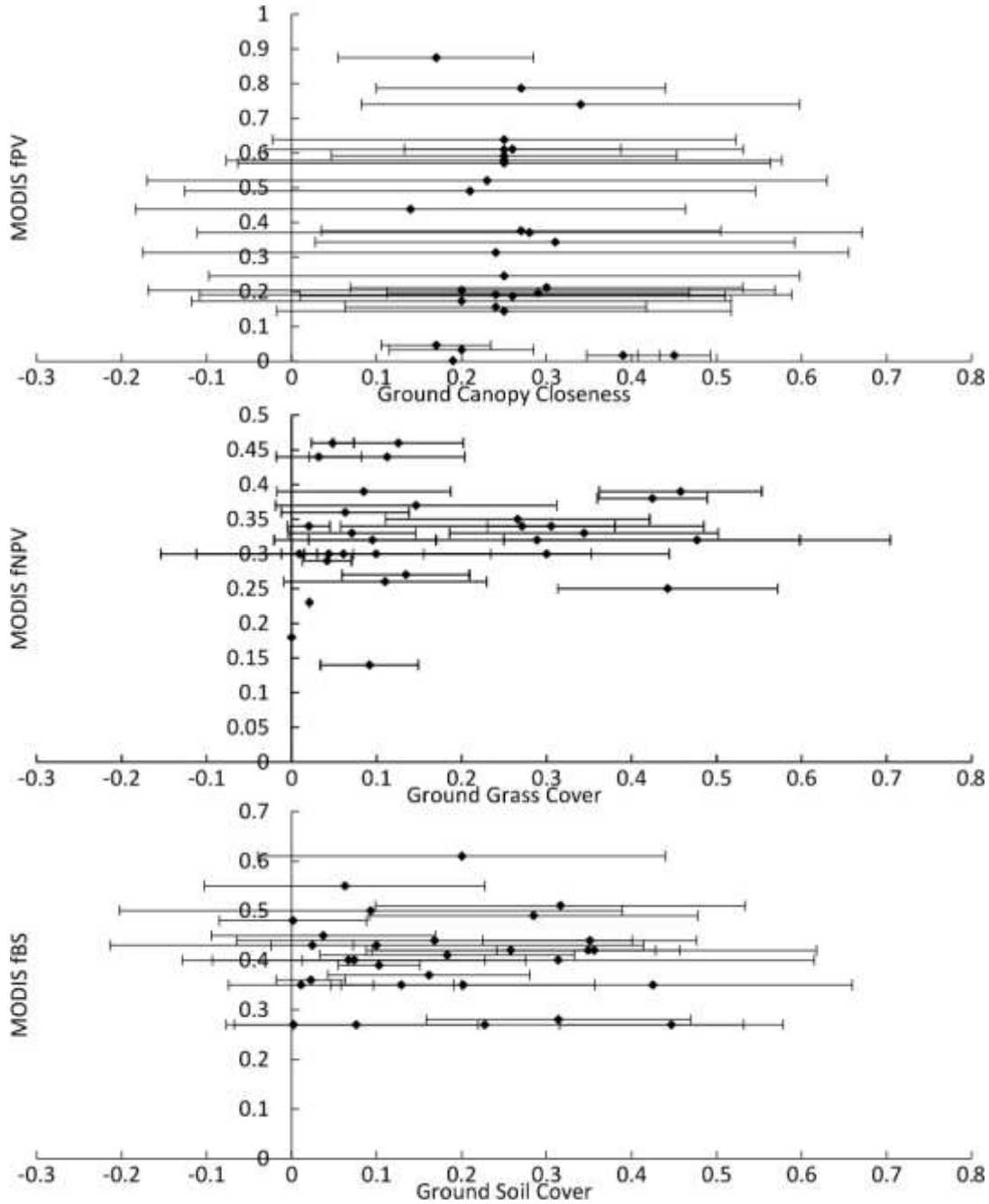

Figure 55. Ground validation of fPV, fNPV and fBS against field observations. Standard deviation of field observations is also shown

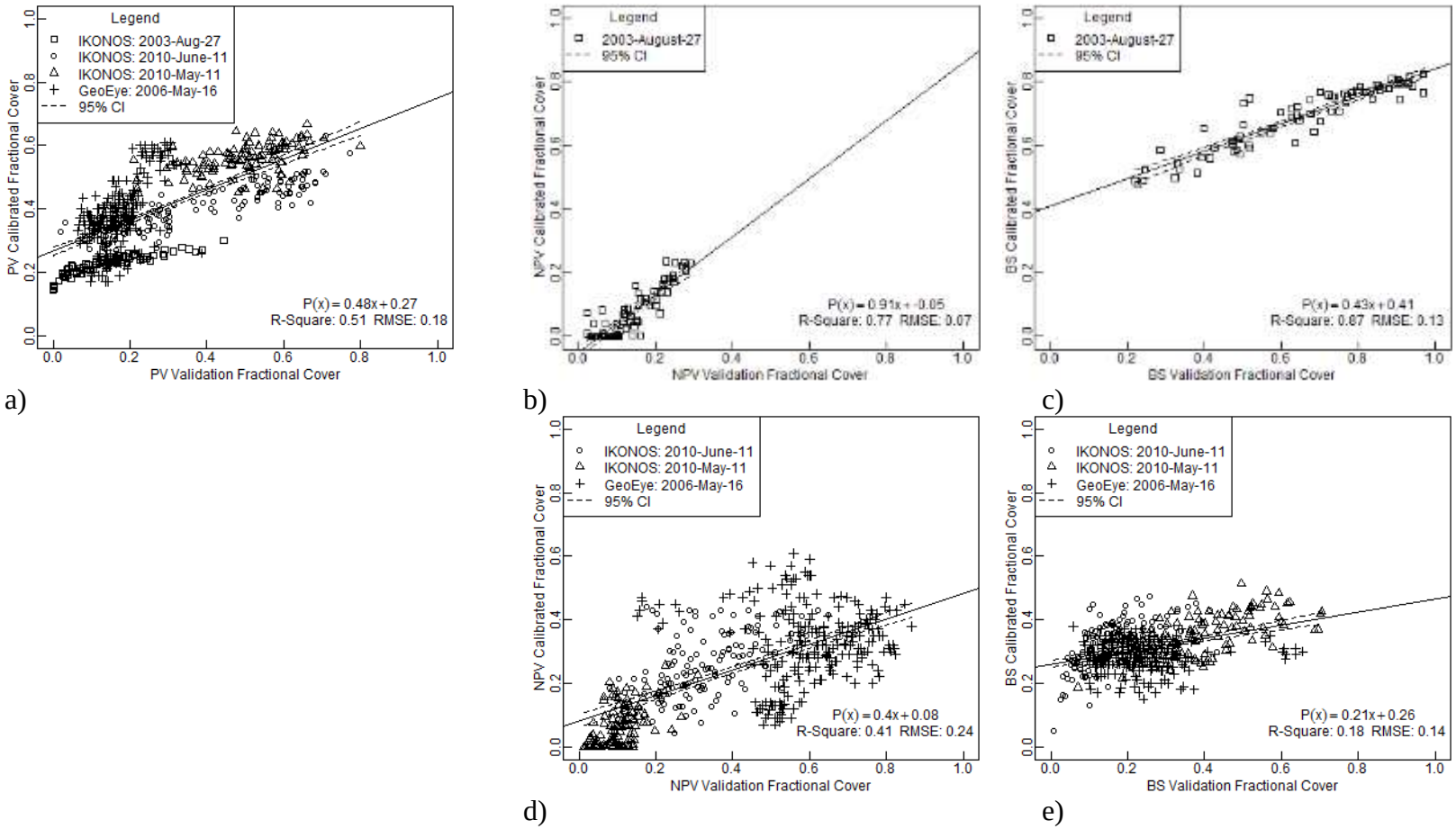

Figure 56 Relationships between a) PV; b) NPV; c) and BS cover fractions derived from MODIS and classified IKONOS imagery in mopane woodland near the Okavango Delta, and between d) NPV; and e) BS cover fractions derived from MODIS and GEOEye imagery in Terminalie arid savanna in a game reserve in Botswana.

In this section, the uncertainty of substituting CAI by SWIR32 was assessed by comparing the fractional covers derived from the NDVI-CAI and NDVI-SWIR32 space. The *f*PV, *f*NPV, and *f*BS were estimated for the two NDVI-CAI and NDVI-SWIR32 spaces. The results were then compared for different ecoregions in order to assess the seasonal variation of the linear correlation across ecosystems. The fractional cover of PV mostly related with the NDVI is highly correlated with the NDVI sensitivity in the two response spaces. Since the replacement of CAI is the main concern, only *f*NPV and *f*BS are plotted in this section. Figure 57 shows the linear correlation of *f*NPV for each response space. The scatter plots show a similar linear relationship but constant overestimation of NDVI-SWIR32 space in Miombo woodland. The comparison at the 500-meter scale indicates a shift at different seasons in the Caprivi mixed vegetation. The shift suggests that NDVI-SWIR32 slightly underestimated *f*NPV in September but overestimated it in February and June. However, the shift is not significant at other locations. Figure 58 is a scatter plot of the *f*BS comparison. The comparison shows better agreement between the NDVI-CAI and NDVI-SWIR32 space with fewer shifts in all ecoregions.

The most significant shifts come from the NPV fraction in Caprivi when using the soil sensitive SWIR32 index to replace the cellulose sensitive CAI index. The difference could be used to explain inconsistent correlation in the NPV and BS validation. The NDVI-SWIR32 performs well in arid areas where vegetation is sparse and SWIR32 mainly detects the abundance of bare soil. However, in dense vegetation areas (Miombo woodlands) or during the wet season (Caprivi), the NDVI-SWIR32 gives higher *f*NPV and lower *f*BS than the NDVI-CAI pair.

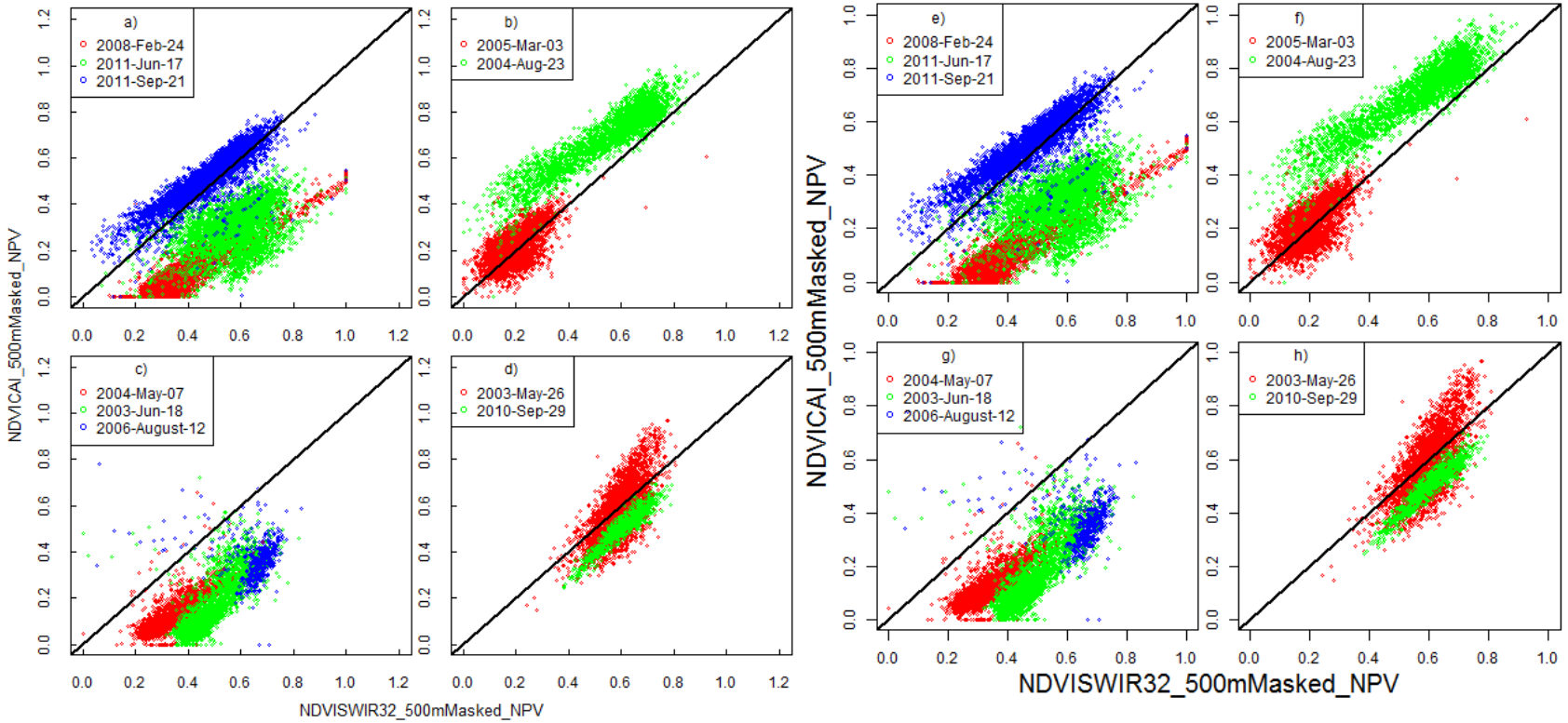

Figure 57. Comparison of the relationships between NPV cover fraction unmixed from NDVI-CAI (a-d) and NDVI-SWIR (e-h) response envelopes for four image time series from different vegetation associations. a, e) Caprivi mixed vegetation types Colophospermum-Baikiaea; b, f) Zambezi Baikiaea woodlands; c,g) Miombo woodland – Brachystegia and Julbernardia spp.; and d, h) Kalahari Acacia-Baikiaea.

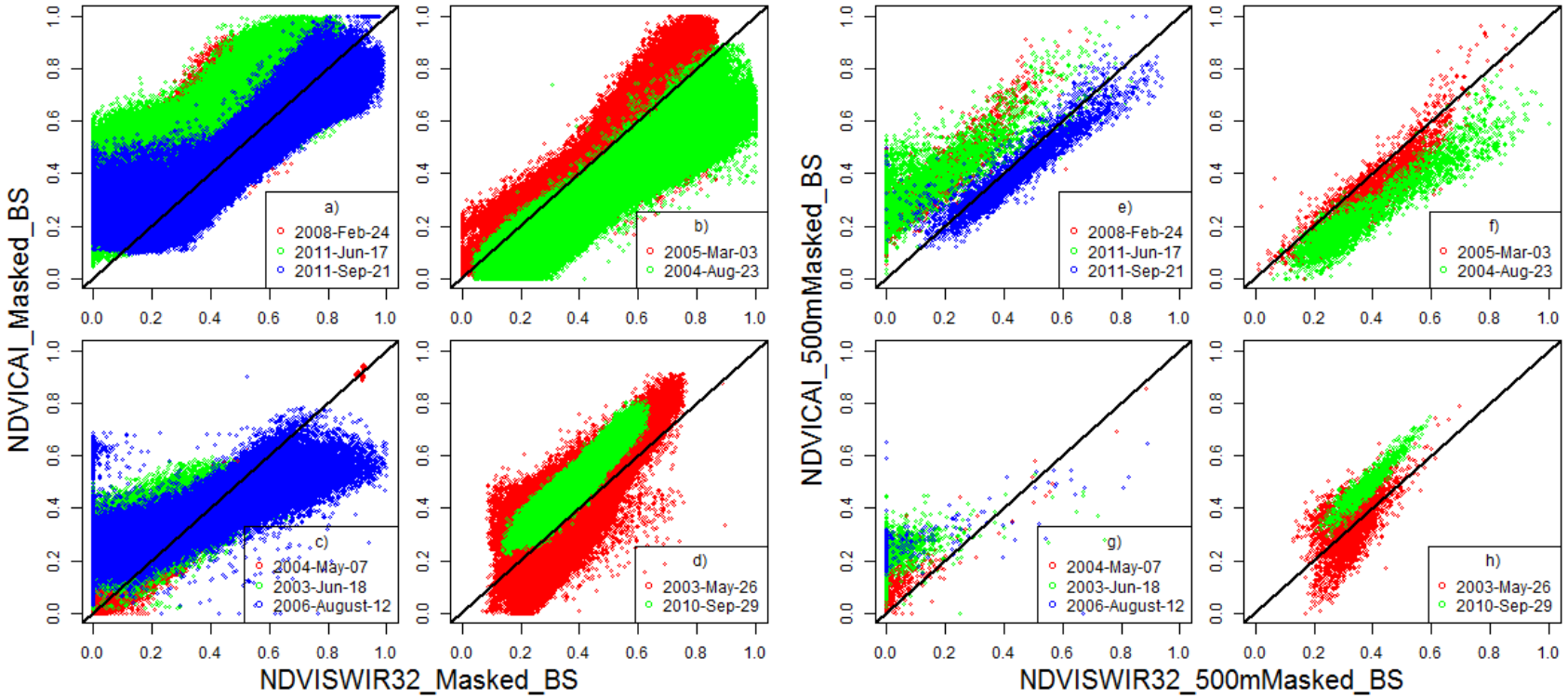

Figure 58. Comparison of the relationships between BS cover fraction unmixed from NDVI-CAI (a-d) and NDVI-SWIR (e-h) response envelopes for four image time series from different vegetation associations. a, e) Caprivi mixed vegetation types Colophospermum-Baikiaea; b, f) Zambezi Baikiaea woodlands; c,g) Miombo woodland – Brachystegia and Julbernardia spp.; and d, h) Kalahari Acacia-Baikiaea.

5.6 Seasonal variation of SWIR2 and SWIR3 in EO-1 Hyperion imagery

Two savanna time series were selected from Hyperion imagery. One subset group contains three Hyperion images over Caprivi mixed vegetation types and another group contains two Hyperion images over Zambezi Baikiaea woodlands. The relationship between CAI, SWIR2, and SWIR3 was plotted in order to explore the relation between vegetation cellulose and SWIR bands respectively. CAI and SWIR3 show a negative correlation through the whole season, though the intercept changes slightly. The relationship between CAI and SWIR2, however, varies significantly in slope (Figure 59). Stepwise multiple linear regressions were used to fit CAI with NDVI, SWIR2, SWIR3, SWIR32, and date of the imagery (*Table 10*). The results indicate that using multiple SWIR bands separately rather than a combined index could improve the estimation of NPV and BS fractions. Figure 60 shows a strong linear relationship between CAI and SWIR bands in ecoregions separately, however, the relationship varies between ecoregions. The SWIR32 combination failed to remove the relationship differences, though restricts the greatest differences to intercepts.

Table 10. The result of stepwise multiple regression (CAI ~ SWIR2, SWIR3, SWIR32, NDVI, day, year)

Model	Remain Parameters	R-square	Residual Standard Error (RSE)
CAI ~ SWIR2 + SWIR3 + NDVI + Day + year	SWIR2, SWIR3, NDVI, Day, year	0.68	0.04
CAI~SWIR2+SWIR3+Day+year	SWIR2, SWIR3, Day, year	0.45	0.06
CAI~SWIR32+Day+year	SWIR32, Day, year	0.37	0.06
CAI ~ SWIR32 + NDVI + Day + year	SWIR32, NDVI, Day, year	0.5	0.05

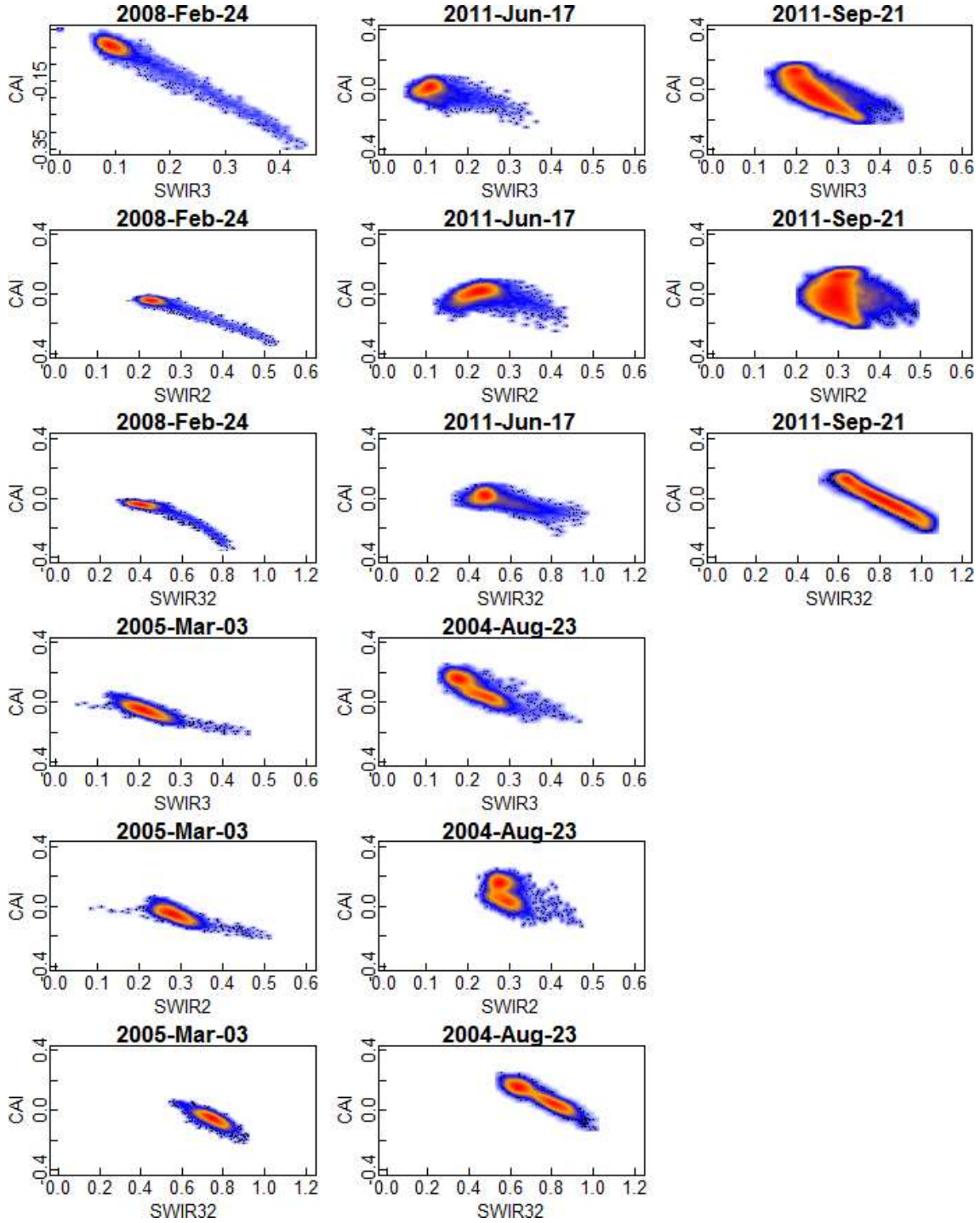

Figure 59. Seasonal responses of spectral indices in pure savanna/grassland. CAI versus SWIR3; CAI versus SWIR2; and CAI versus SWIR32

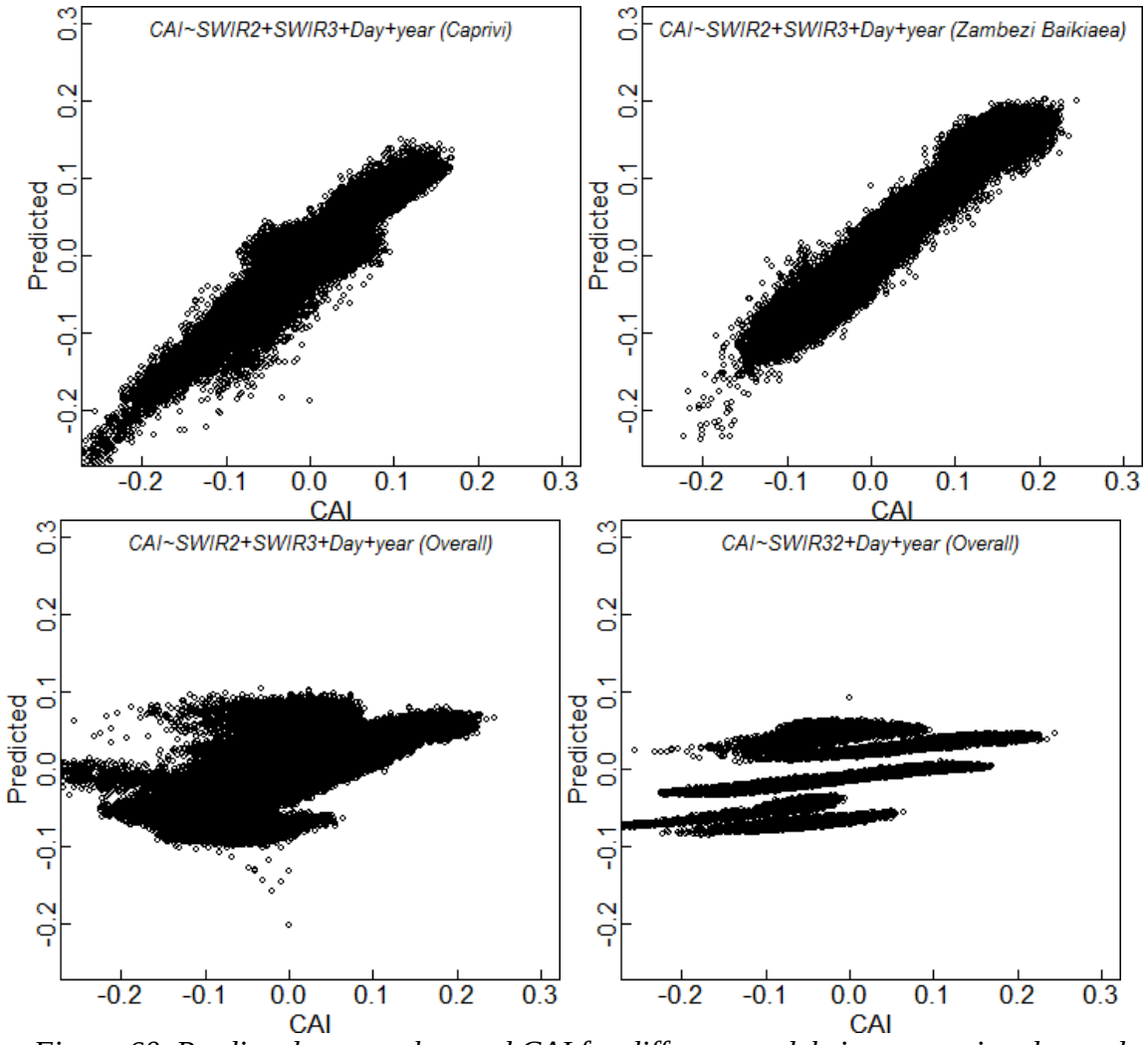

Figure 60. Predicted versus observed CAI for different models incorporating day and year, and contrasting a) using separate SWIR 3 and SWIR 2 spectral channels along with NDVI; b) SWIR3 and SWIR 2 spectral channels alone; c) SWIR32 and NDVI; and d) SWIR32 index alone.

6. Discussion

The result has shown that *f*PV, *f*NPV, and *f*BS in Africa savanna can be retrieved by linear unmixing of NDVI and SWIR32, but that seasonal and geographical variation in the CAI-SWIR32 relationship results in reduced sensitivity of SWIR32 to NPV and BS fractions, and significant bias in retrievals. Daughtry (2001) and Daughtry & Hunt (2005) initially used the NDVI to distinguish green crop from crop residues and soil, while using CAI to separate bare soil and crop residues. Guerschman et al. (2009) found a similar

pattern in the NDVI and SWIR32 space derived from the MODIS data set, and applied the approach to map *f*PV, *f*NPV, and *f*BS in the Australian tropical savanna. However, the author also found that the endmembers could vary on different soil types. Hill et al. (2012) concluded that the endmembers vary across ecoregions and need to be refined when applied to local landscapes. In this current analysis, 12 Hyperion images over different ecosystems at different times of year were used to assess the response envelope relation in the African tropical savanna and to determine the endmember set. All Hyperion images form a triangle in both NDVI-CAI and NDVI-SWIR32 space, except some salty pan area in the NDVI-SWIR32 space. The unified response envelope not only confirms the triangle relation but also suggests that *f*PV, *f*NPV, and *f*BS can be solved using one endmember set. The salty pan exception, however, may suggest that NDVI-SWIR32 space is more sensitive to land cover types than NDVI-CAI space.

The comparison between the linear unmixing results from NDVI-CAI and NDVI-SWIR32 shows a strong agreement of *f*PV, but a shift of *f*NPV and *f*BS over the Caprivi mixed vegetation types. A further comparison between CAI, SWIR3 and SWIR2 at the Caprivi shows a more consistent linear correlation between CAI and SWIR3, but a rotating linear relation between CAI and SWIR2 at different seasons. The difference could be explained by the soil moisture when there is lack of vegetation cover (Guerschman & Scarth 2015). The soil effect was also considered by Guerschman et al. (2009) who assumed that soil types and moisture impact SWIR2 and SWIR3 simultaneously and hence, have less impact on SWIR32. However, our study shows that the assumption is not universally applicable in the African savanna especially when bare surface is prevalent and vegetation coverage is low.

SWIR32 was found linearly correlated with CAI and NDVI in Australian savanna (Guerschman et al. 2009). This chapter investigated the effectiveness of CAI substitutions using multiple stepwise linear regressions. The results show that SWIR2 and SWIR3 independently perform better than SWIR32. The linear relationship between CAI and SWIR bands, however, varies in different ecoregions, which suggests greater diversity of surface reflectance properties in the African savanna than Australian savanna. This means that a simple NDVI-SWIR32 response is insufficient to encompass the observed variation, and that assumptions about the use of SWIR32 to approximate CAI are not valid in this more climatically and biogeochemically diverse savanna. Guerschman & Scarth (2015) explored spectral unmixing algorithm based on a large set of field observation. The study showed less influence from soil color and soil moisture, which indicated a possible solution for the African savanna.

7. Conclusion

In this chapter, a linear unmixing method, based on NDVI and SWIR32, has been tested for evaluating *f*PV, *f*NPV, and *f*BS over the southern African savanna region. Our study systematically compared and extracted endmembers using Hyperion imagery to adapt to local ecosystem feature. Then linear regression was used to evaluate *f*PV, *f*NPV, and *f*BS. The result suggested that this approach has severe limitations in the African savanna especially in relation to SWIR32 sensitivity for the drier, low vegetation coverage areas.

CHAPTER 5 PV FREQUENCY DECOMPOSITION USING FFT

1. Introduction

The previous chapter demonstrated that the simple NDVI-SWIR32 response envelope does not capture the variation in fractional cover of NPV present in the southern African study area. There were significant systematic effects observed in the SWIR32 index attributable to seasonal and interannual variation, as well as differences in vegetation types and land condition. Despite this limitation, retrieval of *f*PV was still satisfactory, hence there is still much benefit in seeking to disaggregate the woody and herbaceous components of the NDVI. In Chapter 3, the potential of the frequency decomposition of the NDVI time series was explored in the Cerrado where there is a short duration and relatively slight amount of leaf loss from the woody stratum in the dry season. The results indicated that only small differences in phase were present. In Africa, with a wide diversity of species and a common occurrence of deciduous behavior, this method should be discriminatory. Hence, in this chapter, the frequency decomposition of the NDVI time series is used to attempt to distinguish between woody plant associations, and detect differences in lagged green-up and senescence of woody and herbaceous layers in response to rainfall.

In the southern African study region, defined in Chapter 4, there are a number of distinct vegetation associations defined by their dominant woody plants: 1) Miombo woodland, often forms dense coverage, and varies from evergreen to deciduous dominant (Fuller 1999; Chidumayo 2002; Richer 2008; Vancutsem et al. 2009); 2) Mopane

woodland, mostly forms open woodland, and is winter deciduous (Fuller 1999; Veenendaal et al. 2008); and 3) the Kalahari Acacia-Baikiaea savanna is mostly deciduous, but the dominant pattern varies due to the climate condition. The deciduous and semi-deciduous vegetation are spatially distinct and associated with the North-South rainfall gradient. Because of the mixture of deciduous woody vegetation, the amplitude and phase metrics retrieved from the frequency decomposition were explored in order to establish different patterns of deciduous tree and understory grass in the frequency domain. Based on the patterns of vegetation types, *f*PV will be decomposed into fractional covers of green semi-deciduous, green deciduous, and green herbaceous vegetation.

2. Method

The frequency decomposition was applied on the *f*PV time series following the method described in chapter 1. The procedure of selecting typical vegetation phenology is described in chapter 3.

3. Data

3.1 MODIS

MODIS NDVI time series was used to explore the vegetation phenology characteristics, while *f*PV, derived in chapter 4 was used to in the frequency decomposition to extract differences in phase and amplitude that could be attributed to separate the green semi-deciduous, green deciduous, and green herbaceous vegetation types.

3.2 Orbview-3

Six Orbview-3 panchromatic images were acquired over the ecoregions (Figure 61) during the dry season in 2006 (September 12, September 29 and October 30), and throughout the growing season in 2007 (January 15, January 18 and February 4). The single band imagery has a 1-meter pixel resolution and a swath of 25km long and 8km wide.

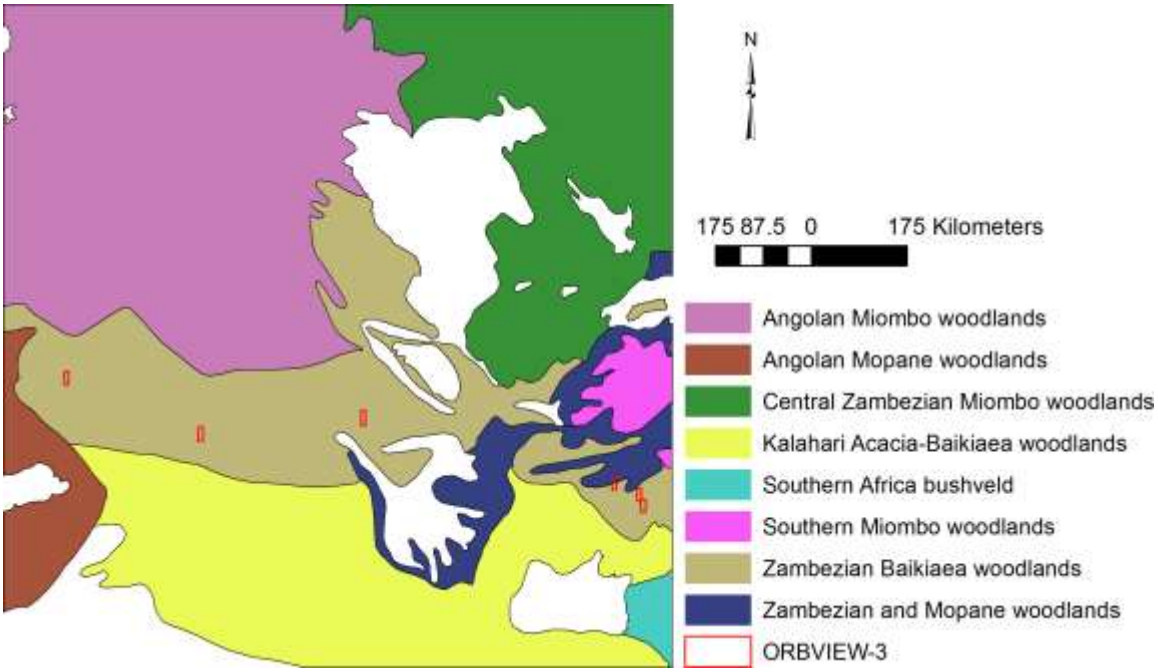

Figure 61 Location of orbview-3 imagery used in validation

3.3 IKONOS

Three IKONOS images were available at different stages of the dry season (Figure 62) during 2003 on August 27, and in 2010 on May 11 and June 11, and covered MODIS pixels 248, 475, and 428 respectively. The 4-meter spatial resolution multispectral bands were fused with the 1-meter panchromatic band. The results were four pan-sharpened bands of 1-meter spatial resolution images.

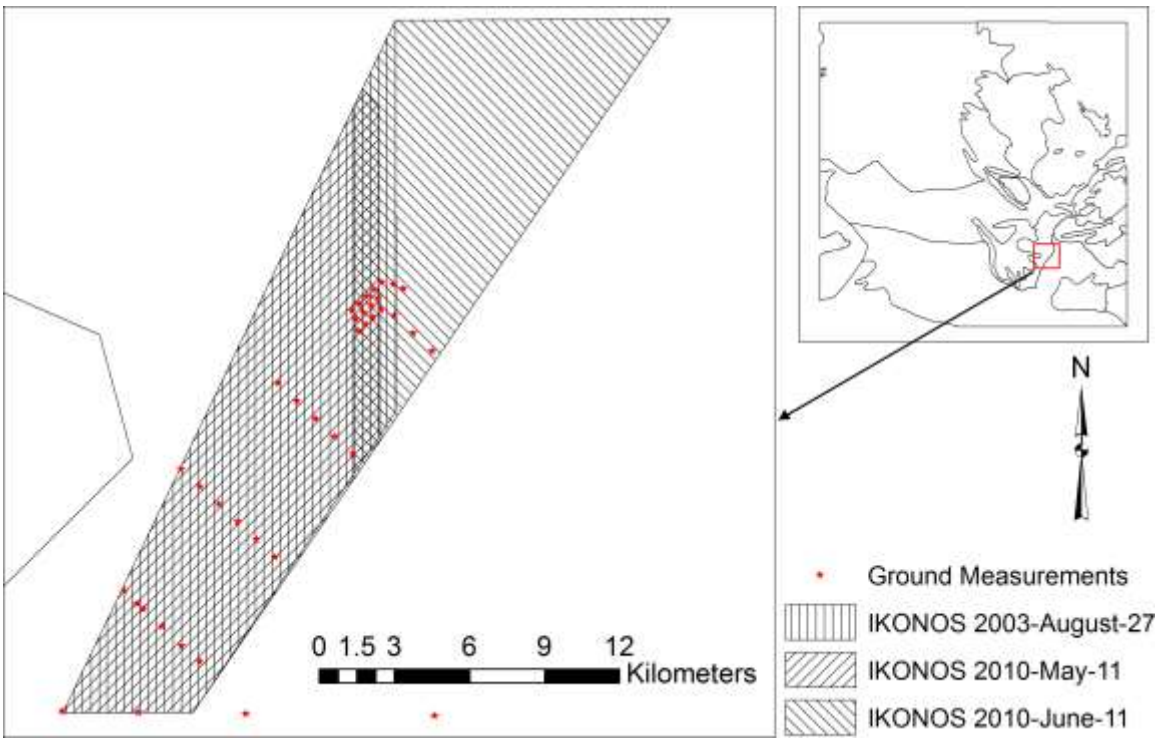

Figure 62 Location of IKONOS imagery and Ground Measurements used in validation

4. Analysis

The analysis was conducted in the following series of stages: i) Exploration of phenology characteristics of different vegetation cover in NDVI. The phase and amplitude of vegetation types were studied in MODIS time series. ii) Determination of the frequency pattern of distinctive vegetation types in MODIS time series. The distinctive vegetation covers were selected as endmembers for frequency decomposition. iii) Estimation of fractional cover of green vegetation components based on *f*PV; and vi) Validation of the green fractions against IKONOS and Orbview-3 classified into woody and herbaceous cover classes.

4.1 Exploration phenology characteristics of woody and herbaceous in NDVI

The NDVI time series were decomposed via the Seasonal-Trend decomposition based on the LOESS (STL) method (Cleveland et al. 1990). The three outputs were long-term trend, seasonal oscillation, and remainder. According to Lu et al. (2003), the

seasonal oscillation was adjusted by including all positive values from the remainder with the purpose of rescuing vegetation information while rejecting atmospheric contamination. Then the slow variations through trough and peak of the adjusted oscillation were estimated and the oscillation was normalized into a -1 to 1 range. The rescaled oscillation, also called shape factor (Lu et al. 2003), represents the phenology characteristics of the land cover.

The shape factor was converted into frequency by using the fast Fourier transform (FFT). The phenology patterns were then extracted over the whole study area by implementation of the following processes: (1) extract key frequencies that define seasonal variations (1 to 1/16 year); 2) explore the amplitude and phase characteristics of vegetation types; (3) classify the images at the key frequencies using the ISODATA unsupervised classification approach; (4) calculate the pure pixel index (PPI) (Boardman 1994) and the average index value for individual classes; (5) determine the typical phenology patterns based on the pure pixel index associated with the high resolution image from Google Earth.

4.2 Frequency decomposition of MODIS fPV

The shape factor of *f*PV was also calculated and converted to frequencies (as described in Chapter 1, section 7.2). The average seasonal frequencies of phenology patterns were extracted based on the typical pixels defined in the last section. Linear unmixing was then used to estimate the proportion of patterns.

4.3 Mapping change of fPVsemi-deciduous, fPVdeciduous, and fPVherbaceous

The yearly maximum $fPV_{semi\text{-}deciduous}$, $fPV_{deciduous}$, and $fPV_{herbaceous}$ were extracted from 2002 to 2011. Then linear regression between the maximum fractional cover from 2002 and 2011 was calculated. This analysis aimed at detecting and mapping any shifts in vegetation over the ten-year period.

4.4 Validation of MODIS Fractional Cover Estimation against IKONOS imagery

The full validation procedure is described in Chapter 2, section 5.8. The fused IKONOS images were converted to Greenness, Brightness and Wetness based on the Tasseled Cap transformation (Kauth & Thomas 1976; Crist & Kauth 1986; Horne 2003).

$$T_{Brightness} = 0.326R_{blue} + 0.509R_{green} + 0.56R_{red} + 0.567R_{nir} \quad \textit{Equation 37}$$

$$T_{Greenness} = -0.311R_{blue} - 0.356R_{green} - 0.325R_{red} + 0.819R_{nir} \quad \textit{Equation 38}$$

$$T_{Wetness} = -0.612R_{blue} - 0.312R_{green} + 0.722R_{red} - 0.081R_{nir} \quad \textit{Equation 39}$$

The proportion of tree, remaining green vegetation, dry vegetation, and bare soil were estimated by integrating the unsupervised classification of the transformed images. The remaining green vegetation includes green herbaceous vegetation and green deciduous woody. This chapter does not separate the green understory vegetation because of the difficulty in distinguishing the two types of vegetation in the IKONOS images.

4.5 Validation of MODIS green cover fractions against Orbview-3

The panchromatic images were classified into 30 classes using the unsupervised classification method and aggregated into tree, bare soil, and remainder (see Chapter 2, section 5.8). The remainder includes green herbaceous vegetation, green deciduous woody and non-photosynthetic vegetation. The accuracy of the aggregated cover classes was assessed against a suite of vegetation patches of different types manually defined and

extracted from Google Earth (*Table 11*). As *Table 11* shows, classification is less accurate throughout the growing season when overstorey and understory are both green. The pixel counts for Orbview-3 classes were summed and converted to cover fractions at MODIS pixel scale for validation analysis. The tree fractional cover was validated against the MODIS $fPV_{semi\text{-}deciduous}$, while the remainder was compared against the sum of $fPV_{deciduous}$, $fPV_{herbaceous}$ and fNPV. It was assumed that deciduous woody is mostly shrubs at the understory.

Table 11 Summary of the accuracy assessment results with supervised classification

Dry Season	Overall Accuracy	Growing Season	Overall Accuracy
2006-Sep-12	0.77	2007-Jan-15	0.58
2006-Sep-29	0.93	2007-Jan-18	0.45
2006-Oct-30	0.83	2007-Feb-4	0.74

5. Result

5.1 Exploration and Decomposition of phenology characteristics of woody and herbaceous

Figure 64 shows amplitudes and phases from the first three significant frequencies (frequency=1, 2, 3). Both maps show the vertical gradient associated with local climate. The red area in the amplitude map corresponds a dominant regular annual phenological cycle. The yellow region in the amplitude map corresponds to a relatively high half-year frequency, which could indicate either a distinct long dry or long wet seasonality according to the phase differences or some form of two layer phenological behavior. Integrated amplitude and phase information should enable the separation of vegetation types with an annual phenological cycle, a long growing season, or a long dry season.

A set of sample sites were used to explore the frequency characteristic of different species composition. The sites were selected based on vegetation maps (SAFARI 2000)

and field observation (Campo-Bescós & Muñoz-Carpena 2013; Gibbes et al. 2013), while the frequency characteristics were delineated by the first five significant frequencies (range 1 per year to 16 per year) (Figure 66). The plots were colored to distinguish herbaceous, deciduous woody, and semi-deciduous woody vegetation. As Figure 66 shows, significant amplitude mostly appears at the first two frequencies. Woody vegetation tends to have higher amplitude at the one-year frequency and lower half-year frequency than herbaceous vegetation and shrubs. This indicates the major annual cycling of woody vegetation. On the other hand, the relatively significant half-year response with close phases between the first two frequencies indicates a shorter growing season and rapid green-up of herbaceous and shrub vegetation. The phase plots show limited variation in patterns among vegetation types and these are convolved with local seasonal climate variation. However, some of the different phases between shrub and herbaceous vegetation may suggest that there may be a possibility of using these end-members to separate the dynamics of these components.

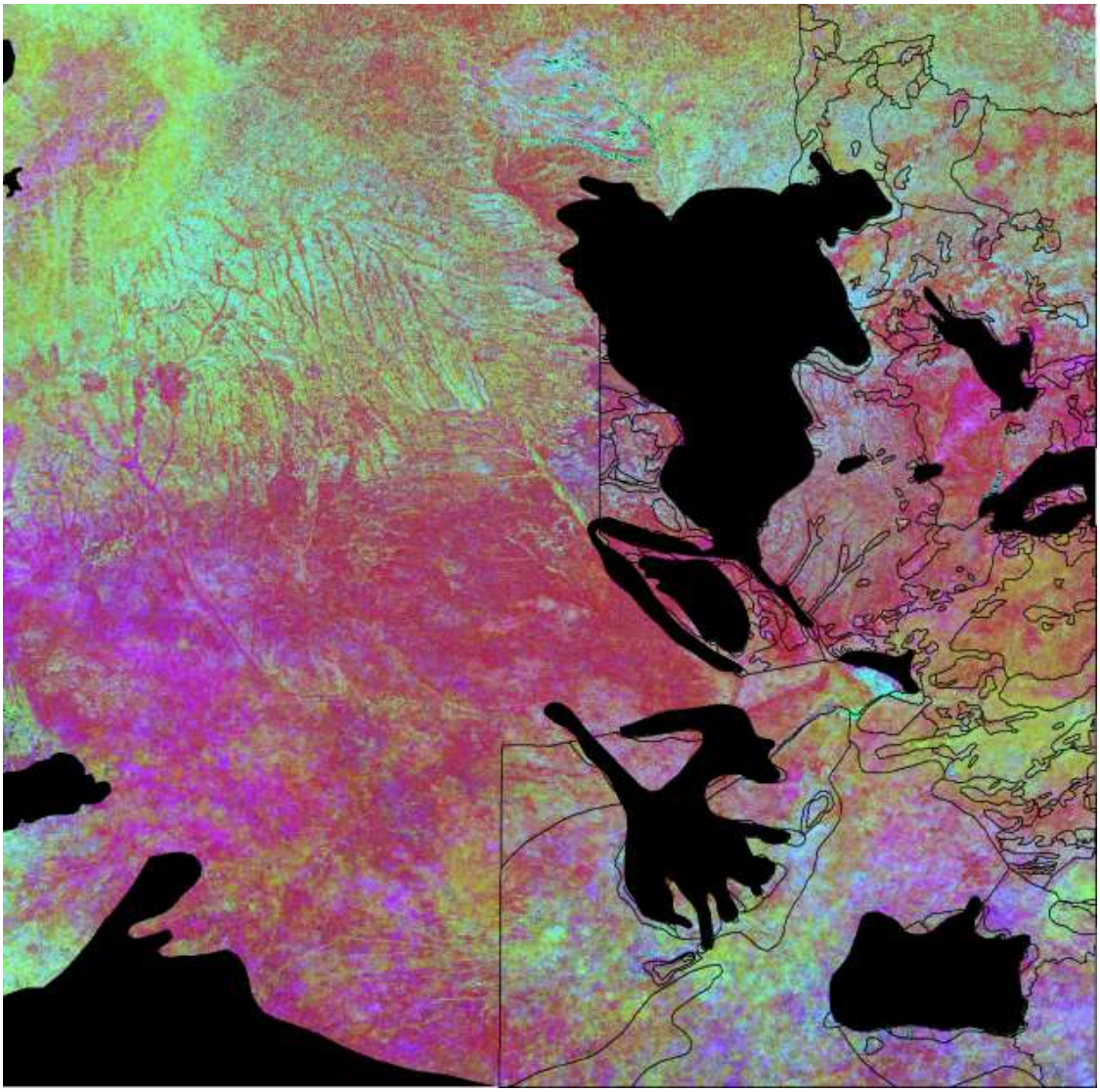

Figure 63. Amplitude frequency characteristic overlaid with vegetation types (black solid line). The maps show Pseudo-color (Period Interval: Red=1 year, Green=0.5 year, Blue=0.25 year)

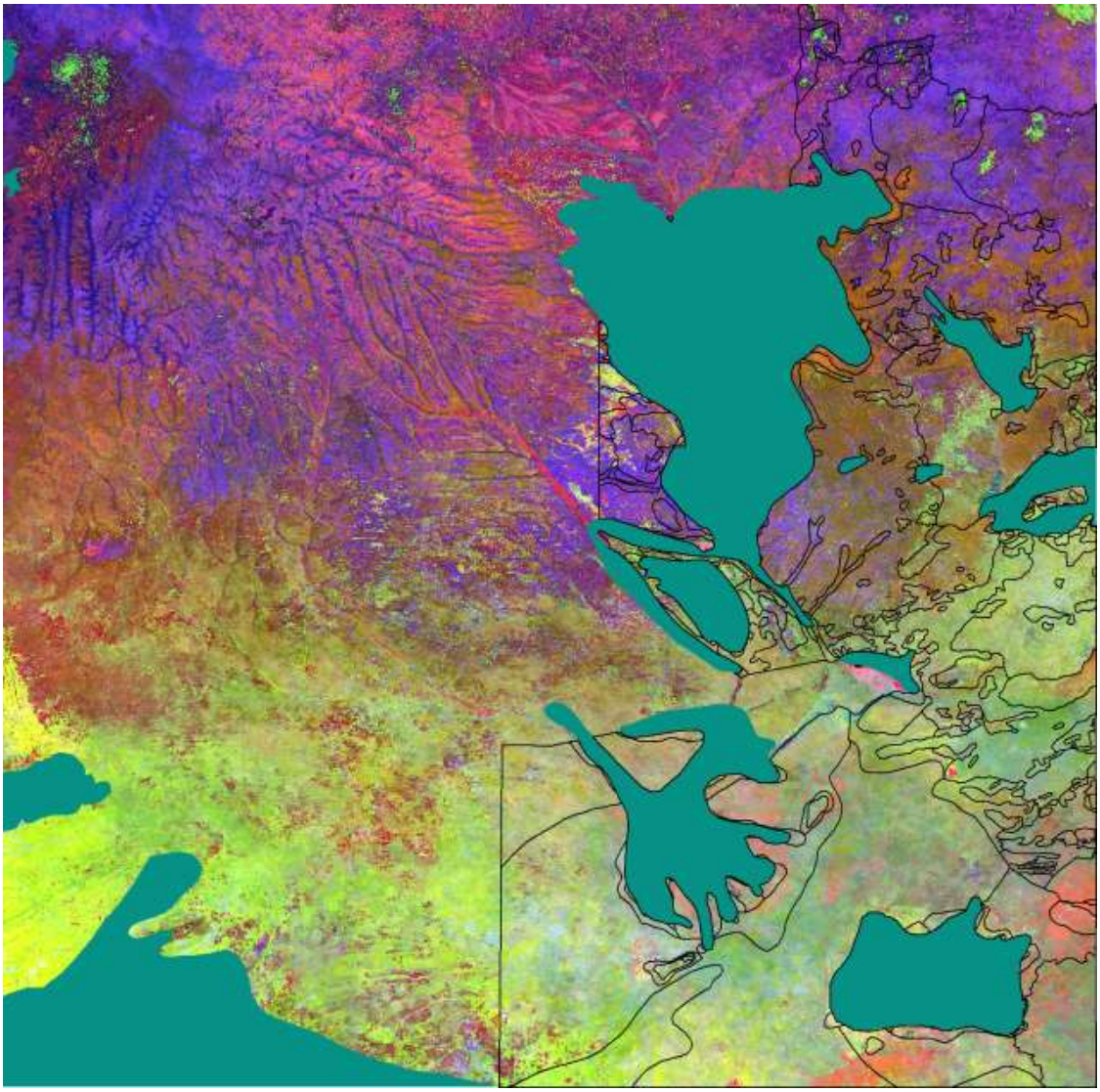

Figure 64. Phase frequency characteristics overlaid with vegetation types (black solid line). The maps show Pseudo-color (Period Interval: Red=1 year, Green=0.5 year, Blue=0.25 year)

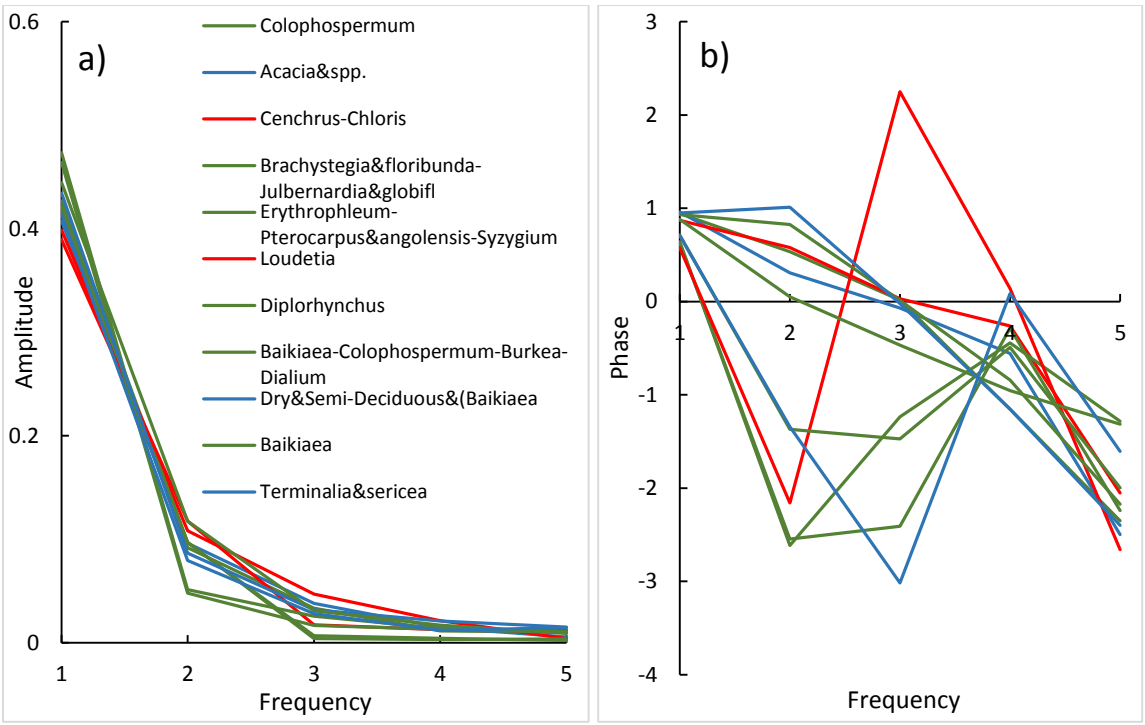

Figure 65. Frequency characteristics of different vegetation types. A) average amplitude of vegetation types based on SAFARI map; b) average phase of vegetation types based on SAFARI map

By assessing the time series variation of the classification map with Google Earth and PPI, three growing patterns were identified (Figure 67). The pattern in the northwest suggests evergreen or semi-deciduous phenology, vegetation that retains most of its leaves during the dry season and flushes again before all old leaves fall off. This area corresponds to the Miombo woodland and is known to receive abundant precipitation and be made up of dense woody cover. The pattern in the southeast indicates that vegetation loses its leaves seasonally and flushes again after a short periods of leaflessness, which indicates a deciduous woody phenology pattern. Examination of high-resolution imagery in Google Earth suggests that this region is dominated by shrubs (where this might be defined by woody plants of 2-m height or less). The pattern in the southwest suggests that most vegetation flushes leaves after the woody shrubs suggesting a strong obligate response to seasonal rainfall, and general exhibits a short growing season. Assessment of

these areas in Google Earth images suggests that herbaceous vegetation predominates with some sparse woody cover present here and there.

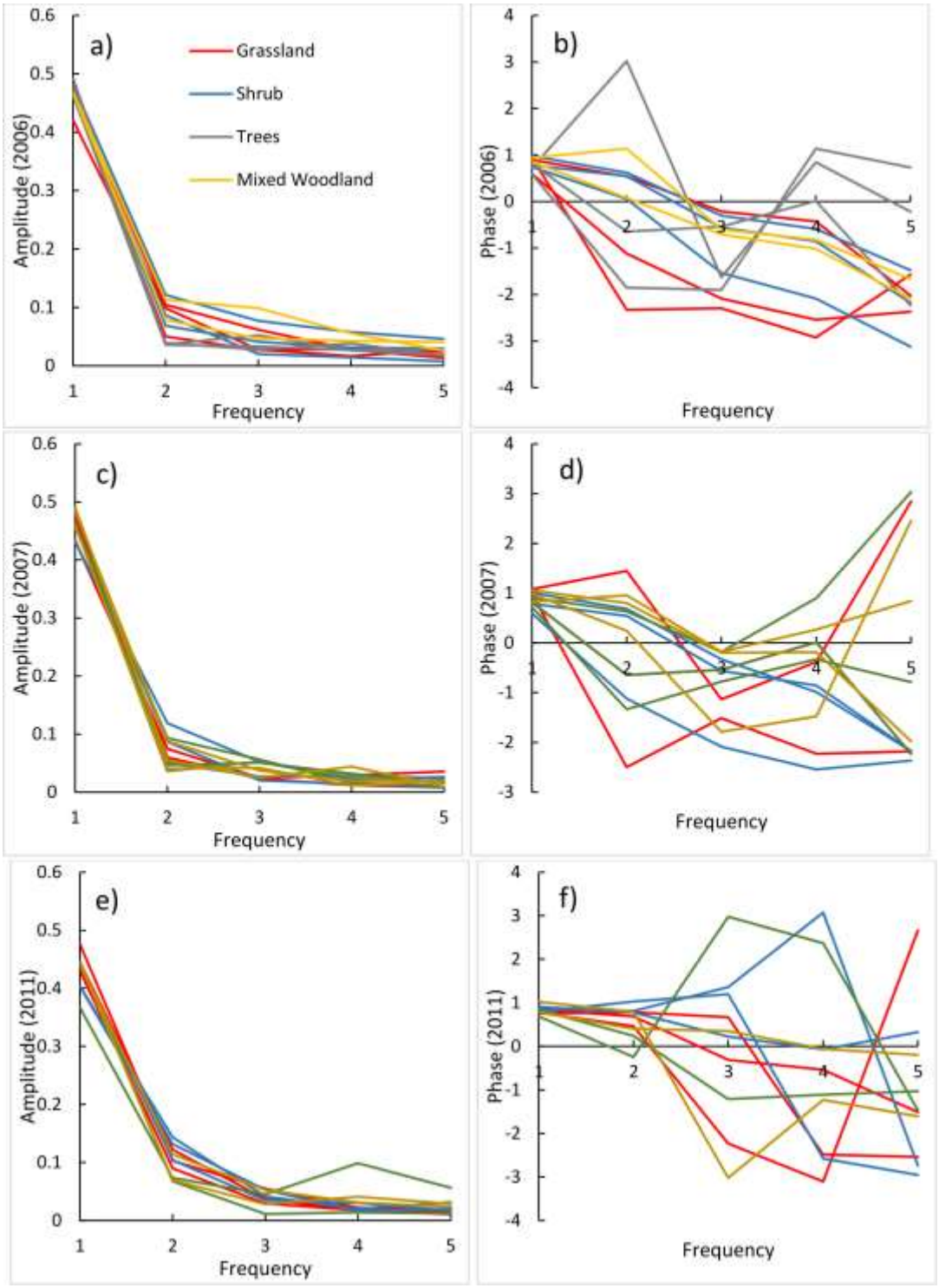

Figure 66. Single pixel amplitude and phase based on field observation (field observation was provided by Jane Southworth)

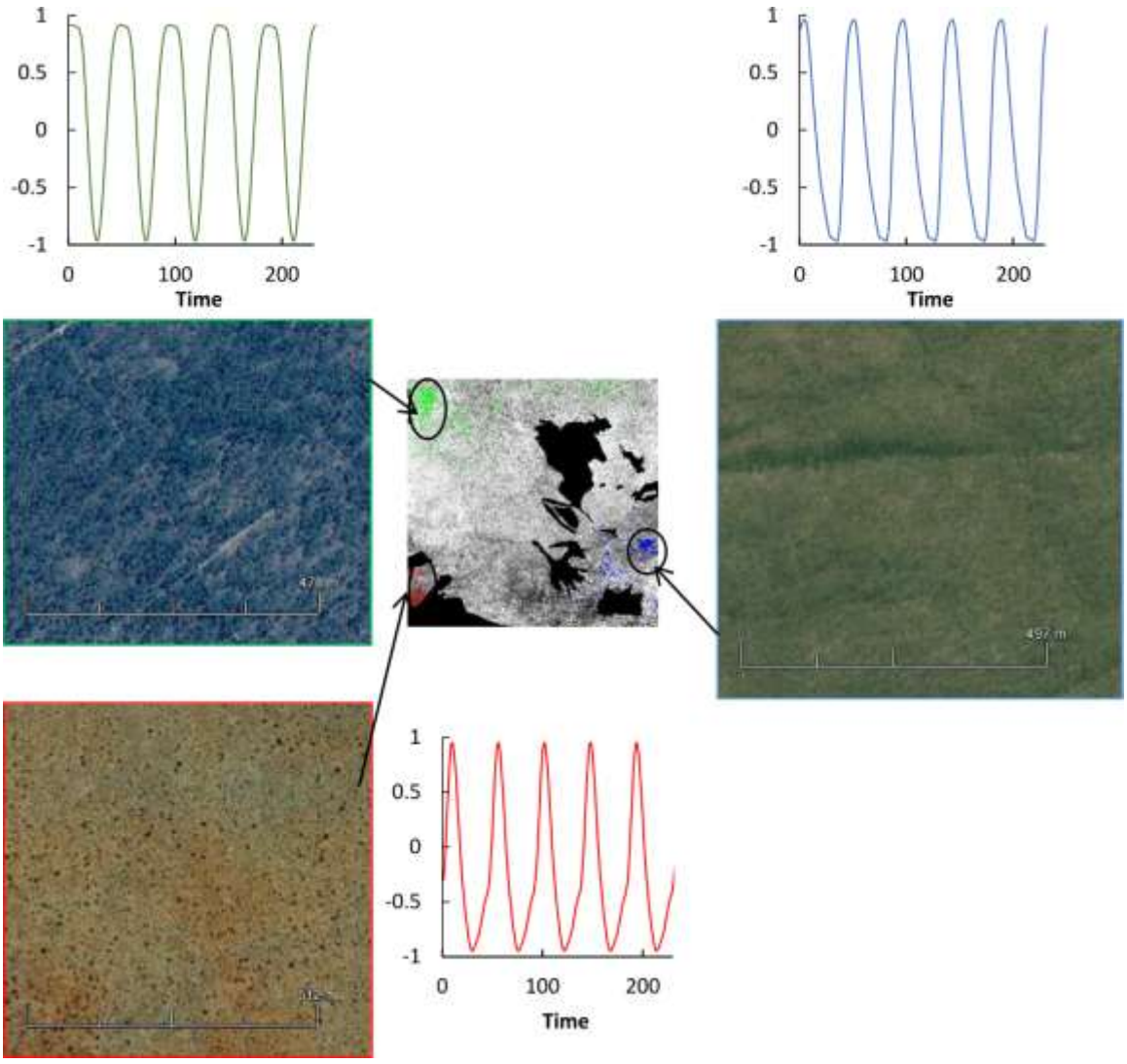

Figure 67 Distribution of the distinctive growing patterns

5.2 Mapping fPVsemi-deciduous, fPVdeciduous, fPVherbaceous and fNPV

The outputs of the model include 8-day time series of fractional cover of $fPV_{semi\text{-}deciduous}$, $fPV_{deciduous}$, and $fPV_{herbaceous}$ from 2002-2011. The RGB color ramp was used to illustrate the monthly average distribution of green overstory ($fPV_{semi\text{-}deciduous}$), green understory ($fPV_{deciduous}$ and $fPV_{herbaceous}$), and dry vegetation (fNPV) (Figure 68). The dark areas suggest a predominantly bare surface with only sparse vegetation cover. The general temporal pattern suggests a dry season between April and October during which dead biomass and litter accumulate resulting in increases in NPV. The flush of vegetation

growth shows distinctive patterns in three regions: the northern part including Angolan Miombo woodlands and the Central Zambezian Miombo woodlands, the central part including Zambezian Baikiaea Woodlands and Zambezian and Mopane Woodlands, and the southern part including Angolan Mopane woodlands and Kalahari Acacia-Baikiaea woodlands. Brevi- and semi-deciduous woody patterns mostly occur in the northern part, while the rest is dominated by deciduous woody and herbaceous vegetation. The central part with more savanna trees like *Colophospermum mopane* drops and flushes leaves earlier than the southern part where more fine-leaved, xeric *Acacia* spp. dominate, although *Terminalia* spp. is fully deciduous.

Table *12*In order to examine the results of the frequency decomposition in detail, a set of sites were selected that sample the main vegetation types (Figure 69; Table 12). These sites were characterized by images from Google Earth and monthly precipitation patterns and statistics from *Terrestrial Precipitation: 1900-2010 Gridded Monthly Time Series* (Matsuura & Willmott 2012), and 10 year time series profiles of the extracted cover fractions (Figure 70 to Figure 88).

The *Brachystegia* and *Erythrophleum* forest sites have a high semi-deciduous component with low deciduous and zero herbaceous components. In contrast, the shrub land and Acacia show significant deciduous fraction with low seasonal variation from the semi-deciduous component. The *Terminalia* site dominated by grassland shows combination of deciduous and herbaceous fraction with near-zero semi-deciduous components. However, *Terminalia* site with a higher shrub cover shows significant deciduous but zero herbaceous fractions, which is inconsistent with the Google Earth

image. This case indicates the limitation of the frequency decomposition when separating deciduous and herbaceous vegetation at some arid areas.

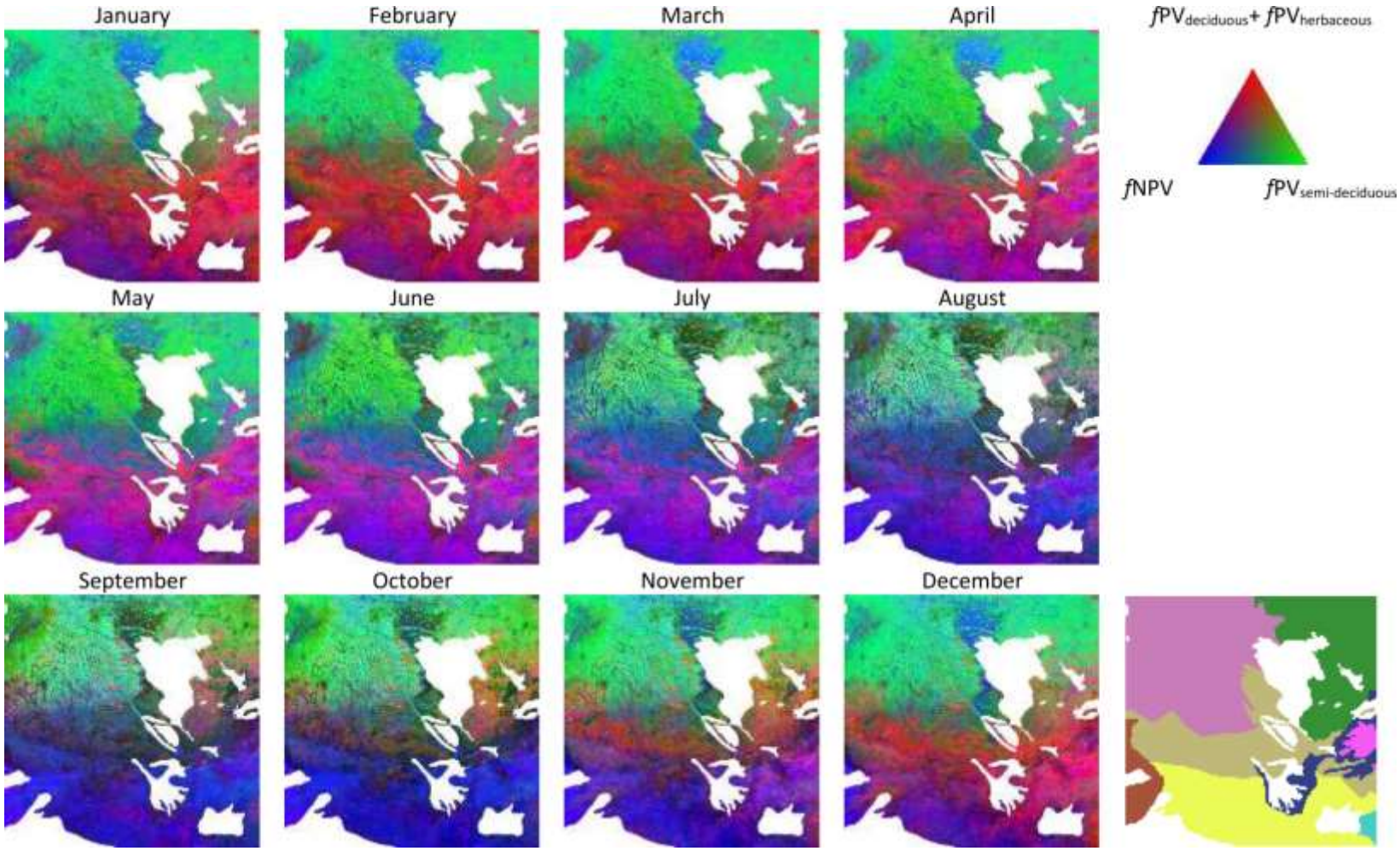

Figure 68 Monthly average of fractional cover for green tree canopy, green deciduous and herbaceous, and NPV in the southern African savanna zone. The proportions of land covers are shown in RGB as specified in the color legend. The dark area suggests high proportion of bare soil. An ecoregion map (Figure 50) is also displayed at the right corner.

Table 12. Samples for vegetation types

Latitude	Longitude	Vegetation Type	Land Cover	Figure Number
-12.25	25.22	Brachystegia floribunda-Julbernardia panicul	Forest	Figure 69
-13.21	26.09	Brachystegia floribunda-Julbernardia globifl	Forest	Figure 70
-15.15	24.85	Brachystegia spiciformis (on Kalahari Sand)	Forest	Figure 71
-16.38	24.26	Brachystegia spiciformis (on Kalahari Sand)	Shrubs - low LD	Figure 72
-18.44	26.09	Colophospermum	Agriculture	Figure 73
-18.9	23.57	Colophospermum	Shrubs - protected	Figure 74
-21.3	23.05	Terminalia sericea	Shrubs - protected	Figure 75
-21.62	23.56	Terminalia sericea	Grasslands - protected	Figure 76
-11.22	24.24	Erythrophleum-Pterocarpus angolensis-Syzygium	Forest	Figure 77
-19.06	26.64	Acacia leuderitzii-Acacia giraffae-Lonchocar	Forest	Figure 78
-18.01	24.91	Baikiaea	Shrubs - protected	Figure 79
-15.81	22.11	Loudetia	Shrubs - protected	Figure 80
-13.93	18.84	Miombo Woodlands	Forest - with agricultural activities	Figure 81
-17.07	17.16	Zambezian Baikiaea Woodlands	Shrubs - moderate livestock density	Figure 82
-18.65	25.5	Colophospermum	Shrubs - low livestock density	Figure 83
-19.92	23.59	Colophospermum	Shrubs - protected	Figure 84
-16.75	23.61	Baikiaea-Colophospermum-Burkea-Dialium	Shrubs - protected	Figure 85
-17.7	24.08	North Forest savanna and woodland	Forest - with moderate or higher livestock density	Figure 86
-19.64	16.67	Mopane savanna	Shrubs - low livestock density	Figure 87

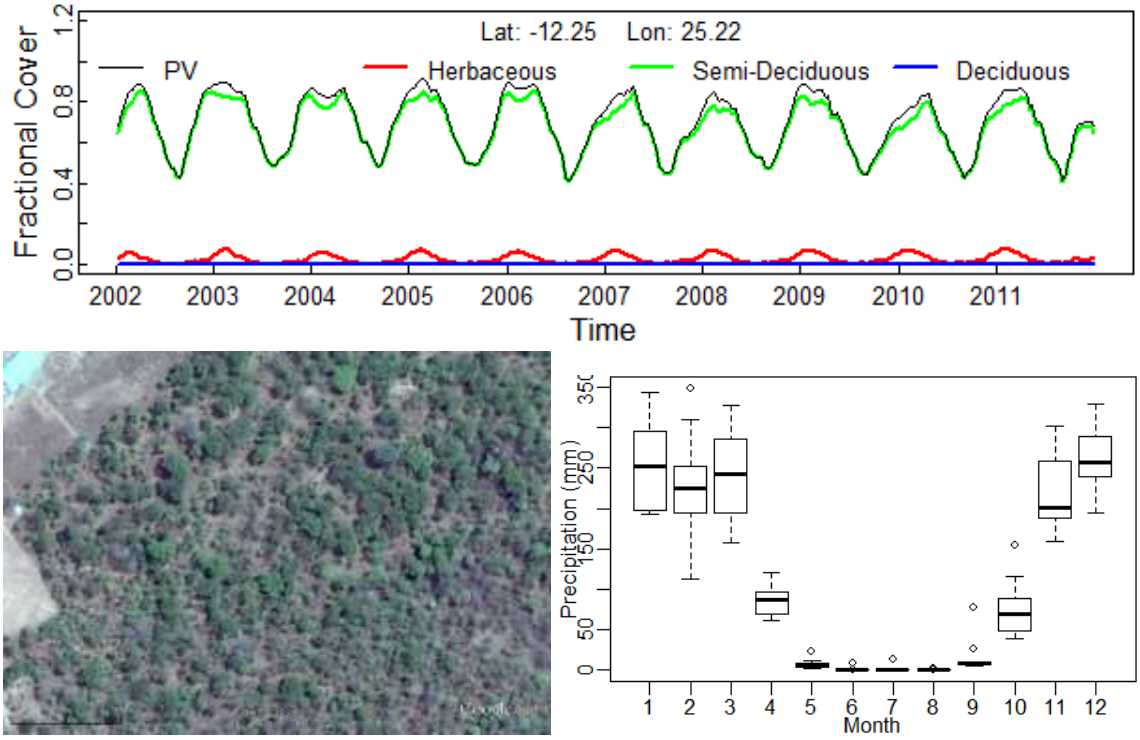

Figure 69. Decomposition fPV into $fPV_{Evergreen}$, $fPV_{Deciduous}$ and $fPV_{Herbaceous}$ for vegetation type 1

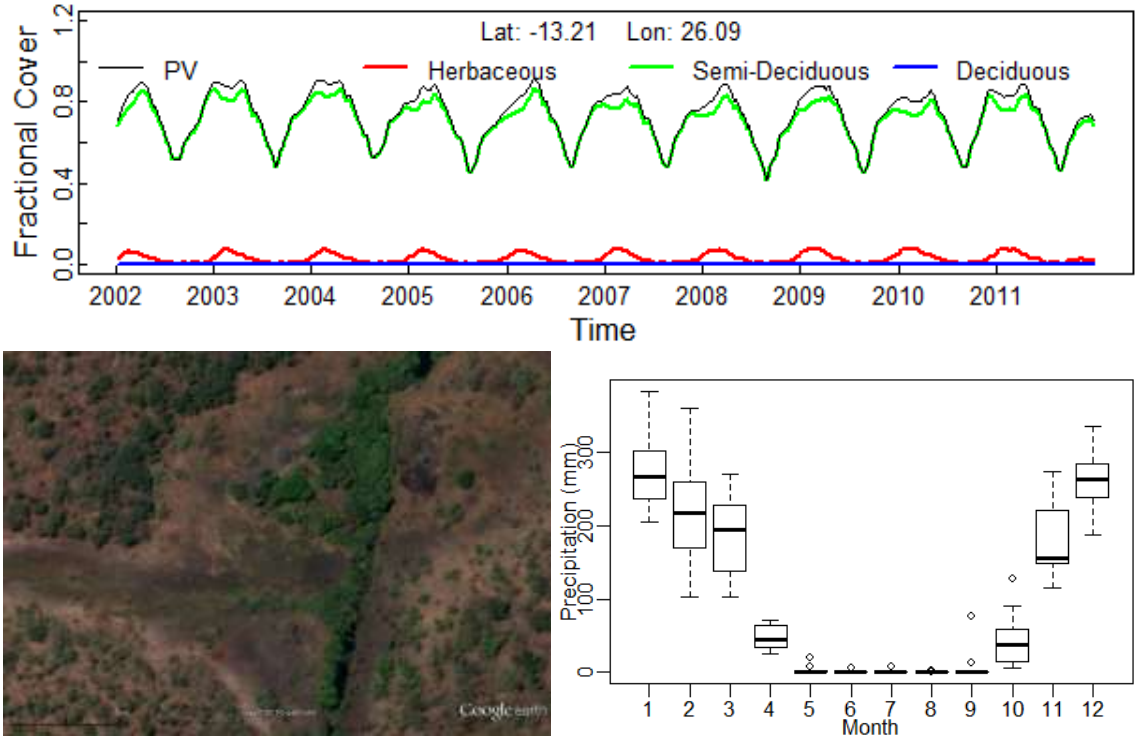

Figure 70. Decomposition fPV into $fPV_{Evergreen}$, $fPV_{Deciduous}$ and $fPV_{Herbaceous}$ for vegetation type 2

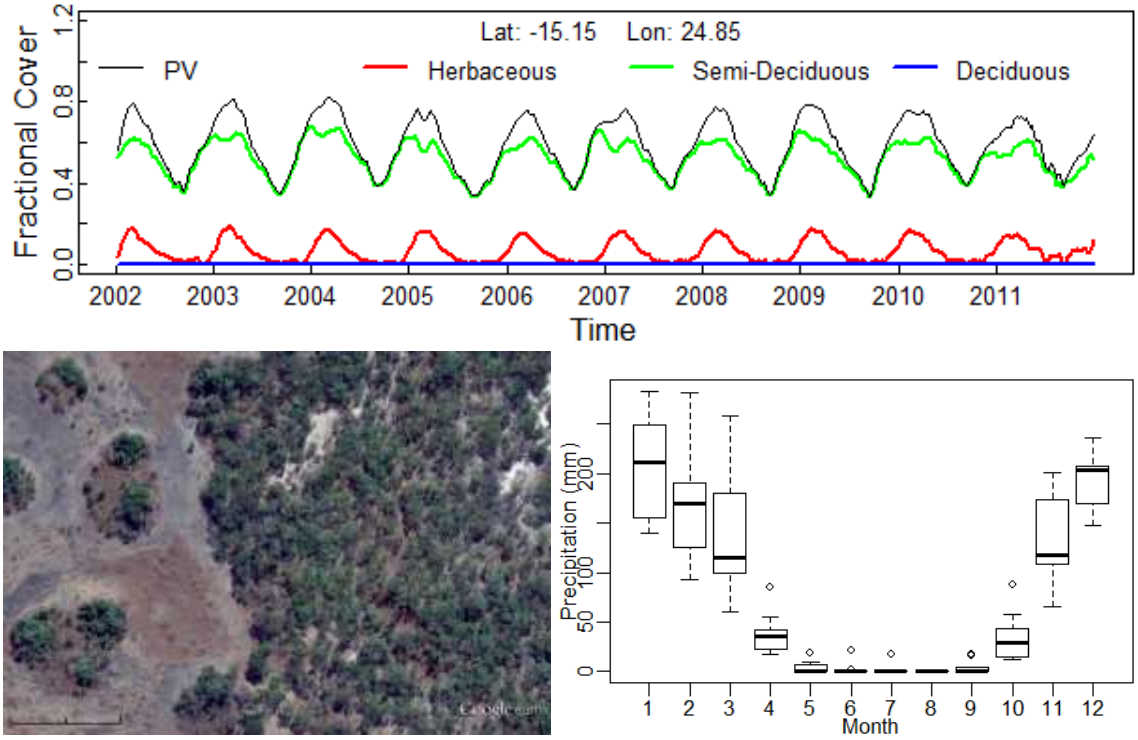

Figure 71. Decomposition fPV into $fPV_{Evergreen}$, $fPV_{Deciduous}$ and $fPV_{Herbaceous}$ for vegetation type 3

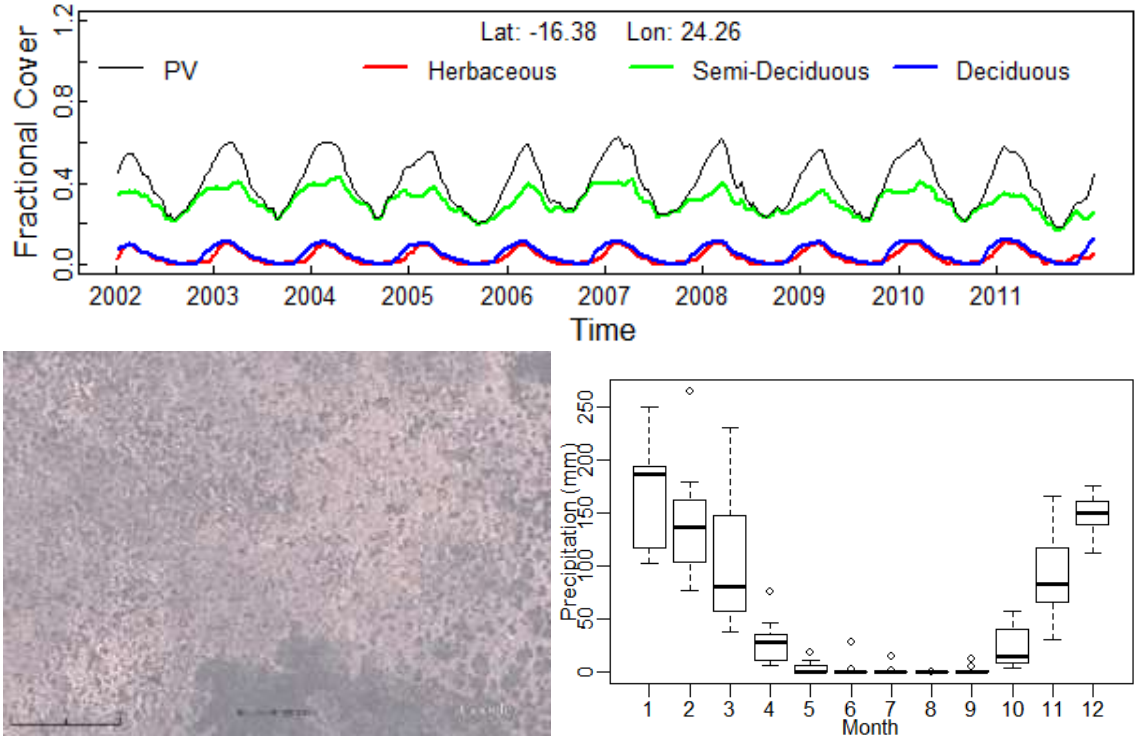

Figure 72. Decomposition fPV into $fPV_{Evergreen}$, $fPV_{Deciduous}$ and $fPV_{Herbaceous}$ for vegetation type 4

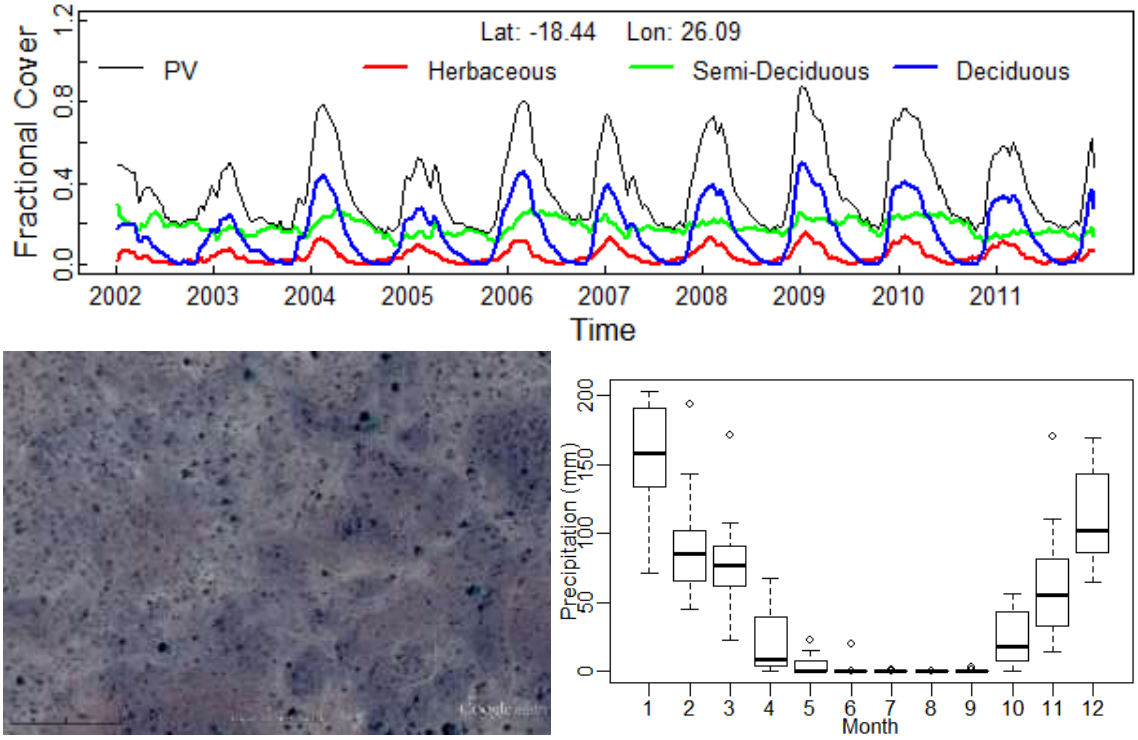

Figure 73. Decomposition fPV into $fPV_{Evergreen}$, $fPV_{Deciduous}$ and $fPV_{Herbaceous}$ for vegetation type 5

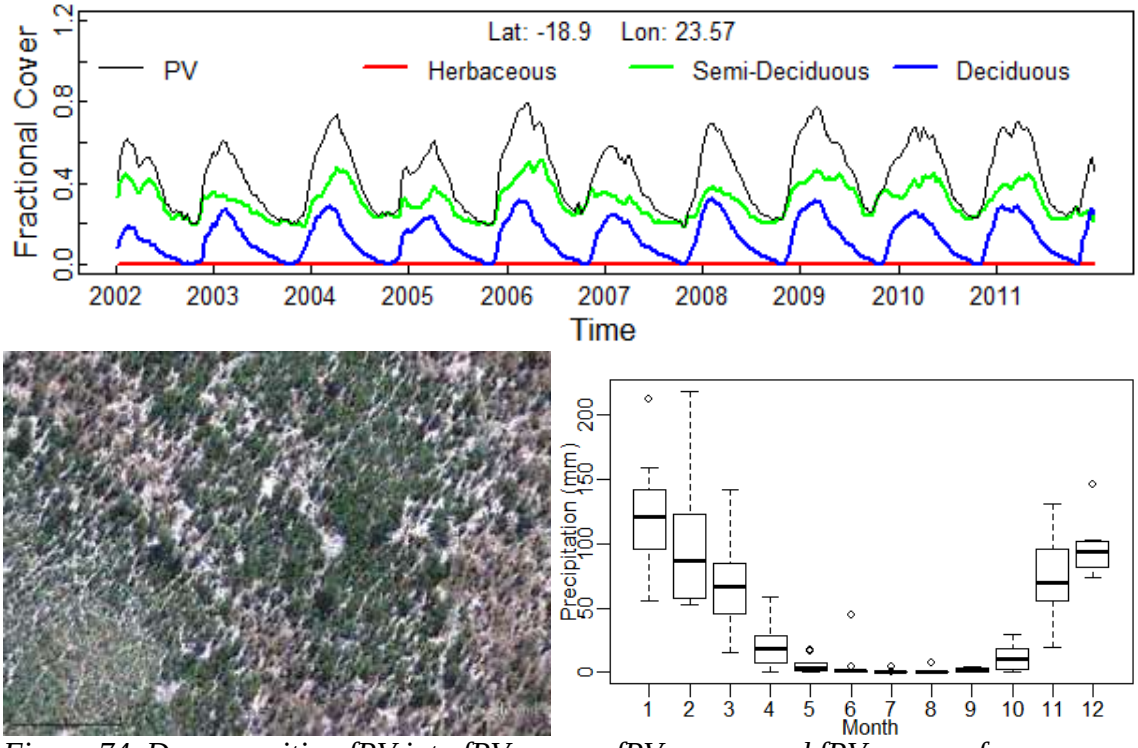

Figure 74. Decomposition fPV into $fPV_{Evergreen}$, $fPV_{Deciduous}$ and $fPV_{Herbaceous}$ for vegetation type 6

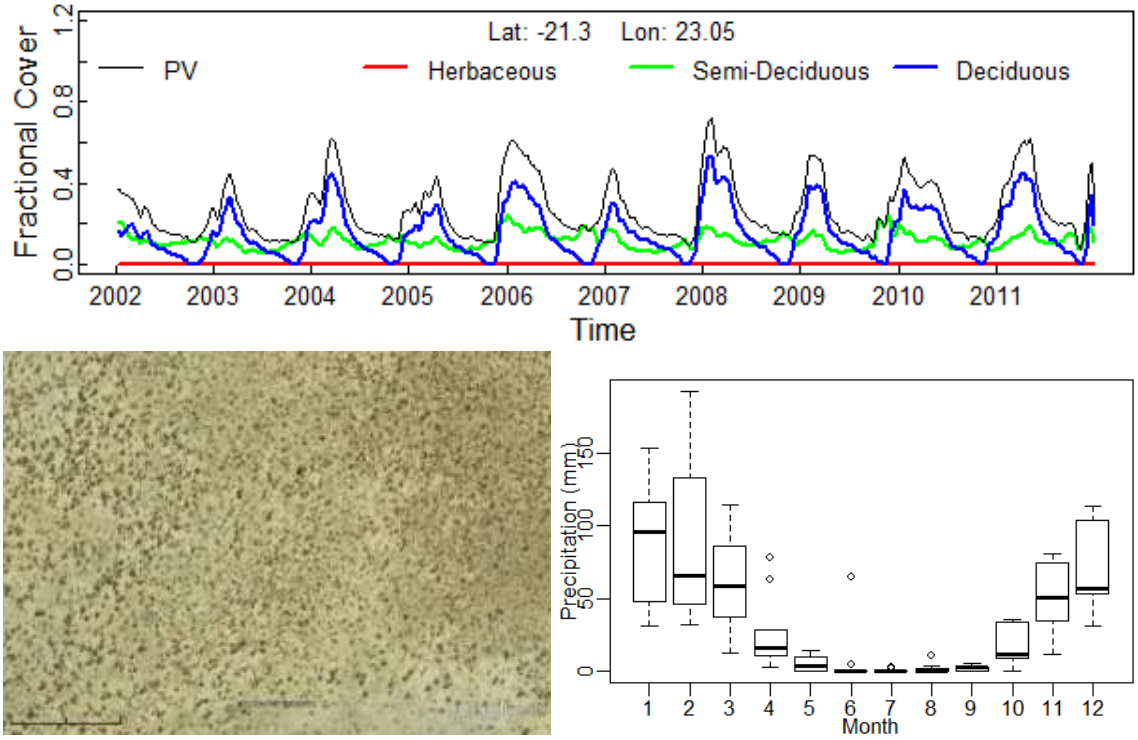

Figure 75. Decomposition fPV into $fPV_{Evergreen}$, $fPV_{Deciduous}$ and $fPV_{Herbaceous}$ for vegetation type 7

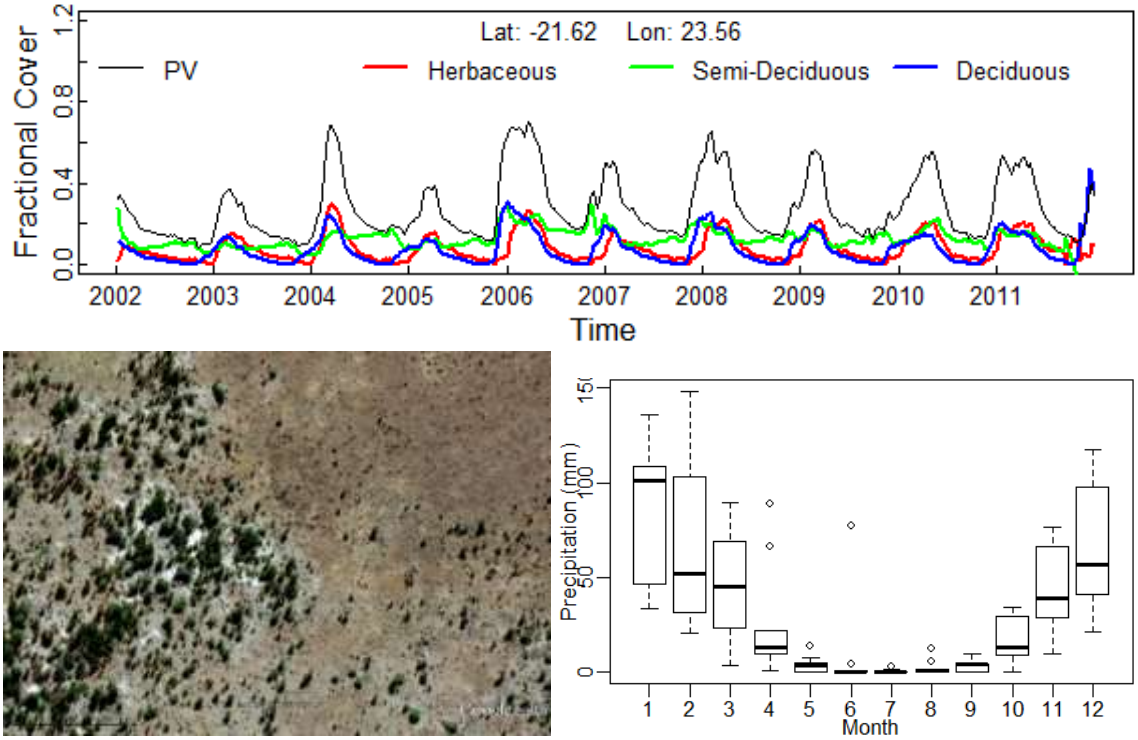

Figure 76. Decomposition fPV into $fPV_{Evergreen}$, $fPV_{Deciduous}$ and $fPV_{Herbaceous}$ for vegetation type 8

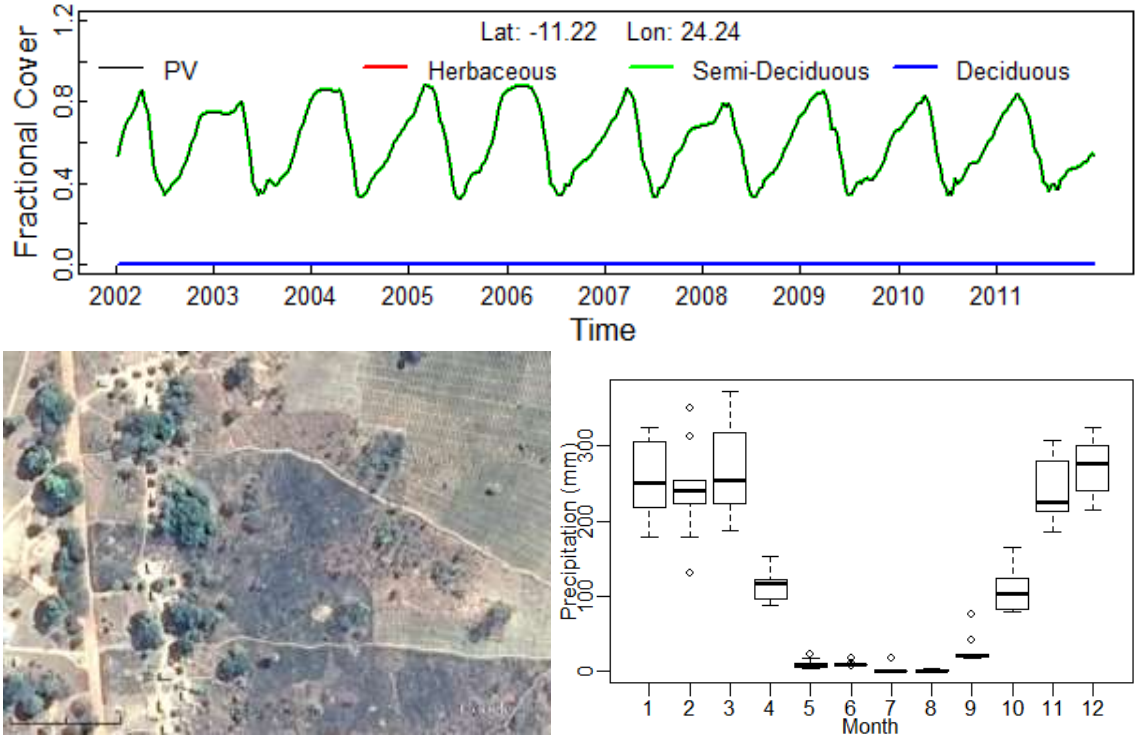

Figure 77. Decomposition fPV into $fPV_{Evergreen}$, $fPV_{Deciduous}$ and $fPV_{Herbaceous}$ for vegetation type 9

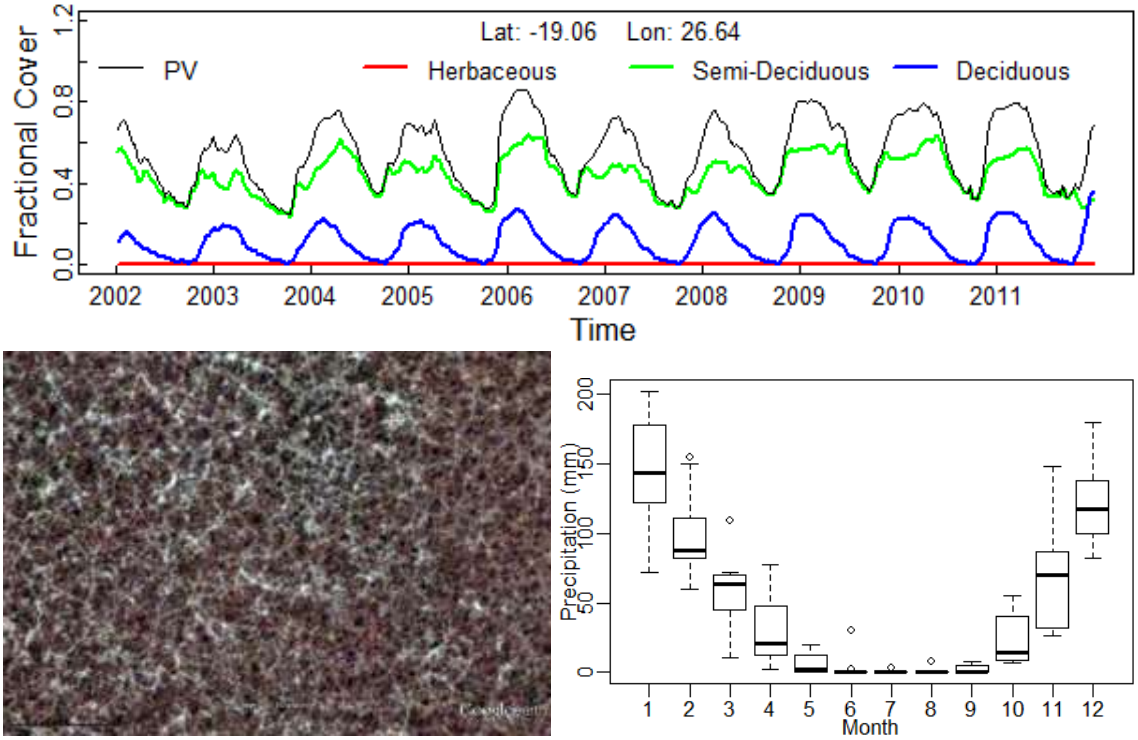

Figure 78. Decomposition fPV into $fPV_{Evergreen}$, $fPV_{Deciduous}$ and $fPV_{Herbaceous}$ for vegetation type 10

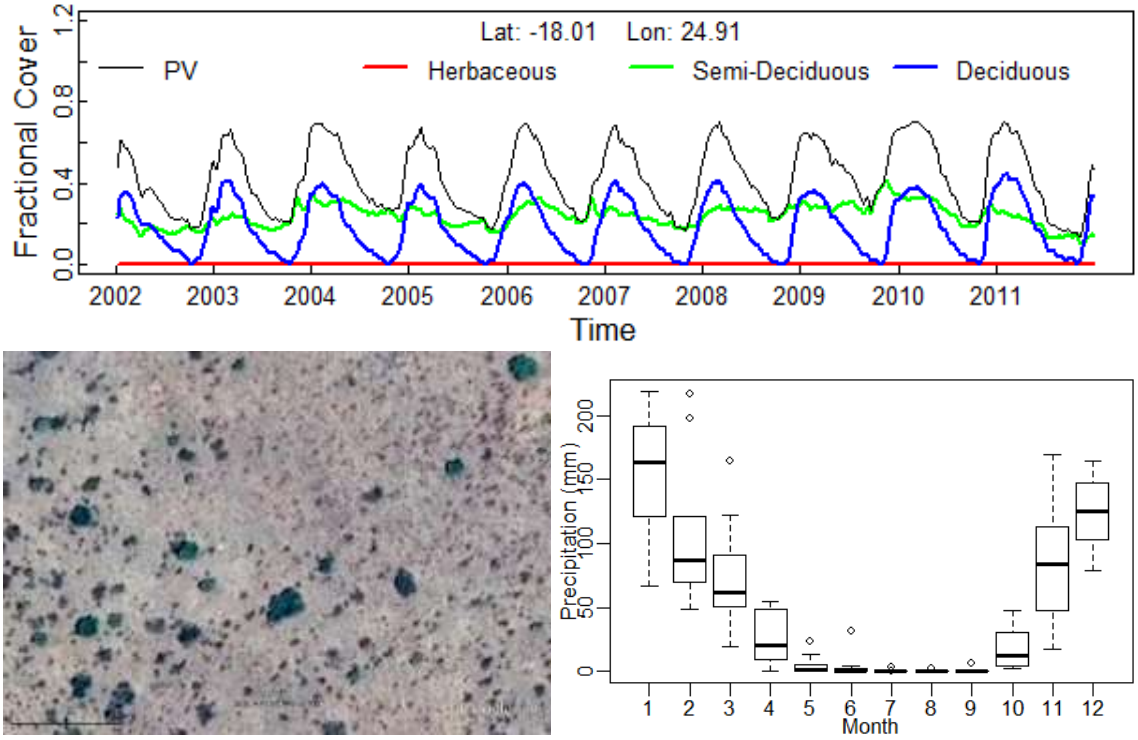

Figure 79. Decomposition fPV into $fPV_{Evergreen}$, $fPV_{Deciduous}$ and $fPV_{Herbaceous}$ for vegetation type 11

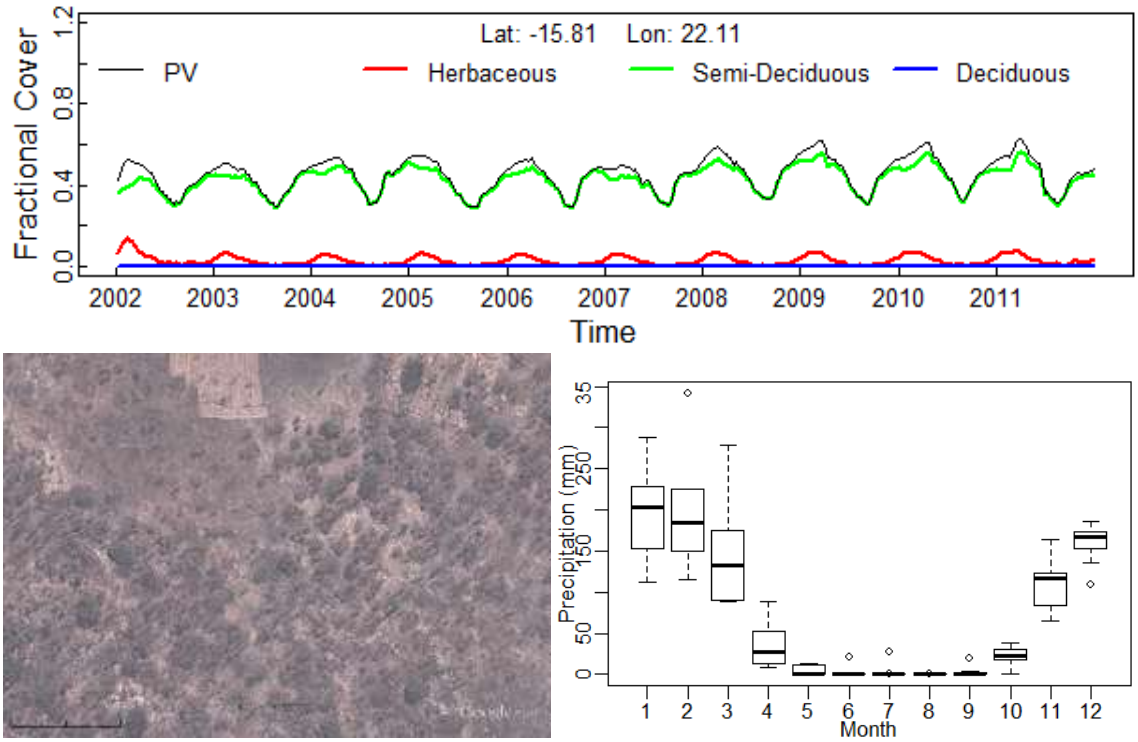

Figure 80. Decomposition fPV into $fPV_{Evergreen}$, $fPV_{Deciduous}$ and $fPV_{Herbaceous}$ for vegetation type 12

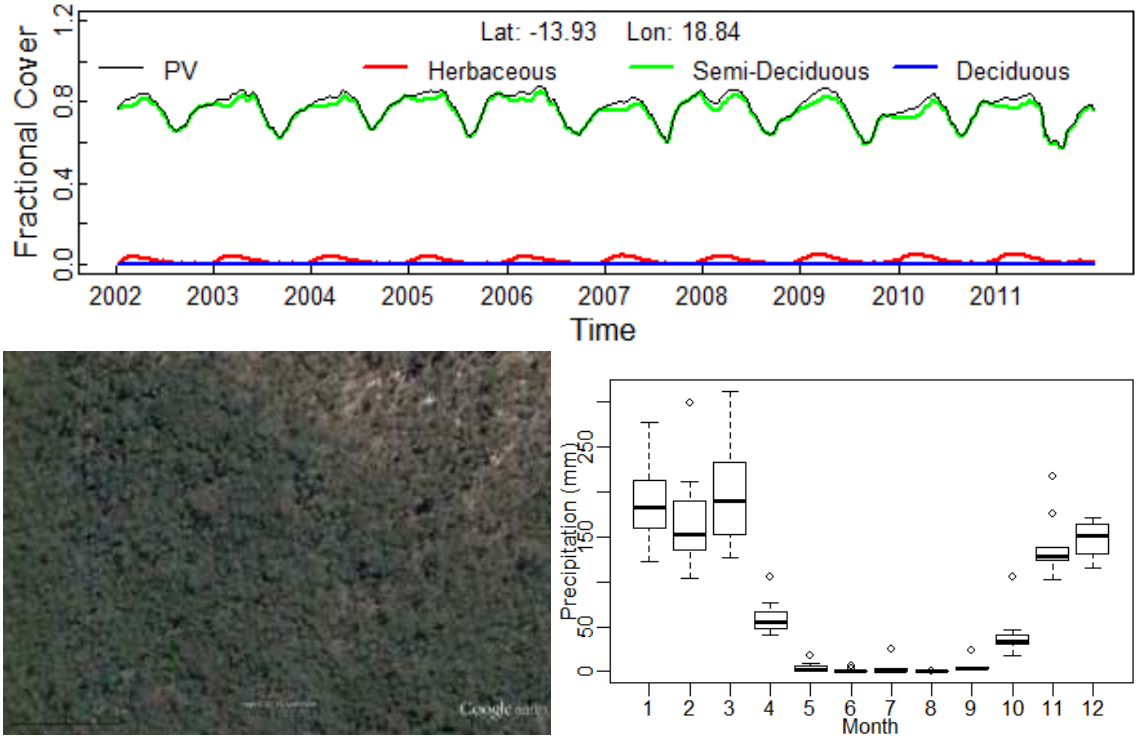

Figure 81. Decomposition fPV into $fPV_{Evergreen}$, $fPV_{Deciduous}$ and $fPV_{Herbaceous}$ for vegetation type 13

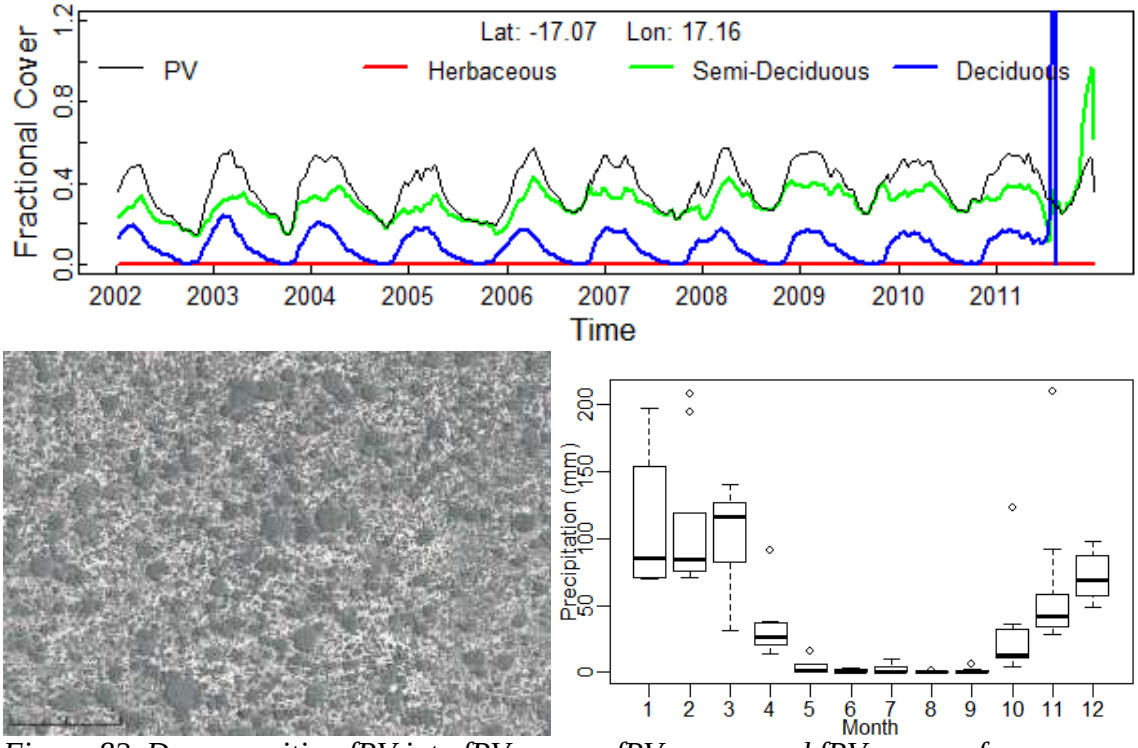

Figure 82. Decomposition fPV into $fPV_{Evergreen}$, $fPV_{Deciduous}$ and $fPV_{Herbaceous}$ for vegetation type 14

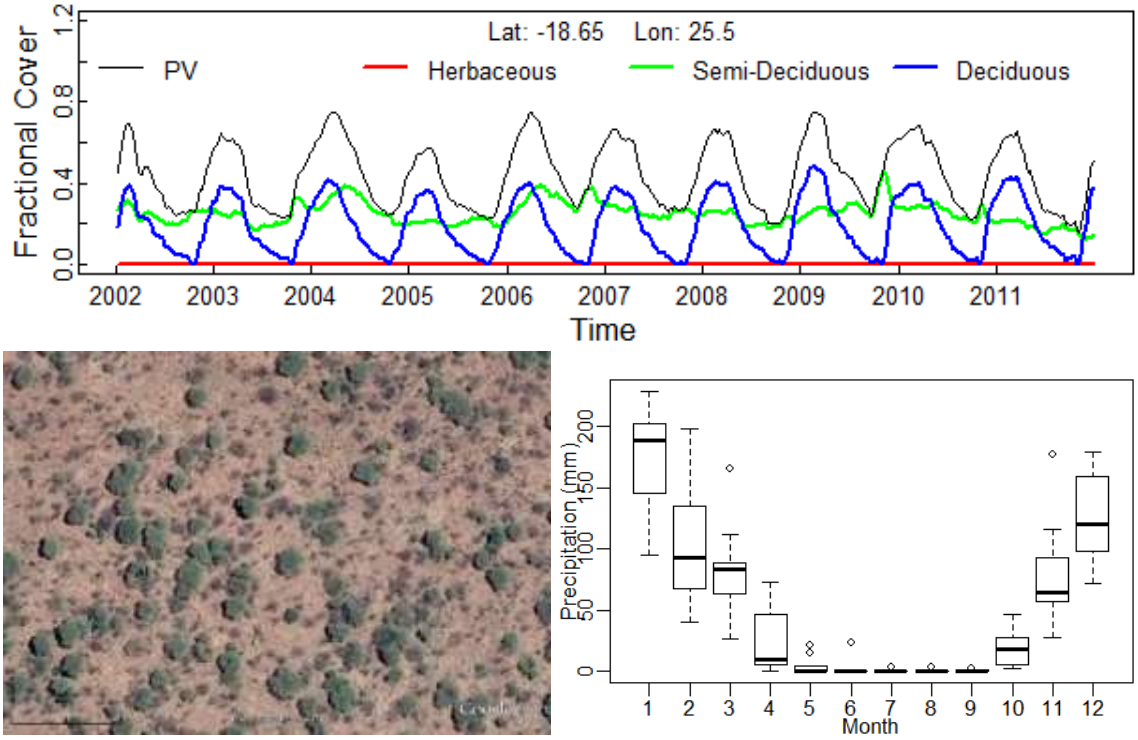

Figure 83. Decomposition fPV into $fPV_{Evergreen}$, $fPV_{Deciduous}$ and $fPV_{Herbaceous}$ for vegetation type 15

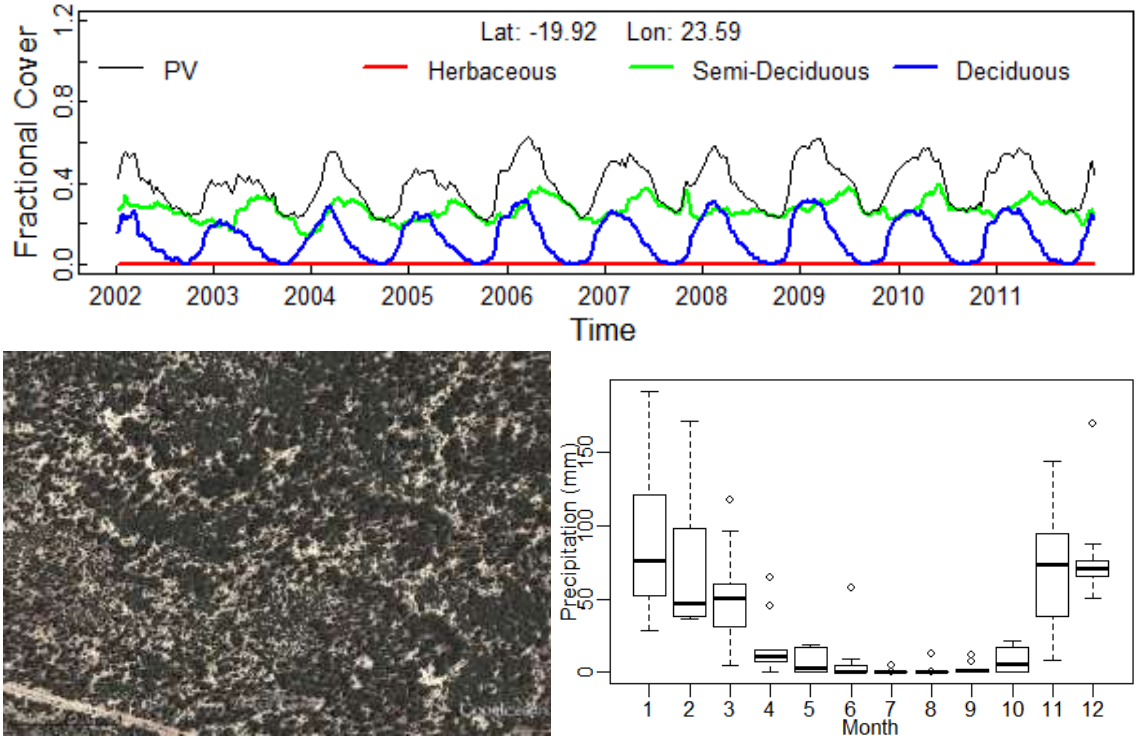

Figure 84. Decomposition fPV into $fPV_{Evergreen}$, $fPV_{Deciduous}$ and $fPV_{Herbaceous}$ for vegetation type 16

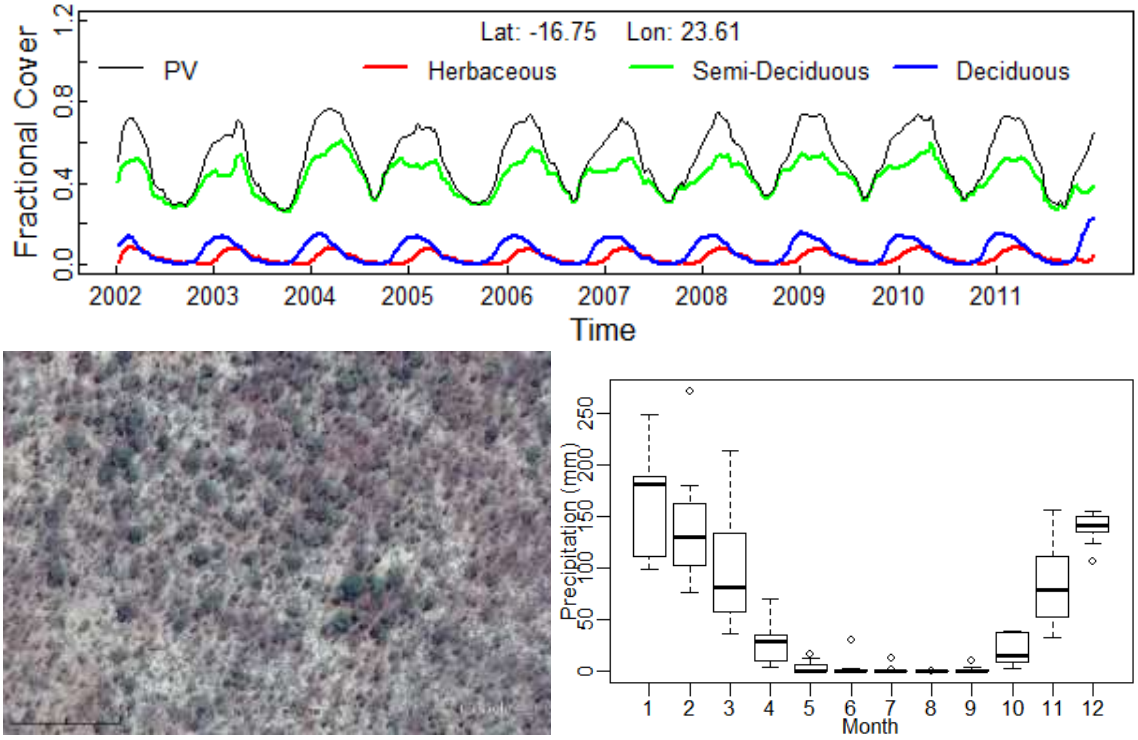

Figure 85. Decomposition fPV into $fPV_{Evergreen}$, $fPV_{Deciduous}$ and $fPV_{Herbaceous}$ for vegetation type 17

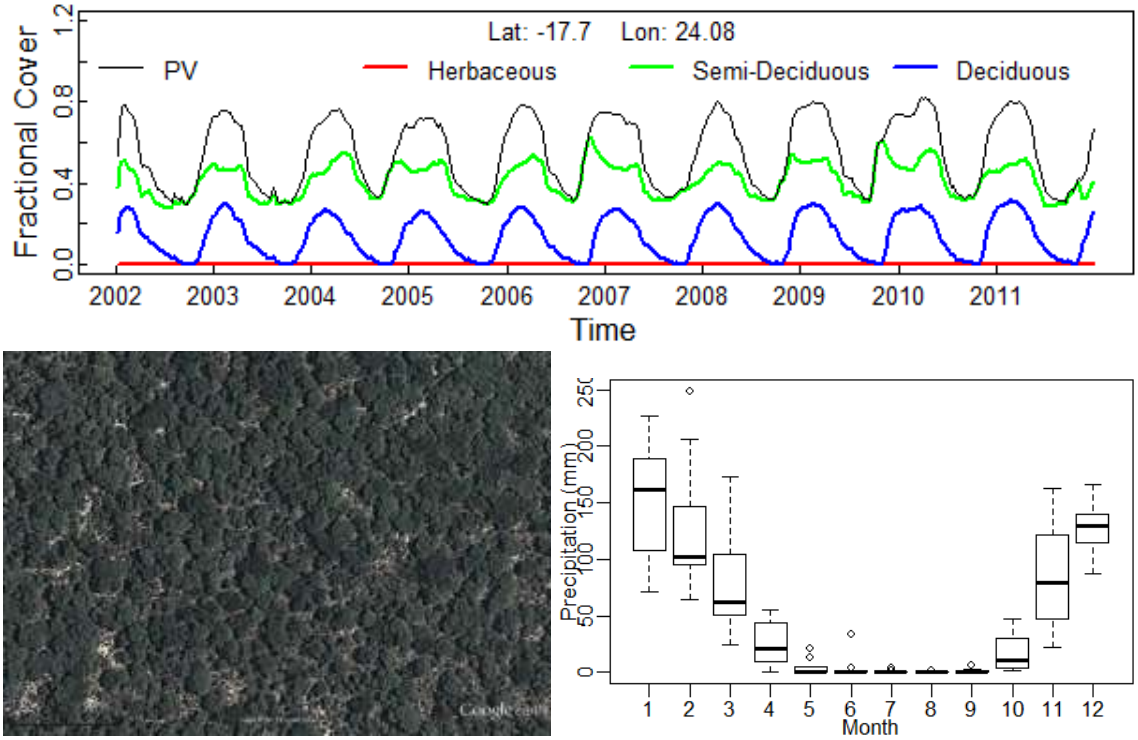

Figure 86. Decomposition fPV into $fPV_{Evergreen}$, $fPV_{Deciduous}$ and $fPV_{Herbaceous}$ for vegetation type 18

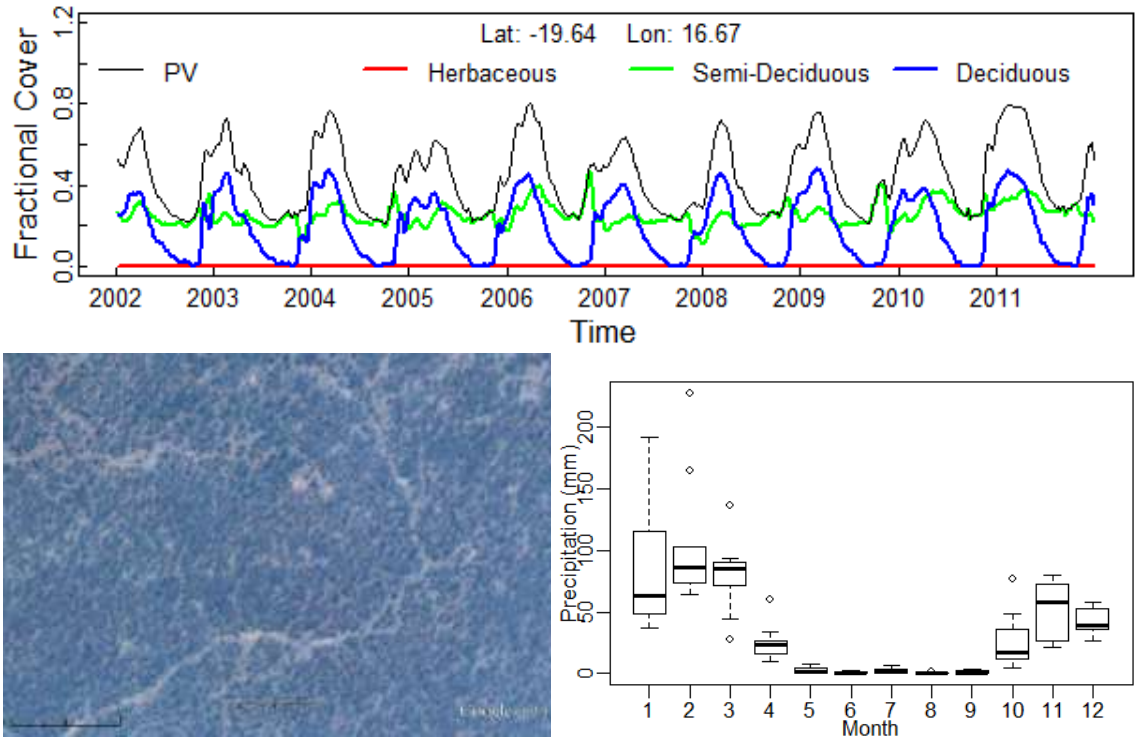

Figure 87 Decomposition fPV into $fPV_{Evergreen}$, $fPV_{Deciduous}$ and $fPV_{Herbaceous}$ for vegetation type 19

5.3 Mapping change of fPVsemi-deciduous, fPVdeciduous, and fPVherbaceous

Error! Reference source not found. reveals the difference of the yearly aximum coverage of tree, shrub, and herbaceous vegetation between 2002 and 2011. Negative values suggest a decrease of the coverage from 2002 to 2010, while positive values mean an increase of the fractional cover. Insignificant changes were displayed as yellow. The results indicate that tree coverage is generally declining in the Angolan Miombo woodland and the Central Zambezian Miombo Woodlands, but significantly rising in the Zambezian Baikiaea Woodlands and Kalahari Acacia-Baikiaea Woodlands. Shrub and herbaceous vegetation, on the other hand, shifted from Zambezian Baikiaea Woodlands to Kalahari Acacia-Baikisea Woodlands and Angolan Mopane Woodlands respectively.

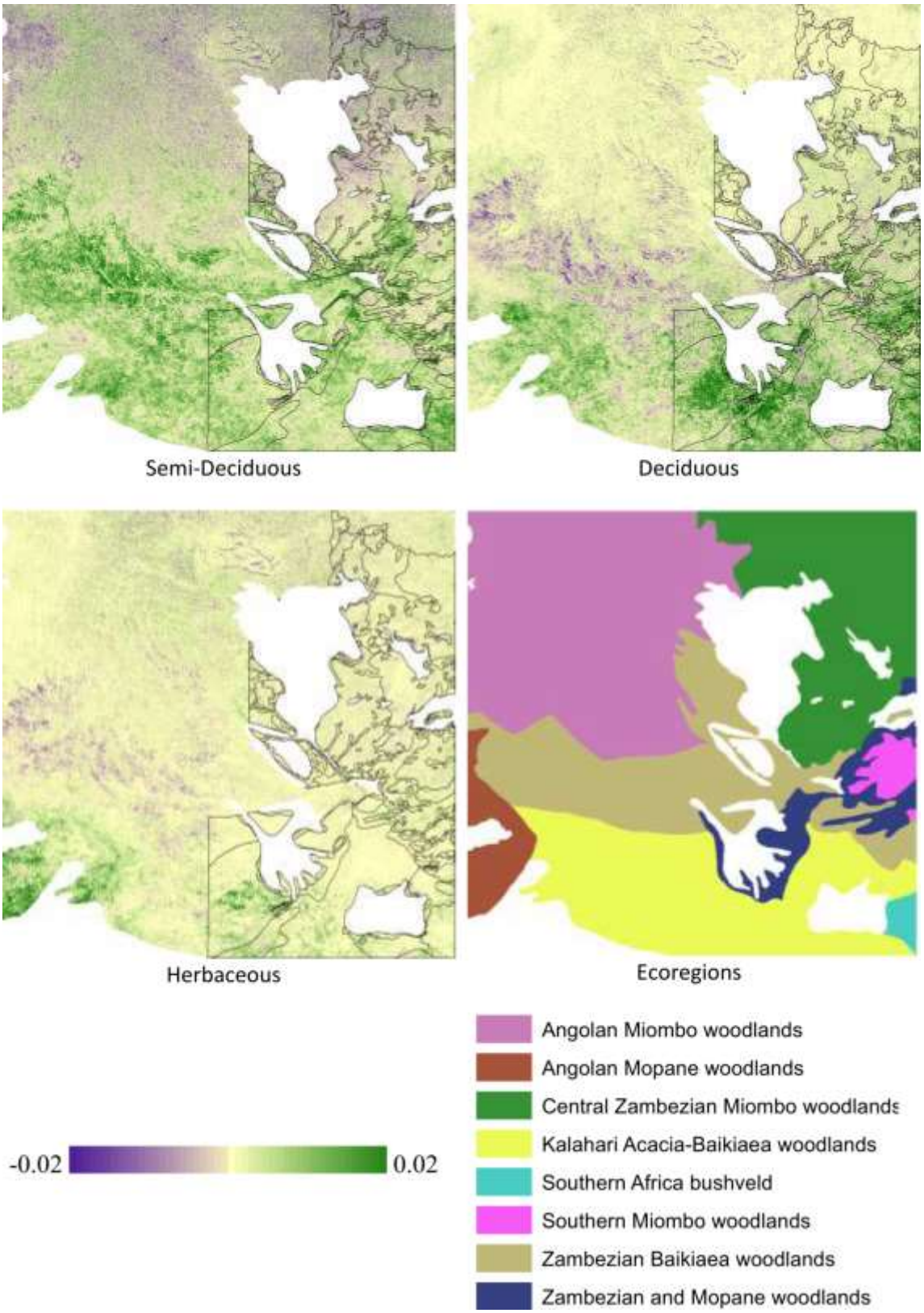

Figure 88 Change of yearly maximum fractional cover from 2002 to 2011. Negative means decreasing of fractional cover in ten years.

5.4 Validation of $fPV_{semi\text{-}deciduous}$ and remaining green vegetation Fractional Cover against IKONOS imagery

Figure 89 shows the assessment of the tree and green understory vegetation fractional cover estimated from IKONOS against those estimated from MODIS. The linear regression suggests that the two data sets produced similar fractional cover with a R^2 ranging from 0.68 to 0.69. Both plots suggest that MODIS tends to slightly underestimate the green vegetation fractional cover. It is possible that drying vegetation leads to a decline of NDVI and an increase of SWIR32, while IKONOS images consider it as green vegetation. Nevertheless, the MODIS estimation still captures the variation of fractional cover as reflected in the low RMSE (less than 0.1).

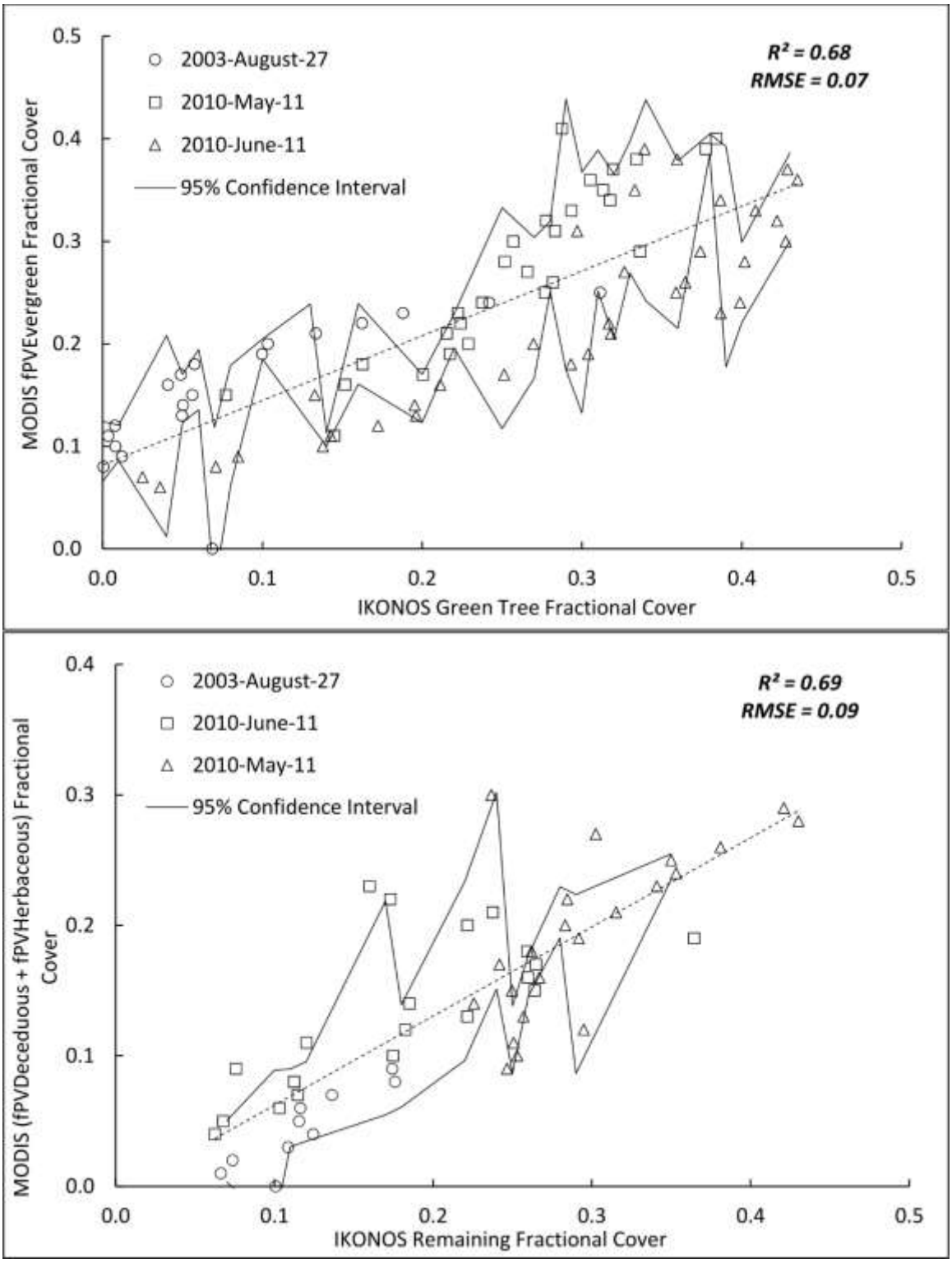

Figure 89 Linear relationship between a) the MODIS Semi-deciduous fraction cover versus the IKONOS canopy fraction cover b) the MODIS green deciduous and green herbaceous fraction cover versus the IKONOS green understory fraction cover.

5.5 Validation of Woody and remaining Vegetation Fractional Cover against Orbview-3 imagery

Figure 90 shows a scatter-plot comparison of Orbview-3 estimated fractional cover and that derived from the MODIS data. The RMSE is 0.1 in both comparisons, suggesting a strong agreement. The linear regression shows close to 1:1 linear correlation for the $fPV_{deciduous}$ and $fPV_{herbaceous}$. The $fPV_{semi\text{-}deciduous}$ is less correlated with the Orbview-3 estimation. The MODIS estimation is insensitive to the $fPV_{semi\text{-}deciduous}$ variation especially when the tree coverage is less than 20% in Orbview-3.

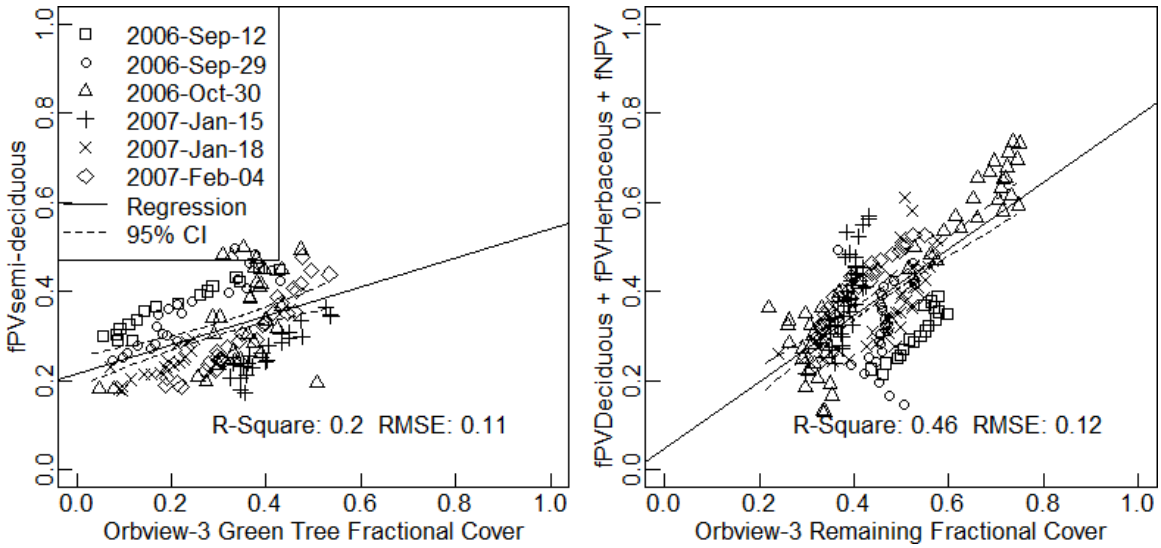

Figure 90 Linear relationship between a) the MODIS Semi-deciduous fraction cover versus the Orbivew-3 canopy fraction cover b) the MODIS green deciduous, green herbaceous, and NPV fraction cover versus the Orbiview-3 non-BS understory fraction cover.

6. Discussion

This chapter explored the possibility of decomposing *f*PV into $fPV_{semi\text{-}deciduous}$, $fPV_{deciduous}$, and $fPV_{herbaceous}$ in the southern African study region spanning diverse vegetation types and a strong precipitation gradient. Lu et al. (2003) decomposed the time series NDVI into woody NDVI and herbaceous NDVI, but the study ignored soil color effect on NDVI, which, in the present study, was excluded from *f*PV. Based on Lu et al. (2003) the time series NDVI is capable of separating evergreen NDVI from seasonal

NDVI by assuming that woody vegetation is mostly evergreen while herbaceous vegetation dries out every year. The assumption is not applicable in the southern African savanna due to the wide range of deciduous woody covers. Therefore, a linear unmixing under frequency domain was developed to separate the frequency of semi-deciduous, deciduous woody, and herbaceous vegetation.

One important assumption in our method is that phenology difference can be grouped into three categories: evergreen or semi-deciduous woody; deciduous woody; and herbaceous vegetation. The assumption has been investigated by previous work. De Bie et al. (1998) examined the phenology of 120 woody species in savanna and found two phenological groups: (1) woody vegetation using water from deeper soil or riverbeds and restricting evaporation via sclerenchyma features; and (2) woody vegetation that have foliage shedding in the dry season. The first group represents evergreen and semi-evergreen woody species, while the second group represents deciduous species. Higgins et al. (2011) found leaf phenology separation between savanna trees and grasses. In this chapter, the seasonal frequencies (from yearly to monthly) were used to explore the differences between eco-regions and major species (such as Miombo woodland, Mopani woodland, and Acacia-Baikiaea shrubland). The significantly different amplitudes and their phases retrieved by the frequency analysis suggested that different phenology patterns were detectable between woody and herbaceous vegetation. Generally, the vegetation defined here as herbaceous and shrubs show more response at the half-year frequency, which is associated with a long dry season. However, the results show a limitation of the method for some arid areas where deciduous woody and herbaceous phenology are similar. Another limitation is that when the phenology patterns were

extracted from the MODIS data set we assumed that there were pure pixels of each vegetation type at the 500-meter scale. In order to better represent the phenology differences in the future, finer spatial and temporal resolution data is needed for the frequency decomposition.

The results of the validation with classified Orbview-3 imagery were relatively poor. This could mainly be attributed to the difficulty of distinguishing overstory and understory with the Orbview-3 pan-chromatic images especially during the growing season. The results of validation using classified IKONOS multispectral images were much better and there was strong agreement between the MODIS green vegetation fractions and IKONOS green vegetation fraction with an RMSE less than 0.1 and a R^2 near 0.7. However, there are also limitations when comparing with high resolution images. First, all three IKONOS images came from the same location, which sampled restricted vegetation types and climate variation. Second, since IKONOS images had 4 m pixel resolution, assumptions about pixel purity had to be made, when in reality, very few 4 m pixels would be pure woody, herbaceous or bar in these savannas. This issue becomes even more important in transition areas between clumps of woody plants trees and patches of grass at sub-4m pixel scale.

7. Conclusion

In this chapter, *f*PV was decomposed into $fPV_{semi\text{-}deciduous}$, $fPV_{deciduous}$, and $fPV_{herbaceous}$. The amplitude and phase of vegetation types were first explored. The amplitude and phase together suggested seasonal differences between woody and herbaceous vegetation. The growing patterns were then extracted from the overall study region referencing PPI and high-resolution images from Google Earth. The results show

the potential effectiveness of the frequency decomposition method for separating phenology of highly seasonal vegetation types where there are distinct differences in the timing of leaf flush/regrowth and leaf fall/senescence in relation to precipitation regimes. The method was able to separate semi-deciduous woody phenology, such as Miombo woodland, from herbaceous understory, however, it was less successful in separating deciduous woody phenology from herbaceous vegetation phenology in typical savanna and semi-arid savanna environments. In these areas, low woody plant density, fine-leaved woody plant morphology and inter-annual variation in timing of herbaceous and woody plant green-up and senescence interact with low MODIS pixel resolutions and 8 day image intervals to limit sensitivity.

CHAPTER 6 DISCUSSION

In order to better understand the land cover change and its interaction with local human society and global climate, we need to understand and monitor the spatial and temporal changes of global savanna vegetation. MODIS data have the potential to provide the needed information. MODIS time series have been shown to be able to distinguish green vegetation, dry vegetation, and bare soil in the Australian tropical savanna, as well as the evergreen and seasonal green vegetation phenology. The integration and the evaluation of those methods from previous studies for a range of applications over global savanna ecosystems are urgent. The research described in this thesis contributes to this development by providing further understanding of the fractional cover of tree/grass and their phenology cycle.

The research was carried on over three continents. All three sites are in the Southern Hemisphere with similar latitude. The Australian and southern African sites are under a rainfall gradients with the southern African site showing a slightly dryer climate. The annual total rainfall generally decreases with the increase of latitude. The Cerrado in South America, in contrast, varied less in annual precipitation and is much wetter than the other two sites.

This study explored different methods based on the different savanna characteristics. First, the green vegetation, dry vegetation, and bare soil were distinguished in all three sites. The method is based on the theory that those three components form a triangle shape in a NDVI-SWIR32 space (Guerschman et al., 2009).

The response envelope, however, varies according to different ecosystems (Hill et al., 2012). Thus, endmembers of the triangle shape were refined for each site. Second, the green vegetation was further separated into green woody and green herbaceous components. The method is based on the assumption that woody and herbaceous vegetation have different phenology. Since woody and herbaceous vegetation have different water use strategies (De Bie et al., 1998), they flush and drop leaves at different times and rates when water is the limiting factor. Lu et al. (2003) first separated evergreen woody (predominantly *Eucalyptus* spp.) and seasonal green herbaceous phenology in Australia. The method assumed that the seasonal variation of evergreen woody is 10% of the overall green vegetation variation, which was applied in the present study. It is, however, not applicable to the southern African site due to the prevalent distribution of deciduous trees. Thus, a frequency decomposition approach was developed to distinguish semi-deciduous woody, deciduous woody, and herbaceous components. The frequency decomposition abandoned the fixed seasonal variation proportion, and was able to dynamically estimate the proportion of variation species. One of the limitations, however, is the difficulty of finding single species dominated patches at the MODIS scale.

The research results have confirmed that fractions of tree/grass can be derived from the MODIS time series, but uncertainty varies among land cover types due to the various vegetation structure and morphology. This final chapter evaluates the results from the research by discussing the findings and formulating conclusions about a few separate aspects: the comparison of the NDVI-SWIR32 response envelopes from each continent;

the comparison of the fractional cover validation; the comparison of the green vegetation fraction accuracy; and the relationship between the fractional covers and latitude/rainfall.

The Australian tropical savanna mostly remains intact. The vegetation shows a distinctive two-layer system. The over layer is dominated by evergreen trees, while the under layer is composed of seasonal green grasses with dry vegetation and bare soil (Olson et al. 2001; Tothill & Gillies 1992; Hill et al. 2012; Eamus 1999; Williams et al. 1997; Lambin et al. 2003). The southern African savanna present also similar two-layer system. The deciduous trees, however, dominate the over layers of some ecosystems due to limited precipitation (Cowling et al. 2004). The Cerrado in Brazil, on the other hand, shows more diversity of vegetation structures (Oliveira & Marquis 2002; Hill et al. 2011). The woody vegetation is often mixed with herbaceous vegetation (Mistry 2000). Moreover, because of the humid climate, herbaceous vegetation could remain green during the dry season and show similar phenology with woody vegetation.

1. Comparisons between Australia, South America and Africa

PV, NPV, and BS show a similar response envelope relationship in the NDVI-SWIR32 space for the three different continents (Figure 91). The African site is enclosed in the Australian site, however, the Cerrado site shows a different response envelope patterns. The major difference comes from the PV end member of the Cerrado site; it suggests a denser vegetation structure in response to higher precipitation. The other two vertices are more similar between the three savanna systems (differences < 0.05).

The validation against high-resolution data shows the best agreement for green woody and PV fractional cover (Figure 92). A similar performance were also found by Mishra et al. (2014), which suggested the *f*PV RMSE is 0.13. The *f*PV in the Australian and southern African sites shows high intercepts (around 0.2). The intercept for fPV_{woody} is lower. The NPV produced mainly two types of regression relationships based on their slope. The first group shows lower slope and higher intercepts (Australia (September); Cerrado; and Southern Africa (May/June)). Another group shows better linear correlation. Similar separation is seen also for the *f*BS, where the South African validation produced higher intercepts and lower slope than the other two sites.

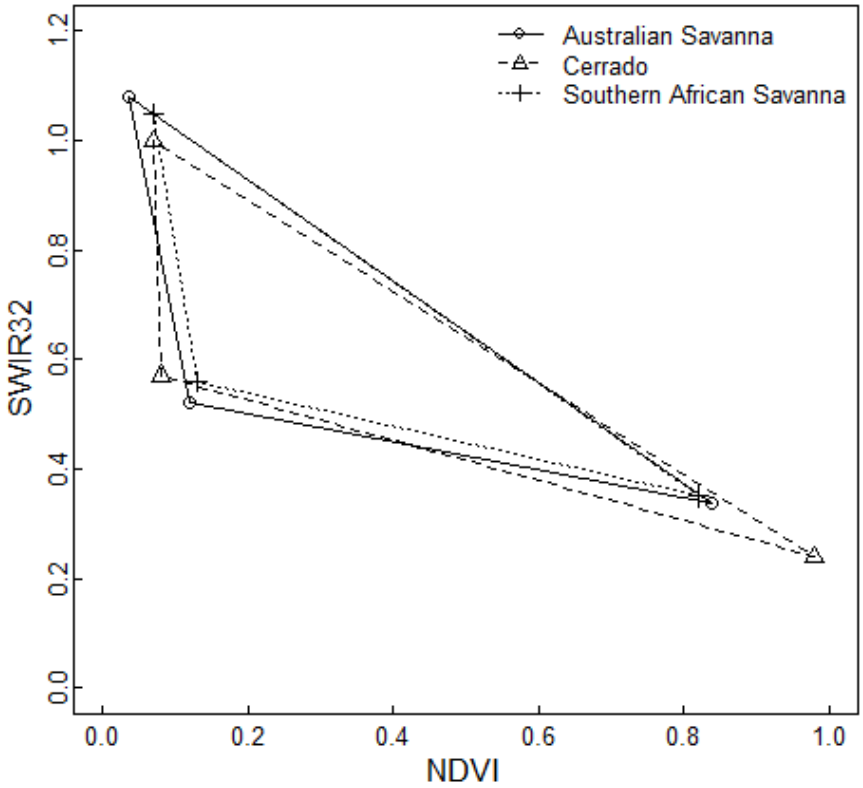

Figure 91. Cross comparison of the NDVI-SWIR32 response envelopes for each study savanna region

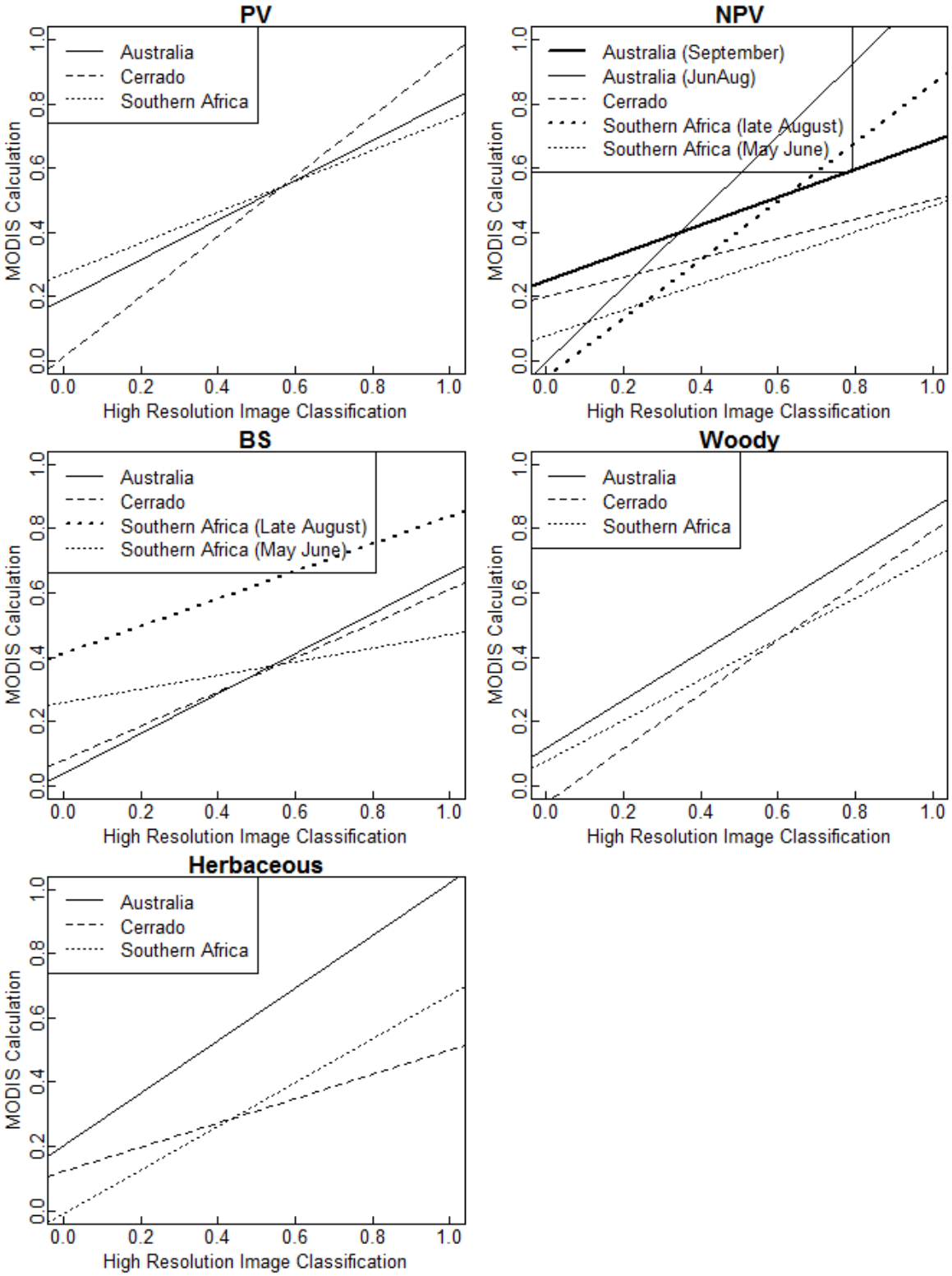

Figure 92. Cross comparison of validation against high-resolution images from each savanna region

Table 13. Effectiveness of the green vegetation decomposition methods in the three continents

Location	Method	R^2 – Evergreen/Semi-deciduous	R^2 – Deciduous/Herbaceous	RMSE – Evergreen/Semi-deciduous	RMSE – Deciduous/Herbaceous	Reference	Limitations
Australia	Lu	0.99	-	0.05	-	Landsat (Persistent Green Product)	
	Lu	0.31	0.57	0.2	0.14	Ground	
	Lu	0.85	0.67	0.1	0.03	Orbview-3 Muti-Spectral	
South America	Bfft	0.56	0.07	0.19	0.13	Quickbird	
	Bfft	0.92	0.5	0.04	0.07	Fire Fuel Survey; Precipitation	
	Lu	0.56	0.52	0.12	0.06	Fire Fuel Survey; Precipitation	
Africa	BFFT	0.68	0.69	0.07	0.09	IKONOS	
		0.2	0.11	0.46	0.12	Orbview-3 Panchromatic	

Table 13 shows the accuracy of green woody and green herbaceous vegetation fractions. The MODIS results showed a better agreement with high-resolution images than with ground observation since the high-resolution images allowed the sampling of the overall heterogeneous MODIS pixel when ground observation usually covers less than 30 meters. The woody fraction, on the other hand, showed a better performance than the herbaceous fraction. One of the reasons is that the over layer is distinctive in both MODIS and high-resolution images, while the green herbaceous vegetation is difficult to discriminate from dry grasses or sparse woody canopy at different seasons. In the South American site, both the frequency decomposition method and time series method from Lu et al. (2003) were tested. The result showed a better performance on the woody vegetation when using the frequency decomposition method, but shows a better agreement on the herbaceous vegetation (lower RMSE) with the method from Lu et al. (2003). The frequency decomposition works better to discriminate different phenology from woody and herbaceous vegetation. Conversely, the other method considered green herbaceous remaining during dry seasons.

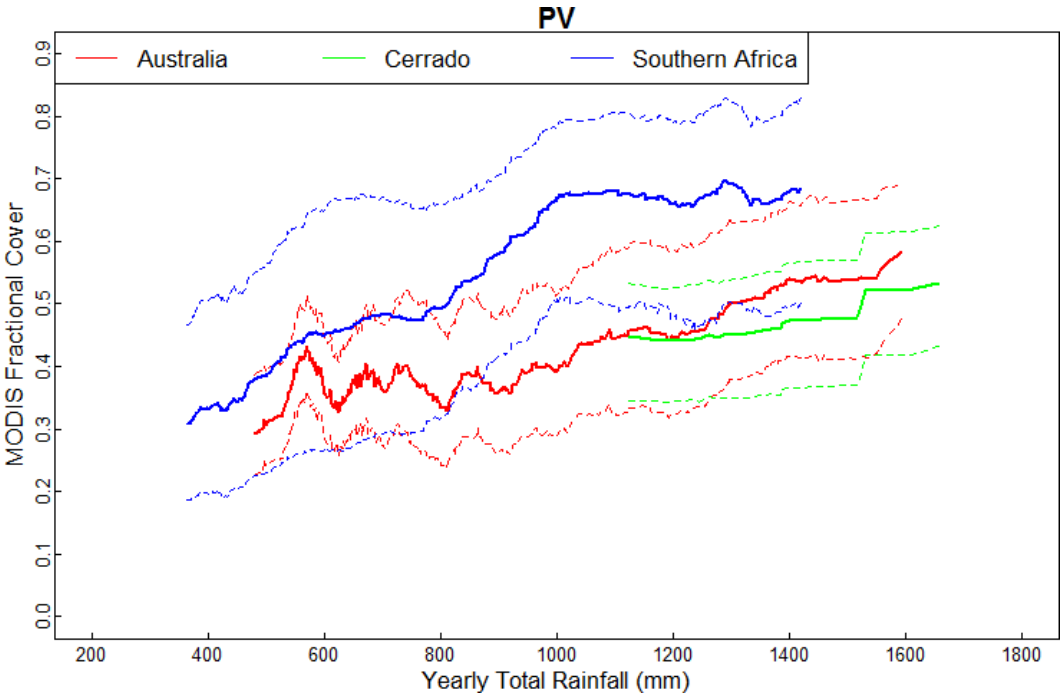

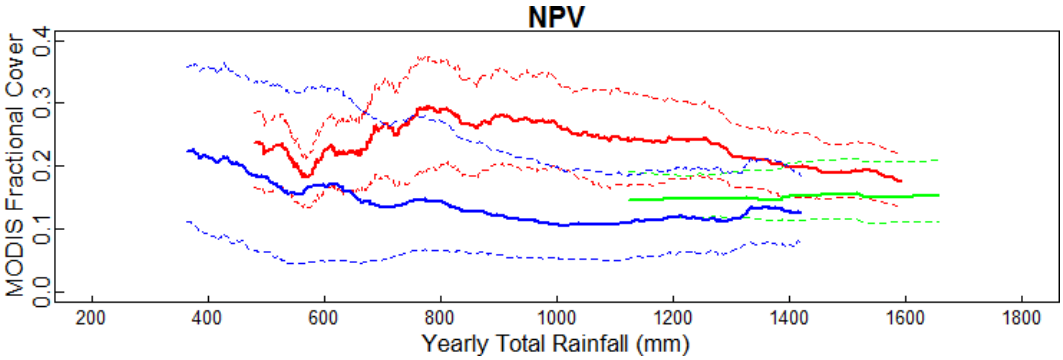

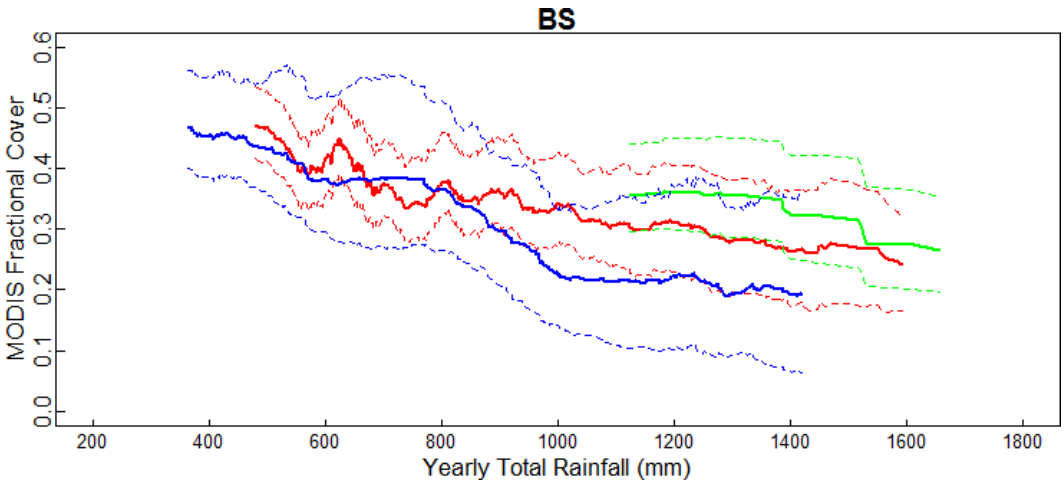

Figure 93 shows the variation of the average, maximum, and minimum fractional cover in relation to the total annual rainfall. The range of fractional cover varies less and is more consistent with the average than the latitude categories. The Cerrado shows overall higher precipitation than the other sites, while the southern African site shows overall higher green vegetation coverage. The Australian and southern African sites have a positive correlation between PV and rainfall, and a negative correlation between BS and rainfall. The correlation is evident when the total annual rainfall is less than approximate 1000mm, but stabilizes when rainfall is higher. The Australian site shows more variance in the average fraction cover and less correlation with rainfall in the arid area (< 700mm). NPV shows less correlation with rainfall, while the range narrows with the increase of rainfall. The average *f*NPV converges to around 0.2 for the three sites when the annual precipitation rises. In addition, the difference between the *f*NPV maximum and minimum also narrows with the raising of rainfall.

The correlations of *f*PV, and *f*BS with rainfall indicate there is a linear relationship between vegetation density and annual rainfall when the rainfall is below a threshold. The limited linear correlation was also observed by previous studies, however, with different rainfall thresholds (see Chapter 1, section 4.4) (Davenport & Nicholson 1993; Farrar et al. 1994; Fuller & Prince 1996; Martiny et al. 2006; Camberlin et al. 2007). The trembling fractional cover of arid areas in the Australian site may suggest various vegetation structures across ecosystems. When rainfall exceeds the threshold, all three fractional covers become stable. The convergence of average, maximum, and minimum *f*NPV may suggest a dominance of semi-deciduous woody and perennial plants where defoliation and decay reaches a balance.

Figure 94 shows a change of the average, maximum, and minimum fractional cover according to latitude. The comparison is based on the rainfall gradients associated with latitude. In the Australian and southern African sites, the annual total rainfall generally decreases with the increasing of latitude. The Cerrado rainfall, however, is more correlated with longitude. The average *f*PV shows a general decrease in the Australian and southern African sites and an increase of the average *f*BS with the rise of latitude. The *f*NPV, however, does not show a significant trend along with the latitude. For a latitude higher than 18 degrees (annual total rainfall between 500mm and 700mm), the maximum *f*PV shows a negative correlation with latitude and a positive correlation with the minimum *f*BS. This indicates the limitation of vegetation density due to water availability. The Cerrado site shows less correlation with latitude for all three fractions as the rainfall gradient do not depend on latitude.

2. Assessment of the Effectiveness of the Methods

Outside of the Australian savanna, the NDVI-SWIR32 response shows limitation in distinguishing NPV and BS, where there are diverse soil types and shrubs are present (southern African savanna) or where there is lack of vegetation layer structure (Cerrado). Recent studies explored spectral linear unmixing PV, NPV, and BS using all seven MODIS bands (Guerschman & Scarth, 2015; Meyer & Okin, 2015); this improved NPV and BS separation and especially reduced soil impact. Using higher resolution data could also improve the linear unmixing performance. Guerschman & Scarth (2015) found that field observations showed stronger agreement with fractional cover derived from Landsat data than from MODIS data.

The frequency decomposition detected phenology differences between tree covers, shrubs, and grass. The technology could be used to map species change associated with climate change in other environments. The frequency end-members, however, need to be refined, because the 500-meter MODIS resolution limits the sampling of pure species patches.

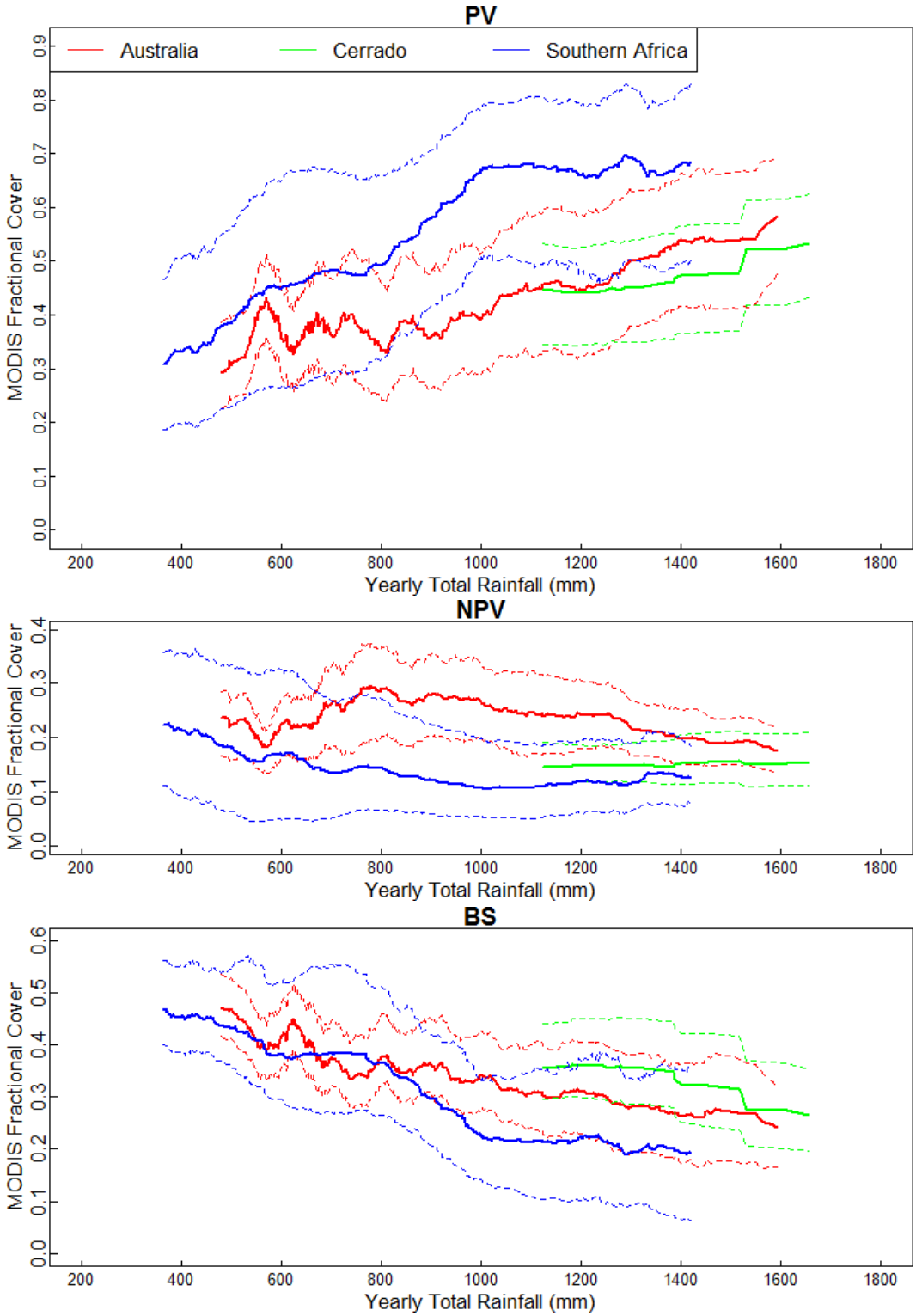

Figure 93. The average (solid line), max (dash line), and min (dash line) of fPV, fNPV, and fBS by yearly total rainfall for the Australian savanna (Red), Cerrado (Green), and Southern African Savanna (Blue) region

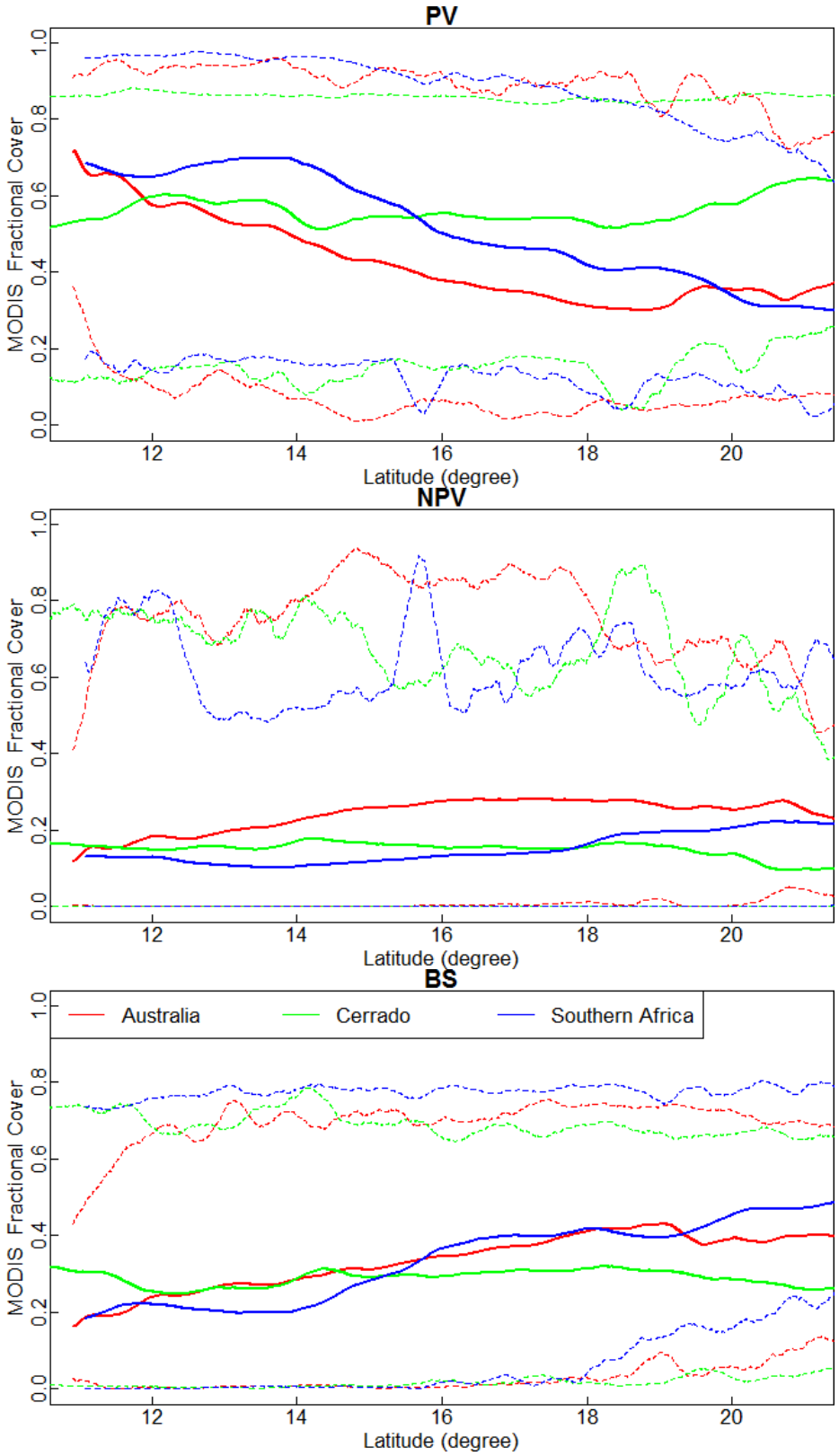

Figure 94. The average (solid line), max (dash line), and min (dash line) of fPV, fNPV, and fBS by latitude for the Australian savanna (Red), Cerrado (Green), and Southern African Savanna (Blue) region

The overall workflow shows good performance on estimating green vegetation and overstory fractional cover. It has been used successfully also to monitor deforestation, urban expansion (Gessner et al., 2013), and hydrodynamics (Guerschman et al., 2009). Moreover, the maps of overstory cover provided a basis for studying the population of browsers and better woody harvest management.

3. Recommendations for Further Work

A number of recommendations can be made for future research in using time series data to derive dynamics of vegetation attributes. Some of the problems experienced were inherent in the research data. The 500 meter MODIS data is naturally insensitive to minor changes of vegetation structure and shows limitations when the vegetation coverage is low. Besides, the coarse resolution also limits the ability of capturing endmembers for both methods, fractional cover unmixing and frequency decomposition. A possible solution is to explore the method with other datasets such as newly launched Landsat 8 and soon-to-be launched Sentinel 2. Another limitation is the stability of SWIR32-NDVI response due to the variation of the relationship between CAI and SWIR32 in different season and vegetation type. Guerschman & Scarth (2015) also confirms that full spectral MODIS or Landsat bands performs better than NDVI-SWIR32 when unmixing PV-NPV-BS components.

4. Conclusions

The conclusions from the research are summarized as follows:

NDVI-SWIR32 response space works best in the Australian savanna and Cerrado where understory is consistent herbaceous vegetation and the overstory is geographically

consistent woody morphology. In the African savanna, however, various types of bare soil introduce more uncertainty to the linear correlation between CAI and SWIR32. Hence, the NDVI-SWIR32 unmixing approach is less effective in African savanna than Australian savanna and Cerrado.

The time series decomposition developed by Lu et al. (2003) works in the Australian savanna where there is a distinctive two-layer system with consistent phenology within each layer. The overstory is evergreen canopy, while the understory is seasonal green herbaceous vegetation. The restriction is not applicable in Cerrado and African savanna because of the hybrid phenology pattern between woody and herbaceous vegetation. In Cerrado, woody vegetation is mostly evergreen. Nevertheless, part of the herbaceous vegetation also remains green even during the dry season; moreover, there are different phenology patterns within the woody or herbaceous vegetation due to the extreme biodiversity. In African savanna, the deciduous woody vegetation dominate overstory in many ecosystems.

The frequency decomposition is developed in this research to separate the deciduous woody vegetation from seasonal herbaceous vegetation. However, more study is needed to investigate the effectiveness of method, such as the representativeness of the frequency endmembers.

The MODIS spatial resolution is one of the biggest challenges when studying the heterogeneous savanna system. The 500-meter pixel integrates reflectance from bare soil, senescent grasses, green grasses, and green trees. The measurements could vary in different vegetation structure due to sheltering and multiple scattering, which reduces or

increases impact from one component. The challenge is rather significant in Cerrado where trees, shrubs, and grasses are intermingled and create synthesized signal at 500-meter scale.

One of the possible improvements in the future study is exploring multi-bands unmixing, instead of using the NDVI-SWIR32 response space. Guerschman & Scarth (2015) found that the spectral unmixing could remarkably reduce the soil color impacts. Another possible improvement is exploring the potential of higher spatial resolution images such as combination of Landsat and Sentinel 2 to reduce the vegetation structure impact in the heterogeneous savanna system.

REFERENCE

Alho, C.J.R. & Martins, E. de S., 1995. Bit by bit the Cerrado loses space. *WWF and PRO-CER, Bras ília, Brazil*.

Anaya, Jesús A., Chuvieco, Emilio & Palacios-Orueta, Alicia, 2009. Aboveground biomass assessment in Colombia: A remote sensing approach. *Forest Ecology and Management*, 257(4), pp.1237–1246.

Apan, A. & Held, A., 2002. In-House Workshop on Hyperion Data Processing: Echo-ing the Sugarcane Project Experience. *Black Mountain Laboratories, Canberra: CSIRO Land and Water*.

Armston, J., Disney, M., Lewis, P., Scarth, P., Bunting, P., Lucas, R., Phinn, S. & Goodwin, N., 2011. Comparison of discrete return and waveform airborne LiDAR derived estimates of fractional cover in an Australian savanna. *Proceedings of SilviLaser 2011*.

Bachoo, A. & Archibald, S., 2007. Influence of using date-specific values when extracting phenological metrics from 8-day composite NDVI data. In *Analysis of Multi-temporal Remote Sensing Images, 2007. MultiTemp 2007. International Workshop on the*. IEEE, pp. 1–4.

Barbosa, H.A., Huete, A.R. & Baethgen, W.E., 2006. A 20-year study of NDVI variability over the Northeast Region of Brazil. *Journal of Arid Environments*, 67(2), pp.288–307.

Barbosa, H.A., Kumar, T.V.L. & da Silva Junior, I.W., 2011. Analysis of the NDVI Temporal Dynamics in Semi-arid Ecosystems: Brazilian Caatinga and African Western Sahel (Análise da Dinâmica Temporal do NDVI nos Ecossistemas Semi-áridos: Caatinga Brasileira e Sahel Ocidental Africano). *Revista Brasileira de Geografia Física*, 4(2), pp.300–306.

Barlow, J. & Peres, C.A., 2008. Fire-mediated dieback and compositional cascade in an Amazonian forest. *Philosophical transactions of the Royal Society of London.Series B, Biological sciences*, 363(1498), pp.1787–1794.

Bastin, GN & Ludwig, JA, 2006. Problems and prospects for mapping vegetation condition in Australia's arid rangelands. *Ecological Management & Restoration*. Available at: http://onlinelibrary.wiley.com/doi/10.1111/j.1442-8903.2006.293_4.x/full [Accessed June 9, 2015].

Bastin, GN, Ludwig, JA & Eager, RW, 2002. Indicators of landscape function: comparing patchiness metrics using remotely-sensed data from rangelands. *Ecological …*. Available at: http://www.sciencedirect.com/science/article/pii/S1470160X02000092 [Accessed June 9, 2015].

Beard, John Stanley, 1953. The savanna vegetation of northern tropical America. *Ecological Monographs*, 23(2), pp.149–215.

Bellefontaine, R., 2000. *Management of natural forests of dry tropical zones.*, Available at: http://www.cabdirect.org/abstracts/20026791423.html [Accessed June 8, 2015].

De Bie, Steven, Ketner, Pieter, Paasse, Martine & Geerling, Chris, 1998. Woody plant phenology in the West Africa savanna. *Journal of Biogeography*, 25(5), pp.883–900.

Blydenstein, John, 1967. Tropical savanna vegetation of the Llanos of Colombia. *Ecology*, pp.1–15.

Boardman, Joseph W., 1994. Geometric mixture analysis of imaging spectrometry data. In *Geoscience and Remote Sensing Symposium, 1994. IGARSS'94. Surface and Atmospheric Remote Sensing: Technologies, Data Analysis and Interpretation., International*. IEEE, pp. 2369–2371.

Bond, William J., 2008. What limits trees in C4 grasslands and savannas? *Annual Review of Ecology, Evolution, and Systematics*, 39, pp.641–659.

Bourliere, Francois & Hadley, M., 1983. Present-day savannas: an overview. *Ecosystems of the World*, 1983.

Bradley, Andrew V, Gerard, France F., Barbier, Nicolas, Weedon, Graham P., Anderson, Liana O., Huntingford, Chris, Aragao, Luiz E.O.C., Zelazowski, Przemyslaw & Arai, Egidio, 2011. Relationships between phenology, radiation and precipitation in the Amazon region. *Global Change Biology*, 17(6), pp.2245–2260.

Brannstrom, Christian, Jepson, Wendy, Filippi, Anthony M., Redo, Daniel, Xu, Zengwang & Ganesh, Srinivasan, 2008. Land change in the Brazilian Savanna (Cerrado), 1986–2002: comparative analysis and implications for land-use policy. *Land Use Policy*, 25(4), pp.579–595.

Brink, Andreas Bernhard & Eva, Hugh Douglas, 2009. Monitoring 25 years of land cover change dynamics in Africa: A sample based remote sensing approach. *Applied Geography*, 29(4), pp.501–512.

Broxton, PD & Zeng, X., 2014. A global land cover climatology using MODIS data. *Journal of Applied …*. Available at:

http://journals.ametsoc.org/doi/abs/10.1175/JAMC-D-13-0270.1 [Accessed July 22, 2015].

Budde, M.E., Tappan, G., Rowland, J., Lewis, J. & Tieszen, Larry L., 2004. Assessing land cover performance in Senegal, West Africa using 1-km integrated NDVI and local variance analysis. *Journal of Arid Environments*, 59(3), pp.481–498.

Bureau of Rural Sciences, 2006. Land Use of Australia, Version 4, 2005/2006 (September 2010 release). *Department of Agriculture : Australian Bureau of Agricultural and Resource Economics and Sciences Data Manager*.

Burgess, Neil, Hales, J.D., Underwood, Emma, Dinerstein, Eric, Olson, David, Itoua, Illanga, Schipper, Jan, Ricketts, Taylor, Newman, Kate & Hales, J.A., 2004. *Terrestrial ecoregions of Africa and Madagascar: a conservation assessment.*, Island Press.

Bustamante, M., Ferreira, L.G., Hill, M.J., Niall, P. & Hanan, N.P., 2010. *Land use change and the carbon budget in the Brazilian Cerrado*, CRC Press: Boca Raton, FL, USA.

Camberlin, Pierre, Martiny, Nadege, Philippon, Nathalie & Richard, Yves, 2007. Determinants of the interannual relationships between remote sensed photosynthetic activity and rainfall in tropical Africa. *Remote Sensing of Environment*, 106(2), pp.199–216.

Campo-Bescós, MA & Muñoz-Carpena, R., 2013. Beyond precipitation: Physiographic gradients dictate the relative importance of environmental drivers on savanna vegetation. *PloS one*. Available at: http://dx.plos.org/10.1371/journal.pone.0072348 [Accessed June 19, 2015].

Capecchi, Valerio, Crisci, Alfonso, Lorenzo, Genesio, Maselli, Fabio & Vignaroli, Patrizio, 2008. Analysis of NDVI trends and their climatic origin in the Sahel 1986-2000. *Geocarto International*, 23(4), pp.297–310. Available at: http://www.informaworld.com/openurl?genre=article&doi=10.1080/10106040801950492&magic=crossref [Accessed March 12, 2013].

CAVALCANTI, Roberto Brandão, 1999. Ações prioritárias para a conservação da biodiversidade do Cerrado e Pantanal. *Conservation International do Brasil, Belo Horizonte*.

Chamaille-Jammes, S., 2006. Spatial patterns of the NDVI–rainfall relationship at the seasonal and interannual time scales in an African savanna. *International Journal of …*. Available at: http://www.tandfonline.com/doi/abs/10.1080/01431160600702392 [Accessed June

14, 2015].

Chamaillé-Jammes, S. & Fritz, H., 2009. Precipitation–NDVI relationships in eastern and southern African savannas vary along a precipitation gradient. *International Journal of Remote Sensing*, 30(13), pp.3409–3422.

Chidumayo, E.N., 2002. Changes in miombo woodland structure under different land tenure and use systems in central Zambia. *Journal of Biogeography*, 29(12), pp.1619–1626.

Chongo, Daniel, Nagasawa, Ryota, Ould Cherif Ahmed, Ahmedou & Perveen, Mst Farida, 2007. Fire monitoring in savanna ecosystems using MODIS data: a case study of Kruger National Park, South Africa. *Landscape and Ecological Engineering*, 3(1), pp.79–88. Available at: http://www.springerlink.com/index/10.1007/s11355-007-0020-5 [Accessed March 12, 2013].

Cleveland, Robert B., Cleveland, William S., McRae, Jean E. & Terpenning, Irma, 1990. STL: A seasonal-trend decomposition procedure based on loess. *Journal of Official Statistics*, 6(1), pp.3–73.

Coutinho, Leopoldo Magno, 1990. Fire in the ecology of the Brazilian cerrado. In *Fire in the tropical biota*. Springer, pp. 82–105.

Cowling, Richard M., Richardson, David M. & Pierce, Shirley M., 2004. *Vegetation of southern Africa*, Cambridge University Press.

Crist, E.P. & Kauth, R.J., 1986. The tasseled cap de-mystified.

Datt, B. & Jupp, D., 2004. No Title. *Hyperion data processing workshop: Hands-on processing instruction*.

Datt, B., McVicar, T.R., Van Niel, T.G., Jupp, D.L.B. & Pearlman, J.S., 2003. Preprocessing EO-1 Hyperion hyperspectral data to support the application of agricultural indexes. *Geoscience and Remote Sensing, IEEE Transactions on*, 41(6), pp.1246–1259.

Daughtry, CST, 2001. Discriminating crop residues from soil by shortwave infrared reflectance. *Agronomy Journal*. Available at: https://dl.sciencesocieties.org/publications/aj/abstracts/93/1/125 [Accessed June 14, 2015].

Daughtry, CST & Hunt, ER, 2005. Remote sensing the spatial distribution of crop residues. *Agronomy …*. Available at: https://dl.sciencesocieties.org/publications/aj/abstracts/97/3/0864 [Accessed June 14,

2015].

Davenport, M.L. & Nicholson, S.E., 1993. On the relation between rainfall and the Normalized Difference Vegetation Index for diverse vegetation types in East Africa. *International Journal of Remote Sensing*, 14(12), pp.2369–2389.

DeFries, Ruth, 2008. Terrestrial vegetation in the coupled human-earth system: Contributions of remote sensing.

Duchemin, B., Goubier, J. & Courrier, G., 1999. Monitoring phenological key stages and cycle duration of temperate deciduous forest ecosystems with NOAA/AVHRR data. *Remote Sensing of Environment*. Available at: http://www.sciencedirect.com/science/article/pii/S0034425798000674 [Accessed June 12, 2015].

Eamus, Derek, 1999. Ecophysiological traits of deciduous and evergreen woody species in the seasonally dry tropics. *Trends in ecology & evolution*, 14(1), pp.11–16.

Eiten, G., 1982. Brazilian "savannas." In *Ecology of tropical savannas*. Springer, pp. 25–47.

Eiten, George, 1972. The cerrado vegetation of Brazil. *The Botanical Review*, 38(2), pp.201–341.

Eiten, George, 1994. Vegeta ção do cerrado. *Cerrado: caracteriza ção, ocupa ção e perspectivas*, 2, pp.17–73.

Erasmi, S., Bothe, M. & Petta, RA, 2006. ENHANCED FILTERING OF MODIS TIME SERIES DATA FOR THE ANALYSIS OF DESERTIFICATION PROCESSES IN NORTHEAST BRAZIL. Available at: http://www.isprs.org/proceedings/xxxvi/part7/pdf/034.pdf [Accessed June 14, 2015].

FAO/ISRIC, 2003. Soil and terrain database for Southern Africa. Land and Water Digital Media Series # 26. *Food and Agriculture Organization of the United Nations, Rome, Italy*.

Farrar, T.J., Nicholson, S.E. & Lare, A.R., 1994. The influence of soil type on the relationships between NDVI, rainfall, and soil moisture in semiarid Botswana. II. NDVI response to soil oisture. *Remote Sensing of Environment*, 50(2), pp.121–133.

Farrell, JAK, 1968. Preliminary notes on the vegetation of the lower Sabi-Lundi basin, Rhodesia. *Kirkia*. Available at: http://www.jstor.org/stable/23501192 [Accessed June 21, 2015].

Fearnside, PM, 2000. Global warming and tropical land-use change: greenhouse gas emissions from biomass burning, decomposition and soils in forest conversion,

shifting cultivation and. *Climatic change*. Available at: http://link.springer.com/article/10.1023/A:1005569915357 [Accessed July 1, 2015].

Ferreira, L.G., Yoshioka, H., Huete, A. & Sano, E.E., 2003. Seasonal landscape and spectral vegetation index dynamics in the Brazilian Cerrado: An analysis within the Large-Scale Biosphere–Atmosphere Experiment in Amaz ônia (LBA). *Remote Sensing of Environment*, 87(4), pp.534–550.

Ferreira, Laerte Guimaraes, Asner, Gregory P., Knapp, David E., Davidson, Eric A., Coe, Michael, Bustamante, Mercedes M.C. & de Oliveira, Eddie Lenza, 2011. Equivalent water thickness in savanna ecosystems: MODIS estimates based on ground and EO-1 Hyperion data. *International Journal of Remote Sensing*, 32(22), pp.7423–7440.

Ferreira, LG, Yoshioka, H., Huete, A. & Sano, EE, 2003. Seasonal landscape and spectral vegetation index dynamics in the Brazilian Cerrado: An analysis within the Large-Scale Biosphere–Atmosphere Experiment in. *Remote Sensing of …*. Available at: http://www.sciencedirect.com/science/article/pii/S0034425703002116 [Accessed July 1, 2015].

Ferreira, M.E., Sano, E.E. & Ferreira, L.G., 2003. Update Vegetation National Park Brasilia Map (Cerrado) By Means Of Orbital Images With High Spatial Resolution. *X Brazilian Symposium Physical Geography Applied*. Available at: http://www.cibergeo.org/XSBGFA/eixo3/3.3/228/228.htm.

Fox, ID, 2001. Vegetation of the Australian tropical savannas. Available at: http://agris.fao.org/agris-search/search.do?recordID=US201300075937 [Accessed June 21, 2015].

Frison, P.L., Mougin, E. & Hiernaux, P., 1998. Observations and interpretation of seasonal ERS-1 wind scatterometer data over Northern Sahel (Mali). *Remote Sensing of Environment*, 63(3), pp.233–242.

Fuller, D.O. & Prince, S.D., 1996. Rainfall and foliar dynamics in tropical southern Africa: potential impacts of global climatic change on savanna vegetation. *Climatic Change*, 33(1), pp.69–96.

Fuller, Douglas O., 1999. Canopy phenology of some mopane and miombo woodlands in eastern Zambia. *Global Ecology and Biogeography*, 8(3-4), pp.199–209.

Gardner, Toby A., 2006. Tree–grass coexistence in the Brazilian cerrado: demographic consequences of environmental instability. *Journal of Biogeography*, 33(3), pp.448–463.

Gaudart, Jean, Tour é, Ousmane, Dessay, Nadine, Dicko, a Lassane, Ranque, St éphane, Forest, Loic, Demongeot, Jacques & Doumbo, Ogobara K., 2009. Modelling malaria

incidence with environmental dependency in a locality of Sudanese savannah area, Mali. *Malaria Journal*, 8(February), p.61. Available at: http://www.pubmedcentral.nih.gov/articlerender.fcgi?artid=2686729&tool=pmcentrez&rendertype=abstract [Accessed March 12, 2013].

Gessner, Ursula, Klein, Doris, Conrad, Christopher, Schmidt, Michael & Dech, Stefan, 2009. Towards an automated estimation of vegetation cover fractions on multiple scales: Examples of Eastern and Southern Africa. In *Proceedings of the 33rd International Symposium on Remote Sensing of Environment*.

Gessner, Ursula, Machwitz, Miriam, Conrad, Christopher & Dech, Stefan, 2013. Estimating the fractional cover of growth forms and bare surface in savannas. A multi-resolution approach based on regression tree ensembles. *Remote Sensing of Environment*, 129, pp.90–102.

Gibbes, C., Cassidy, L., Hartter, J. & Southworth, J., 2013. The monitoring of land-cover change and management across gradient landscapes in Africa. *Human-environment …*. Available at: http://link.springer.com/chapter/10.1007/978-94-007-4780-7_8 [Accessed June 19, 2015].

Gibbes, Cerian, Adhikari, Sanchayeeta, Rostant, Luke, Southworth, Jane & Qiu, Youliang, 2010. Application of object based classification and high resolution satellite imagery for savanna ecosystem analysis. *Remote Sensing*, 2(12), pp.2748–2772.

Giglio, L., Kendall, J.D. & Justice, C.O., 1999. Evaluation of global fire detection algorithms using simulated AVHRR infrared data. *International Journal of Remote Sensing*, 20(10), pp.1947–1985.

Giglio, L., Kendall, J.D. & Mack, R., 2003. A multi-year active fire dataset for the tropics derived from the TRMM VIRS. *International Journal of Remote Sensing*, 24(22), pp.4505–4525.

Giglio, Louis, Kendall, Jacqueline D. & Tucker, C.J., 2000. Remote sensing of fires with the TRMM VIRS. *International Journal of Remote Sensing*, 21(1), pp.203–207.

Goldstein, G., Meinzer, F.C., Bucci, S.J., Scholz, F.G., Franco, A.C. & Hoffmann, W.A., 2008. Water economy of Neotropical savanna trees: six paradigms revisited. *Tree physiology*, 28(3), pp.395–404.

Goodland, Robert & Pollard, R., 1973. The Brazilian cerrado vegetation: a fertility gradient. *The Journal of Ecology*, pp.219–224.

Grace, John, Jos é, Jos éSan, Meir, Patrick, Miranda, Heloisa S. & Montes, Ruben A., 2006. Productivity and carbon fluxes of tropical savannas. *Journal of Biogeography*,

33(3), pp.387–400.

Guerschman, Juan Pablo, Hill, M.J., Renzullo, L.J., Barrett, D.J., Marks, A.S. & Botha, E.J., 2009. Estimating fractional cover of photosynthetic vegetation, non-photosynthetic vegetation and bare soil in the Australian tropical savanna region upscaling the EO-1 Hyperion and MODIS sensors. *Remote Sensing of Environment*, 113(5), pp.928–945.

Guerschman, Juan Pablo, Oyarzabal, Mariano, Malthus, Tim, McVicar, T.R., Byrne, Guy, Randall, L.A. & Stewart, J.B., 2012. Evaluation of the MODIS-based vegetation fractional cover product.

Guerschman, Juan Pablo & Scarth, PF, 2015. Assessing the effects of site heterogeneity and soil properties when unmixing photosynthetic vegetation, non-photosynthetic vegetation and bare soil fractions from. *Remote Sensing of …*. Available at: http://www.sciencedirect.com/science/article/pii/S0034425715000395 [Accessed June 18, 2015].

Guimaraes, R., Hermuche, P., de Carvalho, A., Gomes, R. & Martins, E., 2006. Regional Identification of the Deciduous Forests of Brazil Central Using NDVI Seasonal Variations of the Sensor MODIS and Digital Elevation Model. In *Geoscience and Remote Sensing Symposium, 2006. IGARSS 2006. IEEE International Conference on*. IEEE, pp. 3607–3610.

Gurgel, H.C. & Ferreira, N.J., 2003. Annual and interannual variability of NDVI in Brazil and its connections with climate. *International Journal of Remote Sensing*, 24(18), pp.3595–3609.

Hanan, Niall P., Lehmann, Caroline E.R., Hill, M. & Hanan, N., 2010. *Tree-Grass Interactions in Savannas: Paradigms, Contradictions, and Conceptual Models*, Taylor and Francis Group: Boca Raton, FL, USA.

Herrmann, S.M., Anyamba, a & Tucker, C.J., 2005. Exploring Relationships between Rainfall and Vegetation Dynamics in the Sahel Using Coarse Resolution Satellite Data. *Journal of Arid Environments*. Available at: http://meteo.lcd.lu/globalwarming/Herrmann/Exploring_relationships.pdf.

Higgins, S.I., Delgado-Cartay, M.D., February, E.C. & Combrink, H.J., 2011. Is there a temporal niche separation in the leaf phenology of savanna trees and grasses? *Journal of Biogeography*.

Higgins, Steven I., Bond, William J., February, Edmund C., Bronn, Andries, Euston-Brown, Douglas I.W., Enslin, Beukes, Govender, Navashni, Rademan, Louise, O'Regan, Sean & Potgieter, Andre L.F., 2007. Effects of four decades of fire

manipulation on woody vegetation structure in savanna. *Ecology*, 88(5), pp.1119–1125.

Higgins, Steven I., Bond, William J. & Trollope, Winston S.W., 2000. Fire, resprouting and variability: a recipe for grass–tree coexistence in savanna. *Journal of Ecology*, 88(2), pp.213–229.

Higgins, Steven I., Shackleton, Charlie M. & Robinson, E. Robbie, 1999. Changes in woody community structure and composition under constrasting landuse systems in a semi-arid savanna, South Africa. *Journal of Biogeography*, 26(3), pp.619–627.

Hijmans, RJ, Cameron, S., Parra, J. & Jones, PG, 2005. WorldClim—global climate data. ... *Climate Surfaces for Global* .... Available at: https://scholar.google.com/scholar?q=WorldClim+%E2%80%93+Global+Climate+Data&btnG=&hl=en&as_sdt=0%2C35&as_ylo=2003#1 [Accessed June 20, 2015].

Hill, Michael J., 2013. Vegetation index suites as indicators of vegetation state in grassland and savanna: An analysis with simulated SENTINEL 2 data for a North American transect. *Remote Sensing of Environment*, 137, pp.94–111.

Hill, Michael J. & Donald, Graham E., 2003. Estimating spatio-temporal patterns of agricultural productivity in fragmented landscapes using AVHRR NDVI time series. *Remote Sensing of Environment*, 84(3), pp.367–384. Available at: http://linkinghub.elsevier.com/retrieve/pii/S0034425702001281.

Hill, Michael J. & Hanan, Niall P., 2010. *Ecosystem function in savannas: Measurement and modeling at landscape to global scales*, CRC Press.

Hill, Michael J., Román, Miguel O. & Schaaf, Crystal B., 2012. Dynamics of vegetation indices in tropical and subtropical savannas defined by ecoregions and Moderate Resolution Imaging Spectroradiometer (MODIS) land cover. *Geocarto International*, 27(2), pp.153–191.

Hill, Michael J., Román, Miguel O., Schaaf, Crystal B., Hill, M.J. & Hanan, N.P., 2011. Biogeography and Dynamis of Global Tropical and Subtropical Savannas: A Spatiotemporal View. *Ecosystem function in savannas: Measurement and modeling at landscape to global scales*.

Hirosawa, Yuji, Marsh, Stuart E. & Kliman, Douglas H., 1996. Application of standardized principal component analysis to land-cover characterization using multitemporal AVHRR data. *Remote Sensing of Environment*, 58(3), pp.267–281. Available at: http://linkinghub.elsevier.com/retrieve/pii/S0034425796000685.

Hoffmann, William A., da Silva Jr, Edson Rangel, Machado, Gustavo C., Bucci, Sandra J., Scholz, Fabian G., Goldstein, Guillermo & Meinzer, Frederick C., 2005. Seasonal

leaf dynamics across a tree density gradient in a Brazilian savanna. *Oecologia*, 145(2), pp.306–315.

Horne, James H., 2003. A tasseled cap transformation for IKONOS images. In *ASPRS 2003 Annual conference proceedings*. pp. 60–70.

House, Joanna I., Archer, Steve, Breshears, David D. & Scholes, Robert J., 2003. Conundrums in mixed woody–herbaceous plant systems. *Journal of Biogeography*, 30(11), pp.1763–1777.

Huang, S. & Siegert, F., 2006. Land cover classification optimized to detect areas at risk of desertification in North China based on SPOT VEGETATION imagery. *Journal of Arid Environments*, 67(2), pp.308–327. Available at: http://linkinghub.elsevier.com/retrieve/pii/S0140196306000735 [Accessed March 12, 2013].

Huber, S., Fensholt, R. & Rasmussen, K., 2011. Water availability as the driver of vegetation dynamics in the African Sahel from 1982 to 2007. *Global and Planetary Change*.

Huntley, BJ, 1974. Outlines of wildlife conservation in Angola. *JS Afr. Wildl. Managet. Assoc*. Available at: https://scholar.google.com/scholar?hl=en&as_sdt=0,35&as_ylo=1968&q=outlines+of+wildlife+conservation+in+angola#0 [Accessed June 14, 2015].

Hutley, Lindsay B. & Beringer, Jason, 2010. Disturbance and climatic drivers of carbon dynamics of a north Australian tropical savanna. *Ecosystem Function in Savannas: Measurement and Modeling at Landscape to Global Scales.CRC Press, Boca Raton*, pp.57–75.

Jacquin, Anne, Cheret, Véronique, Sheeren, David & Goulard, Michel, 2010. Impact of Fire on Savanna Vegetation Trends in Madagascar Assessed Using a Remote-Sensing Based Statistical Analysis.

Jacquin, Anne, Dumont, Mélanie, Denux, Jean-Philippe & Gay, Michel, 2007. Mapping annual burned areas in Malagasy savanna environments at landscape scale using MODIS time series analysis. *TOWARDS AN OPERATIONAL USE OF REMOTE SENSING IN FOREST FIRE MANAGEMENT*, p.236.

Jacquin, Anne, Sheeren, David & Lacombe, Jean-Paul, 2010. Vegetation cover degradation assessment in Madagascar savanna based on trend analysis of MODIS NDVI time series. *International Journal of Applied Earth Observation and Geoinformation*, 12(Supplement 1), pp.S3–S10. Available at: http://linkinghub.elsevier.com/retrieve/pii/S0303243409001159 [Accessed March 8,

2013].

Johansen, K., Gill, T., Trevithick, R., Armston, J., Scarth, P., Flood, N. and Phinn, S., 2012. 16th Australasian Remote Sensing and Photogrammery Conference. *16th Australasian Remote Sensing and Photogrammery Conference*.

Jun, Wen, Zhongbo, Su & Yaoming, Ma, 2004. Reconstruction of a cloud-free vegetation index time series for the Tibetan Plateau. *Mountain Research and Development*, 24(4), pp.348–353.

Jupp, D.L.B., Datt, B., Lovell, J., Campbell, S. & King, E., 2002. Discussions around Hyperion Data: Background Notes for the Hyperion Data Users Workshop.

Justice, Christopher O., Giglio, Louis, Roy, David, Boschetti, Luigi, Csiszar, Ivan, Davies, Diane, Korontzi, Stefania, Schroeder, W., O'Neal, Kelley & Morisette, Jeff, 2011. MODIS-derived global fire products. In *Land Remote Sensing and Global Environmental Change*. Springer, pp. 661–679.

Justice, CO & Dugdale, G., 1991. Synergism between NOAA-AVHRR and Meteosat data for studying vegetation development in semi-arid West Africa. ... *Journal of Remote* ..... Available at: http://www.tandfonline.com/doi/abs/10.1080/01431169108929730 [Accessed June 14, 2015].

Kauth, Richard J. & Thomas, G.S., 1976. The tasselled cap--a graphic description of the spectral-temporal development of agricultural crops as seen by Landsat. In *LARS Symposia*. p. 159.

Klein, Doris & Roehrig, Julia, 2006. HOW DOES VEGETATION RESPOND TO RAINFALL VARIABILITY IN A SEMI-HUMID WEST AFRICAN IN COMPARISON TO A SEMI-ARID EAST AFRICAN ENVIRONMENT ? , (September), pp.28–30.

Klink, CA & Machado, RB, 2005. Conservation of the Brazilian cerrado. *Conservation biology*. Available at: http://onlinelibrary.wiley.com/doi/10.1111/j.1523-1739.2005.00702.x/full [Accessed June 12, 2015].

Knapp, Alan K., Briggs, John M., Collins, Scott L., Archer, Steven R., BRET-HARTE, M. SYNDONIA, Ewers, Brent E., Peters, Debra P., Young, Donald R., Shaver, Gaius R. & Pendall, Elise, 2008. Shrub encroachment in North American grasslands: shifts in growth form dominance rapidly alters control of ecosystem carbon inputs. *Global Change Biology*, 14(3), pp.615–623.

Lambin, E.F., Goyvaerts, K. & Petit, C., 2003. Remotely-sensed indicators of burning efficiency of savannah and forest fires. *International Journal of Remote Sensing*,

24(15), pp.3105–3118.

Van Langevelde, Frank, Van De Vijver, Claudius A.D.M., Kumar, Lalit, Van De Koppel, Johan, De Ridder, Nico, Van Andel, Jelte, Skidmore, Andrew K., Hearne, John W., Stroosnijder, Leo & Bond, William J., 2003. Effects of fire and herbivory on the stability of savanna ecosystems. *Ecology*, 84(2), pp.337–350.

Legendre, P. & Legendre, LFJ, 2012. *Numerical ecology*, Available at: https://books.google.com/books?hl=en&lr=&id=6ZBOA-iDviQC&oi=fnd&pg=PP1&dq=Numerical+ecology,+2nd+English+edition&ots=ux8m18PaUe&sig=AayLIWQiYVMwRBCKIHMzFUZEBPs [Accessed June 21, 2015].

Leinenkugel, Patrick, Kuenzer, Claudia, Oppelt, Natascha & Dech, Stefan, 2013. Characterisation of land surface phenology and land cover based on moderate resolution satellite data in cloud prone areas—A novel product for the Mekong Basin. *Remote Sensing of Environment*, 136, pp.180–198.

Lhermitte, Stefaan, Verbesselt, Jan, Jonckheere, Inge, Nackaerts, Kris, Van Aardt, Jan a N., Verstraeten, Willem W. & Coppin, Pol, 2008. Hierarchical image segmentation based on similarity of NDVI time series. *Remote Sensing of Environment*, 112(2), pp.506–521. Available at: http://linkinghub.elsevier.com/retrieve/pii/S0034425707002301 [Accessed March 4, 2013].

Li, Hui, Mausel, Paul, Brondizio, Eduardo & Deardorff, David, 2010. A framework for creating and validating a non-linear spectrum-biomass model to estimate the secondary succession biomass in moist tropical forests. *ISPRS Journal of Photogrammetry and Remote Sensing*, 65(2), pp.241–254.

Lovell, J.L. & Graetz, R.D., 2001. Filtering pathfinder AVHRR land NDVI data for Australia. *International Journal of Remote Sensing*, 22(13), pp.2649–2654.

Low, A.B...T.G. Rebelo, 1996. Vegetation of South Africa Lesotho and Swaziland. *Pretoria South Africa Dept. of Environmental Affairs and Tourism Pretoria*.

Lu, Hua, Raupach, Michael R., McVicar, Tim R. & Barrett, Damian J., 2003. Decomposition of vegetation cover into woody and herbaceous components using AVHRR NDVI time series. *Remote Sensing of Environment*, 86(1), pp.1–18. Available at: http://linkinghub.elsevier.com/retrieve/pii/S0034425703000543 [Accessed March 5, 2013].

Ludwig, JA, Eager, RW & Bastin, GN, 2002. A leakiness index for assessing landscape function using remote sensing. *Landscape* …. Available at:

http://link.springer.com/article/10.1023/A:1016579010499 [Accessed June 9, 2015].

Ludwig, JA, Wiens, JA & Tongway, DJ, 2000. A scaling rule for landscape patches and how it applies to conserving soil resources in savannas. *Ecosystems*. Available at: http://link.springer.com/article/10.1007/s100210000012 [Accessed June 9, 2015].

Lymburner, L., Tan, P., Mueller, N., Thackway, R., Lewis, A., Thankappan, M., Randall, L., Islam, A. & Senarath, U., 2011. Dynamic Land Cover Dataset Version 1. *Geoscience Australia*.

M.M., Cole., 1986. The Savannas: Biogeography and Geobotany. *Academic Press, London*.

Maignan, F., Bréon, F.M., Bacour, C., Demarty, J. & Poirson, a, 2008. Interannual vegetation phenology estimates from global AVHRR measurements. *Remote Sensing of Environment*, 112(2), pp.496–505. Available at: http://linkinghub.elsevier.com/retrieve/pii/S0034425707002143 [Accessed March 12, 2013].

Malo, Ada R. & Nicholson, Sharon E., 1990. A study of rainfall and vegetation dynamics in the African Sahel using normalized difference vegetation index. *Journal of Arid Environments*, 19(1), pp.1–24.

Marañón, Teodoro, Pugnaire, Francisco I. & Callaway, Ragan M., 2009. Mediterranean-climate oak savannas: the interplay between abiotic environment and species interactions. *Web Ecology*, 9, pp.30–43.

Martiny, N., Camberlin, P., Richard, Y. & Philippon, N., 2006. Compared regimes of NDVI and rainfall in semi-arid regions of Africa. *International Journal of Remote Sensing*, 27(23), pp.5201–5223.

Matsuura, K. & Willmott, CJ, 2012. Terrestrial Precipitation: 1900-2010 Gridded Monthly Time Series (V. 3.01). *Center for Climatic Research, Department of …*. Available at: https://scholar.google.com/scholar?q=Terrestrial+Precipitation%3A+1900-2010+Gridded+Monthly+Time+Series&btnG=&hl=en&as_sdt=0%2C35&as_ylo=1968#1 [Accessed June 14, 2015].

Menenti, Massimo, Azzali, S., Verhoef, W. & Van Swol, R., 1991. *Mapping agroecological zones and time lag in vegetation growth by means of Fourier analysis of time series of NDVI images*, BCRS, Netherlands Remote Sensing Board.

Miranda, Sabrina do Couto, Bustamante, Mercedes, Palace, Michael, Hagen, Stephen, Keller, Michael & Ferreira, Laerte Guimarães, 2014. Regional Variations in Biomass Distribution in Brazilian Savanna Woodland. *Biotropica*, 46(2), pp.125–

138.

Mishra, Niti B. & Crews, Kelley A., 2014. Mapping vegetation morphology types in a dry savanna ecosystem: integrating hierarchical object-based image analysis with Random Forest. *International Journal of Remote Sensing*, 35(3), pp.1175–1198.

Mishra, Niti B., Crews, Kelley A. & Okin, Gregory S., 2014. Relating spatial patterns of fractional land cover to savanna vegetation morphology using multi-scale remote sensing in the Central Kalahari. *International Journal of Remote Sensing*, 35(6), pp.2082–2104.

Mistry, Jayalaxshmi, 2000. *World savannas: ecology and human use*, Pearson Education.

Mitchard, E.T.A., Saatchi, S.S., Gerard, F.F., Lewis, S.L. & Meir, P., 2009. Measuring woody encroachment along a forest-savanna boundary in Central Africa. *Earth Interactions*, 13(8), pp.1–29.

Monasterio, MAXIMINA, 1970. Ecología de las sabanas de América Tropical II. Caracterización ecológica del clima en los Llanos de Calabozo, Venezuela. *Revista Geográfica*, 21, pp.5–38.

Moody, Aaron & Johnson, David M., 2001. Land-surface phenologies from AVHRR using the discrete fourier transform. *Remote Sensing of Environment*, 75(3), pp.305–323. Available at: http://linkinghub.elsevier.com/retrieve/pii/S0034425700001759.

Muir, J., Schmidt, M., Tindall, D. & Trevithick, R., 2011. Guidelines for field measurement of fractional ground cover: a technical handbook supporting the Australian collaborative land use and management. *... : Queensland Department of ...*. Available at: https://scholar.google.com/scholar?q=Guidelines+for+Field+measurement+of+fractional+ground+cover%3A+a+technical+handbook+supporting+the+Australian+collaborative+land+use+and+management+program&btnG=&hl=en&as_sdt=0%2C35&as_ylo=1968#0 [Accessed June 14, 2015].

MUSYIMI, Z., 2011. TEMPORAL RELATIONSHIPS BETWEEN REMOTELY SENSED SOIL MOISTURE AND NDVI OVER AFRICA: POTENTIAL FOR DROUGHT EARLY WARNING?

Nagler, P.L., Inoue, Y., Glenn, E.P., Russ, A.L. & Daughtry, C.S.T., 2003. Cellulose absorption index (CAI) to quantify mixed soil-plant litter scenes. *Remote Sensing of Environment*, 87(2-3), pp.310–325.

National Forest Inventory, 2003. Australia's State of the Forests Report 2003. *Bureau of Rural Sciences, Canberra*.

Nicholson, Sharon E., 2000. The nature of rainfall variability over Africa on time scales of decades to millenia. *Global and Planetary Change*, 26(1), pp.137–158.

Nix, H.A., 1983. Climate of tropical savannas. *Elsevier, Amsterdam*, pp.37 – 62.

Ogbazghi, Woldeselassie, Rijkers, Toon, Wessel, Marius & Bongers, Frans, 2006. Distribution of the frankincense tree Boswellia papyrifera in Eritrea: the role of environment and land use. *Journal of Biogeography*, 33(3), pp.524–535.

Oliveira, Paulo S. & Marquis, Robert J., 2002. The cerrados of Brazil. *Ecology and natural history of a neotropical savanna.Columbia University Press, New York*.

Oliveira-Filho, Ary T. & Ratter, James A., 2002. Vegetation physiognomies and woody flora of the cerrado biome. *The Cerrados of Brazil.Ecology and natural history of a neotropical savanna*, pp.91–120.

Olson, David M., Dinerstein, Eric, Wikramanayake, Eric D., Burgess, Neil D., Powell, George V.N., Underwood, Emma C., D'amico, Jennifer A., Itoua, Illanga, Strand, Holly E. & Morrison, John C., 2001. Terrestrial Ecoregions of the World: A New Map of Life on Earth A new global map of terrestrial ecoregions provides an innovative tool for conserving biodiversity. *Bioscience*, 51(11), pp.933–938.

Olson, David M., Dinerstein, Eric, Wikramanayake, Eric D., Burgess, Neil D., Powell, George V.N., Underwood, Emma C., D'amico, Jennifer a., Itoua, Illanga, Strand, Holly E., Morrison, John C., Loucks, Colby J., Allnutt, Thomas F., Ricketts, Taylor H., Kura, Yumiko, Lamoreux, John F., Wettengel, Wesley W., Hedao, Prashant & Kassem, Kenneth R., 2001. Terrestrial Ecoregions of the World: A New Map of Life on Earth. *BioScience*, 51(11), p.933.

Ottmar, RD, Vihnanek, RE & Miranda, HS, 2001. Stereo photo series for quantifying cerrado fuels in Central Brazil—volume I. Available at: http://www.srs.fs.usda.gov/pubs/viewpub.php?index=5516 [Accessed June 17, 2015].

Pennington, R. Toby, Lewis, G.P., Ratter, James A., Pennington, R.T., Lewis, G.P. & Ratter, J.A., 2006. An overview of the plant diversity, biogeography and conservation of neotropical savannas and seasonally dry forests. *Neotropical savannas and seasonally dry forests: plant biodiversity, biogeography and conservation*, pp.1–29.

Pettorelli, Nathalie, Vik, Jon Olav, Mysterud, Atle, Gaillard, Jean-Michel, Tucker, Compton J. & Stenseth, Nils Chr, 2005. Using the satellite-derived NDVI to assess ecological responses to environmental change. *Trends in Ecology & Evolution*, 20(9), pp.503–510. Available at: http://www.ncbi.nlm.nih.gov/pubmed/16701427

[Accessed March 4, 2013].

Philippon, N., Jarlan, L., Martiny, N., Camberlin, P. & Mougin, E., 2007. Characterization of the Interannual and Intraseasonal Variability of West African Vegetation between 1982 and 2002 by Means of NOAA AVHRR NDVI Data. *Journal of Climate*, 20(7), pp.1202–1218. Available at: http://journals.ametsoc.org/doi/abs/10.1175/JCLI4067.1 [Accessed March 12, 2013].

Du Plessis, W.P., 1999. Linear regression relationships between NDVI, vegetation and rainfall in Etosha National Park, Namibia. *Journal of Arid Environments*, 42(4), pp.235–260. Available at: http://linkinghub.elsevier.com/retrieve/pii/S0140196399905050.

Prince, S.D., 1991. Satellite remote sensing of primary production: comparison of results for Sahelian grasslands 1981-1988. *International Journal of Remote Sensing*, 12(6), pp.1301–1311.

Prince, S.D. & Tucker, C.J., 1986. Satellite remote sensing of rangelands in Botswana II. NOAA AVHRR and herbaceous vegetation. *International Journal of Remote Sensing*, 7(11), pp.1555–1570.

Privette, JL & Roy, DP, 2005. Southern Africa as a remote sensing test bed: the SAFARI 2000 Special Issue overview. *International journal of remote sensing*. Available at: http://www.tandfonline.com/doi/abs/10.1080/01431160500113401 [Accessed June 17, 2015].

Privette, JL, Tian, Y. & Roberts, G., 2004. Vegetation structure characteristics and relationships of Kalahari woodlands and savannas. *Global Change …*. Available at: http://onlinelibrary.wiley.com/doi/10.1111/j.1365-2486.2004.00740.x/full [Accessed June 17, 2015].

Ratter, James A., Ribeiro, Jos éFelipe & Bridgewater, Samuel, 1997. The Brazilian cerrado vegetation and threats to its biodiversity. *Annals of Botany*, 80(3), pp.223–230.

Reed, B.C., 2006. Trend analysis of time-series phenology of North America derived from satellite data. *GIScience & Remote Sensing*, 43(1), pp.24–38.

Richer, R.A., 2008. Leaf phenology and carbon dynamics in six leguminous trees. *African Journal of Ecology*, 46(1), pp.88–95.

Rigina, O. & Rasmussen, M.S., 2003. Comparing time series of AVHRR LAC data with the IGBP 1 km and the Pathfinder 8 km datasets. *GEOGRAFISK TIDSSKRIFT*, (1), pp.17–30.

Roderick, Michael L., Noble, Ian R. & Cridland, Shane W., 1999. Estimating woody and herbaceous vegetation cover from time series satellite observations. *Global Ecology and Biogeography*, 8(6), pp.501–508.

Roerink, G.J., Menenti, M., Soepboer, W. & Su, Z., 2003. Assessment of climate impact on vegetation dynamics by using remote sensing. *Physics and Chemistry of the Earth Parts ABC*, 28(1-3), pp.103–109. Available at: http://linkinghub.elsevier.com/retrieve/pii/S1474706503000111 [Accessed March 7, 2013].

Román, Miguel O., Schaaf, Crystal B., Woodcock, Curtis E., Strahler, Alan H., Yang, Xiaoyuan, Braswell, Rob H., Curtis, Peter S., Davis, Kenneth J., Dragoni, Danilo & Goulden, Michael L., 2009. The MODIS (Collection V005) BRDF/albedo product: Assessment of spatial representativeness over forested landscapes. *Remote Sensing of Environment*, 113(11), pp.2476–2498.

Romero-Ruiz, M.H., Flantua, S.G.A., Tansey, K. & Berrio, J.C., 2012. Landscape transformations in savannas of northern South America: Land use/cover changes since 1987 in the Llanos Orientales of Colombia. *Applied Geography*, 32(2), pp.766–776.

Roy, D.P., Lewis, P.E. & Justice, C.O., 2002. Burned area mapping using multi-temporal moderate spatial resolution data—A bi-directional reflectance model-based expectation approach. *Remote Sensing of Environment*, 83(1), pp.263–286.

Roy, Dp, Jin, Y., Lewis, Pe & Justice, Co, 2005. Prototyping a global algorithm for systematic fire-affected area mapping using MODIS time series data. *Remote Sensing of Environment*, 97(2), pp.137–162. Available at: http://discovery.ucl.ac.uk/11136/ [Accessed March 1, 2013].

Rutherford, M.C., 1997. Categorization of biomes. *Vegetation of southern Africa*, pp.91–98.

Sankaran, Mahesh, Hanan, Niall P., Scholes, Robert J., Ratnam, Jayashree, Augustine, David J., Cade, Brian S., Gignoux, Jacques, Higgins, Steven I., Le Roux, Xavier & Ludwig, Fulco, 2005. Determinants of woody cover in African savannas. *Nature*, 438(7069), pp.846–849.

Sano, EE, Rosa, R., Brito, JLS & Ferreira, LG, 2010. Land cover mapping of the tropical savanna region in Brazil. *Environmental monitoring and …*. Available at: http://link.springer.com/article/10.1007/s10661-009-0988-4 [Accessed June 12, 2015].

Sano, EE, Rose, R., Brito, JLS & Ferreira, LG, 2007. vegetation mapping the Cerrado

biome. *Planaltina: Embrapa Cerrado*. Available at: http://core.ac.uk/download/pdf/15445589.pdf [Accessed June 17, 2015].

Santos, P. & Negri, A.J., 1997. A comparison of the normalized difference vegetation index and rainfall for the Amazon and northeastern Brazil. *Journal of Applied Meteorology*, 36(7), pp.958–965.

Sarmiento, G., 1983. The savannas of tropical America. *ECOSYSTEMS OF THE WORLD.1983*.

Scanlon, Todd M., Albertson, John D., Caylor, Kelly K. & Williams, Chris a, 2002. Determining land surface fractional cover from NDVI and rainfall time series for a savanna ecosystem. *Remote Sensing of Environment*, 82(2-3), pp.376–388. Available at: http://linkinghub.elsevier.com/retrieve/pii/S0034425702000548.

Scarth, P., Röder, A., Schmidt, M. & Denham, R., 2010. Tracking grazing pressure and climate interaction—The role of Landsat fractional cover in time series analysis. *... of the 15th Australasian Remote Sensing ...*. Available at: https://scholar.google.com/scholar?q=Tracking+grazing+pressure+and+climate+interaction+-+the+role+of+Landsat+fractional+cover+in+time+series+analysis&btnG=&hl=en&as_sdt=0%2C35&as_ylo=1968#0 [Accessed June 14, 2015].

Schaaf, Crystal B., Gao, Feng, Strahler, Alan H., Lucht, Wolfgang, Li, Xiaowen, Tsang, Trevor, Strugnell, Nicholas C., Zhang, Xiaoyang, Jin, Yufang & Muller, Jan-Peter, 2002. First operational BRDF, albedo nadir reflectance products from MODIS. *Remote Sensing of Environment*, 83(1), pp.135–148.

Scholes, R.J. & Archer, S.R., 1997. Tree-grass interactions in savannas 1. *Annual Review of Ecology and Systematics*, 28(1), pp.517–544.

Scholes, RJ & Dowty, PR, 2002. Trends in savanna structure and composition along an aridity gradient in the Kalahari. *Journal of ...*. Available at: http://onlinelibrary.wiley.com/doi/10.1111/j.1654-1103.2002.tb02066.x/full [Accessed June 5, 2015].

Scholes, RJ, Frost, PGH & Tian, Y., 2004. Canopy structure in savannas along a moisture gradient on Kalahari sands. *Global Change Biology*. Available at: http://onlinelibrary.wiley.com/doi/10.1046/j.1365-2486.2003.00703.x/full [Accessed June 17, 2015].

Schulze, B.R., 1965. *Climate of South Africa: General Survey by BR Schulze*, Government Printer, South Africa.

Silva, J.F., Fariñas, M.R., Felfili, J.M. & Klink, C.A., 2006. Spatial heterogeneity, land

use and conservation in the cerrado region of Brazil. *Journal of Biogeography*, 33(3), pp.536–548.

Smith, PP, 1998. A reconnaissance survey of the vegetation of the North Luangwa National Park, Zambia. *Bothalia*. Available at: http://www.abcjournal.org/index.php/ABC/article/view/641 [Accessed June 21, 2015].

Smitinand, T., 1977. Vegetation and ground cover of Thailand. *Technical Paper*. Available at: http://kukr.lib.ku.ac.th/Fulltext/KU0024046.pdf [Accessed June 5, 2015].

SMITINAND, TEM, 1962. Types of Forests of Thailand. *Bangkok. Ministry of Agriculture, Royal Forest …*. Available at: https://scholar.google.com/scholar?start=70&q=types+of+forests+of+thailand+Smitinand&hl=en&as_sdt=0,35#5 [Accessed June 5, 2015].

Sokal, R. R., & Rohlf, F.J., 1995. "Model II regression". In Biometry (3rd ed). *New York: W. H. Freeman*, pp.541 – 549.

Spessa, Allan, McBeth, Bevan & Prentice, Colin, 2005. Relationships among fire frequency, rainfall and vegetation patterns in the wet–dry tropics of northern Australia: an analysis based on NOAA-AVHRR data. *Global Ecology and Biogeography*, 14(5), pp.439–454.

Staver, A. Carla, Archibald, Sally & Levin, Simon, 2011. Tree cover in sub-Saharan Africa: rainfall and fire constrain forest and savanna as alternative stable states. *Ecology*, 92(5), pp.1063–1072.

Staver, AC, Archibald, S. & Levin, SA, 2011. The global extent and determinants of savanna and forest as alternative biome states. *Science*. Available at: http://www.sciencemag.org/content/334/6053/230.short [Accessed June 8, 2015].

Stott, P., 1991. Recent trends in the ecology and management of the world's savanna formations. *Progress in Physical Geography*. Available at: http://ppg.sagepub.com/content/15/1/18.short [Accessed June 5, 2015].

Stott, P., 1988. Savanna forest and seasonal fire in Southeast Asia. *Plants today*. Available at: https://scholar.google.com/scholar?q=savanna+forest+and+seasonal+fires+in+south+east+asia&btnG=&hl=en&as_sdt=0%2C35#0 [Accessed June 5, 2015].

Tothill, JC & Gillies, C., 1992. The pasture lands of northern Australia: their condition, productivity and sustainability., Occasional Publication No. 5.(Tropical Grassland Society of. Available at:

https://scholar.google.com/scholar?q=the+pasture+lands+of+northern+australia+their+condition+productivity+and+sustainability&btnG=&hl=en&as_sdt=0%2C35&as_ylo=1991#0 [Accessed June 14, 2015].

Tucker, C.J. & Sellers, P.J., 1986. Satellite remote sensing of primary production. *International Journal of Remote Sensing*, 7(11), pp.1395–1416.

Vanak, Abi Tamim, Shannon, Graeme, Thaker, Maria, Page, Bruce, Grant, Rina & Slotow, Rob, 2012. Biocomplexity in large tree mortality: interactions between elephant, fire and landscape in an African savanna. *Ecography*, 35(4), pp.315–321.

Vancutsem, Christine, Pekel, J.F., Evrard, C., Malaisse, Francois & Defourny, Pierre, 2009. Mapping and characterizing the vegetation types of the Democratic Republic of Congo using SPOT VEGETATION time series. *International Journal of Applied Earth Observation and Geoinformation*, 11(1), pp.62–76.

Veenendaal, E.M., Mantlana, K.B., Pammenter, N.W., Weber, P., Huntsman-Mapila, P. & Lloyd, J., 2008. Growth form and seasonal variation in leaf gas exchange of Colophospermum mopane savanna trees in northwest Botswana. *Tree physiology*, 28(3), pp.417–424.

Verbesselt, J., Jonsson, P., Lhermitte, S., Van Aardt, J. & Coppin, P., 2006. Evaluating satellite and climate data-derived indices as fire risk indicators in savanna ecosystems. *Geoscience and Remote Sensing, IEEE Transactions on*, 44(6), pp.1622–1632.

Verbesselt, J., Somers, B., Van Aardt, J., Jonckheere, I. & Coppin, P., 2006. Monitoring herbaceous biomass and water content with SPOT VEGETATION time-series to improve fire risk assessment in savanna ecosystems. *Remote Sensing of Environment*, 101(3), pp.399–414. Available at: http://linkinghub.elsevier.com/retrieve/pii/S0034425706000332 [Accessed March 9, 2013].

Verbesselt, J., Somers, B., Lhermitte, S., Jonckheere, I., Van Aardt, J. & Coppin, P., 2007. Monitoring herbaceous fuel moisture content with SPOT VEGETATION time-series for fire risk prediction in savanna ecosystems. *Remote Sensing of Environment*, 108(4), pp.357–368. Available at: http://linkinghub.elsevier.com/retrieve/pii/S0034425706004962 [Accessed March 9, 2013].

Viovy, N., Arino, O. & Belward, A.S., 1992. The Best Index Slope Extraction (BISE): A method for reducing noise in NDVI time-series. *International Journal of Remote Sensing*, 13(8), pp.1585–1590.

Vourlitis, GL & Rocha, HR da, 2011. Flux dynamics in the cerrado and cerrado-forest transition of Brazil. *... function in global ...*. Available at: https://scholar.google.com/scholar?q=flux+dynamics+in+the+cerrado+and+cerrado+forest+transistion+of+brazil&btnG=&hl=en&as_sdt=0%2C35#0 [Accessed July 1, 2015].

Wagenseil, H. & Samimi, C., 2006. Assessing spatio-temporal variations in plant phenology using Fourier analysis on NDVI time series: results from a dry savannah environment in Namibia. *International Journal of Remote Sensing*, 27(16), pp.3455–3471.

White, Frank, 1983. The vegetation of Africa: A descriptive memoir to accompany the UNESCO/AETFAT/UNSO vegetation map of Africa (Natural Resources Research 20). *UN Educational, Scientific and Cultural Organization, Paris*.

White, MA, 1997. A continental phenology model for monitoring vegetation responses to interannual climatic variability. *Global biogeochemical ...*. Available at: http://onlinelibrary.wiley.com/doi/10.1029/97GB00330/full [Accessed June 5, 2015].

Wiegand, Kerstin, Saltz, David & Ward, David, 2006. A patch-dynamics approach to savanna dynamics and woody plant encroachment–insights from an arid savanna. *Perspectives in Plant Ecology, Evolution and Systematics*, 7(4), pp.229–242.

WILD, H. & Fernandes, A., 1968. Flora Zam-besiaca. Suppl. Vegetation map of the Flora Zambesiaca area. *... . Vegetation map of the Flora Zambesiaca ...*. Available at: http://www.cabdirect.org/abstracts/19690701641.html [Accessed June 21, 2015].

Williams, Christopher A., Hanan, Niall P., Neff, Jason C., Scholes, Robert J., Berry, Joseph A., Denning, A. Scott & Baker, David F., 2007. Africa and the global carbon cycle. *Carbon Balance and Management*, 2(3), pp.1–13.

Williams, R.J., Myers, B.A., Muller, W.J., Duff, G.A. & Eamus, Derek, 1997. Leaf phenology of woody species in a north Australian tropical savanna. *Ecology*, 78(8), pp.2542–2558.

Williams, Richard J., Hutley, Lindsay B., Cook, Garry D., Russell-Smith, Jeremy, Edwards, Andrew & Chen, Xiayong, 2004. Viewpoint: Assessing the carbon sequestration potential of mesic savannas in the Northern Territory, Australia: approaches, uncertainties and potential impacts of fire. *Functional Plant Biology*, 31(5), pp.415–422.

Williams, RJ & Duff, GA, 1996. Variation in the composition and structure of tropical savannas as a function of rainfall and soil texture along a large-scale climatic gradient in the Northern Territory,. *Journal of ...*. Available at:

http://onlinelibrary.wiley.com/doi/10.1111/j.1365-2699.1996.tb00036.x/abstract [Accessed June 5, 2015].

Yarbrough, Lance D., Easson, Greg & Kuszmaul, Joel S., 2005. QuickBird 2 tasseled cap transform coefficients: a comparison of derivation methods. In *Pecora*. pp. 23–27.

Zhang, X., Friedl, MA & Schaaf, CB, 2003. Monitoring vegetation phenology using MODIS. *Remote sensing of …*. Available at: http://www.sciencedirect.com/science/article/pii/S0034425702001359 [Accessed June 12, 2015].

Zhang, Xiaoyang, Friedl, Mark A., Schaaf, Crystal B., Strahler, Alan H. & Liu, Zhong, 2005. Monitoring the response of vegetation phenology to precipitation in Africa by coupling MODIS and TRMM instruments. *Journal of Geophysical Research: Atmospheres (1984–2012)*, 110(D12).

Zine, Sonia, Jarlan, Lionel, Frison, P.L., Mougin, Eric, Hiernaux, Pierre & Rudant, J.P., 2005. Land surface parameter monitoring with ERS scatterometer data over the Sahel: A comparison between agro-pastoral and pastoral areas. *Remote Sensing of Environment*, 96(3), pp.438–452.